Delft University of Technology

SET 3901 - Graduation project

Validation of *New*Gust

and a comparison with other wind gust simulation methods

with respect to the load response of a wind turbine

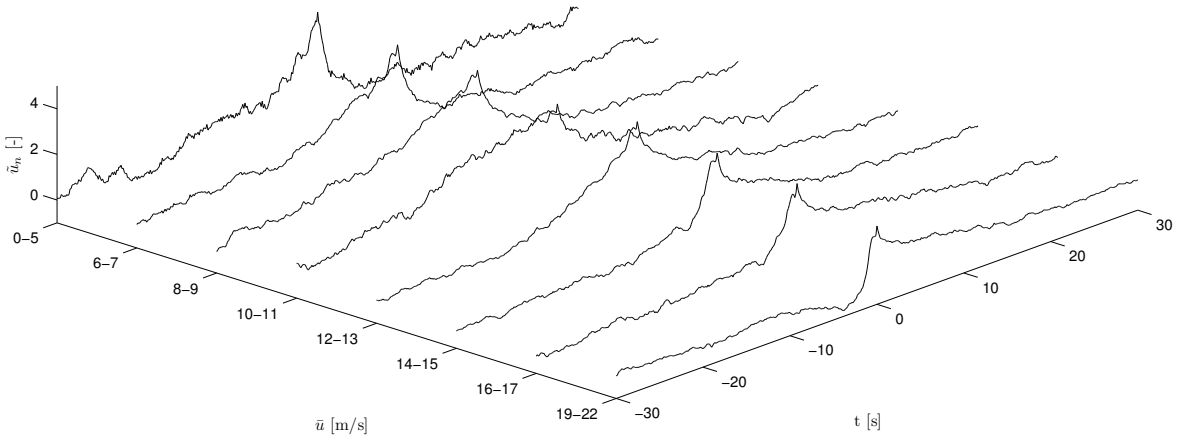

A.K. de Wit
Delft

April 20, 2010

Delft University of Technology

SET 3901 - Graduation project

Validation of *New*Gust

and a comparison with other wind gust simulation methods

with respect to the load response of a wind turbine

Author:
ing. Kundert de Wit

Supervisor:
dr. Wim Bierbooms

Examination committee:
dr. W.A.A.M. Bierbooms
prof. dr. G.J.W. van Bussel
prof. dr. F.M. Mulder

Delft
April 20, 2010

Preface

For the acquisition of the Master of Science degree at Delft Technical University it is required to do a master thesis project. The master programme I am following is Sustainable Energy Technology (SET). As my specialization is wind energy, I wanted to do my master thesis within this department. Because atmospheric wind and, more specific, turbulence had my interest for a long time, I looked for a project with a relation to this topic. I found this in the topic of wind gusts, which was part of the course "wind and site conditions" given by Wim Bierbooms. He has developed a method to numerically simulate wind gusts of a desired length and amplitude called *New*Gust. The validity of the mean gust shape has already been proved by several articles, but until now nobody looked at the validity of the load response of a wind turbine resulting from wind gusts simulated according to the *New*Gust method.

Hence, the main topic of my thesis became to investigate the validity of the mean load response resulting from *New*Gust wind speed gusts with respect to measured wind speed gusts. During the process of this thesis it turned out that there are several methods to simulate wind speed gusts. A number of these methods have been compared with respect to the mean shape of the load response and the 50-years extreme value of the load response.

First of all I want to thank my supervisor Wim Bierbooms for his kind guidance during my literature study and following thesis work. Through his coaching I could give this thesis a scientific value. I want to thank Maaike for always being interested in what I do. I also want to name my parents, who enabled me to follow this course by always giving a safe home. I should not forget my brother Jan for his kind review of my English. Above all I have to thank the Lord God, who gave me the strength, knowledge and intellect to do this.

This research would not have been possible without the kind permission of "Database of Wind Characteristics" to download measurements from their internet database located at DTU, Denmark. Internet: "http://www.winddata.com/". Wind field time series from the following sites have been applied: Hornsrev (with acknowledgments to ELSAM Engineering, Denmark), Oak Creek and Toboel (both with acknowledgments to Risø National Laboratories, Denmark).

Kundert de Wit

Abstract

This thesis report has been made in the context of acquiring the Master of Science degree for the master Sustainable Energy Technology at Delft Technical University, faculty of applied sciences. The thesis work has been conducted at the faculty of aerospace engineering, section wind energy.

As wind turbines become larger and larger, optimization of material usage becomes relatively more important. The reason lies in the direct connection of material use with investment costs, which are becoming more important with larger turbines. For this optimization, proper fatigue analysis and assessment of the extreme loads is highly important. For the assessment of extreme loads wind gusts are important. Until now, gusts of a deterministic shape have been used, which is in contrast with the common practise for fatigue analysis. Therefore, Wim Bierbooms developed the *New*Gust method for simulating wind speed gusts of any desired length and amplitude at DUWIND. The validity of the resulting gust shape has already been proved by several articles, but until now nobody looked into the validity of the load response of a wind turbine resulting from wind gusts simulated according to the *New*Gust method.

The main research question of this thesis is:

> *What is the validity of the mean load response resulting from wind speed gusts simulated with the NewGust method with respect to measured gusts?*

In this context, also some different stochastic gust simulation methods have been compared with respect to mean gust and load response shape. During the process, two other topics became of interest:

> *What is the gust shape causing the extreme loads of a pitch-regulated wind turbine?*
>
> *How do different stochastic methods compare to each other with respect to the 50-years' extreme value?*

The first question has been answered by comparing load responses from measured wind speed gusts and wind speed gusts that were simulated with *New*Gust. The *New*Gust method is based upon the assumption of Gaussian distributed turbulence. It has therefore been verified whether gusts extracted from simulated time series with the same non-Gaussian distribution as the measured time series give different load responses when compared to the gusts simulated according to the *New*Gust method. Risø National Laboratories has developed a method to simulate non-Gaussian gusts in the same way as the *New*Gust method. The non-Gaussian gusts simulated with the Risø method have been compared to the gusts simulated with the *New*Gust method.

It appeared that, with respect to the load responses, the *New*Gust gusts are similar to measured gusts for the upper range of wind speeds and amplitudes. The more equal the gust

shapes from different methods are, the more equal are their load responses. The non-Gaussian Risø gusts are almost equal to the Gaussian *New*Gust gusts. The gusts from simulated non-Gaussian turbulence are equal to the gusts from measurements.

The second question has been answered by taking 60 seconds of wind speed data around a maximum in the corresponding load response. By averaging for certain classes of wind speed, and load response amplitude the gust shape causing the extreme loads is obtained for a range of mean wind speeds. If the pitch is active, extreme rise time gusts cause the extreme loads, otherwise the extreme loads are caused by extreme amplitude gusts.

For the third question, extreme values of the load response with a 50-years' return period have been calculated. This has been done for Gaussian theory, measurements and conditional simulations with *New*Gust and *Load*Gust. It appears that conditional simulations give a good indication of the 50-years' extreme value, better than the Gaussian theory. This, however, is only the case if the statistics (skewness and kurtosis) are not too far from the Gaussian values. For Oak Creek a very high 50-years' extreme value is found, due to more frequent large negative gusts, indicated by a large negative skewness.

The most important conclusions are that the resemblance between measured and *New*Gust gusts is particularly good in the extreme cases for which *New*Gust has been designed (high mean wind speed, high relative amplitude). The comparison of *New*Gust and non-Gaussian gusts shows that in these extreme cases there is no need for non-Gaussian simulations of wind speed gusts. However, in the case of lower mean wind speeds, non-Gaussian theory is required.

The extreme loading of a pitch-regulated wind turbine is caused by an extreme rise time gust if the pitch control is active (this in contrast with stall-regulated wind turbines, where maximum amplitude gusts always cause the extreme load response). However, the most extreme loads of a pitch-regulated wind turbine occur in the wind speed range just before the pitch control becomes active. In this wind speed region the extreme load response is caused by gusts with an extreme amplitude.

In order to assess the extreme wind turbine loading which occurs on average ones in 50 years, conditional simulation with *New*- or *Load*Gust can be applied if the turbulence statistics are not too much different from Gaussian statistics. If the deviation from Gaussian statistics becomes too large and, in particular, if many large negative gusts are observed, proper non-Gaussian simulation is required.

The necessary programming for the data analysis and the simulations has been done with use of MATLAB.

Contents

List of Figures

List of Tables

Nomenclature

Roman Symbols

A	Normalized gust amplitude at t_0	-
B	Acceleration of the wind speed at t_0	$\mathrm{m/s^2}$
c	Scale parameter of the Weibull probability distribution	m/s
$E(\cdot)$	Energy spectral density function	$\mathrm{m^2/s}$
e	Mean square error	
$F(\cdot)$	Cumulative distribution function	-
f	Cyclic frequency	$1/s$
$f(\cdot)$	Probability density function	-
G	Parameter in the theoretical spectrum	s
$g(\cdot)$	Transformation function	-
H	Parameter in the theoretical spectrum	s
$\mathrm{He}_n(\cdot)$	n^{th} order Hermite polynomial	-
I	Turbulence intensity	-
I_g	Gust interval	s
k	Shape parameter of the Weibull probability distribution	-
l	Load response	N
$m_{f,n}$	n^{th} order cyclic spectral moment	m^2/s^{n+2}
$m_{\omega,n}$	n^{th} order angular spectral moment	m^2/s^{n+2}
N	Number of maximums in a certain period	-
$P(\cdot)$	Power spectral density function	$\mathrm{m^2/s}$
$R(\cdot)$	Autocorrelation function	$\mathrm{m^2/s^2}$
$r(\cdot)$	Normalized autocorrelation function	-
Re	Reynolds number	-
$S(\cdot)$	Spectral density function	$\mathrm{m^2/s}$
T	Recurrence or total period	

t	Time	s
t_0	Time of the maximum wind speed of a gust	s
t_{end}	Time of the end of detecting a gust	s
t_{start}	Time of the start of detecting a gust	s
$u(t)$	Instantaneous wind speed	m/s
$\bar{u}$	Ten-minute mean wind speed	m/s
$\tilde{u}(t)$	Fluctuating wind speed	m/s
$u_c(t)$	Constrained fluctuating wind speed	m/s
u_{ex}	Extreme wind speed	m/s
$\tilde{u}_n(t)$	Normalized wind speed	-
w	Width of a moving window	s
z	Height	m

Greek Symbols

$\Delta\tilde{u}$	Height of a moving window	m/s
κ	Wavenumber	rad/m
λ	Second order normalized spectral moment	$1/s^2$
μ	Fourth order normalized spectral moment	$1/s^4$
ν_0	Mean zero crossing frequency	1/s
σ	Standard deviation	m/s
τ	Time lag or period between two subsequent temporal points	s
ω	Radial or angular frequency	rad/s

Other Symbols

$\mathcal{K}$	Kurtosis	-
$\mathcal{S}$	Skewness	-
$\mathcal{T}$	integral time scale	s

Acronyms

ABL	Atmospheric Boundary Layer
acf	Autocorrelation function
cdf	Cumulative distribution function
Coh	Coherence function
CSD	Cross Spectral Density

CTRW	Continuous Time Random Walks
ECD	ECG in combination with EDC
ECG	Extreme coherent gust
EDC	Extreme direction gust
EOG	Extreme operating gust
ESD	Energy spectral density
EWS	Extreme wind shear
FFT	Fast Fourier transform
FT	Fourier transform
GEV	Generalized Extreme Value
GL	Germanischer Lloyd
IEC	International Electrotechnical Commission
IFT	Inverse Fourier transform
pdf	Probability density function
POT	Peak over threshold
PSD	Power spectral density

Chapter 1

Introduction

This document is the final report of the master thesis project "validation of *New*Gust". This thesis was conducted in the context of the master Sustainable Energy Technology at Delft Technical University, faculty of aerospace engineering, section wind energy.

As wind turbines are getting persistently larger, optimization of the wind turbine with respect to strength and material usage is getting more and more important. The relative increase in importance of the optimization of material usage lies in its direct connection with investment costs. The mass and costs of a turbine rotor scales with (blade length)$^{2.6}$, while the energy yield scales with (blade length)$^{2.2}$. This shows that at a certain point, costs will exceed revenues. Hence, optimization is becoming more important with larger turbines, in order to outsmart the current scaling laws. For this optimization, proper fatigue analysis and assessment of the extreme loads is highly important. Fatigue analysis has been done in a stochastic way for a long time. This basically means that for load calculations a stochastic representation of a turbulent wind field is generated, which is used as the input for a simulation program of the wind turbine. For the assessment of extreme loads wind gusts are important. Until now, gusts of a deterministic shape have been used, which is in contrast with the common practice for fatigue analysis.

In this context the *New*Gust method has been developed by Wim Bierbooms at DUWIND. *New*Gust is a method for simulating wind speed gusts of any desired length and amplitude. The validity of the resulting gust shape has already been proved by several articles, but until now nobody looked at the validity of the load response resulting from wind gusts simulated according to the *New*Gust method.

The main research question of this thesis is:

> *What is the validity of the mean load response resulting from wind speed gusts simulated with the NewGust method with respect to measured gusts?*

Within this context, also some different stochastic gust simulation methods have been compared with respect to mean gust and load response shape. During the process, two other question arose:

> *What is the gust shape causing the extreme loads of a pitch-regulated wind turbine?*

> *How do different stochastic methods compare to each other with respect to the 50-years' extreme value?*

This report is basically divided into three parts: In part I the theoretical context of wind speed gusts is described. In part II the practise of validating *New*Gust and the extreme value analysis is described. Part III contains the appendices. Each part contains a number of chapters belonging to the topic of that part; in chapter 2 a description is given of atmospheric wind. In chapter 3 and 4 atmospheric turbulence and wind gusts are treated in more detail. In chapter 5 the procedure for validating the *New*Gust expression is outlined. In chapter 6 and 7 the practise of analyzing numerical wind speed data and the simulation of numerical wind speed gusts is described. In chapter 8 the method used to simulate the load response is given. In chapter 9 the results obtained from the data analysis are described. In chapter 10 some questions about extremes are addressed and a comparison is made between several methods for the analysis of extreme values. Finally, the last chapter contains the conclusions and recommendations. Additional information and results can be found in the appendices.

This report is written for the examination committee, to be able to give credit to this thesis work. It also is written to provide other students who want to continue on this research with a thorough overview of what has already been done. Finally, other people from the SET master and wind energy department might also be interested in the topic of wind speed gusts.

Part I

Theoretical background of wind speed gusts

Chapter 2

Atmospheric wind

In this chapter a description is given of the physical context of the phenomenon of wind gusts. To do this, an explanation is given of (1) the atmospheric boundary layer of the earth, (2) how the wind resource is structured according to temporal and spatial scales, (3) the seasonal variations of wind velocity and (4) extreme wind speeds and extreme loads. Turbulence and wind gusts are treated as separate topics and described in chapter 3 and 4.

2.1 The atmospheric boundary layer

The part of the universe of interest with respect to wind turbines is the earth atmosphere. The earth atmosphere consists of four characteristic thermally-defined layers; (1) the troposphere ($0 \leq z \leq 11$ km), (2) the stratosphere ($11 \leq z \leq 47$ km), (3) the mesosphere ($47 \leq z \leq 85$ km) and (4) the thermosphere ($z \geq 85$ km) (cf. figure 2.1). The troposphere is of importance for

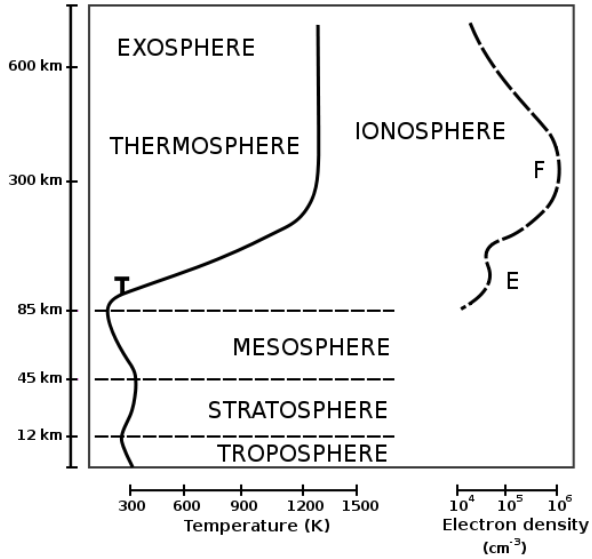

Figure 2.1: Graphical representation of the earth atmosphere. The heights (z) of the layers are indicative and vary with solar activity. The iono- and exosphere are part of the thermosphere [taken from Wikipedia, 2009c]

wind energy conversion. Within this layer the atmospheric boundary layer (ABL) exists up to ∼4 km. This layer experiences a daily cycle in temperature, humidity and wind variations caused by the daily cycle of heating and cooling due to the sun. The bottom 5 to ∼10% of the ABL is called the surface layer, where today still most of the wind energy conversion takes place. For this part of the ABL, semi-empirical profiles have been found for the wind speed variation with height z (cf. figure 2.2).

$$u(z) = \frac{u_*}{\kappa} \ln\left(\frac{z}{z_0}\right) \qquad \text{(neutral surface layer)} \tag{2.1}$$

$$u(z) = \frac{u_*}{\kappa} \left[\ln\left(\frac{z}{z_0}\right) + 6\frac{z}{L}\right] \qquad \text{(stable surface layer)} \tag{2.2}$$

Where z_0 is the aerodynamic roughness length, which quantifies the surface roughness. A table with the Davenport-Wieringa roughness length classification can be found in appendix B. κ is the von Karman constant which equals ≈ 0.4, u_* is the friction velocity and L the Obukhov length:

$$u_* = \frac{\kappa u_r}{\ln\left(z_r/z_0\right)} \tag{2.3}$$

$$L = \frac{-u_*^3}{\kappa\left(g/T_v\right) F_{Hsfc}} \tag{2.4}$$

Where u_r is the wind speed at reference height z_r. $r = 10$ m for the standard anemometer height for measuring 'surface winds'. g is the gravitational acceleration, T_v is the absolute virtual temperature and F_{Hsfc} is the kinematic surface heat flux[1]. The variation of wind speed with height (also called 'wind shear') is caused by surface drag, thermal effects and turbulence. The Reynolds number (Re) of the flow in the ABL is in the order of $10^7 - 10^8$, which shows that turbulence is a characteristic feature of atmospheric wind.

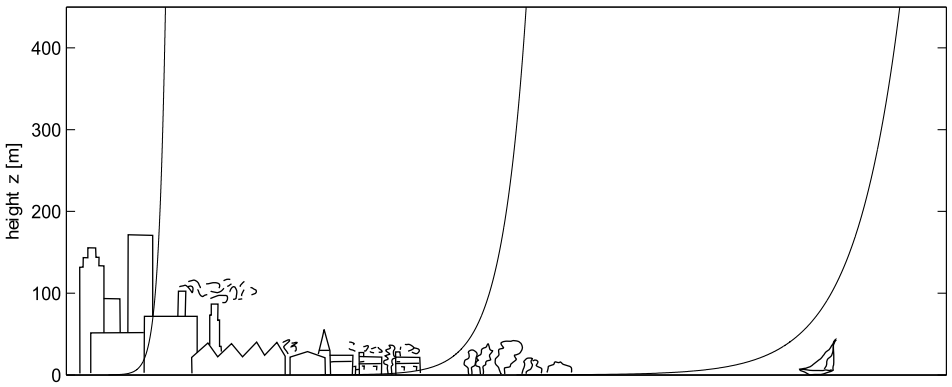

Figure 2.2: Example of the variation of mean wind speed with height in the atmospheric boundary layer. The plot shows the variation of mean wind speed versus height over different terrain types (roughness lengths).

[1]The notation in this section has been adapted from Stull [2000].

2.2 Structure of the wind resource

The power available in wind is the resource for a wind turbine[2]. The positive side of this resource is that it is for free, the negative side is its fluctuating behavior. The fluctuations in the power available in wind are characterized by the wind speed.

$$P_{wind} = \frac{1}{2}\rho\bar{u}^3 A_r \tag{2.5}$$

Where ρ is the air density, $\bar{u}$ the mean wind speed and A_r the rotor area of the wind turbine.

The wind speed varies on many different scales both in space and time. In figure 2.3 the range of space and time scales of atmospheric motion is given. Large scale temporal variations

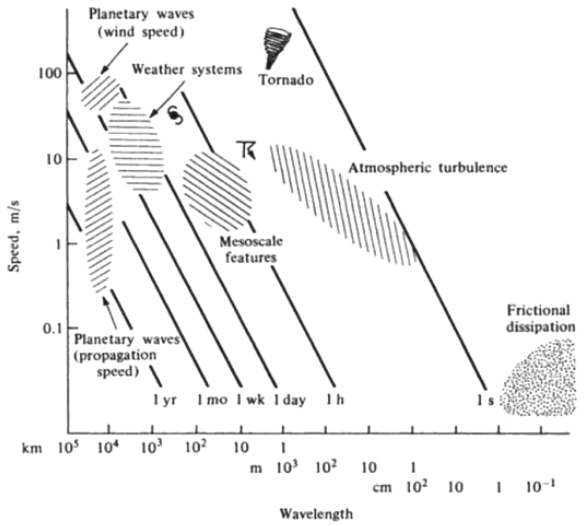

Figure 2.3: Range of temporal and spatial scales in atmospheric motion (taken from Dutton [1976]).

correspond to wind speed variations from year to year or even from decade to decade at a certain location. These variations can be connected to global climate fluctuations or other global phenomena, such as large volcanic eruptions or sunspot activity. Long term variations are important for the prediction of the economic viability of a wind farm. However, they are not understood well, which makes an accurate prediction difficult. Within the time-scale of a year there are seasonal variations, which can be predicted much better. Variations related to a time scale of a couple of days and a single day are respectively called synoptic and diurnal variations. These variations are more random and therefore less predictable. Synoptic variations are related to large scale spatial variations like high and low pressure areas. Diurnal variations are caused by, for example, heating of the earth surface in daytime and cooling at night. Fluctuations on a time scale of less than ten minutes are called turbulence. It is useful to think about turbulence as the fluctuation of the wind speed around the mean wind speed. This mean wind speed is determined by the larger scale variations described above, averaged over a period of ten minutes. The distinction between the mean flow and its

[2]Not all the power available in wind can be extracted by the wind turbine. The ratio between the power available and the power which can be extracted from wind is called the 'power coefficient' C_p. The power coefficient has a maximum of $16/27 \approx 0.593$, which is known as the Betz limit.

fluctuations is justified by the existence of a spectral gap between 10 minutes and 2 hours (cf. figure 2.4). To understand this graph, imagine that the energy at a certain frequency is linked to some physical phenomenon with the same frequency. It thus gives a view of the scales of the physical phenomena behind the wind speed variations. Note however that the empirical evidence for and therefore the existence of this spectral or meso-scale gap is strongly criticized[3] (see e.g. Schertzer and Lovejoy [2004] and references therein).

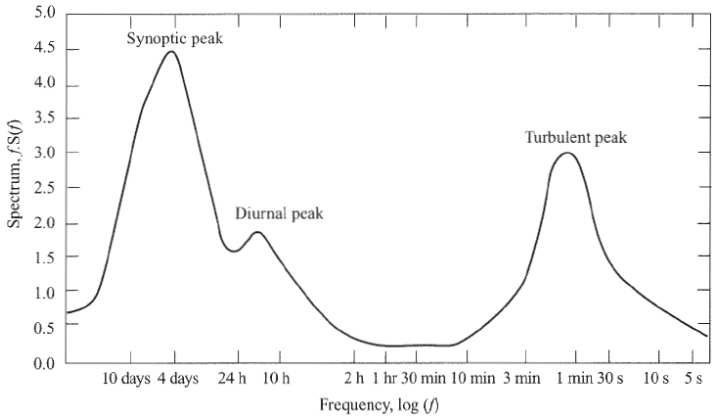

Figure 2.4: Wind spectrum based on work by van der Hoven. taken from Burton et al. [2008].

Within turbulence, large fluctuations of the wind speed with respect to the mean can occur on a small time scale. The typical time scale of these large fluctuations is in the range of couple of seconds up to approximately one minute. This phenomenon is called wind gust.

2.3 Seasonal variations

Wind speed variations within a year can be described well for many typical sites by a Weibull cumulative probability distribution (cdf). This distribution gives the variations of the mean wind speed over a year. Usually, hourly or ten-minute mean wind speeds are described. The equation describing the Weibull cdf is

$$F(u) = 1 - e^{-\left(\frac{\bar{u}_{hr}}{c}\right)^k} \tag{2.6}$$

Where $\bar{u}_{hr}$ is the hourly mean wind speed and $F(u)$ the fraction of time in which $\bar{u}_{hr}$ is not exceeded. The distribution is characterized by respectively a shape parameter k, which describes the variability around the mean, and a scale parameter c. For Northern Europe, $k \approx 2$. c is obtained from the annual mean wind speed $\bar{u}_{yr}$ and the complete gamma function:

$$c = \frac{\bar{u}_{yr}}{\Gamma\left(1 + \frac{1}{k}\right)} \tag{2.7}$$

A typical plot of $f(u)$ and $F(u)$ for the Netherlands is given in figure 2.5. The values for the

[3]The main criticism about the graph in figure 2.4 is that it is based upon four different measurements with different sampling frequencies and different atmospheric conditions. In Schertzer and Lovejoy [2004] it is mentioned that due to the intermittent nature of atmospheric turbulence, such an atmospheric flow is only turbulent in tiny fractions of space and time. The use of a limited temporal or spatial frame to characterize turbulence is thus justified. In wind energy research usually a time fraction of ten-minutes is taken, which is followed in this thesis as well.

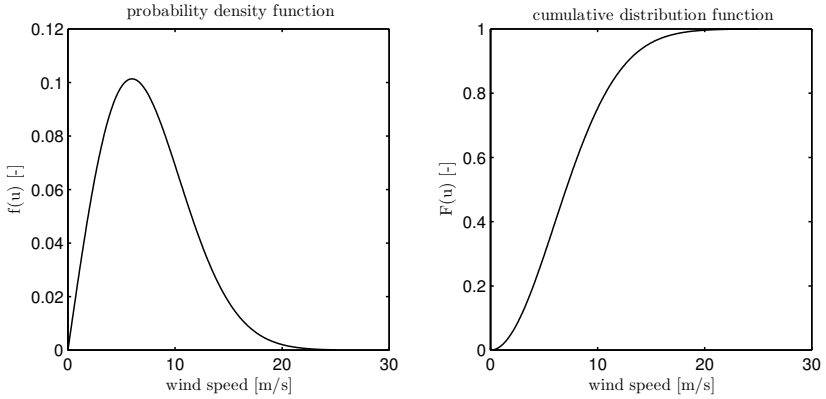

Figure 2.5: Typical wind velocity probability density and distribution function for The Netherlands ($k = 2$, $\bar{u} = 7.5$ m/s).

parameters k and c are obtained by fitting the Weibull distribution to the distribution of the measured data of a particular site. The measurement time span should be long enough to get a good Weibull distribution for a certain location.

2.4 Extremes

The former description of wind speed distributions cannot be used for a reliable estimation of the probability of extreme wind speeds. Almost all of the data used to fit the distribution will correspond to lower wind speeds, and thus the tails of the distribution does not represent the real situation well. For a good estimation of the extreme wind speeds corresponding to a certain recurrence period, the tail of the cdf is important. In the wind turbine design standards GL and IEC 61400-1, the wind speed with a recurrence period of 50 years is used for extreme load calculations. For a good estimation of the tail of the distribution, a record of ∼500 years is needed for a 50-years' return period. Such long data records of hourly or ten-minute mean wind speeds would be in the order of respectively 10^8 and 10^9 data points and are not available. Therefore, extreme value analysis has to be used to get a good estimate of the distribution tail from a shorter record.

An easy method to obtain the extreme cumulative distribution is to use a known cdf of, let's say hourly, mean wind speed (e.g. the Weibull distribution). The probability of $u_{ex} < u$ for a return period of one hour is $F(u)$. The probability of an extreme value for a return period of T hours is $F^T(u)$. In figure 2.6 an example is given. The standard method to obtain the extreme cdf, is to consider a long time record of mean wind speeds (e.g. ten-minute averages for a time period of six months). From this record, extreme values above a certain threshold are selected. The threshold should be large enough to get independent extreme values. From this data a cumulative probability distribution $F(u)$ can be determined. To obtain from this cdf the cdf of e.g. annual maxima, $F(u)$ has to be scaled with $F_{yr}(u) = F^N(u)$. Where N is the number of extremes for a year, observed in the data, from where the cdf $F(u)$ is obtained. From the resulting cdf, the extreme wind speed u_{ex} corresponding to a return period T can be obtained.

$$T = \frac{1}{1 - F} \tag{2.8}$$

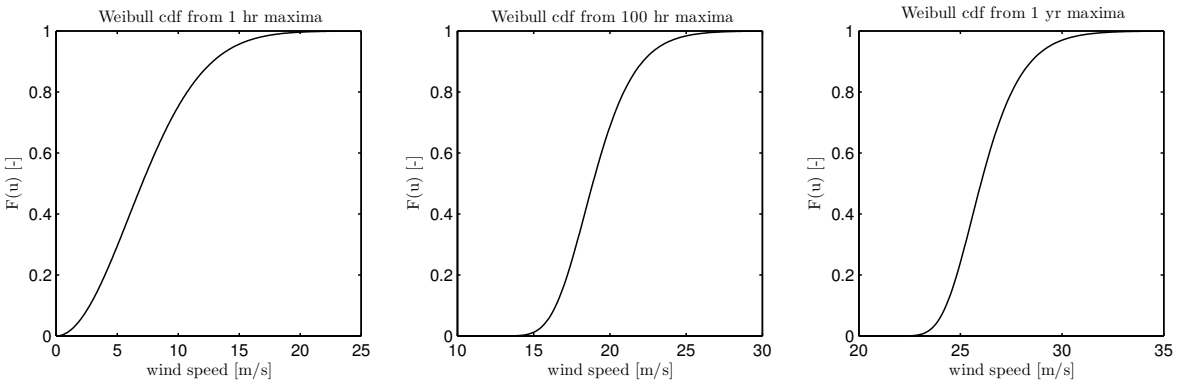

Figure 2.6: Example of an extreme value distribution based on the Weibull cdf, for 1 hr ($F(u)$), 100 hr ($F^{100}(u)$) and 1 yr ($F^{8760}(u)$) maximums. The probability and extreme values for $T = 50$ year are respectively $F = 0.9999977, u_{ex.} = 30.5$ m/s, $F = 0.99977, u_{ex.} = 30.5$ m/s, $F = 0.98, u_{ex.} = 30.5$ m/s (k=2, $\bar{u}$=7.5 m/s).

For a return period of $T = 50$ year, the wind speed corresponding to $F = 0.98$ should be used, if the cdf is based on 1-yr extremes.

2.4.1 50-years' extreme load response

Extreme value analysis can also be used to determine the extreme load response resulting from wind speeds. The loads can for example be calculated for a number of time series of ten minutes length. The maximum load response in each time series can be used to derive a distribution function of the ten-minute maximum loads. Because each time series has a certain mean wind speed $\bar{u}$, a conditional distribution $F(l_{max}|\bar{u})$ is obtained for a number of mean wind speeds. To derive from this conditional distribution the cdf of ten-minute maxima for all wind speeds $F(l_{max})$, the following relations are used:

$$f(l_{max}|\bar{u}) = \frac{f(l_{max}, \bar{u})}{f(\bar{u})} = \frac{dF(l_{max}|\bar{u})}{dl_{max}} \tag{2.9}$$

$$f(l_{max}) = \int_{-\infty}^{\infty} f(l_{max}, \bar{u})\, d\bar{u} \tag{2.10}$$

$$F(l_{max}) = \int_{-\infty}^{l_{max}} f(l_{max})\, dl_{max} \tag{2.11}$$

By Combining these equations, the distribution of extreme loads can be derived:

$$F(l_{max}) = \int_{-\infty}^{l_{max}} \int_{-\infty}^{\infty} f(l_{max}, \bar{u})\, d\bar{u}\, dl_{max} \tag{2.12}$$

$$F(l_{max}) = \int_{-\infty}^{l_{max}} \int_{-\infty}^{\infty} f(l_{max}|\bar{u}) f(\bar{u})\, d\bar{u}\, dl_{max} \tag{2.13}$$

$$F(l_{max}) = \int_{-\infty}^{\infty} F(l_{max}|\bar{u}) f(\bar{u})\, d\bar{u} \tag{2.14}$$

The probability for the 50-years extreme load F_{50} can be derived as explained above, where for T the number of ten-minutes in 50 year should be taken. This theory has been applied in section 10.1.3.

Gaussian reference value

With respect to the extreme loads of a wind turbine, the response level with a return period of 50 years is of primary interest. It determines the failure rate together with the statistics of the structure strength. For a Gaussian random variable a theoretical expression exists for the mean level up-crossing frequency of level l_n [Bierbooms, 2008].

$$\nu_n = \frac{1}{T_n} = \nu_0 e^{\frac{l_n^2}{2\sigma^2}} \tag{2.15}$$

Where T_n is the number of seconds in n year, $\nu_0 = \sqrt{\frac{m_{f,2}}{\sigma^2}}$ is the mean zero crossing frequency, with $m_{f,2}$ the second order spectral moment (cf. section 3.2.3) and σ the standard deviation of the load response. The n-years' response level can be derived from this expression.

$$l_n = \sigma\sqrt{2\ln\left(\nu_0 T_n\right)} \tag{2.16}$$

In the latter part of this thesis, this equation will be denoted as the 'Rice equation'.

A function describing the probability of local maxima in a Gaussian random process is the Rice probability density function of local maxima;

$$f(\eta) = \eta\sqrt{1-\varphi^2}e^{-\frac{\eta^2}{2}}\,\Phi\left(\frac{\eta\sqrt{1-\varphi^2}}{\varphi}\right) + \frac{1}{\sqrt{2\pi}}\varphi e^{-\frac{\eta^2}{2\varphi^2}} \tag{2.17}$$

Where $\eta = C/\sqrt{m_{f,0}}$ is the dimensionless level of the local maxima, with $m_{f,0}$ the zeroth order spectral moment (variance) of the load response and C the amplitude of the local maximum. $\varphi = \sqrt{1 - \frac{m_{f,2}^2}{m_{f,0}m_{f,4}}}$ is the bandwidth parameter, with $m_{f,2}$ and $m_{f,4}$ the second and fourth order spectral moment of the load response (cf. section 3.2.3). Φ indicates the standard Gaussian distribution function[4]. In the latter part of this thesis, this function will be denoted as the 'Rice pdf'.

This theory gives the possibility to compare the obtained extreme values with a theoretical value for the 50-years' response. Note that for the above equations the number of seconds in 50 year should be taken for T_{50}.

[4]The standard Gaussian distribution function can be written as $\Phi\left(\frac{x-\bar{x}}{\sigma_x}\right) = \frac{1}{\sigma_x\sqrt{2\pi}}\int_{-\infty}^{x}\exp\left(\frac{-(t-\bar{x})^2}{2\sigma_x^2}\right)dt$. For a standard Gaussian random variable, $\bar{x} = 0$ and $\sigma_x = 1$.

Chapter 3

Turbulence description

The atmosphere is a very complex system, as briefly shown in chapter 2. What shows the complexity even more is the fact that it has more than 10^{30} degrees of freedom. It is impossible to compute the temporal evolution or to make enough measurements to get the right initial conditions of such a complex system. The only possibility to describe it is by statistical physics [Hense and Friederichs, 2006]. One of the many interesting parts of the atmosphere is its turbulence. Because turbulent flow is not deterministic, it has to be treated as a random or stochastic process. This chapter, therefore, deals with the statistical description of turbulence. Only the features of turbulence relevant for this research are explained. These include: (1) the statistical definition of turbulence as it is used in the context of this research, (2) the statistical description of turbulence with spectra, autocorrelation functions and the probability distribution of turbulence. The last section (3) of this chapter deals with numeric simulation of turbulence.

3.1 Statistical definition

Turbulence, as it is used in the context of this research, is defined as the fluctuations of the instantaneous wind speed around its ten-minute average (cf. section 2.2). The decomposition of the instantaneous wind speed $u(t)$ into its ten-minute mean $\bar{u}$ and fluctuation $\tilde{u}(t)$ is very useful, because the turbulent part of the wind speed can now be separated from the instantaneous wind speed, $\tilde{u}(t) = u(t) - \bar{u}$. The mean of $\tilde{u}(t)$ is zero by definition, because $\langle \tilde{u}(t) \rangle = \langle u(t) - \bar{u} \rangle = \bar{u} - \bar{u} = 0$. The variance of $\tilde{u}(t)$, $\left\langle \tilde{u}(t)^2 \right\rangle$ is a measure of the turbulence kinetic energy. $\langle \cdot \rangle$ denotes the ensemble averaging operator.

Turbulence in the atmospheric boundary layer consists of many scales, ranging from scales as large as the boundary layer thickness, to the Kolmogorov scales where the turbulent kinetic energy dissipates into heat by viscous forces (cf. figure 2.3). In the context of wind being the resource for wind turbines, the medium scale (inertial range, cf. figure 3.1) turbulence is important. This part of the turbulence can assumed to be isotropic[1]. In section 2.2 the use of a limited temporal or spatial frame to characterize turbulence is justified. The averaging time span has to be small compared to the changing frequency of the average properties. The spectral gap in the energy spectrum of atmospheric wind speed (cf. figure 2.4) allows to assume a stationary wind speed on a time scale of ten minutes up to two hours. In this framework, ten minutes is the shortest time allowed for averaging, which is thus defined as

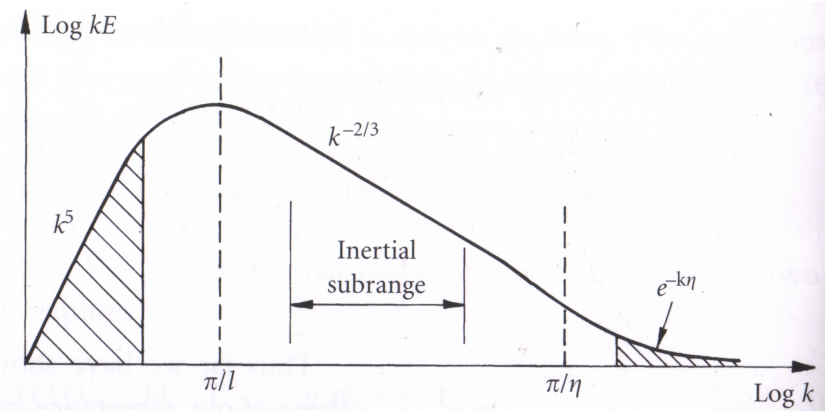

Figure 3.1: Theoretical spectrum of physical isotropic turbulence. Taken from Davidson [2007].

the time span to characterize turbulence.

A common measure of the level of turbulence is the turbulence intensity I,

$$I = \frac{\sigma_u}{\bar{u}} \tag{3.1}$$

Where σ_u is the standard deviation of $u(t)$. I can be calculated for each velocity component (longitudinal u, lateral v, transversal w). For the longitudinal component, σ is almost constant with height. This implicates a decrease of I with respect to height, because the mean wind speed increases with height. Different models for all components of turbulence intensity as a function of height and mean wind speed are given in standards of wind turbine design (e.g. Germanischer Lloyd, IEC and Danish standards). This method of describing turbulence is not distinctive, because the same level of intensity can be obtained for many different mean and standard deviation of the wind speed. A given turbulence intensity hence does not contain any information about the fluctuations itself and is therefore not useful for gaining insight in wind gusts.

An important hypothesis about small-scale turbulence is the Taylor hypothesis of frozen turbulence. Although it seems that wind speed is measured as variations in time, in reality variations are not measured in time but in space. Taylor's frozen turbulence hypothesis says that fluctuations in wind speed are felt by a fixed observer, because eddies (imagine blobs of vorticity) are convected by the mean flow. These eddies are fixed or frozen into the mean flow, i.e. they do not change considerably as they are convected (cf. figure 3.2). This hypothesis holds well for turbulence with lower intensity (high mean wind speed, moderate wind shear), because then the variations in time due to passage are much smaller than the variations in space (small turbulence intensity indicates that the passing time of an eddy is small compared to its life time). To satisfy this requirement, $\sigma_u < \frac{1}{2}\bar{u}$ [Stull, 1988]. In mathematical form, the transformation from time to space and from frequency (f (cyclic) or ω (angular)) to

[1]Isotropy is uniformity in all directions, which for turbulence means measuring the same values of properties like velocity and dissipation along axes in all directions. Homogeneous is independence of physical properties on (absolute) position

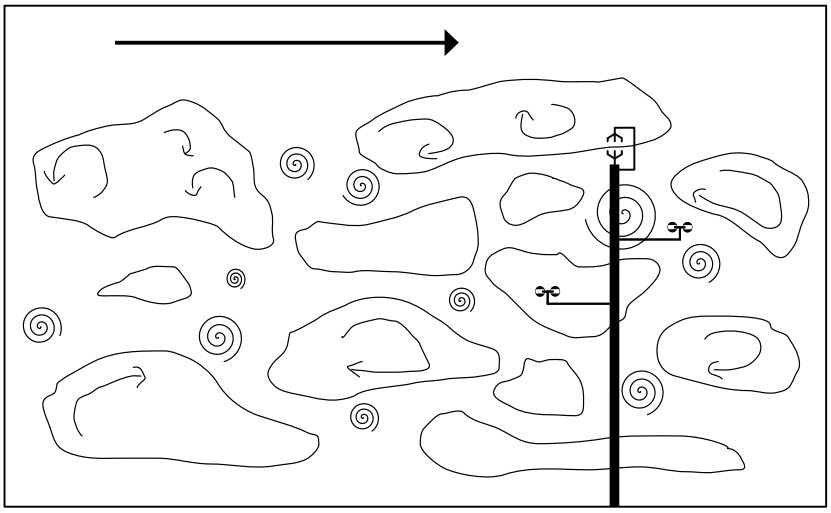

Figure 3.2: Example of (artificial) blobs of vorticity convected in the mean flow.

wave-number (κ) is defined as

$$u(x, y, z, t) = u(x - \bar{u}t, y, z, 0) \tag{3.2}$$

$$\kappa = \frac{2\pi f}{\bar{u}} = \frac{\omega}{\bar{u}} \tag{3.3}$$

Where x is the coordinate in the mean flow direction, $u(t)$. Officially $\bar{u}$ should be the total magnitude s of the horizontal wind speed, $s = \sqrt{\bar{u}^2 + \bar{v}^2}$ [Stull, 1988]. Since often only the longitudinal wind speed is known, it is assumed that $s \cong \bar{u}$. For ultimate gusts, the Taylor hypothesis is assumed valid, because they are closely related to high mean wind speeds [Larsen et al., 2003].

3.2 Statistical description

For numerically simulating turbulence (c.f. section 3.3), it is necessary to have a statistical description of turbulence, both in time and frequency domain. The common way to do this is by means of a spectral density function for the frequency domain and an autocorrelation function for the time domain.

3.2.1 Spectral density

The spectral density (spectrum) is used in statistical signal processing and physics to describe the frequency content of a stochastic process. Two routes are possible to derive the spectral density of a stochastic process; (1) via the power spectrum and (2) via the energy spectrum. Both methods are used in the context of this research and are described below. The practice of estimating a spectrum from discrete time series of turbulent wind speed is described in section 6.5.

Energy spectral density

The energy spectral density (ESD) describes how the energy (variance) of a signal or time series is distributed over the frequencies it contains. The following definition of ESD requires that the Fourier transform of the signal exists, which means that the signal should be a well-behaved continuous function[2]. This requirement ensures that the signal $\tilde{u}(t)$ is of finite energy. The ESD is then defined as

$$E_{\tilde{u}}(f) = \left| \int_{-\infty}^{\infty} \tilde{u}(t) e^{-i2\pi f t} dt \right|^2 = F(f)F^*(f) \tag{3.4}$$

$$\sigma_{\tilde{u}}^2 = \int_{-\infty}^{\infty} E_{\tilde{u}}(f) df \tag{3.5}$$

Where f is the cycle frequency, $F(f)$ the Fourier transform of $\tilde{u}(t)$ and $F^*(f)$ its complex conjugate. In the case of discrete time series, with a finite number of points, the sequence can be treated as periodic, using a discrete Fourier transform to make a discrete spectrum. This is further explained in section 6.5.

Power spectral density

The power spectral density (PSD) describes how the power of a signal or time series is distributed with frequency. Power can be the actual physical power, or for convenience with abstract signals, the squared value of the signal, $\tilde{u}^2(t)$. Because the instantaneous power has a nonzero average root, its Fourier transform doesn't exist. Therefore, the PSD is defined as the Fourier transform of the autocorrelation function $R(\tau)$ of the signal (Wiener - Khinchin theorem). This is only possible if the signal is a wide-sense stationary process[3]. If the signal is not wide-sense stationary, then the autocorrelation function cannot be a function of only one variable, so no PSD exists. The PSD is then defined as

$$P_{\tilde{u}}(f) = \int_{-\infty}^{\infty} R_{\tilde{u}}(\tau) e^{-i2\pi f \tau} d\tau \tag{3.6}$$

$$\sigma_{\tilde{u}}^2 = \int_{-\infty}^{\infty} P_{\tilde{u}}(f) df \tag{3.7}$$

The power spectral density and energy spectral density equal each other in the case of $\tilde{u}(t)$ being a real function[4]. This gives the opportunity to derive the autocorrelation function (acf) from the spectral density (cf. section 3.2.2). In the latter part of this report, the spectral density will be denoted by S.

Theoretical models of atmospheric spectra

For atmospheric turbulence, the spectrum of turbulence must[5], according to Kolmogorov's five-thirds law ($S_{\tilde{u}}(f) = \alpha_{\tilde{u}} \varepsilon^{2/3} f^{-5/3}$), approach an asymptotic limit proportional to $f^{-5/3}$

[2] In fact the signal (function of a variable) must be square-integrable (or square-summable) over an interval. This requires that the integral of the square of its absolute value over that interval, is finite, $\int_a^b |\tilde{u}(t)|^2 \, dt \neq \infty$. Function and variable can be both real- or complex-valued.

[3] Wide sense stationary means a stochastic process with constant mean; strict sense stationary requires also all other statistical properties to be invariant with time.

[4] In the case of $\tilde{u}(t)$ being a real function, $R_{\tilde{u}}(f) = F(f)F^*(f)$ [see e.g. Beers, 2007, p. 450], then $R_{\tilde{u}}(\tau) = IFT(R_{\tilde{u}}(f))$. This makes that $P_{\tilde{u}}(f) = F(f)F^*(f) = E_{\tilde{u}}(f)$.

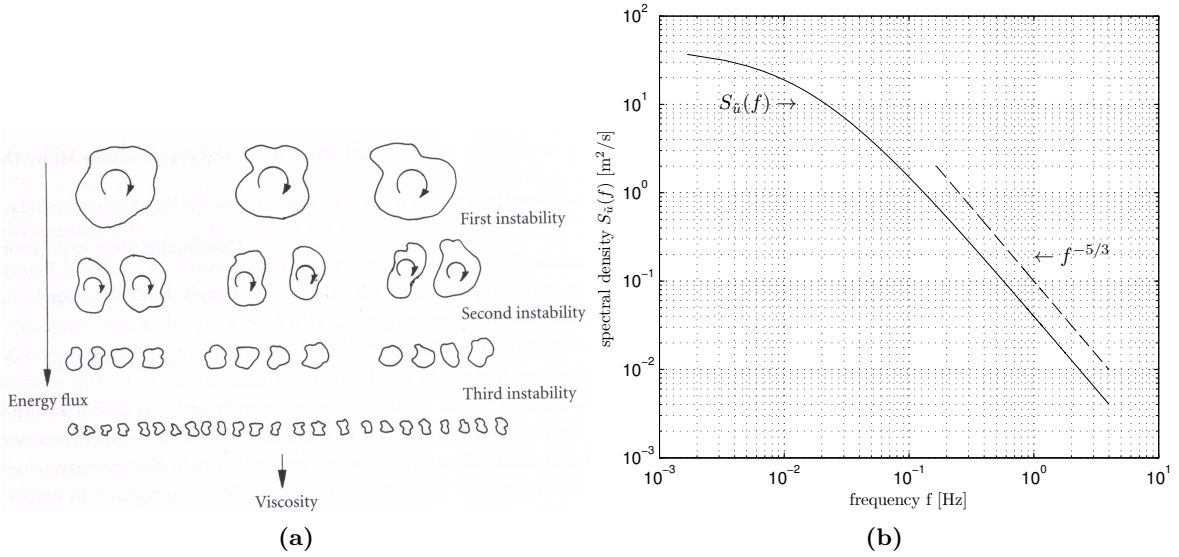

(a) **(b)**

Figure 3.3: (a) Graphical representation of the energy cascading (taken from Davidson [2007]) and (b) an example of the five-third law

at the inertial subrange ($f > 1$) (cf. figure 3.3b). Here ε is the dissipation rate of turbulent kinetic energy and $\alpha_{\tilde{u}}$ is a universal constant [Tieleman, 1995]. This relationship is based upon the energy decay of turbulent eddies from low to high frequencies called 'energy cascade' (cf. figure 3.3a) and is universal for the inertial frequency (or wavenumber) subrange. For low frequencies, the definition of the spectral density function in eq. (3.6) requires[6] that $\lim_{f\to 0} S_{\tilde{u}}(f)$ is proportional to 1. A theoretical representation of the spectrum must hence exhibit these two asymptotes with a maximum in between. A simple and common interpolation expression is

$$\frac{fS_{\tilde{u}}(f)}{\sigma_{\tilde{u}}^2} = \frac{Gf^{\gamma}}{(1+Hf^{\alpha})^{\beta}} \tag{3.8}$$

Where in the case of neutral thermal conditions, $\alpha = 1$, $\beta = 5/3$ and $\gamma = 1$ for the longitudinal velocity component [Tieleman, 1995; Olesen et al., 1984]. A plot of the left hand side of eq. 3.8 on a double logarithmic scale has a low-frequency slope of γ and a high-frequency slope[7] of $\gamma - \alpha\beta$. G and H depend on atmospheric conditions [Olesen et al., 1984]. In this article several criteria for the construction of models describing atmospheric spectra are given. Eq. (3.8) is valid in the frequency range representing turbulent motion and gives a smooth curve with only one maximum. In the case of complex terrain, the factor one in the denominator of the right hand side of eq. (3.8) can be replaced by a variable $I \leq 1$ [Tieleman, 1995]. Two commonly used theoretical expressions of the spectrum for the longitudinal turbulence

[5] Kolmogorov's five-thirds law is derived from the Navier-Stokes equation, assuming an infinite Reynolds number [Laubrich, 2009, Ch. 4.5], which is indeed approached by atmospheric flows due to large length scales [Kundu and Cohen, 2004]

[6] $S_{\tilde{u}}(f) = \int_{-\infty}^{\infty} R_{\tilde{u}}(\tau) e^{-i2\pi f\tau} d\tau$ and $\mathcal{T} = \int_0^{\infty} r(\tau) d\tau$. In the limiting case $f \to 0$ and a one-sided spectrum, $S_{\tilde{u}}(0) = \int_0^{\infty} R_{\tilde{u}}(\tau) d\tau$, $\frac{S_{\tilde{u}}(0)}{\sigma_{\tilde{u}}^2} = \int_0^{\infty} r_{\tilde{u}}(\tau) d\tau = \mathcal{T} = 4L_{\tilde{u}}/\bar{u}$ (cf. also Kundu and Cohen [2004, Ch. 13]).

[7] In the case of eq. (3.8) this gives a high-frequency slope of -2/3, which seems to be in contradiction with Kolmogorov's five-thirds law. The reason lies in the scaling of the spectrum with the frequency (left hand side of eq. 3.8), which causes γ to be one. If the frequency scaling of the spectrum is leaved out, γ would be zero

component are the Kaimal and the von Karman spectrum. The Kaimal description applies better for atmospheric turbulence, while the von Karman spectrum applies well for turbulence in wind tunnels [Burton et al., 2008]. The Kaimal spectrum is specified in the IEC61400-1 standard as

$$S_{\tilde{u}}(f) = \sigma_{\tilde{u}}^2 \frac{4L_{\tilde{u}}/\bar{u}}{(1 + 6fL_{\tilde{u}}/\bar{u})^{5/3}} \tag{3.9}$$

Where $L_{\tilde{u}}$ is the integral length scale for $\tilde{u}$ and $S_{\tilde{u}}(f)$ is the spectral density function for $\tilde{u}$. An example of this spectrum is given in figure 3.3b. Appropriate values for $\sigma_{\tilde{u}}$ and $L_{\tilde{u}}$ are specified in wind turbine design standards. Note that many different spectra are possible for one and the same probability density function, because there are many possibilities to distribute the same variance over the frequencies in a stochastic process. Spectra of physical stationary stochastic processes exist only for the positive frequencies (called one-sided spectra). For computational reasons it can, however, be convenient to have double-sided spectra (also defined for negative frequencies). In such a case, the spectral values should be equally divided over the positive and negative frequencies (cf. figure 6.4). In appendix B some other theoretical spectra descriptions can be found.

3.2.2 Autocorrelation function

As the spectral density is used to describe the frequency domain properties of turbulence, the autocorrelation function is used to represent the time domain properties of turbulence. It measures the persistence of a wave within a time series. The spectral density and autocorrelation function form a Fourier transform pair; from the definition given above it follows that

$$R_{\tilde{u}}(\tau) = \int_{-\infty}^{\infty} S_{\tilde{u}}(f) e^{i2\pi f\tau} df \tag{3.10}$$

$$R_{\tilde{u}}(\tau) = \langle \tilde{u}(t)\tilde{u}(t+\tau) \rangle \tag{3.11}$$

$$r_{\tilde{u}}(\tau) = \frac{R_{\tilde{u}}(\tau)}{\sigma_{\tilde{u}}^2} \tag{3.12}$$

Where $r_{\tilde{u}}(\tau)$ is the normalized autocorrelation function of $\tilde{u}(t)$. If $\tau = 0$, $R(0) = \sigma_{\tilde{u}}^2 = \langle \tilde{u}^2 \rangle$, is the average power of $\tilde{u}(t)$. For a stationary process R is a symmetric function and its average power is independent on time. If R is small, this indicates a weak correlation. If R is large and positive, it indicates a strong correlation. If R is large and negative, it indicates a strong inverse correlation. In the limiting cases $\tau \to \infty$ and $\tau \to 0$, $r(\tau)$ becomes respectively 0 (totally uncorrelated) and 1 (perfectly correlated). For large time lag τ, the autocorrelation of turbulence goes to zero, which thus indicates a random process with no regularly-recurring structures. The area under $r(\tau)$ is called the integral time scale $\mathcal{T}$;

$$\mathcal{T} = \int_0^{\infty} r(\tau) d\tau \tag{3.13}$$

The integral time scale is a measure of the memory of the process and indicates the time over which the turbulence highly correlates with itself. Note that the integral time scale as it

and the high frequency slope indeed is -5/3 (cf. e.g. eq. 3.9). The low frequency slope then goes towards zero and is thus proportional to one (on a double logarithmic plot). This type of scaling is also the reason why in literature both values for the high frequency slope can be found.

is defined here, equals in the limiting case $f \to 0$, the factor $4L_{\tilde{u}}/\bar{u}$ in the Kaimal spectrum description given above (eq. 3.9, cf. footnote 6). The derivatives of the autocorrelation function can be very easily derived via the inverse Fourier transform of the spectrum.

$$\frac{d^n}{d\tau^n}R(\tau) = \int_{-\infty}^{\infty} (i2\pi f)^n \, S_{\tilde{u}}(f) e^{i2\pi f\tau} df \tag{3.14}$$

3.2.3 Spectral moments

Spectral moments are defined in order to characterize the spectrum. Unfortunately, two definitions of the spectral moments exist, because the spectrum can be expressed in cyclic frequency f or angular frequency ω.

$$m_{f,n} = \int_{-\infty}^{\infty} (f)^n \, S_{f,\tilde{u}}(f) \, df \tag{3.15}$$

$$m_{\omega,n} = \int_{-\infty}^{\infty} (\omega)^n \, S_{\omega,\tilde{u}}(\omega) \, d\omega \tag{3.16}$$

Because in this thesis both definitions are used, the subscript f and ω are used to denote which definition is used. Of course $m_{f,n}$ and $m_{\omega,n}$ are connected, because $2\pi f = \omega$, which gives that $(2\pi)^n m_{f,n} = m_{\omega,n}$. The connection between the spectral density and autocorrelation function is also noticeable in the spectral moments.

$$m_{f,n} = (2\pi i)^{-n} \frac{d^n R(0)}{d\tau^n} \tag{3.17}$$

$$m_{\omega,n} = (i)^{-n} \frac{d^n R(0)}{d\tau^n} \tag{3.18}$$

If the acf is normalized by the variance contained in the spectrum, normalized moments are obtained. For the second and fourth order normalized spectral moments a notation of respectively λ and μ is used, to be in agreement with the notation used in eq. (4.12). The derivation of the above mentioned equalities can be found in appendix C.

3.2.4 Probability distribution

The probability density of a stochastic variable describes the relative number of times a certain value of the variable is likely to occur.

$$f(\tilde{u}) = \lim_{M\to\infty} \frac{M(\tilde{u})}{M} \tag{3.19}$$

Where $M(\tilde{u})$ is the number of times $\tilde{u}$ is observed, and M quantifies the total amount of data. According to this definition, the area below the pdf is normalized to unity. The cumulative distribution function (cdf) is related to the pdf by

$$F(\tilde{u}) = \int_{-\infty}^{\tilde{u}} f(\tilde{u}) d\tilde{u} \tag{3.20}$$

Where $F(\tilde{u})$ describes the fraction of time for which $\tilde{u} \leq \tilde{u}$. In this section the distribution of turbulence is described for (1) the case when turbulence can be treated as Gaussian and (2) when turbulence is non-Gaussian.

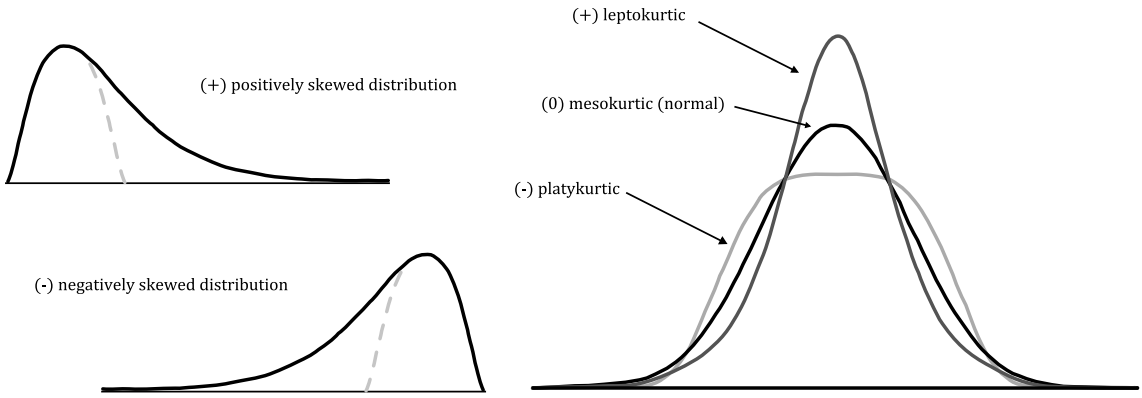

Figure 3.4: Example probability density functions for different skewness (left) and kurtosis (right). For a Gaussian pdf, skewness is zero, which means the pdf is fully symmetric. The kurtosis for a Gaussian pdf is three. The pdf related to a high kurtosis has a high central peak and broad skirts. Values near the mean and unexpectedly high deviations are thus more common than in a Gaussian process.

Gaussian distributed turbulence

The central limit theorem tells that a random variable, which itself is a sum of many other random variables, is approximately Gaussian distributed. This type of statistics is often observed in nature and also applies to turbulence. The probability density function of single-point grid turbulence is indeed close to the Gaussian pdf. It is symmetric and has a flatness factor of approximately three. Therefore, small scale wind speed fluctuations (turbulence) are often assumed to have a Gaussian probability density function (pdf) (cf. figure 3.4).

$$f(\tilde{u}) = \frac{1}{\sigma\sqrt{2\pi}} e^{\frac{-\tilde{u}^2}{2\sigma^2}} \tag{3.21}$$

The approximation of the Gaussian distribution of turbulence holds for single point fluctuations. For difference in wind speeds between two points in space, separated by a distance ξ, $\tilde{u}_\xi(x) = |\tilde{u}(x+\xi) - \tilde{u}(x)|$, the probability distribution is non-Gaussian [Davidson, 2007; Schmitt, 2007; Böttcher et al., 2007]. The departure of the pdf from being Gaussian can be seen from the skewness $\mathcal{S} = \langle\tilde{u}^3\rangle / \left(\sigma_{\tilde{u}}^2\right)^{3/2}$ and kurtosis (or flatness) $\mathcal{K} = \langle\tilde{u}^4\rangle / \left(\sigma_{\tilde{u}}^2\right)^2$ of the pdf (cf. also figure 3.4). For a Gaussian pdf, $\mathcal{S} = 0$ and $\mathcal{K} = 3$. For two-point velocity differences, the tails of the real distribution are significantly different from being Gaussian. This part of the probability distribution is related to high wind speed fluctuations (gusts). The approximation of Gaussian distributed turbulence therefore does not estimate the correct probability of larger wind gusts. In e.g. Peinke et al. [2004], certain gusts are measured each hour, while these gusts would be expected only once in a century for a corresponding wind field following Gaussian statistics. The following section, therefore, deals with non-Gaussian turbulence.

Non-Gaussian distributed turbulence

The departure of the distribution from being Gaussian depends on the Reynolds number and the distance ξ between the points. Davidson [2007] gives for $\xi = 0$ a variation of the flatness factor with $\mathcal{K} \sim 4$ for modest Re to $\mathcal{K} \sim 40$ for high Re (e.g. in the ABL, where Re $\sim 10^7$). High flatness factors are typical for intermittent signals. Such signals are close to the mean for a long period of time, suddenly increase and return to the mean again (cf. figure 3.5). The degree of intermittency thus increases with increasing Re (turbulence). The skewness

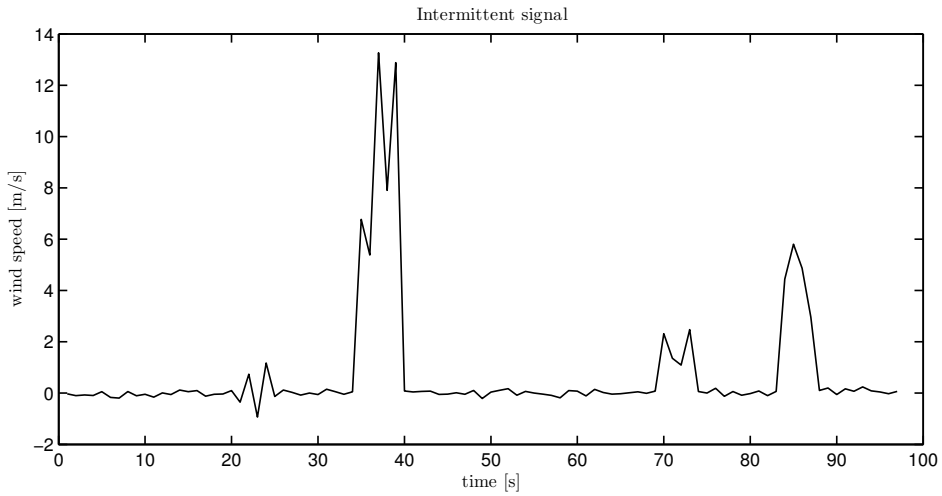

Figure 3.5: Example of an intermittent signal. The signal stays around its mean value (zero) for most of the time and occasionally increases suddenly and goes back to its mean.

factor is in the range of $\sim$ -0.4 – 0.1 for Re up to 10^6 with slightly higher values for higher Re. The deviation of the real turbulence pdf from being Gaussian decreases if ξ increases. These results are in agreement with the kurtosis and skewness for Oak Creek in Larsen et al. [2003]. It depends on terrain types and atmospheric conditions how non-Gaussian the turbulence actually is [Larsen et al., 2003].

In real (atmospheric) turbulence an unexpected (assuming Gaussian turbulence) high probability of large velocity fluctuations (gusts) exists. This behavior is related to the phenomenon of intermittency in turbulence explained above. This feature of turbulence, however, is still not fully understood and remains an important area of research. A plausible explanation of its causes is e.g. mixing in internal boundary layers or unsteady flow phenomena like recirculation zones [Nielsen et al., 2007]. In She [1991] intermittency is explained by highly localized turbulent structures, which are occasionally excited by self-interaction. These isolated turbulent structures exists within the largely random stochastic velocity field (which is thus a mixture of random eddies and structures). The random eddies are characterized by velocities $\tilde{u}$ of $\sigma_{\tilde{u}}$ amplitude. The structures are in contrast characterized by much higher velocities ($\tilde{u} >> \sigma_{\tilde{u}}$). The self-interaction of the structures happens due to their exceptionally high amplitudes.

Any assumption about the distribution of wind speed fluctuations has influence on the probability of simulating extreme wind gusts. For simulating extreme wind gusts with a correct probability, the tails of the probability distribution for the real wind speed must compare with the distribution used for simulation. The difference between non-Gaussian and

Gaussian distributed turbulence lies mainly in the tails of the probability distribution [Gontier et al., 2007; Böttcher et al., 2003; Peinke et al., 2004; Böttcher et al., 2007]. Peinke et al. [2004] shows that the Fokker-Planck equation with adapted coefficients describes the changing behavior of the anomalous pdf well.

$$\begin{aligned} -\xi \frac{\partial}{\partial \xi} f(\tilde{u}_\xi, \xi) &= \left[-\frac{\partial}{\partial \tilde{u}_\xi} D^1(\tilde{u}_\xi, \xi) + \frac{\partial^2}{\partial \tilde{u}_\xi^2} D^2(\tilde{u}_\xi, \xi) \right] f(\tilde{u}_\xi, \xi) \\ D^1(\tilde{u}_\xi, \xi) &= -\gamma(\xi)\tilde{u}_\xi \\ D^2(\tilde{u}_\xi, \xi) &= \alpha(\xi) - \delta(\xi)\tilde{u}_\xi + \beta\xi\tilde{u}_\xi^2 \end{aligned} \tag{3.22}$$

Where $f(\tilde{u}_\xi, \xi)$ is the pdf of $\tilde{u}_\xi$. The Kramers-Moyal coefficients $D^1(\tilde{u}_\xi, \xi)$ and $D^2(\tilde{u}_\xi, \xi)$ can be estimated from experimental data (see also Nawroth and Peinke [2006]). In Böttcher et al. [2003], the same behavior of the pdf of wind speed increments is observed with increasing time lag between two temporal points ($\tilde{u}_\tau(t) = |\tilde{u}(t+\tau) - \tilde{u}(t)|$) as in Davidson [2007] with increasing distance between two spatial points (cf. figure 3.6). Their pdf goes from an

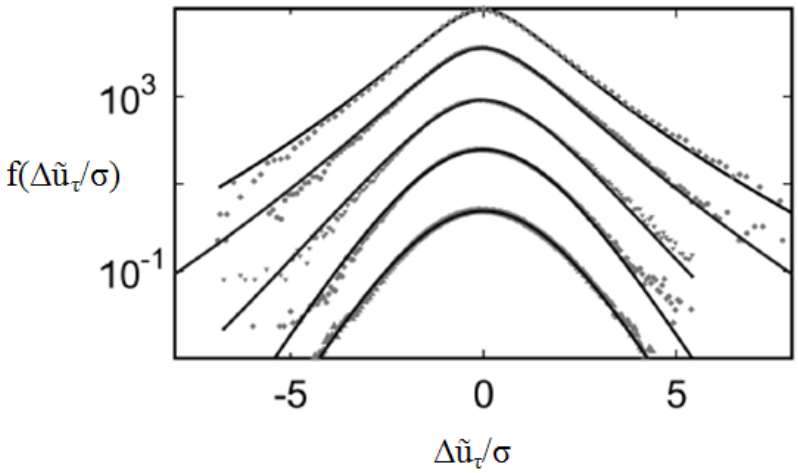

Figure 3.6: Conditioned atmospheric pdfs, where τ is $0.008\mathcal{T}$, $0.03\mathcal{T}$, $0.2\mathcal{T}$, $0.95\mathcal{T}$ and $1.9\mathcal{T}$. The mean wind interval on which the increments are conditioned is [4.5, 5.6] m/s. The distributions are shifted vertically against each other for a clearer presentation. (taken from Böttcher et al. [2003]).

intermittent shape to an almost Gaussian shape when the time lag is near the integral time scale (The same is given by Bergström [1987]). This is in agreement with the central limit theorem, which requires uncorrelated variables to get a Gaussian probability distribution. It also shows the validity of Taylor's hypothesis of frozen turbulence (Schmitt [2007] confirms this for large mean velocities). However, this changing behavior of the pdf is only observed for stationary turbulence, which is never the case for atmospheric wind. To observe the same behavior for measured wind speed, conditioned pdf's of the wind speed increments can be calculated for intervals (approximately 1 m/s width) of the mean wind speed. Böttcher et al. [2003] shows from these observations that the anomalous statistics of wind speed fluctuations on discrete time intervals (wind gusts) can be reduced to the intermittent statistics of local isotropic turbulence. This is based upon a model proposed by Castaing et al. [1990] which

tells that the velocity increment distribution $f(\tilde{u}_\tau)$ can be interpreted as a superposition of Gaussian distributions $f(\tilde{u}_\tau|\sigma)$ with standard deviation σ (distributed according to a log-normal distribution $f(\sigma)$). This model of $f(\tilde{u}_\tau)$ is in turn based upon the basis of Kolmogorovs understanding of turbulent cascade. The pdf of wind speed increments is than described as

$$f(\tilde{u}_\tau) = \int_0^\infty f(\tilde{u}_\tau|\sigma) f(\sigma) d\sigma \tag{3.23}$$

$$= \int_0^\infty \frac{1}{\sigma\sqrt{2\pi}} e^{\frac{-\tilde{u}_\tau^2}{2\sigma^2}} \frac{1}{\sigma\lambda\sqrt{2\pi}} e^{\frac{-\ln^2(\sigma/\sigma_0)}{2\lambda^2}} d\sigma \tag{3.24}$$

Where σ_0 is the median and λ^2 is the variance of the log-normal distribution. In the limit of $\lambda \to 0$, the log-normal distribution converges toward a delta function, which causes $f(\tilde{u}_\tau)$ to become a Gaussian distribution with variance σ_0^2. This 'Castaing distribution' is used by Böttcher et al. [2003] to fit the measured pdf's in figure 3.6 by choosing an appropriate λ. The form of the resulting pdf $f(\tilde{u}_\tau)$ is determined by λ^2, which is therefore called 'form parameter'. This form parameter can be used to compare the pdf's with each other in a quantitative way. A further elaboration of this topic is given in Böttcher et al. [2007]. In this paper it is proposed that the observed intermittency in the increment pdf's of atmospheric turbulence should be explained by mixing different Gaussian distributions rather than by a fractional (Lévy) stochastic process. Thus, in analogy with the 'Castaing distribution', atmospheric turbulence can be considered as a superposition of a number of homogeneous, isotropic, stationary (Gaussian) turbulent flow segments. These flow segments are characterized by their mean wind speed (instead of standard deviation in the case of the 'Castaing distribution') and denoted by $f(\tilde{u}_\tau|\bar{u})$. The mean wind speed is distributed according to a two parameter Weibull distribution

$$f(\bar{u}) = \frac{k}{c^k} \bar{u}^{k-1} e^{-(\frac{\bar{u}}{c}^k)} \tag{3.25}$$

In this way an explicit expression for atmospheric wind speed increment pdf's is obtained

$$f(\tilde{u}_\tau) = \int_0^\infty f(\bar{u}) f(\tilde{u}_\tau|\bar{u}) d\bar{u} \tag{3.26}$$

$$= \frac{k}{2\pi c^k} \int_0^\infty \int_0^\infty \bar{u}^{k-1} e^{-(\frac{\bar{u}}{c}^k)} \frac{1}{\sigma^2\lambda} e^{\frac{-\tilde{u}_\tau^2}{2\sigma^2}} e^{\frac{-\ln^2(\sigma/\sigma_0)}{2\lambda^2}} d\sigma d\bar{u} \tag{3.27}$$

Here k plays a similar role as λ in determining the shape of the distribution. In the limiting case $k \to \infty$ and $\lambda \to 0$ (which happens if $\tau \to \infty$), $f(\tilde{u}_\tau)$ becomes a Gaussian pdf. To apply eq. (3.27), c, k, σ_0 and λ^2 should be known. The parameters for the Weibull distribution can be obtained from a fit to measured wind speed data. The other two parameters can be fitted by using the approximations

$$\lambda^2 = a_{\bar{u}} - b_{\bar{u}} \ln(\tau) \tag{3.28}$$

$$\sigma_0 = b_\tau \bar{u} \tag{3.29}$$

This description of the velocity increment pdf can for example be used as input for simulation of turbulence with use of continuous time random walks. This is briefly explained in section 3.3.3. For more information the reader is directed to Böttcher et al. [2007]; Peinke et al. [2008].

As already said above, the deviation of the pdf of real turbulence from being Gaussian causes a much smaller probability of extreme wind gusts compared to real wind when simulating Gaussian wind fields. In section 10.2 the effect of non-Gaussian distributed turbulence on the distribution of the extreme load response of a wind turbine is shown. The deviation of simulated wind from real wind has influence on the dynamic loads of the turbine, but it's not known how significant this influence is. Mann [2007] reports from a Danish study at Risø National Laboratory an increase of some loads with 15% for rather complex terrain. Gontier et al. [2007] reports major influence of non-Gaussian wind simulation on the fatigue loads. For complex terrain Hansen and Larsen [2007] has found large deviations of extreme coherent wind speed and direction change (ECD) from the IEC 61400-1 standard. The difference between loads from Gaussian and non-Gaussian simulation for complex terrain is reasonable. This is the type of terrain where non-Gaussian time series occur most frequently and non-Gaussian simulation thus has a greater impact. Despite these deviations from reality, the assumption of Gaussian turbulence is still made because it simplifies the simulation algorithms so much and applies well for easier applications.

3.3 Simulation of turbulence

The relation between atmospheric turbulence and the loads on wind turbine blades is highly nonlinear. Turbulence is the source of a large part of the blade fatigue and extreme gust loading. The IEC 61400-1 standard states that a number of load calculations must be made to verify structural safety. For the load calculation of mid- to large size wind turbines numerical simulation of 3D turbulent wind speed is required. The simulation of numerical turbulence is done by means of stochastic simulation. In conventional stochastic simulation of turbulence, it is assumed that turbulence is a stationary Gaussian process specified by a given (cross) spectral density. However, extensions to general probability distributions are possible. This section deals with (1) simulation of Gaussian distributed turbulence and (2) correction of this method to obtain non-Gaussian distributed turbulence.

3.3.1 Gaussian turbulence

The Generation of stochastic time series described in this chapter is based upon a method for stochastic simulation developed by Shinozuka [1971]. A description of this method for simulations of turbulent wind fields applied to wind turbines is given by Veers [1988] and is commonly denoted as "Veers method". Other more general names are: "Multivariate Fourier simulation" and "Spectral representation method". The idea behind this method is that for simulating almost Gaussian distributed turbulence, the auto- and cross-spectra of the inflowing turbulent wind field are sufficient. Wind speed time series are simulated at predefined points in a plane perpendicular to the mean wind direction. When using Taylor's frozen turbulence hypothesis (cf. section 3.1) the wind speed time series can be moved through the rotor plane of a wind turbine in the mean wind direction at the mean wind speed. In this method empirical one-sided spectra and coherences are used as input. It is necessary to have a realistic model for the spectral density and coherence to get results comparable to the real situation. The assumptions about the turbulent wind speed are; stationary, homogeneous, Gaussian distributed and incompressible flow. When the terrain is complex or in the case of wind farms, these assumptions can be questioned, because in these situations special phenomena like micro-bursts or weird gusts can occur. Extensions of

this method are possible for inhomogeneous, non-stationary processes of general probability distribution (i.e. non-Gaussian) [Nielsen et al., 2007]. For a one-dimensional Gaussian process, a stationary stochastic time series $\tilde{u}(t)$ can be obtained by summing harmonics with random phase ϕ and amplitudes which follow from a given two-sided spectral density function $S_{uu}(f)$.

$$\tilde{u}(t) = \sum_{k=1}^{K} \sqrt{\frac{2S_{uu}(f_k)}{T}} \cos(2\pi f_k t + \phi_k) \tag{3.30}$$

Where the independent random phase angles ϕ_k are uniformly distributed between 0 and 2π, t is the discretized time, T is the total sampling time (period) and f a set of K equidistant frequencies. If the number of time steps becomes large, $\tilde{u}(t)$ will be Gaussian and the statistical properties measured over multiple realizations of $\tilde{u}(t)$ at a fixed time instant t will be invariant to the chosen time instant. The simulated stochastic process $\tilde{u}(t)$ is periodic with the period T. An alternative description is

$$\tilde{u}(t) = \sum_{k=1}^{K} a_k \cos(2\pi f_k t) + b_k \sin(2\pi f_k t) \tag{3.31}$$

For a Gaussian process with zero mean (i.e. single point turbulence, cf. section 3.2.4), the Fourier coefficients a_k and b_k should be Gaussian distributed. They have to be mutually uncorrelated, with zero mean and variance of $S_{uu}(f_k)/T$ (cf. Papoulis and Pillai [2002, p. 411-412]). The advantage of eq. (3.31) over eq. (3.30) is that the former one is always Gaussian distributed, even for a small number of time steps.

The general procedure for N spatial points is described below according to Veers [1988]. The procedure followed by the Veers method is basically to generate Fourier coefficients with proper statistics and next perform an inverse Fourier transform to obtain a discrete wind speed time series. An example is given in appendix D.

The base of the Veers method is the spectral matrix $\mathbf{S}$, which contains the information about the wind field which has to be represented. This matrix consists of a power spectral density (PSD) for each spatial point and a cross spectral density (CSD) for between spatially separated points. The CSD depends solely on the PSD's and the coherence function (Coh).

$$\mathbf{S}_{j,k}(f) = Coh_{j,k}(f, \xi, \bar{u}) \sqrt{\mathbf{S}_{j,j}(f)\mathbf{S}_{k,k}(f)} \tag{3.32}$$

Where ξ is the distance between points j and k. Thus, in order to construct $\mathbf{S}$, only models for PSD's and Coh are needed. The used input models for turbulence PSD and Coh determine the accuracy of the simulation method. Hence, it is important to have accurate models for PSD and Coh, depending on the situation the wind is simulated for. Standards on wind turbine design give recommendations for some input models. In appendix B several descriptions of PSD and Coh can be found.

The spectral matrix $\mathbf{S}$ has to be decomposed into the lower triangular transformation matrix $\mathbf{H}$ and its transpose $\mathbf{H}^T$ (e.g. with Cholesky factorization).

$$\mathbf{S}(f) = \begin{bmatrix} PSD_{1,1} & CSD_{1,2} & \cdots & CSD_{1,N} \\ CSD_{2,1} & PSD_{2,2} & \cdots & CSD_{2,N} \\ \vdots & \vdots & \ddots & \vdots \\ CSD_{N,1} & CSD_{N,2} & \cdots & PSD_{N,N} \end{bmatrix} = \mathbf{H}\mathbf{H}^T \tag{3.33}$$

All elements of **S**, and hence of **H**, are one-sided functions of the frequency f [Hz]. For all N spatial points, correlated time series of length M must be created. To obtain these N time series, N independent random processes (white noise) should be generated and stored into the diagonal matrix **X**. These white noise inputs are complex exponentials with unit magnitude and random phase ϕ. To obtain a Gaussian distributed input, ϕ should be uniformly distributed within $0 - 2\pi$.

$$\mathbf{X}(f) = \begin{bmatrix} e^{i\phi_1(f)} & 0 & \cdots & 0 \\ 0 & e^{i\phi_2(f)} & \cdots & 0 \\ \vdots & \vdots & \ddots & 0 \\ 0 & 0 & \cdots & e^{i\phi_N(f)} \end{bmatrix} \tag{3.34}$$

The Fourier coefficients for all N points (stored in the vector $\mathbf{V}(\mathbf{f})$) are obtained by

$$\mathbf{V}(f) = \mathbf{H}(f)\mathbf{X}(f)\mathbf{e} = \begin{bmatrix} \sum_{n=1}^{1} H_{1,n} e^{i\theta_n(f)} \\ \sum_{n=1}^{2} H_{2,n} e^{i\theta_n(f)} \\ \vdots \\ \sum_{n=1}^{N} H_{N,n} e^{i\theta_n(f)} \end{bmatrix} \tag{3.35}$$

Where **e** is a column vector of N ones. Thus the sum of each row of the matrix **HX** is obtained. With the multiplication of **H** and **X**, the independent input in **X** is correlated according to the information of the turbulence PSD and Coh model contained in **H**. Fourier transformation (FT) is used to transform Fourier coefficients from frequency to time domain. In order to obtain the correct Fourier coefficients, the correct frequency components should be used. The total period $T = M\Delta t$ contains the frequency components $f = \Delta f(1, \ldots, M/2-1)$, with $\Delta f = 1/T$. In Fourier transformation, the number of frequency components should be exactly equal to M, to get time series of length M. By using the same amount of neg. and positive frequencies, the inverse Fourier transform of the Fourier coefficients will sum up cosines and sines. This results in a time series with only real values.

A physical spectrum can only be one-sided. Therefore, only the positive half of frequencies is taken into account to obtain the Fourier coefficients. This is corrected in the inverse Fourier transform below, to get a time series of length M, by assuming an artificial double-sided symmetric spectrum[8] (cf. figure 6.4). For each spatial point N, The inverse Fourier transform of each row of **V** is

$$T = M * IFT(\begin{bmatrix} 0 & \mathbf{V} & 0 & \text{rot90}(\mathbf{V}^T) \end{bmatrix})$$

The first Fourier coefficient for the positive frequencies is set to zero, to get a zero mean. The first of the Fourier coefficients for the negative frequencies is also set to zero, to avoid imaginary values. In order to keep the area below the spectrum equal to the variance, the discrete values $S_{\tilde{u}}(f)$ obtained from the spectrum should be multiplied with $\Delta f/2$. This method thus produces a Gaussian time series from the prescribed spectral density and Fourier coefficients (see appendix D for an example). An additional method to infuse a prescribed non-Gaussian content in the signal is described in the next section.

[8]The imaginary Fourier coefficients for the positive frequencies are rotated ninety degrees in the imaginary plane, to create the Fourier coefficients for the negative frequencies. In this case $S_{\tilde{u}}(-f) = S_{\tilde{u}}(+f)$

3.3.2 Non-Gaussian turbulence

Extensions of the Veers method are possible for inhomogeneous, non-stationary processes of general probability distribution, as already stated above. A practical description of these extensions is given by Nielsen et al. [2007]. In the context of this thesis only the extension to non-Gaussian probability distributions is of relevance. The extension to non-Gaussian distributed variables can be done by the monotone memoryless transformation

$$\tilde{u}(t) = g(\tilde{x}(t)) \tag{3.36}$$

Where $\tilde{x}(t)$ is a real-valued stationary Gaussian process, simulated as explained above, with zero mean, unit variance and autocorrelation function $R(\tau) = \langle \tilde{x}(t+\tau)\tilde{x}(t) \rangle$. Eq. (3.36) can either be an analytical relation or an empirical mapping scheme [Masters and Gurley, 2003]. The transformation function g should be nonlinear to obtain non-Gaussian distributions [Grigoriu, 1995, p. 43].

g as an empirical mapping scheme

A non-Gaussian time series can be obtained from a Gaussian one by mapping $x(t)$ to the realization of the non-Gaussian stochastic process $\tilde{u}(t)$.

$$\tilde{u}(t) = F^{-1}\left[X(\tilde{x}(t))\right] \tag{3.37}$$

Where X is the cumulative distribution function (cdf) of $\tilde{x}(t)$ and F is a prescribed non-Gaussian marginal cdf. For every $\tilde{x}$ at time t, the corresponding $\tilde{u}$ at time t is calculated in such a way that $F(\tilde{u}(t)) = X(\tilde{x}(t))$ (cf. figure 3.7). This method of non-Gaussian mapping can also be used in a numerical discretized form, by means of interpolation. However, using a theoretical model obtained from a fit to an empirical cdf is much faster.

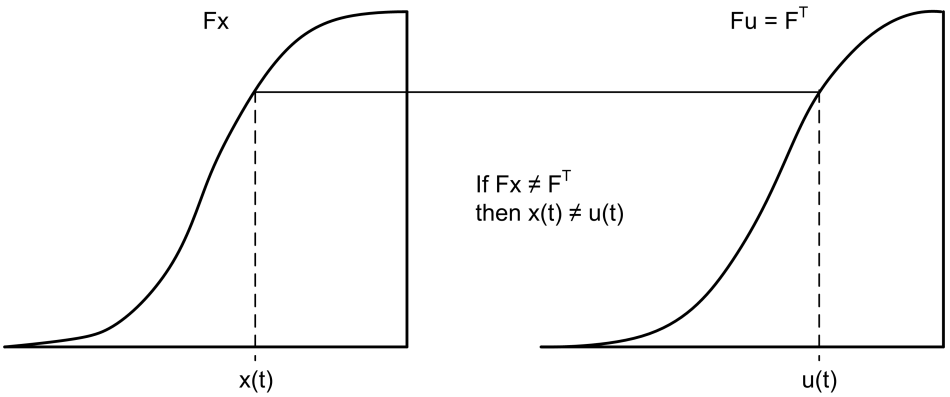

Figure 3.7: Procedure for cdf-mapping. Each value in $x(t)$ is mapped to a value $u(t)$ of the correct probability. A cdf instead of pdf is used to avoid ambiguity.

g as an analytical relation

Winterstein [1985] uses Hermite expansion estimates of g to provide a useful model for a transformation to a non-Gaussian process based on known central moments of $\tilde{u}(t)$. The

methods of simulating non-Gaussian stochastic processes in Gurley et al. [1996]; Gurley and Kareem [1998]; Nielsen et al. [2007] are based on this principle.

$$\tilde{u}(t) = \sum_{n=1}^{N} a_n He_n(\tilde{x}(t)) \tag{3.38}$$

Where $He_n(x)$ is the Hermite polynomial of order n, which can be obtained by $He_0 = 1$, He_x and the recurrence relationship $He_n = xHe_{n-1}(x) - (x-1)He_{n-2}(x)$, $n \geq 2$. A proof of this approximation is given in Grigoriu [2009]. The Hermite polynomial definition used here is actually the probabilists' version of the Hermite polynomial[9] [Weisstein, 2009; Wikipedia, 2009b]. The coefficients a_n can be found by the following integral, where $\phi(x)$ is the Gaussian probability density function.

$$a_n = \int_{-\infty}^{\infty} u(t) He_n(\tilde{x}(t)) \phi(\tilde{x}(t)) d\tilde{x} \tag{3.39}$$

When the pdf of $\tilde{u}(t)$ is only mild non-Gaussian, the Hermite expansion can be truncated at the third order ($N = 3$), as has been done in Winterstein [1988]. The Hermite coefficients can hence be expressed as a function of skewness and kurtosis and can be found by solving the following system of equations [Ditlevsen et al., 1996; Nielsen et al., 2007].

$$\begin{aligned} 1 &= a_1^2 + 2a_2^2 + 6a_3^2 \\ \mathcal{S} &= 2a_2\left(2 + a_2^2 + 18a_1a_3 + 42a_3^2\right) \\ \mathcal{K} &= 15 - 12a_1^4 - 264a_1^3a_3 - 864a_1^2a_3^2 - 432a_1a_3^3 + 288a_1a_3 + 936a_3^2 - 2808a_3^4 \end{aligned} \tag{3.40}$$

Where $\mathcal{S}$ stands for skewness, $\mathcal{S} = \langle\tilde{u}^3\rangle / \left(\sigma_{\tilde{u}}^2\right)^{3/2}$ and $\mathcal{K}$ for kurtosis, $\mathcal{K} = \langle\tilde{u}^4\rangle / \left(\sigma_{\tilde{u}}^2\right)^2$ (cf. section 3.2.4). An approximation of the solution of this system can be found in Winterstein [1988]. This transformation method is used, for instance, in Gurley et al. [1996].

Spectrum distortion

The nonlinear transformation g forces the probability content of $\tilde{u}(t)$ to be conform to the specified target distribution function. However, the spectral contents of $\tilde{u}(t)$ will be distorted due to the nonlinearity of this transformation. Spectral correction can be used to address this issue (cf. figure 3.8). The idea is to seek an underlying spectral density $S_{\tilde{x}}$ to assign to the initial Gaussian function $\tilde{x}(t)$, which differs from the target spectral density of the final non-Gaussian function $S_{\tilde{u}}^T$. The spectral density $S_{\tilde{x}}$ should be chosen in such a way, that the transformation g distorts the spectral content of $\tilde{x}(t)$ into the target spectral density $S_{\tilde{u}}^T$, without causing an inaccurate representation of the target distribution function. Several spectral correction methods are available, see e.g. Shinozuka and Yamazaki [1988]; Deodatis and Micaletti [2001]; Gurley and Kareem [1998]. A comparison of these methods has been

[9] Hermite polynomials are defined as $He_n(x) = (-1)^n e^{x^2} \frac{d^n}{dx^n} e^{-x^2}$ ("physicists' Hermite polynomial"), or as $He_n(x) = (-1)^n e^{\frac{x^2}{2}} \frac{d^n}{dx^n} e^{-\frac{x^2}{2}}$ ("probabilists' Hermite polynomial"). The latter one is used by Winterstein [1985, 1988]; Nielsen et al. [2007]; Grigoriu [2009]; Gurley and Kareem [1998]. For x being standard Gaussian, these latter Hermite polynomials all have zero mean and are uncorrelated. According to Papoulis and Pillai [2002, p. 281], they form a complete orthogonal set on the real line. Note that these Hermite polynomials are used by Papoulis and Pillai [2002] for error correction to a Gaussian pdf.

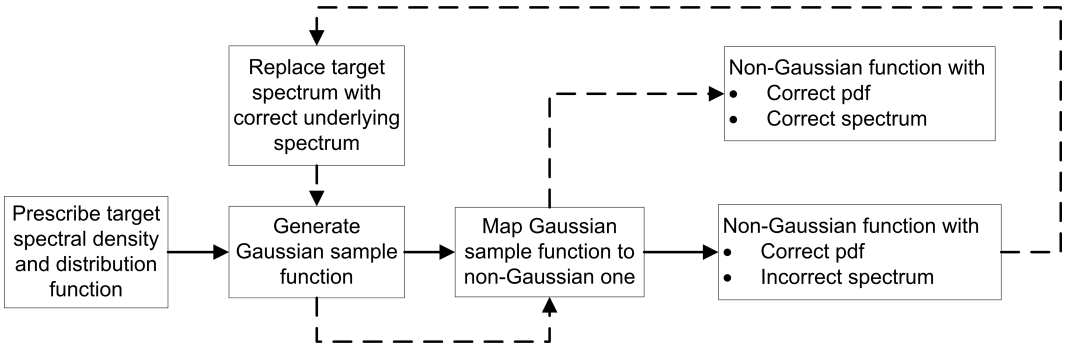

Figure 3.8: Schematic diagram of non-Gaussian simulation with (dashed line) and without (solid line) spectral correction.

made in Masters and Gurley [2003]. The method described by Deodatis and Micaletti [2001] is a revision of the method described by Shinozuka and Yamazaki [1988]. The characteristic feature of this method is the spectrum updating scheme

$$S_{\tilde{x}}^{j+1} = S_{\tilde{x}}^{j}(\omega) \left[\frac{S_{\tilde{u}}^{T}(\omega)}{S_{\tilde{u}}^{j}(\omega)} \right]^{\alpha} \tag{3.41}$$

Where j denotes the iterative step and $S_{\tilde{u}}^{j}(\omega)$ is the spectrum of the current simulation of $\tilde{u}(t)$ and α is a parameter for enhancing convergence, set to 0.3 by Deodatis and Micaletti [2001] and 1 in [Shinozuka and Yamazaki, 1988]. This scheme is used to iteratively alter the underlying spectral density until the difference between $S_{\tilde{u}}^{T}$ and $S_{\tilde{u}}^{j}$ is acceptably small. Although $\alpha = 0.3$ causes better convergence than $\alpha = 1$, it still happens that eq. (3.41) does not converge for combinations of a highly non-Gaussian spectrum and acf. The reason lies in an incompatible pair of an underlying Gaussian spectral density function and a non-Gaussian distribution function [Deodatis and Micaletti, 2001]. In Lagaros et al. [2005], the spectrum updating scheme is replaced by approximating the unknown Gaussian spectrum $S_{\tilde{x}}$ with a neural network regression model. This drastically reduces the computational effort of the non-Gaussian simulation and always shows convergence, even for highly skewed distribution functions.

In this thesis the method described by Deodatis and Micaletti [2001] is used, since only mild non-Gaussianity is observed. The difference between $S_{\tilde{u}}^{T}$ and $S_{\tilde{u}}^{j}$ is quantified by the mean square error

$$e = \frac{1}{K} \sum_{k=1}^{K} \left(S_{\tilde{u}}^{T} - S_{\tilde{u}}^{j} \right)^2 \tag{3.42}$$

Now, the largest error allowed has to be chosen. The procedure to arrive at a non-Gaussian stochastic time series is described by the following steps:

1. find the spectrum $S_{\tilde{u}}^{T}$ of the measured process $\tilde{u}(t)$;
2. apply Fourier simulation to generate stochastic Gaussian time series $\tilde{x}(t)$;
3. transform $\tilde{x}(t)$ into a non-Gaussian time series $\tilde{u}(t)$;
4. apply iterative spectral correction until the spectral density is sufficiently accurate.

See figure 3.9 for a flowchart of the process and figure 3.10 for an example of an in this way obtained non-Gaussian time series.

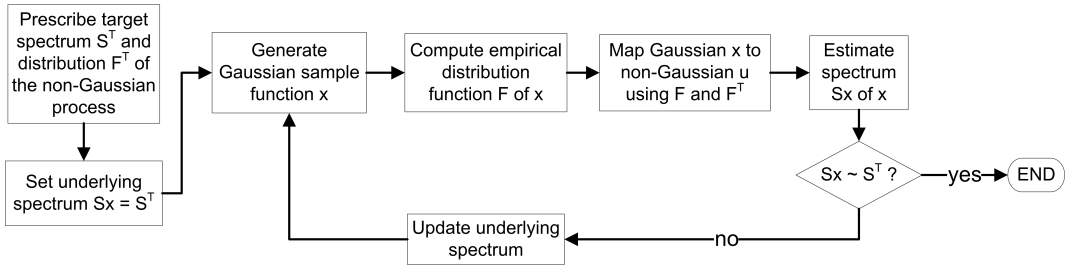

Figure 3.9: Flowchart of the iterative spectral correction procedure

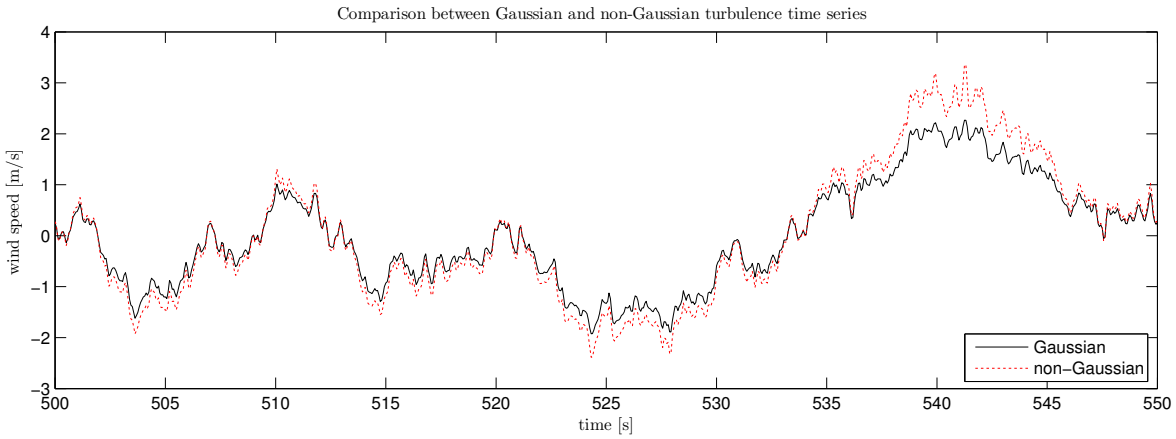

Figure 3.10: Comparison between a Gaussian and non-Gaussian turbulence time series

Correlation distortion

The iterative method described above may be avoided if the autocorrelation function of the non-Gaussian time series is transformed to the underlying Gaussian process. This approach is called correlation distortion and is, among others, described by Grigoriu [1995]; Gurley et al. [1996]; Nielsen et al. [2004, 2007]. In this report only the general procedure is given. In, for instance, Nielsen et al. [2004]; Grigoriu [1995] the general equations can be found. The correlation distortion method goes as follows:

1. find the autocorrelation function $r_{\tilde{u}}(\tau)$ of the measured process $\tilde{u}(t)$;
2. transform $r_{\tilde{u}}(\tau)$ to the acf $r_{\tilde{x}}(\tau)$ of the underlying Gaussian process. The method to do this is e.g. described in Nielsen et al. [2004];
3. simulate a Gaussian time series $\tilde{x}(t)$ using the Gaussian spectrum $S_{\tilde{x}}(f)$ associated with $r_{\tilde{x}}(\tau)$;
4. transform the Gaussian process to a non-Gaussian process.

In section 2.2 it is explained that gusts are an inherent part of turbulence. By just simulating a very long time series, gusts can be selected and taken as input for load calculations. This would take much time and will hence be expensive. An alternative is to perform a special kind of stochastic simulation during which the desired events are automatically selected. In this context the *New*Gust method has been developed, which is explained in section 4.4.

3.3.3 Other turbulence simulation methods

Another important method for simulating 3D wind fields in the Fourier domain is the Mann model. The characteristic difference with the Veers method is the use of a semi-empirical 3D spectral tensor instead of a 1D PSD. A 3D spectral tensor is physically more correct and the Mann model should therefore give a better representation of turbulent wind. Another difference is that the Veers method performs an FFT from frequencies to time domain whereas the Mann model performs an FFT from wave numbers to space domain. In Gontier et al. [2007] a comparison between both methods is made.

The single-point statistics of turbulence are Gaussian distributed, as explained in section 3.2.4. Gaussian statistics can be properly represented by spectral representation models, but the thus simulated turbulende does not include intermittency observed in physical turbulence. The two-point statistics of turbulence are non-Gaussian distributed and include intermittency (cf. eq. 3.27). These statistics can be used to simulate turbulence including intermittency. A model for simulating turbulence, which uses these two-point statistics as input is the Friedrich-Kleinhans model [Peinke et al., 2004; Gontier et al., 2007; Friederichs and Kleinhans, 2007; Peinke et al., 2008]. This model generates non-Markovian[10] data series in real space domain. The simulation is based on the theory of 'continuous time random walks' (CTRW), which is a generalization of random walk processes. A CTRW $\tilde{u}_j(t_j)$ is iteratively defined by

$$\tilde{u}_{j+1} = \tilde{u}_j + \eta_j \quad \text{and} \quad t_{j+1} = t_j + \tau_j \tag{3.43}$$

For $j \in \mathbb{N}$, $\tilde{u}_0 = t_0 = 0$, $\tau_j \geq 0$, $\forall\ j$. The step width and waiting time of the step j are respectively η_j and τ_j and are generally random numbers. To make the process applicable to physical problems, the discrete variable j should be transitioned to a continuous time s. The equations above (3.43) in this way become stochastic differential equations, coupled via the intrinsic time s. The latter equation corresponds to the mapping of s on the physical time t. From a comparison of this model with the Sandia-Veers method with Kaimal, von Karman PSD's and the Mann model, it is concluded that the form of the tails of the probability distribution of the velocity increments has a major influence on the wind turbine fatigue loads [Gontier et al., 2007].

In Kleinhans et al. [2009] an overview is given of models for simulating turbulence for wind turbine applications, including a short description of their capabilities, limitations and current developing state.

[10] A Markov process is a mathematical model for the random evolution of a memoryless system. In such a system, the likelihood of a given future state, at any given moment, is independent on any past states and depends only on its present state. Thus, if the present is specified, the past has no influence on the future. A non-Markovian process covers all random processes except the ones that have the Markov property. Note, however, that a Markov process is an (extensively studied) exception. A stochastic model of a process is non-Markovian, if the idealized assumption of exponential distributions is removed.

Chapter 4

Wind speed gusts

In section 2.2 and 3.2.4, the physical context of wind speed gusts was described. From this description, a gust can be defined as a short term wind speed fluctuation in a turbulent wind field. This chapter describes (1) which definitions of gusts are given in standards and which gusts are of relevance for this thesis, (2) how gusts are characterized in this thesis, (3) detection methods for wind gusts from measured wind speed, (4) the *New*Gust and Risø constrained simulation method and (5) typical load responses to wind speed gusts and how to obtain the distribution of extreme loads with *New*Gust and *Load*Gust.

4.1 Gust definitions

In literature several definitions of gusts exist. With the IEC 61400-1 standard, the gust definition has been standardized. In the 2005 version the following gusts are described as extreme wind conditions:

- *Extreme operating gust (EOG)*: A sudden increase in wind speed within a short time period smaller then 60 seconds;
- *Extreme direction change (EDC)*: A sustained wind direction change;
- *Extreme coherent gust (ECG)*: A sustained change in wind speed;
- *Extreme coherent gust with direction change (ECD)*: A combination of EDC and ECG;
- *Extreme wind shear (EWS)*: A fluctuation in the horizontal or vertical wind speed gradient across the rotor.

In the context of this thesis, only positive wind speed gusts are of importance, because this is the type of gust for which *New*Gust has been developed. Extreme wind speed gusts are described in the IEC 61400-1 standard as EOG, which is mathematically represented by eq. (4.1). If negative wind speed gusts are required, this definition can simply be adapted by adding instead of subtracting the second term in the right hand side of eq. (4.1).

$$V(z,t) = V(z) - 0.37 V_{gust} \sin\left(\frac{3\pi t}{T}\right)\left(1 - \cos\left(\frac{2\pi t}{T}\right)\right); \quad t \in 0,\ldots,T \tag{4.1}$$

$$V_{gust} = \min\left\{1.35\left(V_{e1} - V_{hub}\right); \quad 3.3\left(\frac{\sigma_1}{1 + 0.1\frac{D}{\Lambda_1}}\right)\right\} \tag{4.2}$$

Where T is the duration of the gust (10.5 s) and V_{gust} is the maximum magnitude of the gust at the wind turbine hub height. For the explanation and calculation of the other variables

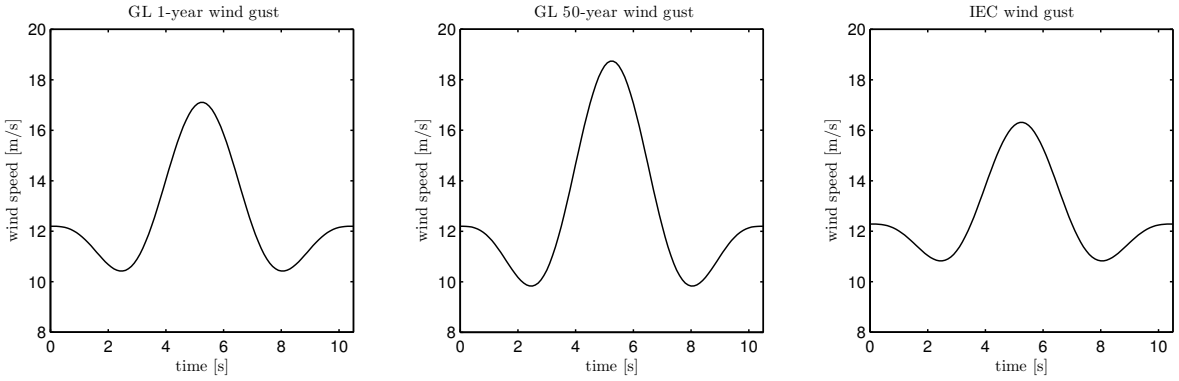

Figure 4.1: Examples of different extreme operating gusts defined in the standards of Germanische Lloyd [2005] and IEC 64100-1 [2005]

is referred to the standard itself. The magnitude and shape of the obtained gust depends on the wind turbine and turbulence class which applies (defined in the standard). The EOG should be considered for ultimate load calculations during start-up, power production plus occurrence of a fault and normal shut down. In the GL standard a slightly different EOG is used

$$V_{gust} = \beta \left(\frac{\sigma_1}{1 + 0.1 \frac{D}{\Lambda_1}} \right) \tag{4.3}$$

Where β depends on the recurrence period (β is 4.8 or 6.4 for the recurrence period of respectively 1 year and 50 years). An example of both EOG's is given in figure 4.1. These types of gusts are called 'Mexican hat gust' referring to the shape of a Mexican hat.

4.2 Characterization of gusts

For the purpose of research, a more precise statistical description of wind speed gusts is necessary. Therefore the statistical parameters to characterize gusts are defined in table 4.1 (inspired by Branlard [2009]; Bergström [1987]; Larsen et al. [2003]). In figure 4.2 the parameters are visualized. An example of the effect of normalization on the time series is shown in figure 4.2 (including linear trend removal). For the calculation of the parameters in table 4.1, ten-minute averages are taken, because this is the typical timescale for turbulence as described in section 2.2. The gust time period typically ranges between 5 – 60 seconds.

4.3 Methods for detecting wind gusts

Several methods exist to detect extreme wind speed gusts from time series. Each method can be seen as a different definition of gusts and hence gives different types of gusts. The methods found in literature are described and compared according to results from a study by Branlard [2009].

Wind speed time series	$u(t)$
Wind speed average	$\bar{u}$
Wind speed standard deviation	σ_u
Turbulent time series	$\tilde{u}(t) = u(t) - \bar{u}$
Normalized time series	$\tilde{u}_n(t) = \frac{\tilde{u}(t)}{\sigma_u}$
Time of the maximum wind speed of the gust	$t_0 = \max_{t \in I_g}(\tilde{u}(t))$
Time of the start of detecting the gust	t_{start}
Time of the end of detecting the gust	$t_{end} = t_{start} + \tau$
Gust relative amplitude	$\tilde{u}_n(t_0) = \frac{\tilde{u}(t_0)}{\sigma_u}$
Gust time period	τ
Gust interval	$I_g = [t_{start}, \ldots, t_{end}]$

Table 4.1: Characteristic gust parameters

4.3.1 Peak-peak and velocity increment

Used, among others, by Bergström [1987]; Branlard [2009]; Böttcher et al. [2003]; Peinke et al. [2004]; Larsen et al. [2003]. The peak-peak method is used to detect extreme values within a certain time period T (e.g. 10 minutes, an hour, a year etc.). The method can be visualized by a moving window with a predefined width[1] $w = \tau/2$ and height or velocity increment $\Delta\tilde{u}$. The minimum and maximum of each window is defined as

$$\tilde{u}_{min} = \min\left(\tilde{u}(t), \ldots, \tilde{u}(t+w)\right) \tag{4.4}$$

$$\tilde{u}_{max} = \max\left(\tilde{u}(t), \ldots, \tilde{u}(t+w)\right) \tag{4.5}$$

The height is the difference between the minimum and maximum of the window.

$$\Delta\tilde{u} = \tilde{u}_{max} - \tilde{u}_{min} \tag{4.6}$$

The velocity increment or velocity difference method looks for the maximum velocity rise and is essentially the same as the peak-peak procedure, but defined somewhat differently. Instead of taking the height $\Delta\tilde{u}$ as the difference between the minimum and maximum within the window, it takes the difference between the first and last point of the window.

$$\Delta\tilde{u} = \tilde{u}(t+w) - \tilde{u}(t) \tag{4.7}$$

The maximum height of all windows in the period T is defined as the extreme gust for that time period. t_0 is the time of the maximum in the window with maximum height. t_{start} and t_{end} are respectively $t_0 \mp w$. The disadvantage of these two methods is that only the extremes are selected and many other interesting and important gusts are ignored. These methods only look at the shape of the gust (the steepness of the rise). For both methods it does not make any difference whether $\tilde{u}(t)$ or $u(t)$ is used. However, less computation time is needed if gusts are selected from the instantaneous wind speed, because averaging is avoided. The

[1] The width of $w = \tau/2$ is taken to be consistent with the other methods. The Peak-peak and velocity increment method only take into account half of the gust. The peak over threshold and correlation method take the whole gust into account. As τ is defined as the gust time period, it becomes clear that $w = \tau/2$ for the first two methods.

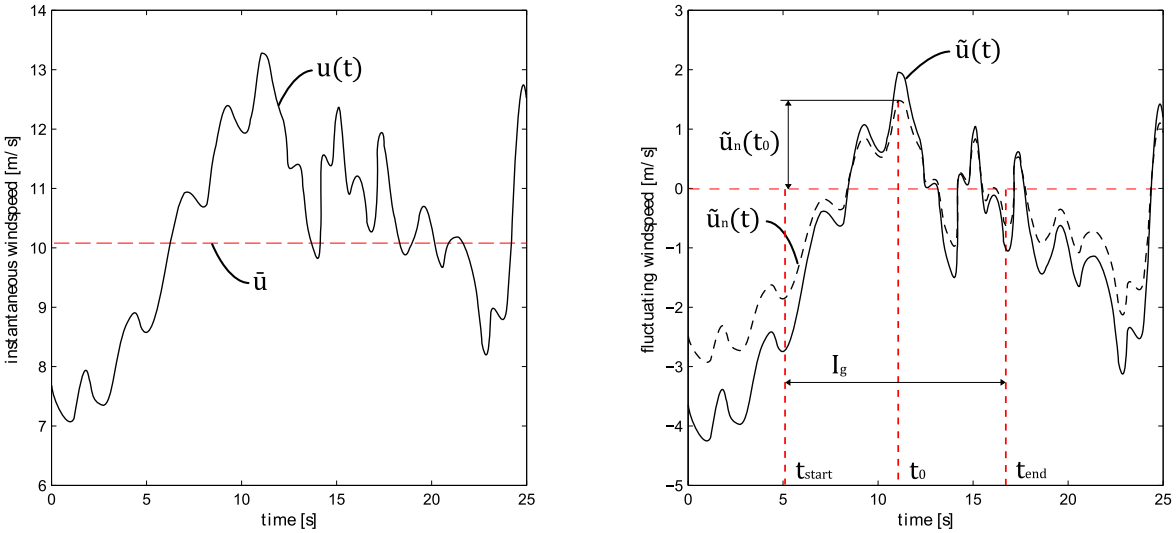

Figure 4.2: Example of the characterization parameters, note that the displayed time series is part of a larger time series and that in the right hand figure the linear trend has also been removed

time period T relevant for selection of gusts is the integral time scale $\mathcal{T}$ of the process (to obtain uncorrelated gusts).

The velocity increment method can also be used to calculate the structure function $D(w)$, which is equal to the variance of $\Delta\tilde{u}$ and related to the spectral density function

$$\left\langle \Delta\tilde{u}^2 \right\rangle = D(w) = \left\langle \left(\tilde{u}(t+w) - \tilde{u}(t)\right)^2 \right\rangle = 2\sigma_{\tilde{u}}^2 \left(1 - r(w)\right) \tag{4.8}$$

$$D(w) = 2\int_0^\infty (1 - \cos(2\pi f w)) S_{\tilde{u}}(f) df \tag{4.9}$$

Where f is the frequency in Hz and $S_{\tilde{u}}(f)$ is the spectral density function of the wind speed.

4.3.2 Peak over threshold

Used, among others, by Bergström [1987]; Branlard [2009]; Bierbooms et al. [1999]; Larsen et al. [2003]. This method is used to detect high amplitude gusts. The restricting parameter is a certain threshold $\Delta\tilde{u}$ which should be exceeded. Therefore, instead of the two former methods, a series of gusts can be detected. This method does not take into account the shape of the gusts and is not dependent on the duration of the gust either. Because of fluctuating wind speed during a gust, a window (or time instant) with width $w = \tau$ is used to prevent obtaining several results for one gust. In mathematical form, a gust is detected if

$$\max\left(\tilde{u}(t), \ldots, \tilde{u}(t+w)\right) > \Delta\tilde{u} \tag{4.10}$$

t_{start} and t_{end} are respectively $t_0 \mp \tau/2$. The peak over threshold method is similar to the zero (or mean) passage method if the threshold is set to zero (or the mean). The fluctuating wind speed has to be used to obtain consistent results, since stationarity is assumed implicitly.

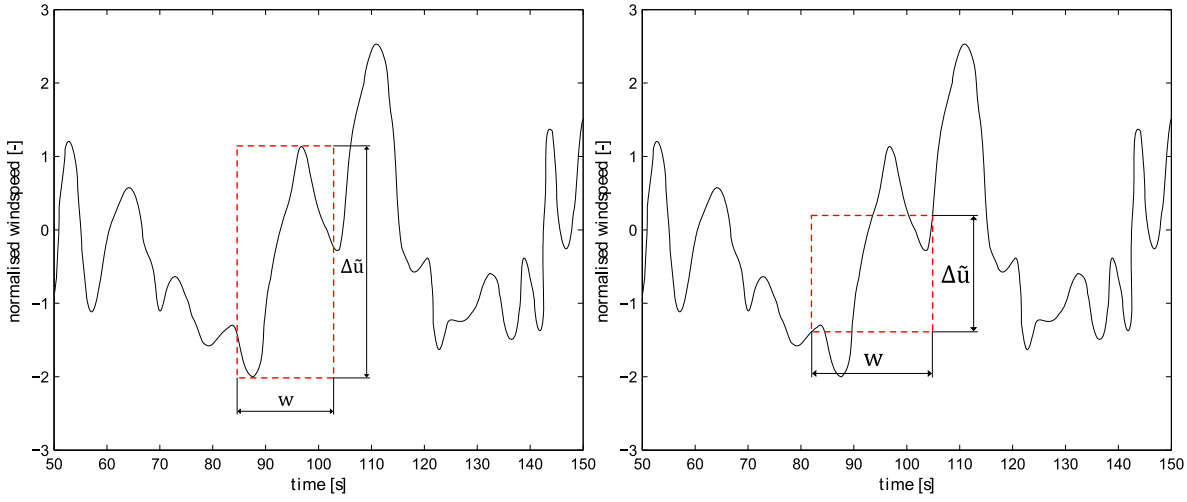

Figure 4.3: Gust detection methods; (a) peak-peak and (b) velocity increment

4.3.3 Correlation

Used by [Branlard, 2009]. With this method gusts with a specific shape can be obtained. A reference signal (e.g. a gust shape from the IEC standard) with duration τ is correlated with the data. To restrict the amount of detectable gusts, a threshold for the relative amplitude and the minimum correlation coefficient r_{min} has to be defined. Only gusts with the same τ as the reference gust can be found, because correlation is only possible for signals of the same size. There is no dependence on the amplitude of the reference gust. For this method t_0 is the time where r is maximum in the interval where $r > r_{min}$. t_{start} and t_{end} are respectively $t_0 \mp \tau/2$.

4.3.4 Velocity increment over threshold

Used, among others, by [Branlard, 2009; Schmitt, 2007]. This method can be used to detect long time-scale events such as fronts. In addition to the velocity increment method described above, a constraint is added to the height of the window $\Delta u \geq |u(t+w) - u(t)|$. Hence, there is a threshold to the acceleration of the wind speed. Long time scale events can be detected by taking a large width (e.g. 10 minutes). This method is in between the velocity increment and peak over threshold method.

4.3.5 Comparison of detection methods

Each detection method provides different types of gusts (cf. figure 4.5). The characteristic parameters described in section 4.2 can be used to compare the different gusts. From studies done by Branlard [2009]; Bergström [1987] the following interesting conclusions can be drawn:

- The correlation and velocity increment method are selective for the rise time due to the dependency on window width w (in contrast to the peak over threshold method);
- For small τ, time dependent methods will be more likely to provide high acceleration values;

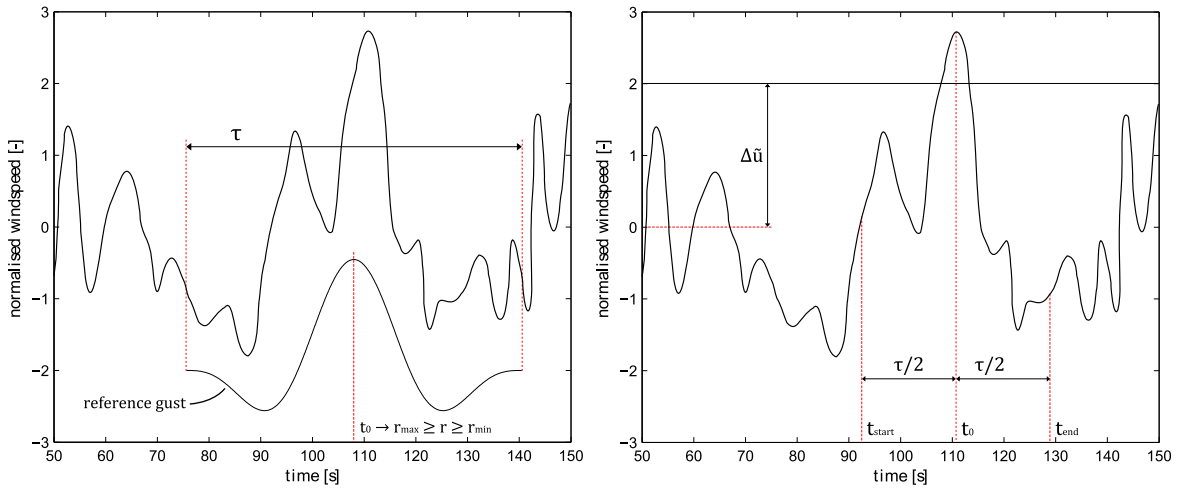

Figure 4.4: Gust detection methods; (a) correlation and (b) peak over threshold

- If the gusts are not centered around their maximum, but in the middle of the interval where the wind speed is above a threshold, the peak over threshold method gives two peaks for the mean gust shape, centered around the middle;
- The peak over threshold method can quickly select high amplitude gusts;
- The velocity increment method provides gusts with a far from symmetric shape;
- The correlation method provides more symmetric gusts;
- The correlation coefficient $r(\tau)$ is independent on stability and surface roughness.

For more information about these conclusions, the reader is directed to the above mentioned documents.

4.4 Simulation of *New*Gust wind speed gusts

In the current wind turbine design standards (IEC 61400-1, 2005; GL wind, 2005), extreme gusts are defined as coherent with an inherent deterministic character as described in section 4.1. In reality gusts are of a stochastic nature and spatially limited. This difference can cause significant differences in the calculated and real loads (cf. section 3.2.4). In order to obtain more realistic load situations, the *New*Gust method has been developed. This probabilistic method simulates gusts of a stochastic nature with a predefined amplitude and is in line with the common practice for fatigue loading. The *New*Gust method is based upon constrained stochastic simulation[2], which applicability is restricted to events (constraints) which can be expressed as a linear relation:

$$\mathbf{y} = \mathbf{G}\mathbf{x} \tag{4.11}$$

Where $\mathbf{G}$ is a matrix of constants, depending on the desired event. $\mathbf{y}$ and $\mathbf{x}$ are random vectors describing respectively the event and the process. Thus, the wind velocities which

[2]A special kind of stochastic simulation during which the desired events are automatically selected by considering the conditional density matching the specified constraints.

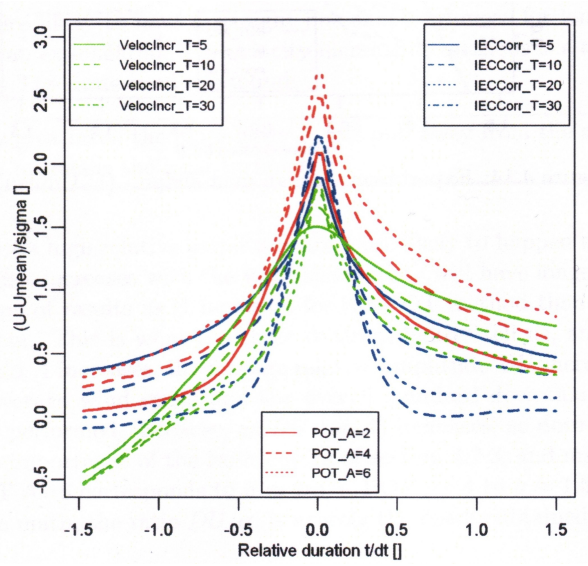

Figure 4.5: Different mean gust shape for different detection methods (taken from Branlard [2009]).

are Gaussian distributed should satisfy these constraints to obtain the desired event. The derivation of an explicit expression in time domain has been done by Bierbooms [2006] for local maxima and velocity jumps. The time domain expression for local maxima is given by

$$\begin{aligned} u_c(t) = u(t) &+ \left(\frac{\mu_\omega}{\mu_\omega - \lambda_\omega^2} r\left(t - t_0\right) + \frac{\lambda_\omega}{\mu_\omega - \lambda_\omega^2} \ddot{r}\left(t - t_0\right) \right) \left(A - u(t_0)\right) \\ &+ \frac{\dot{r}\left(t - t_0\right)}{\lambda_\omega} \dot{u}\left(t_0\right) \\ &+ \left(\frac{\lambda_\omega}{\mu_\omega - \lambda_\omega^2} r\left(t - t_0\right) + \frac{1}{\mu_\omega - \lambda_\omega^2} \ddot{r}\left(t - t_0\right) \right) \left(B - \ddot{u}(t_0)\right) \end{aligned} \tag{4.12}$$

Where $u(t)$ is a turbulent time series (simulated as explained in section 3.3), $r(\tau)$ is the normalized autocorrelation function (cf. section 3.2.2), λ_ω and μ_ω are respectively the second and fourth order normalized spectral moments (cf. section 3.2.3) and A and B specify the local maxima:

$$\begin{aligned} u(t_0) &= A \\ \dot{u}(t_0) &= 0 \\ \ddot{u}(t_0) &= B < 0 \end{aligned} \tag{4.13}$$

An example of a gust resulting from eq. (4.12) is shown in figure 4.6. The statistics of B can be derived, which has been done by Bierbooms [2009a, appendix]. The probability density

function of B is

$$f_B(B) = \frac{|B|\, f_1(B)}{\int_{-\infty}^{0} |B|\, f_1(B) dB} \tag{4.14}$$

$$f_1(B) = |B|\, e^{\frac{-(B-\mu_0)^2}{2\sigma_0^2}} \tag{4.15}$$

$$\mu_0 = -\lambda_\omega A \tag{4.16}$$

$$\sigma_0 = \sigma_u \sqrt{\mu_\omega - \lambda_\omega^2} \tag{4.17}$$

Where μ_ω and λ_ω are the second and fourth order normalized spectral moments as defined in section 3.2.3 and σ is the standard deviation of the turbulence. The mean gust shape resulting from equation (4.12) is

$$\begin{aligned} \bar{u}_c(t) = &\left(\frac{\mu_\omega}{\mu_\omega - \lambda_\omega^2} r\,(t - t_0) + \frac{\lambda_\omega}{\mu_\omega - \lambda_\omega^2} \ddot{r}\,(t - t_0) \right) A \\ &+ \left(\frac{\lambda_\omega}{\mu_\omega - \lambda_\omega^2} r\,(t - t_0) + \frac{1}{\mu_\omega - \lambda_\omega^2} \ddot{r}\,(t - t_0) \right) \overline{B} \end{aligned} \tag{4.18}$$

$$\overline{B} = \int_{-\infty}^{0} B f_B(B) dB \tag{4.19}$$

With increasing A, the second term on the right hand side of eq. (4.12) will become more dominant. This causes the constrained time series to be more and more deterministic in their shape, proportional to the autocorrelation function. In Bierbooms [2006], it is shown that for large A the asymptotic form of eq. (4.12) can be considered to be equal to

$$\begin{aligned} u_{c2}(t) = u(t) &+ r\,(t - t_0)\,(A - u(t_0)) \\ &+ \frac{\dot{r}\,(t - t_0)}{\lambda_\omega} \dot{u}\,(t_0) \end{aligned} \tag{4.20}$$

In this case local extremes rather than local maxima are considered (its unlikely to encounter a local minimum for large A, which allows to omit B).

The gusts resulting from the *New*Gust expression are the same as those selected from a very long stochastic time series generated by e.g. the Veers method (cf. section 3.3.1). The advantage of constrained simulation is the reduction in computation time. The basic assumption behind *New*Gust is that extreme wind gusts can be described by means of Gaussian processes. The main aim of this thesis project is to validate this assumption, which is described in part II. From validation work done by Bierbooms et al. [1999]; Larsen et al. [2003]; Branlard [2009] on the mean gust shape, some interesting conclusions can be drawn:

- In contrast to standards, the mean gust has a rather sharp peak;
- The peak in the mean gust shape is of a universal character;
- The theoretical mean gust shape has to take into account the change of the wind speed spectrum with the mean wind speed;
- A better resemblance is obtained between the theoretical and measured mean gust shape for higher wind speed, sampling frequency and amplitude;
- The gust shapes are independent of terrain;

For more information about these conclusions, the reader is directed to the above mentioned documents.

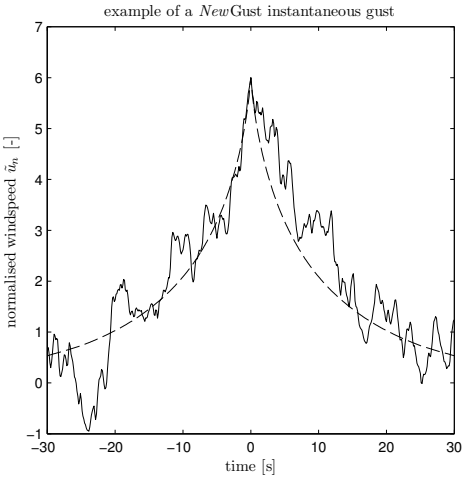

Figure 4.6: Example of an instantaneous *New*Gust gust shape with and without turbulence added.

4.5 Other gust simulation methods

The *New*Gust method described above is not the only method to describe theoretical wind speed gusts. In Nielsen et al. [2004] a gust simulation method is described, which is based upon selection of desired events in a time series with use of a filter function. The filter function contains the constraints of the desired event. By applying certain constraints, wind speed gusts can be simulated. The theoretical description of the mean gust obtained in this way is identical to the *New*Gust description and gives the same type of gusts. It therefore does not add anything to the theory described above. However, this gust description is also defined for non-Gaussian turbulence, which gives the ability to check whether there is a difference between the mean gust shape resulting from Gaussian and non-Gaussian theory or not. The gusts resulting from this method are denoted in this report by Risø gusts.

An extensive mathematical derivation of theoretical Gaussian and non-Gaussian gusts can be found in Nielsen et al. [2004]. The instantaneous Gaussian time series containing a desired Gaussian gust event is

$$\tilde{u}(t) = x(t) + \frac{v_c - (\phi(t), x(t))}{v_c}\tilde{u}_g(t) \tag{4.21}$$

Where $x(t)$ is a Gaussian time series simulated as explained in section 3.3. $\tilde{u}_g(t)$ is the Gaussian ensemble mean gust shape, of which the analytical expression is

$$\tilde{u}_g(t) = v_c \frac{R * \check{\phi}}{(\phi, R * \phi)} \tag{4.22}$$

Where the notation $f * g$ denotes the convolution $\int f(t - t')g(t')dt'$ and (f, g) denotes the inner product $\int f(t)g(t)dt$. The notation $\check{\phi}(t)$ means $\phi(-t)$. In case $\tilde{u}(t)$ should attain some large value v_c at $t = t_0$, the filter function becomes $\phi(t) = \delta(t - t_0)$, which leads to

$$\tilde{u}_g(t) = v_c \frac{R(t - t_0)}{R(0)} = Ar(t), \quad t_0 = 0 \tag{4.23}$$

Where v_c is a certain (large) value, which is identical to A in the *New*Gust expression. $\delta(\cdot)$ is the Dirac function. The expression of the mean gust given here is identical to the mean

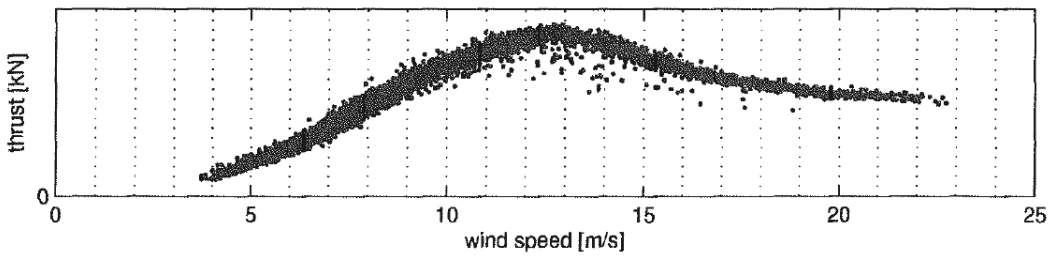

Figure 4.7: Evolution of the thrust with the incoming mean wind speed (taken from Branlard [2009]).

gust resulting from the second *New*Gust expression (eq. 4.20). When implemented in the expression for the instantaneous time series (eq. 4.21) exactly the same theoretical expression as equation (4.20) is obtained [Nielsen et al., 2004, Appendix F].

For the derivation of the non-Gaussian wind speed gust, the same theory as explained in section 3.3.2 is used. For the mathematical derivations of the following theoretical expressions, the reader is directed to Nielsen et al. [2004, Ch. 6]. The ensemble average non-Gaussian gust according to the filter function $\phi(t) = \delta(t_0 - t)$ is

$$\tilde{u}_g(t) = g\left(g^{-1}(v_c)\frac{R(t_0 - t)}{R(0)}\right) \tag{4.24}$$

Where g denotes the transformation function as explained in section 3.3.2. The resulting instantaneous non-Gaussian time series containing the specified gust event is

$$\tilde{u}_r(t) = \tilde{u}(t) - g\left(g^{-1}(v_p)\frac{R(t_0 - t)}{R(0)}\right) + g\left(g^{-1}(v_c)\frac{R(t_0 - t)}{R(0)}\right) \tag{4.25}$$

Where $\tilde{u}(t)$ is a non-Gaussian time series simulated as explained in section 3.3.2. $v_p = \int \phi(t)\tilde{u}(t)dt$, which is equal to $\tilde{u}(t_0)$ for $\phi(t)$ being a Dirac function as given above. v_c is in this case the desired amplitude of the gust in the non-Gaussian time series. In section 7.3 the practice of numerical simulation of these gusts is explained.

4.6 Load response to a wind gust

In Bierbooms [2006, 2005] research has been done on the extreme loads of wind turbines. It appears that stall regulated wind turbines (fixed blades) are significantly effected by extreme wind speed gusts. This is not, however, the case for pitch regulated wind turbines, due to pitch actions initiated by the control system. Pitch regulated wind turbines are assumed to be more sensitive to extreme rise time gusts than to extreme amplitude gusts. This is shown, for instance, in Branlard [2009, Ch. 8], where a study was performed on the load response of a pitch regulated wind turbine to a wind speed gust. Figure 4.7 shows that for above rated mean wind speeds, a negative wind gust (below mean wind speed) causes the loads to increase and for a positive wind gust to decrease. This is the opposite for below rated mean wind speeds. For stall regulated wind turbines, the thrust always increases with wind speed, so maximum amplitude wind speed gusts are more dangerous for this kind of turbines then for pitch regulated ones. However, in Bierbooms [2005] a preliminary conclusions is drawn that extreme rise time gusts at above rated wind speed do not lead to extreme loads of pitch-regulated wind turbines. Section 10.1 investigates which wind speed gust type leads to the extreme load response of pitch-regulated wind turbines.

4.6.1 Determination of extreme loads with use of *New*Gust

One of the goals behind analyzing atmospheric wind is to find the extreme load response of a wind turbine with a return period of 50 years. This extreme load then should represent the worst load case a wind turbine has to deal with during its working life time. Just like explained in section 2.4, the tails of the load response cdf are of importance for a good estimation of the 50 year load response. Neither the amount of wind speed data nor the amount of load response data is available to get a proper estimation of the cdf tail. To compensate this lack of data, simulations can be done to obtain the required amount of data. By applying constrained stochastic simulation (cf. section 4.4) the number of simulations needed to arrive at the extreme 50-years load response can be reduced [Bierbooms, 2008, 2009b]. By simulating a number of gusts with a certain amplitude A and mean wind speed $\bar{u}$, a conditional distribution of the maximum load resulting from these gusts can be obtained;

$$f(l_{max}|\bar{u},A) = \frac{f(l_{max},\bar{u},A)}{f(\bar{u},A)} = \frac{dF(l_{max}|\bar{u},A)}{dl_{max}} \tag{4.26}$$

By inserting eq. (4.26) in eq. (4.27), the distribution of extreme loads can be derived in a similar way as has been done in section 2.4:

$$F(l_{max}) = \int_{-\infty}^{l_{max}} \int_{-\infty}^{\infty} \int_{-\infty}^{\infty} f(l_{max},\bar{u},A)\, dA\, d\bar{u}\, dl_{max} \tag{4.27}$$

$$F(l_{max}) = \int_{-\infty}^{l_{max}} \int_{-\infty}^{\infty} \int_{-\infty}^{\infty} f(l_{max}|\bar{u},A) f(\bar{u},A)\, dA d\bar{u}\, dl_{max} \tag{4.28}$$

$$F(l_{max}) = \int_{-\infty}^{\infty} \int_{-\infty}^{\infty} F(l_{max}|\bar{u},A) f(\bar{u},A)\, dA\, d\bar{u} \tag{4.29}$$

In [Bierbooms, 2008] a slightly different method is used, which requires the assumption of independent[3] A and $\bar{u}$, which then gives that $f(\bar{u},A) = f(\bar{u})f(A)$. Eq. (4.29) can than be rewritten as

$$F(l_{max}) = \int_{-\infty}^{\infty} f(\bar{u}) \int_{-\infty}^{\infty} F(l_{max}|\bar{u},A) f(A)\, dA\, d\bar{u} \tag{4.30}$$

which is equal to the method used by [Bierbooms, 2008, 2009b]. In these latter papers it is reasoned that the simulated gusts represent ten-minute maxima and that the obtained distribution is thus constructed from ten-minute extreme loads. The probability for the 50-years extreme load F_{50} can be derived from the following equation,

$$F_{50} = 1 - \frac{1}{T_{50}} \tag{4.31}$$

where T_{50} is the 50-years return period, in this case equal to the number of ten minutes in 50 year. In section 10.1.3 this theory has been applied.

[3] If random variables are independent, then they are uncorrelated. However, uncorrelated variables are only necessarily independent for Gaussian random variables [Papoulis and Pillai, 2002, Theorem 6-5]. If random variables are independent, then $\langle g_1(z_1)\cdots g_n(z_n)\rangle$ equals $\langle g_1(z_1)\rangle\cdots\langle g_n(z_n)\rangle$ [Papoulis and Pillai, 2002, Ch. 7-1]. In section 9.3.4 this has been applied to the random variables $\bar{u}$ and A.

4.6.2 Determination of extreme loads with use of *Load*Gust

Instead of using *New*Gust to derive the distribution function of the maximum loads, also another expression can be used. In Bierbooms [2007] an expression is derived to obtain a gust leading to an extreme in the load response.

$$\begin{aligned} u_c(t) = u(t) &+ \frac{1}{\Delta}\left(\dddot{R}_{ll}(0)R_{uu}(t+\delta) - \ddot{R}_{ul}(\delta)\ddot{R}_{lu}(t)\right)(A - u(-\delta)) \\ &- \frac{\dot{R}_{lu}(t)}{\ddot{R}_{ll}(0)}\dot{l}(0) \\ &+ \frac{1}{\Delta}\left(-\ddot{R}_{ul}(\delta)R_{uu}(t+\delta) + R_{uu}(0)\ddot{R}_{lu}(t)\right)(B - \ddot{r}(0)) \end{aligned} \tag{4.32}$$

With $\Delta = R_{uu}(0)\dddot{R}_{ll}(0) - \ddot{R}^2_{ul}(\delta)$. In case the load response $l(t)$ is defined by a linear system, the expression for the load response can also be derived.

$$\begin{aligned} l_c(t) = l(t) &+ \frac{1}{\Delta}\left(\dddot{R}_{ll}(0)R_{ul}(t+\delta) - \ddot{R}_{ul}(\delta)\ddot{R}_{ll}(t)\right)(A - u(-\delta)) \\ &- \frac{\dot{R}_{ll}(t)}{\ddot{R}_{ll}(0)}\dot{l}(0) \\ &+ \frac{1}{\Delta}\left(-\ddot{R}_{ul}(\delta)R_{ul}(t+\delta) + R_{uu}(0)\ddot{R}_{ll}(t)\right)(B - \ddot{r}(0)) \end{aligned} \tag{4.33}$$

In these equations, R_{ll} and R_{uu} are the autocorrelation function of respectively the load response and the wind speed. R_{lu} is the cross-correlation function between the load response and the wind speed. δ denotes the time delay between the extreme in the wind speed and in the load response. It has been chosen such, that $\dot{R}_{lu}(\delta) = 0$, which ensured that $R_{lu}(-\delta) = R_{ul}(\delta)$ is a local extreme and $l_c(0)$ is a local maximum [Bierbooms, 2007]. Equation (4.33) is therefore denoted with *Load*Gust. The cross- and autocorrelation function of wind speed and load response can be derived from the spectrum of the wind speed S_u and the transfer function H; if $\cdot^*$ denotes the complex conjugate, then $S_{lu} = H^* S_{uu}$; and $S_{ll} = |H|^2 S_{uu}$. From these spectra, the correlation functions can be derived as described in section 3.2.2. The probability of B can be obtained in the same way as described in section 4.4, with this difference that μ_0 and σ_0 are defined as

$$\mu_0 = A\frac{\ddot{R}_{ul}(\delta)}{R_{uu}(0)} \tag{4.34}$$

$$\sigma_0 = \dddot{R}_{ll}(0) - \frac{\ddot{R}^2_{ul}(\delta)}{R_{uu}(0)} \tag{4.35}$$

In section 10.1.3 this theory has been applied.

Part II

Validation of *New*Gust

Chapter 5

Validation procedure

In the preceding chapters, the theoretical background of turbulence and wind gusts has been explained. Since the theory has been defined, it can be used to validate the assumption of Gaussian distributed turbulence in atmospheric wind, made in the derivation of the *New*Gust mean gust shape (explained in section 4.4). From former validation done on this method, it can be concluded that the effect of non-Gaussian distributed turbulence does not make a big difference in the mean gust shape.

> *The theoretical mean gust shape has been verified by means of simulated and measured wind data. The resemblance between the theoretical and experimental curves is good, in particular for the shape in time. [Bierbooms et al., 1999]*

> *The theoretical expression for the mean gust shape is verified by comparison with simulated wind fields as well as with full scale measured wind fields related to different wind climate conditions. ...No significant tendencies of terrain dependent gust shapes are identified. ...For the comparison between the model prediction and the simulated wind field, where the ACF is known a priori, the resemblance between "measured" and predicted gust shapes is good for the investigated gust amplitudes and mean wind speeds. [Larsen et al., 2003]*

The probability of gust occurrence has been verified by Bierbooms et al. [2001]. *New*Gust is developed to compute loads resulting from wind gusts in the same stochastic manner as has been common practice for fatigue loading for a long time [Bierbooms et al., 1999; Bierbooms, 2006] (cf. also section 4.4). However, resemblance of only the mean gust shape is not enough to conclude that the resulting loads will not show any difference between the theoretical and physical gusts either. Therefore, it is necessary to verify if there is a difference between mean load responses resulting from theoretical and physical gusts. If there is a difference, it should be determined whether it is due to the assumption of Gaussian distributed turbulence or to something else.

The procedure which has been used for the validation can be found in figure 5.1. First of all, data of measured wind speed has to be acquired. This data is analysed for wind speed gusts and used as the bases for simulations of *New*Gust gusts and non-Gaussian time series[1]. The gusts, load responses, spectra and probability distributions are compared for each type of gust (measured, *New*Gust, non-Gaussian).

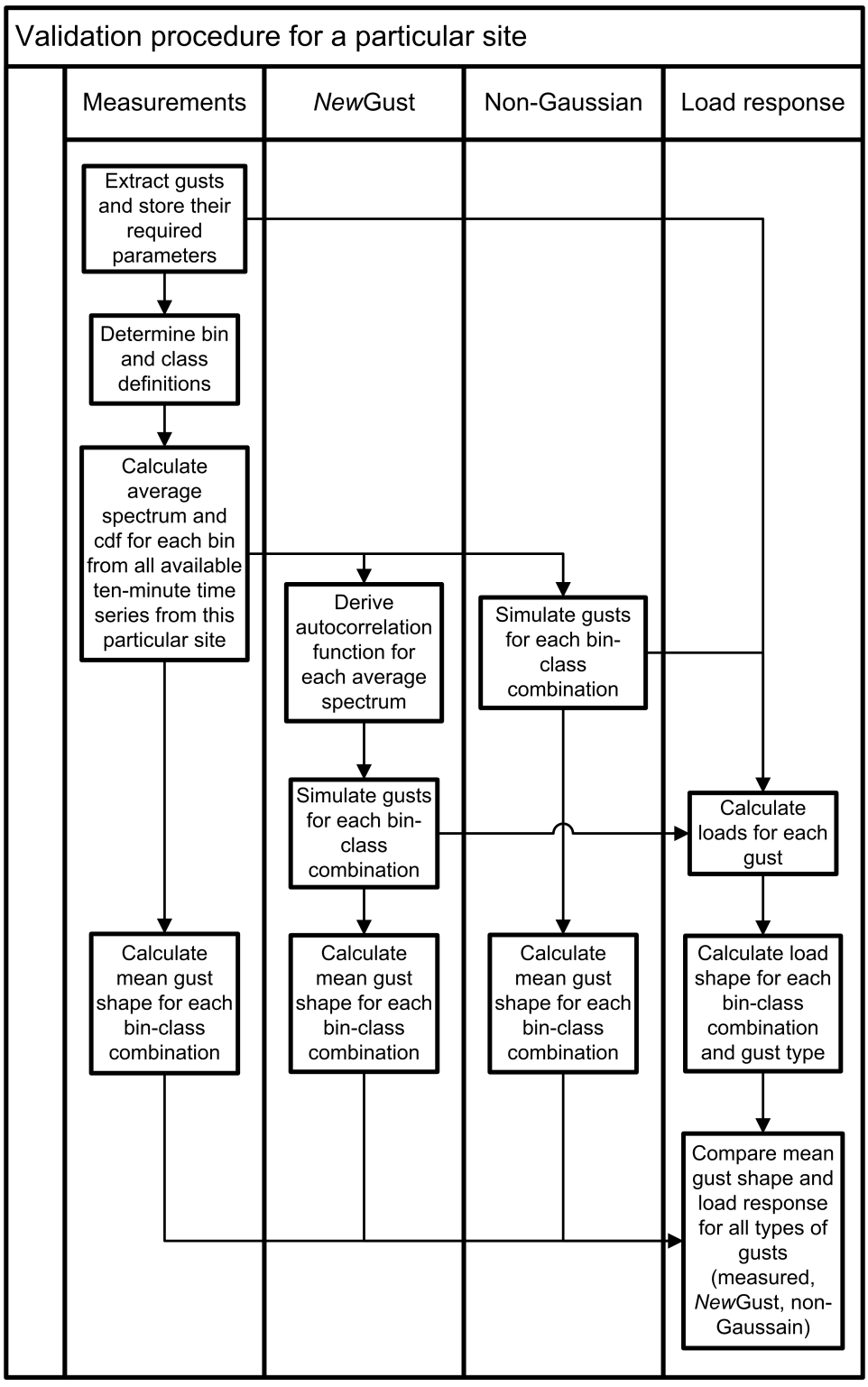

Figure 5.1: Procedure for validating *New*Gust

In the following chapters, the practical considerations as well as all decisions made with respect to the validation are explained. The necessary data processing for the validation procedure has been done with MATLAB.

[1]Someone might question the value of validating a model based on measurements of the past; Who does guarantee that observations from past events will give the same results in the future? The answer lies in one of the very basic assumptions behind physical science. Expecting a model, confirmed by measurements from the past, to represent the behavior in future, is only allowed because of the assumption that there is some continuity in the physical behaviour of natural processes. This assumption of continuity can be observed if physics, e.g. atmospheric wind, are measured as a spatial quantity, which in the case of wind reduces the complex overall physical feature of wind to wind speeds.

The validity of a model based upon observations from the past is hence only sufficient for situations where the future behaviour of the measured physical quantity, the model describes, is expected to be equal to its behaviour in the past. This clearly shows the limited validity of the validation work done in the context of this thesis project.

Chapter 6

Data analysis

In this chapter the process of data analyses and related topics are described. The goal of data analysis in the context of this thesis is (1) to acquire sequences of measured wind gusts, and (2) to obtain spectra, autocorrelation functions and spectral moments of the actual turbulence on a specific site. In appendix H detailed flowcharts of the whole analysis process can be found.

6.1 Data acquisition

To reach these goals, time series of measured wind speed have been obtained from the internet database "Database of Wind Characteristics". In this database, more than 172000 hours of high sampled meteorological data from as many as 60 sites is available. To be able to make a rational selection of data, appropriate for the purpose of this project, the following pre-requirements are used:

- The sampling frequency should be at least 5 Hz, to be able to make accurate load calculations;
- The measuring wind speed sensor should be at least at a height of 40 meters, to be of relevance for today's wind turbine rotor heights;
- The measurements should contain enough data on a broad range of wind speeds. A time span of at least 400 hrs distributed on approximately 5 – 20 m/s is required, to be able to select enough gusts to calculate a qualitatively good mean;
- In order to make the validation as broad as possible, data has been acquired for three sites with different types of terrain and orography. These are: offshore, flat; scrub, hill and pastoral, flat.

According to these requirements, the following three sites are selected:

Toboel: Measurements from a meteorological met-mast situated at Toboel site, Ribe, Denmark. This is a place in the south-west of Denmark, east of Esbjerg. Its coordinates are: 55° 25' 51.96" N, 8° 52' 4.95" E. The surroundings are classified as a flat landscape, with open fields and meadows. The wind speed measurements are conducted with a sonic Gill anemometer at a height of 49 m. The time series are stored with a frequency of 8 Hz. For the analysis 12000 ten-minute time series are used from this site (equivalent to $\sim$ 83 days). The data is divided over the years 1999 (day 306 – 355) and 2000 (day 28 – 182)[1].

Horns Rev: Measurements from a meteorological met-mast from the offshore wind farm Horns Rev, Esbjerg, Denmark. The met-mast is located at a reef approximately 18 km off Jutland in the North Sea in a very harsh environment. The water depths at the site vary between 6 and 12 m. Its coordinates are: 55° 30' 0" N, 8° 0' 0" E. The surroundings are classified as offshore (open sea) with a flat landscape. The wind speed measurements are conducted with a 3-D sonic METEK anemometer at a height of 50 m above sea level. The time series are stored with a frequency of 12 and 20 Hz. During the analysis it appeared that the 20 Hz data of Hornsrev is corrupt (cf. appendix G). Hence, the 12 Hz data has been used. For the analysis 40830 ten-minute time series are used from this site (equivalent to $\sim$ 284 days). The data is divided over the years 2001 (day 290 – 365), 2002 (day 1 – 114, 315 – 363) and 2003 (day 1 – 148, 338 – 362).

Oak Creek: Measurements from a meteorological met-mast situated in Oak Creek, near Tehachapi, California. The wind farm consists of wind turbines erected on a ridge in a very complex terrain with high wind speeds. Its coordinates are: 35° 2' 32.64" N, 118° 22' 5.54" W. The surroundings are classified as rolling hills, with open bushes and small trees. The wind speed measurements are conducted with a sonic anemometer at a height of 80 m. The time series are stored with a frequency of 8 and 16 Hz. For the analysis 14993 ten-minute time series of the 16 Hz data are used from this site (equivalent to $\sim$ 104 days). The data is divided over the years 1998 (day 167 – 365), 1999 (day 7 – 162) and 2000 (day 199 – 309).

6.2 Data conditioning

For each of the sites described above, a drawing of the met-mast can be found in appendix F. The data of each selected site is stored in ten-minute time series on the ftp server of "http://www.winddata.com". Before storage, the following screening has been applied by "Database on wind characteristics" [taken from Hansen and Larsen, 2001], to ensure a reasonable and documented data quality:

1. $\sigma > 0.0$: to ensure that only active signals are registered and used in the database;
2. $|\text{max-min}| < 6\sigma$: to ensure that extreme ranges correspond to "something" like a normal distribution - failure in this check item indicates possible spikes;
3. normalized statistical fourth order moment is calculated and range checked (>1.5 and < 5.0);
4. normalized statistical sixth order moment is calculated and range checked (>8.0 and $<$ 20.0);
5. signal minimum and maximum values are checked according to specified instrument upper and lower measurement values. Note, that the instrument upper and lower measurement values are entered through the master sensor table;
6. detection of possible (signal) noise;
7. detection of possible (signal) spikes;
8. detection of possible (signal) level jumps.

[1]This is only a rough indication of the time span, not all days are (completely) included, mainly because of the data conditioning and the requirement for normal wind turbine operating conditions ($\bar{u} \leq 25$ m/s).

These screening criteria can be used to select proper data. For this thesis, the first, fifth, sixth and seventh criteria are used, to avoid distortion of the spectrum. For Sonic anemometer signal co-ordinate transformations, the standard Risø alignment procedure for sonic signals is used. This means that the unaligned (x,y,z) co-ordinate system is transformed to a second orthogonal system (u,v,w) where the u vector points in the direction of the mean flow; and hence the mean speeds in the v and w directions are zero. The sonic component $s = \sqrt{u^2 + v^2}$ has been used for this research. The ten-minute time series are downloaded and stored on a local disk. For analyzing purposes, only the data series of the required measurement height is extracted and stored with a follow-up number depending on the measurement date of the time series. It appeared that the Toboel measurements were not checked for the fifth criteria, because no information about the instrument's upper and lower values is available. To exclude some extreme data for Toboel, further selection criteria are placed on the standard deviation ($\sigma < 4$) and the kurtosis ($-2 < \mathcal{K} < 8$). Before analyzing the ten-minute time series for gusts, the data has been conditioned by (1) removal of a linear trend and (2) normalization to $\tilde{u}_n(t)$ as described in section 4.2.

6.3 Extracting gusts

As already explained in chapter 5, extraction of gusts from measured wind speed time series is necessary to have a reference mean gust shape. The simulated mean wind gusts and their mean load response should resemble this reference mean gust shape and its resulting mean load shape. In section 4.3 a number of detection methods for wind gusts are given. As already explained there, these definitions can be used to detect gusts in a data sequence. In Branlard [2009] an extensive comparison has been made between the resulting mean gusts of each method. It appears that for the purpose of this analysis, the peak over threshold method has several advantages over the other methods:

- the POT method is not sensitive for the shape of a gust;
- it is independent of the duration of the gust compared to other methods;
- several gusts within a certain time-frame can be detected;
- it is in line with former research done on *New*Gust [Bierbooms et al., 1999; Bierbooms, 2006; Larsen et al., 2003].

The POT method used in this analysis is slightly different from the method used by Branlard [2009]. Instead of extracting for each gust a specific time around the peak of the gust, a fixed time τ of 60 seconds is extracted for each gust. Branlard [2009] correctly says that by using a fixed time, parts of the gusts are left out and that for a large part of the gusts only their extreme is taken into account. But according to Larsen et al. [2003] it is only this extreme part which is of importance (for validation of *New*Gust). The time period of 60 seconds has been chosen to make a compromise, because most gusts are of shorter duration. The time period of 60 seconds is in agreement with the maximum time period used by "Database on wind characteristics" to detect wind speed gusts [Hansen and Larsen, 2001, p. 20-21]. The POT method is roughly programmed as follows:

1. subtraction of the mean and removing the trend of the ten-minute time series $u(t)$. This ensures that the procedure 'sees' stationary turbulence;

2. weighing each data point, by moving a window of $\tau/2$ (30 seconds) over the whole ten-minute time series (cf. figure 6.1). The maximum data point in the window is weighted

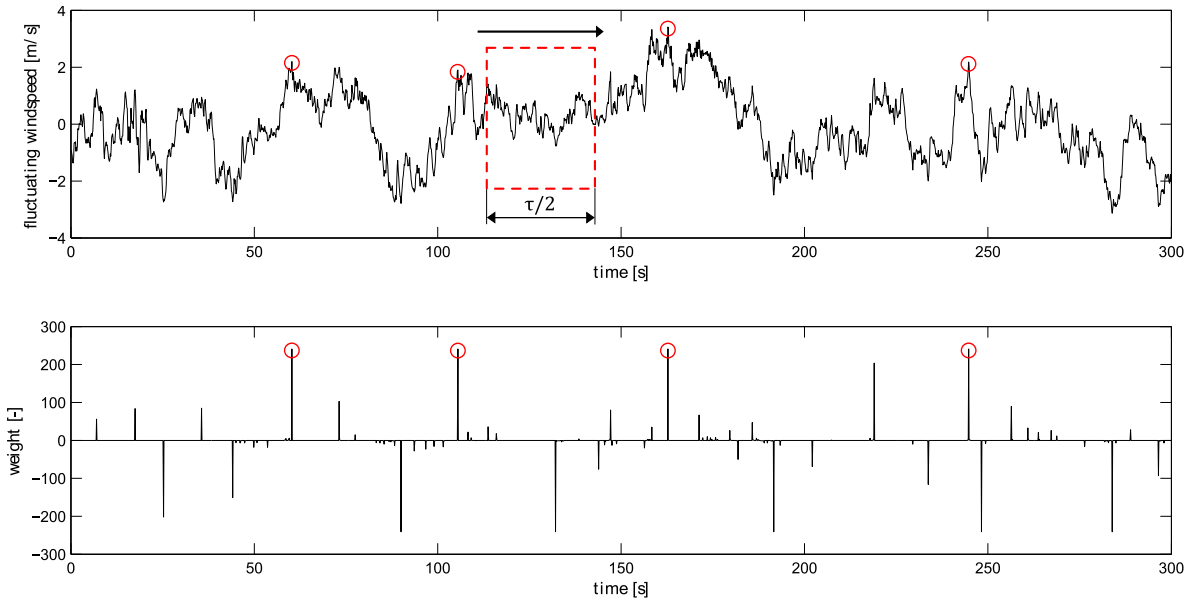

Figure 6.1: Peak over threshold method, weighing each data point in a time series with a moving window.

+1 and the minimum -1.

$$u(t_{max}) = \max\left(\tilde{u}(t)\right), \quad t \in t, \ldots, t + \tau/2 \tag{6.1}$$

$$u(t_{min}) = \min\left(\tilde{u}(t)\right), \quad t \in t, \ldots, t + \tau/2 \tag{6.2}$$

$$w(t) = w(t) \pm 1, \quad t = t_{max}, t_{min} \tag{6.3}$$

3. If a data point is the maximum for the whole gust time period τ, it will have a weight of $w = f\frac{\tau}{2} + 1$ and is defined as the center of a gust.

Gusts are extracted if (1) their amplitude ratio is above a minimum of $\tilde{u}_n(t) = 1$, to detect only gusts larger than the standard deviation and (2) the peak of the former gust is at least a distance τ away from the peak of the present gust. This more or less ensures independent gusts.

After all gusts are detected for all ten-minute time series, each gust is classified in a certain bin-class of mean wind speed and amplitude ratio (cf. table 6.1). These bins and classes are specifically defined for each site and depend on the number of gusts which could be detected for each bin-class. At least ~ 50 gusts are needed to construct a qualitatively good mean gust shape [Larsen et al., 2003]. Thus, a minimum of 50 gusts is used to restrict and define the number of bin-classes. For each bin-class the ensemble average is calculated. To be able to do the classification, to reconstruct the origin of each gust and to find each gust in the local database, the following properties are stored for each gust:

- index of the ten-minute time series;
- index of the gust (within the ten-minute time series);
- time of the maximum of the gust in the ten-minute time series;
- ten-minute mean;
- ten-minute standard deviation;

Toboel		Horns Rev		Oak Creek		
bin [m/s]	class [-]	bin [m/s]	class [-]	bin [m/s]	class [-]	index
0-5	1-1.5	0-2	1-1.5	0-1	1-1.5	1
5-6	1.5-2	2-3	1.5-2	1-2	1.5-2	2
6-7	2-2.5	3-4	2-2.5	2-3	2-2.5	3
7-8	2.5-3	4-5	2.5-3	3-4	2.5-3	4
8-9	3-3.5	5-6	3-3.5	4-5	3-3.5	5
9-10	3.5-6	6-7	3.5-6	5-6	3.5-6	6
10-11		7-8		6-7		7
11-12		8-9		7-8		8
12-13		9-10		8-9		9
13-14		10-11		9-10		10
14-15		11-12		10-11		11
15-16		12-13		11-12		12
16-17		13-14		12-13		13
17-19		14-15		13-14		14
19-22		15-16		14-15		15
22-30		16-17		15-16		16
		17-18		16-17		17
		18-19		17-18		18
		19-20		18-19		19
		20-21		19-20		20
		21-30		20-21		21
				21-22		22
				22-23		23
				23-24		24
				24-25		25
				25-26		26
				26-30		27

Table 6.1: Definitions of wind speed bin and gust amplitude class.

- amplitude ratio;
- B at the gust maximum;
- bin index;
- class index.

The mean and standard deviation have been calculated with the MATLAB comments `mean` and `std`. The second time-derivative at the maximum of each gust (B) has been calculated by

$$\frac{d^2\tilde{u}(t_0)}{dt^2} = \frac{\tilde{u}(j+1) - \tilde{u}(j) + \tilde{u}(j-1)}{\Delta t^2} \tag{6.4}$$

Where j indicates the position of the gust maximum in the time series and Δt is the time step between each data point.

6.4 Probability density function

For the simulation of non-Gaussian distributed turbulence time series cumulative distribution functions are required (cf. section 3.3.2). For each measured time series, the cdf has been estimated with use of the MATLAB function `ksdensity`. This function uses kernel smoothing based on a Gaussian kernel function to estimate the cdf. The bandwidth of the kernel smoothing-window is a function of the number of points in the time series and is optimal for the Gaussian kernel function. For each bin the ensemble average distribution is calculated. To be able to do the classification, to reconstruct the origin of each distribution and to find each distribution in the local database, the following properties are stored for each distribution:

- index of the ten-minute time series;
- ten-minute mean;
- ten-minute standard deviation;
- ten-minute skewness;
- ten-minute kurtosis;
- bin index.

For the multi-variate probability density functions presented in chapter 9, the MATLAB function `gmdistribution` has been used. This function uses the Expectation Maximization algorithm to obtain the maximum-likelihood estimates of the parameters in a Gaussian mixture model. The skewness and kurtosis have been calculated with the MATLAB commands `skewness` and `kurtosis`.

6.5 Estimating spectra

Estimating spectral density and autocorrelation functions is necessary to simulate turbulence with the same characteristics as the turbulence measured on a specific site (cf. section 3.3). The goal of spectral density estimation is to estimate the spectrum from a finite sequence of time samples. This is basically done by converting a signal from time domain to frequency domain by discrete Fourier transforms (cf. section 3.2.1). Many possible methods exist for estimating the spectral density. A common method is the Welch method of averaged periodograms, which is computationally one of the most efficient methods [Jokinen et al., 2000]. Although this method is available in the library of MATLAB, it has been specifically programmed to meet the needs of estimating atmospheric spectra[2]. For each ten-minute time series the spectrum is estimated. The obtained spectra are classified according to the wind speed bins defined for the gusts (cf. table 6.1). Classification according to classes of amplitude ratio is avoided by normalizing the spectrum to unit variance. For each bin, an average spectrum is defined as the ensemble average of all spectra in that bin. The followed procedure for estimating the spectra is:

1. Removal of the trend and the mean from the original time series $u(t)$;
2. Windowing of the resulting time series $\tilde{u}(t)$;

[2]The purpose of spectral analysis in MATLAB is to identify distinct peaks at certain frequencies. In such a case, an accurate representation of the total variance is not of great importance. The reason for this can be found in the history of MATLAB, since it was originally designed for control engineering. For representation of atmospheric turbulence, the variance of the spectrum is very important. Less or more variance would mean less or more turbulence than actually exists in the physical wind where the spectrum results from.

3. For $\tilde{u}(t)$ the two-sided periodogram is computed by $P = |FFT(U)|^2$;
4. The resulting periodogram is corrected for the use of a window by dividing P by the periodogram of the window function;
5. The one-sided periodogram is derived from the two-sided periodogram by $P(f) = 2P(f)$ for $f = \Delta f \ldots f_N$, where f_N is the Nyquist frequency[3];
6. The spectral density is calculated by $S = \frac{P}{\Delta f}$;
7. The spectral density is normalized to unit variance by $S_n = \frac{S}{\sigma_{\tilde{u}}^2}$.

The perceptive reader might notice that this is not exactly the Welch method, because no overlap of windows is used. This is justified by the fact that overlap reduces the frequency resolution of the resulting spectrum. A reduction in the frequency resolution is not desired, because for simulating turbulence with the same frequency as the measured data, a spectrum with the same frequency resolution as the data is required to avoid interpolation (cf. section 3.3). This method of spectrum estimation only differs from the Bartlett method, because of a window function, which is characteristic for the Welch method [see e.g. Wikipedia, 2009a,d]. The trend removal has been done to prevent distortion of the spectrum by red noise. The window function[4] is used to reduce the problem of leakage which arises from a sharp truncation of the data sequence. The use of a ten-minute time series for the estimation of the spectrum is in effect the same as multiplying an infinite time series by a square window function with a length of ten minutes. The reason for leakage is that the square window function turns on and off so rapidly. Its Fourier transform therefore has substantial components at high frequencies, to be able to follow the square window function. The resulting noise in the spectrum is reduced by multiplying the finite sequence by a smoother window function before conversion to frequency domain. In this way, the sequence is truncated gradually rather than abruptly.

Since many windows have been developed it is difficult to select one. The principal trade-off is between making the central peak as narrow as possible versus making the tails of the distribution fall off as rapidly as possible (in frequency domain). Effective window widths are of the order of $T/2$ (T is the total sampling time). In general, the advantages of windows whose rise and fall time are only fractions of the data length are minor or nonexistent, and such small window widths should thus be avoided [Press et al., 1992]. To reduce the effect of unequal weighing of the data by the window, a proper choice of overlapping is required. Jokinen et al. [2000] shows that for the Blackman and Hann window an overlap of at least respectively 80% and 66.7% is required to reduce this unequal weighing and resulting incorrect variance. From the results of this latter paper, the Hann window would be chosen. But as already explained above, overlap has unwanted effects on the frequency resolution. To avoid the unequal weighing of the data points and maintain the positive tapering effect of a window function, the window function is only applied to the initial and final 10% of the sequence[5]. This is in agreement with the method for estimating spectra of atmospheric

[3] It never makes sense to obtain the spectral density of a sampled function outside of the Nyquist interval since, according to the sampling theorem, there spectral power will have been aliased into the Nyquist interval [see e.g. Press et al., 1992; Stull, 1988]. The sampling theorem indicates that a continuous signal can be properly sampled, only if it does not contain frequency components above one-half of the sampling rate [Smith, 1997].

[4] In signal processing, a window function is a function which is zero-valued, or goes sufficiently rapidly toward zero, outside of a chosen interval. When a data signal is multiplied by the window function, the product is a zero-valued signal outside the chosen interval. Typical window functions are non-negative smooth "bell shaped" curves. Selecting a finite time series is the same as multiplying an infinite run of sampled data by a window function which is unity during sampling time T and zero everywhere else (a square window function).

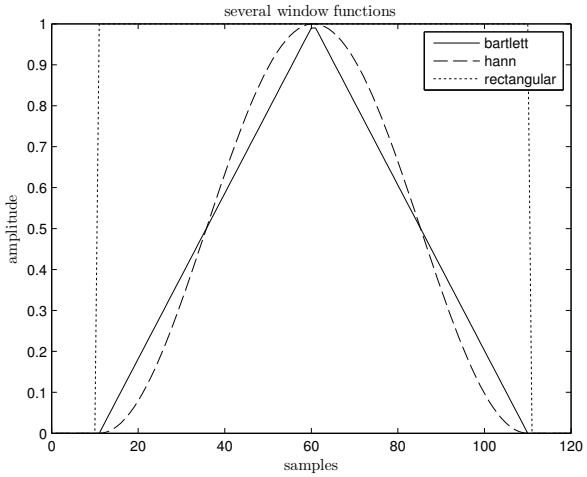

Figure 6.2: Example of several window functions.

turbulence described by Stull [1988]. The noise reduction in the spectrum, which is another advantage of using overlapping window functions is gained by ensemble averaging the spectra per wind speed bin.

The spectral density function is normalized with the variance of the time series $\tilde{u}(t)$ instead of dividing by the area of the spectrum. In this way it provides a measure of how well the estimated spectrum represents the variance of the original time series $\tilde{u}(t)$. For example, the average spectrum with a window function applied to the full time series shows a normalized variance of 1.02, compared to a normalized variance of 1 for the average spectrum with a window function applied only to the ends of the sequence (which is in agreement with Jokinen et al. [2000]). In some cases, the time series appeared to be a bit shorter than ten minutes, these time series are extended with zeros to the required length. To be able to do the classification and to find back the statistic properties of each spectrum, the following properties are stored for each spectrum:

- index of the ten-minute time series;
- ten-minute mean;
- ten-minute standard deviation;
- bin index;
- class index.

For each mean spectrum, a least squares fit has been made with Eq. (3.8). This has been done to represent the real turbulence as much as possible. The estimated spectra show a smoothing behaviour at the high frequencies, which is due to the estimation procedure and not a feature of the real turbulence (cf. appendix G). See e.g. Kaimal et al. [1989] for an interesting reading about the effect of finite sampling on atmospheric spectra.

[5]This type of window function is not available in the MATLAB library, for the same reasons as why the standard Welch method from MATLAB could not be used.

6.6 Deriving autocorrelation functions and spectral moments

For each average spectrum, an autocorrelation function has to be derived for the simulation of *New*Gust gusts. This can be done by inverse Fourier transforms, as already shown in paragraph 3.2.2. In practice, this is basically done in three steps:

1. smoothing the cut-off of the spectrum;
2. applying an inverse Fourier transform;
3. shifting the zero-frequency component to the center of the acf.

The smoothing of the spectrum cut-off is done to prevent oscillatory behaviour of the resulting autocorrelation function. The smoothing is done by multiplying the spectrum with a window function which gradually goes from one to zero. After this smoothing, the spectrum is renormalized to its original variance. The effect can be seen in the derivatives of the acf, of which an example is shown in figure 6.3. For the *New*Gust expression a double-sided auto-

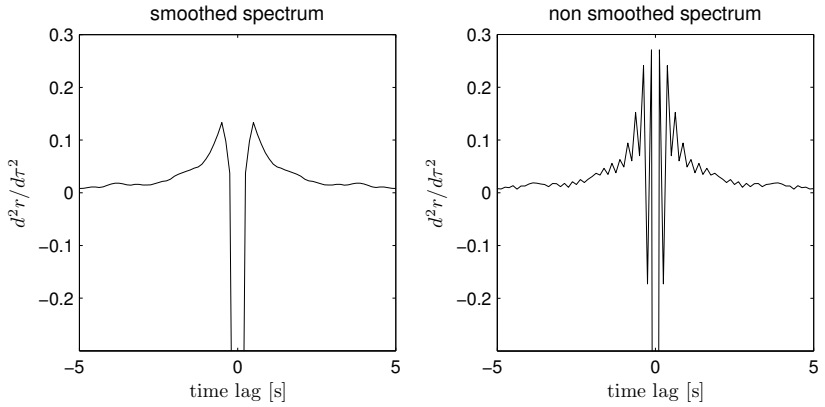

Figure 6.3: The effect of smoothing the spectrum on the second derivative of the acf.

correlation function is required. The estimated spectra are one-sided, but in order to derive a two-sided acf, a two-sided spectrum is required. This requirement is fulfilled by assuming a symmetric two-sided spectrum S_2, which can be constructed from the physical one-sided spectrum S_1 by assuming an artificial double-sided symmetric spectrum. To maintain the correct variance, the spectral values are multiplied with a factor 1/2 (cf. figure 6.4). This

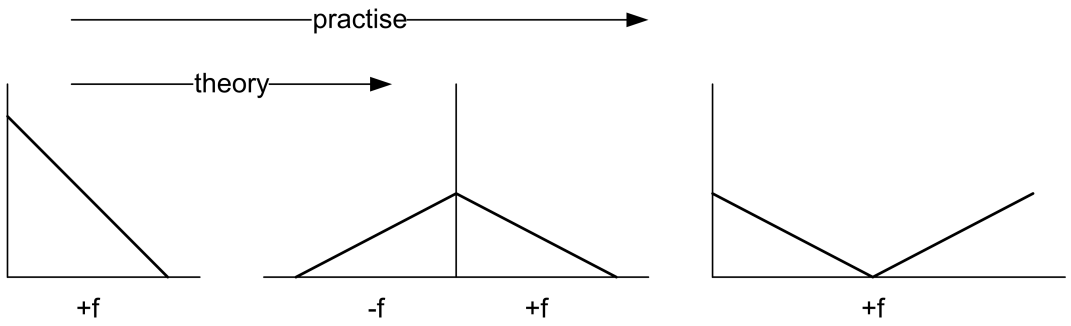

Figure 6.4: construction of an artificial double sided spectral from a physical one-sided real spectrum.

is allowed, because the spectrum results from a stationary time series. The inverse Fourier

transform of the resulting double-sided spectrum is taken to obtain the acf. As a result of the operation shown in figure 6.4, the negative frequency components are on the wrong side of the acf and should be shifted towards the left hand side of the acf, to get the correct shape (cf. figure 6.5). The acf is normalized by dividing it by the variance of the spectrum. The

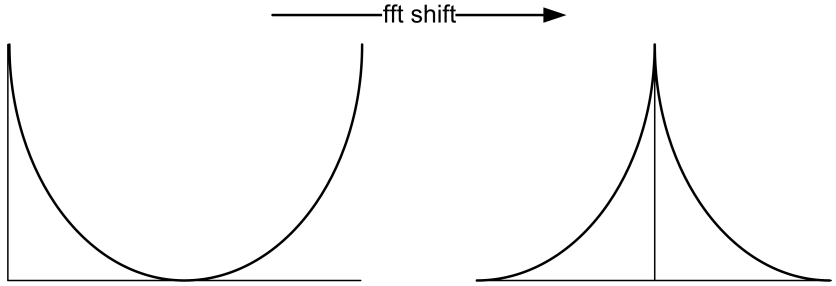

Figure 6.5: Application of a `fftshift` to obtain a zero-centered autocorrelation function.

equation used to derive the spectral moments from the spectrum is given in section 3.2.3. To be consistent, the spectrum is conditioned in the same manner as for the derivation of the acf.

Chapter 7

Simulating turbulence and gusts

The theory regarding simulation of turbulence and gusts is explained in section 3.3 and 4.4. In this chapter the practical side of programming these simulation methods into MATLAB is described. Gaussian distributed turbulence time series has been simulated exactly as described in section 3.3.1. The required spectra are obtained as described in section 6.5. The cut-off of the spectrum is done as in section 6.6. This is necessary in order to be consistent with the derivation of the acf, which is used in the simulation of *New*Gust.

7.1 Non-Gaussian turbulence

For the simulation of non-Gaussian gusts, a Gaussian distributed turbulence time series, a target spectral density and a cumulative distribution function is required. The time series are simulated as described above; target spectrum and cdf are obtained as described in respectively section 6.5 and 6.4. The cdf mapping and iterative procedure for seeking the underlying Gaussian spectrum are implemented as described in section 3.3.2. Note that for the cdf-mapping the empirical cdf of the measured and simulated data is used, which requires interpolation (no theoretical cdf is used). The requirement on the mean square error (mse) has been set as the average mse between the instantaneous spectra and their corresponding fitted average spectra. It appeared that this varied from 5.5 – 1.8 for Oak Creek. One to three iterations are enough to meet the required mean square error. For the simulation of non-Gaussian time series a normalized spectrum (unit variance) is used. The resulting time series are thus already normalized to $\tilde{u}_n(t)$.

7.2 *New*Gust gusts

For the simulation of gusts with the *New*Gust method, the acf, second and fourth order spectral moments λ and μ, constraints A and B and a Gaussian distributed turbulence time series is required. The acf and spectral moments are derived from the estimated spectrum as described in section 6.6. The turbulent time series has been simulated as described above. Gusts with a length of the gust time period τ, defined in section 6.3, have been simulated for all bins and classes defined in table 6.1. A fixed number of gusts has been simulated for each bin. Constraint A is randomly generated with a distribution corresponding to the distribution of $\tilde{u}_n(t_0)$ of all gusts. Constraint B is derived from A, λ and μ as described in section 4.4. The integrals mentioned there are solved numerically with use of the MATLAB

command `quadl`. Because A is specified in terms of σ and the generated turbulence has unit variance, the resulting gusts are already normalized to $\tilde{u}_n(t)$.

7.3 Risø gusts

For the simulation of gusts with the Risø method, a non-Gaussian distributed turbulence time series, a spectral density and autocorrelation function is required. The acf's are derived from the estimated spectrum as described in paragraph 6.6. For the transformation function, the cdf-mapping transformation has been used (cf. section 3.3.2). Only the mean non-Gaussian gusts of each bin is simulated. The amplitude v_c has been taken the same as for the class wherefore the comparison of measured and *New*Gust gusts has been done (cf. figure 9.10). Because v_c is specified in terms of σ and the generated turbulence has unit variance, the resulting gusts are already normalized to $\tilde{u}_n(t)$.

Chapter 8

Calculating the load response

In section 4.6 a short introduction about loads resulting from wind gusts was given. In order to validate the assumption of Gaussian distributed turbulence, it is necessary to compare the load responses resulting from measured, non-Gaussian wind speed gusts and with *New*Gust simulated wind speed gusts. Because the measured time series are for one point in space, the loads are calculated with a uniform flow over the rotor area. This is done with a linearized model of the wind turbine. The wind turbine for which the loads are simulated is the "NREL offshore 5-MW baseline wind turbine".

8.1 Description of wind turbine

The "NREL offshore 5-MW baseline wind turbine" is specified in Jonkman et al. [2009]. This wind turbine was developed by NREL to be a representative utility-scale turbine for research, to standardize baseline offshore wind turbine specifications. It is a conventional three-bladed upwind variable-speed variable blade-pitch-to-feather-controlled turbine. The properties of this turbine taken into account for the simulation are given in table 8.1. Note that the tip speed ratio and rotor collective blade-pitch at peak power coefficient has been set according to the Cp-lambda curve obtained from the simplified model. The aerodynamic blade properties are taken from a custom table of lift and drag coefficients for one airfoil type. The blade is constructed according to the regions specified in Jonkman et al. [2009, table 3-1].

8.2 Model for load calculations

The calculation of load responses to a wind gust is done with a simulation of the loads based on the blade element - momentum method. Simplifications made in this code are:

- uniform flow (i.e. wind speed constant over rotor plane; no yawed flow, windshear or tower shadow);
- no wake rotation (i.e. no tangential induction factor);
- no blade tip loss factor;
- small flap angle;
- gravity is neglected;
- the dynamics of all subsystem are reduced to 'mass-spring-damper' systems.

The transfer function of the wind turbine is determined by linearizing the equations of motion of the following states of the wind turbine:

- Flap angle of rotor blade;
- Flap angular velocity of rotor blade;
- Tower top displacement;
- Tower top speed;
- Rotor angular velocity;
- Torsion angle transmission;
- Torsion angular velocity transmission.

The MATLAB function `lsim` is used to simulate the response of the discrete linear systems to arbitrary inputs specified in the transfer function. In figure 8.1 a diagram of the procedure is shown. The loads are calculated for the aerodynamic flap moment. The blade pitch comes

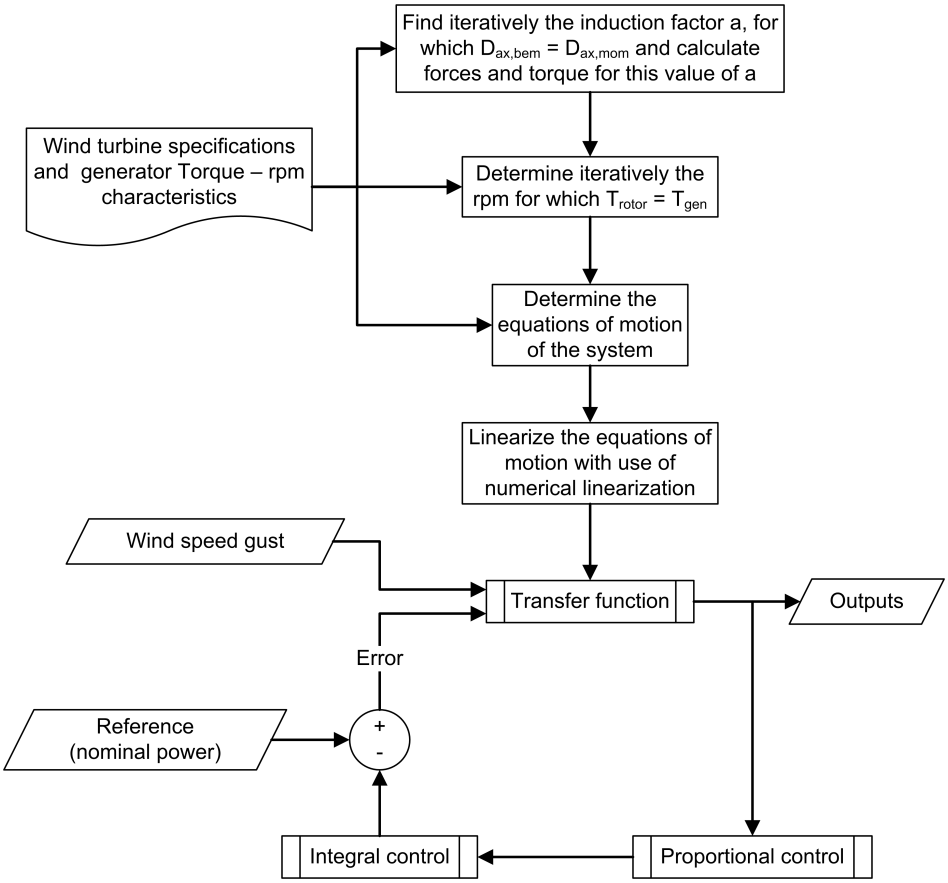

Figure 8.1: Diagram for the calculation of the load response

into action if the wind speed exceeds its rated value. The applied control on the blade pitch has been visualized in figure 8.1 and a description can be found in appendix A. The inputs and outputs of the transfer function of the wind turbine are:

- inputs of wind turbine:
  - blade pitch angle;

  - undisturbed wind speed.

- outputs of wind turbine:
  - axial force;
  - aerodynamic flap moment;
  - aerodynamic rotor torque;
  - generator power;
  - blade pitch angle;
  - undisturbed wind speed.

The transfer function is determined separately for each mean wind speed bin. In case the wind speed is e.g 8 m/s, and a wind gust of 4 m/s happens, no pitch control is applied, because the transfer function depends on the mean wind speed and does not change during the calculation of one time series. This implies that the load response calculated for gusts in the bin-classes with gusts exceeding the rated wind speed are not representative for reality.

Overall turbine properties	
rating	5 MW
rotor orientation, configuration	upwind, 3 blades
drivetrain	high speed, multiple stage gearbox
rotor, hub diameter	126 m, 3 m
hub height	90
cut-in, rated, cut-out wind speed	3 m/s, 11.4 m/s, 25 m/s
cut-in, rated rotor speed	6.9 rpm, 12.1 rpm
rated tip speed	80 m/s
rotor, nacelle, tower mass	110000 kg, 240000 kg, 347460 kg
Blade properties	
length	61.5 m
overall (integrated) mass	17740 kg
second mass moment of inertia w.r.t. root	11776047 kgm^2
first mass moment of inertia w.r.t. root	363231 kgm^2
Hub and nacelle properties	
critical damping ratio	2%
Drivetrain properties	
rated generator speed	1173.7 rpm
driveshaft critical structural-damping ratio	5%
gearbox ratio	97:1
electrical generator efficiency	94.4%
generator inertia about high-speed shaft	534116 kgm^2
Tower properties	
critical structural-damping ratio	1%
Baseline control system properties	
peak power coefficient	0.482
tip-speed ratio at peak power coeff.	7.55
rotor collective blade-pitch angle at peak power coeff.	0.0°
Full-system natural frequencies	
first tower fore-after	0.32 Hz
first blade asymmetric flapwise pitch	0.67 Hz

Table 8.1: Properties for the NREL 5 MW baseline wind turbine according to Jonkman et al. [2009].

Chapter 9

Results

In the preceding chapters, the practice of each step taken in the analysis of the data for the validation of *New*Gust has been described. In this chapter the results from the data analysis are described and explained for (1) the spectral density functions, (2) the cumulative distribution functions, (3) statistical properties of the time series, (4) the evolution of the mean gust shape and (5) the resemblance of the mean gusts and their resulting load responses. Figures of all different spectra, autocorrelation functions, cumulative density functions, gusts and load responses can be found in appendix J.

9.1 Spectral density function

An example of an estimated spectrum is given in figure 9.1. Due to the cut-off of each spectrum at the Nyquist frequency, each spectrum shows a smooth round-off at the high frequency tail. If the spectrum does not show this round-off it points towards aliasing [Smith, 1997]. This round-off behavior of the spectrum is not an effect from something existing into physical turbulence. It should therefore not be taken into account when simulating gusts. Hence, a least squares fit has been made with eq. (3.8) for each average spectrum. It appeared that the resulting values for G and H exactly matches the Kaimal spectrum (eq. 3.9). The ratio G/H is indeed[1] equal to 4/6. In figure 9.2 the parameter G has been plotted against the mean wind speed. The plot clearly shows that the spectra are the same for all three sites and equal to the Kaimal spectrum. This is in agreement with the IEC standard, where $\Lambda_{\tilde{u}} = \min(0.678 z_{hub}, 20.3)$. As the hub heights are 49, 50 and 80 meter, this gives in each case $L_{\tilde{u}} = 8.1\Lambda_{\tilde{u}} = 164.43$. The parameter $G = 4L_{\tilde{u}}/\bar{u}$ and thus scales with the mean wind speed. In section 3.2.1 (footnote 6) it has been shown that G equals the integral time scale $\mathcal{T} = 4L_{\tilde{u}}/\bar{u}$. In Kaimal et al. [1989] it is shown that in order to obtain a correct spectrum from finite sampled time series with length T, it is required that $T > 10\mathcal{T}_m$, where $\mathcal{T}_m \cong \mathcal{T}$ (compare Kaimal et al. [1989, eq. (18)] with eq. (3.9)). In figure 9.3 this requirement has been depicted along the mean wind speed. The used time period of 600 seconds is clearly too short for the wind speeds below 11 m/s, which, according to Kaimal et al. [1989], will result in an overestimation of the spectrum of approximately 10 – 50%.

[1] The ratio 2/3 comes from the fact that $\sigma_{\tilde{u}}^2 = \int_{-\infty}^{\infty} S_{\tilde{u}}(f)df$. For the one-sided spectrum in eq. (3.8), with $\alpha = 1$, $\beta = 5/3$ and $\gamma = 1$, $\int_0^{\infty} S_{\tilde{u}}(f)df = \frac{3G}{2H}\sigma_{\tilde{u}}^2$. This gives that $\frac{3G}{2H} = 1$ and $G/H = 2/3$. This result is in agreement with Tieleman [1995, eq. 20] and required for the equality $\sigma_{\tilde{u}}^2 = \int_0^{\infty} S_{\tilde{u}}(f)df$ to be true. Finally, because $G = 4L_{\tilde{u}}/\bar{u}$, $H = \frac{3}{2}G = 6L_{\tilde{u}}/\bar{u}$.

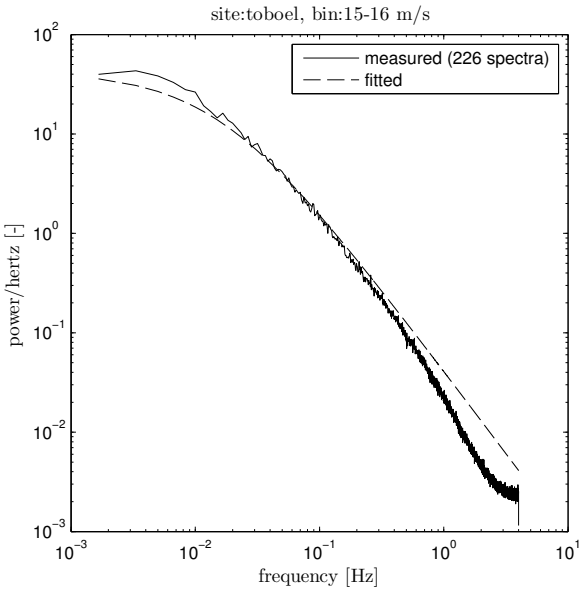

Figure 9.1: Example of an estimated spectrum and the corresponding theoretical fit.

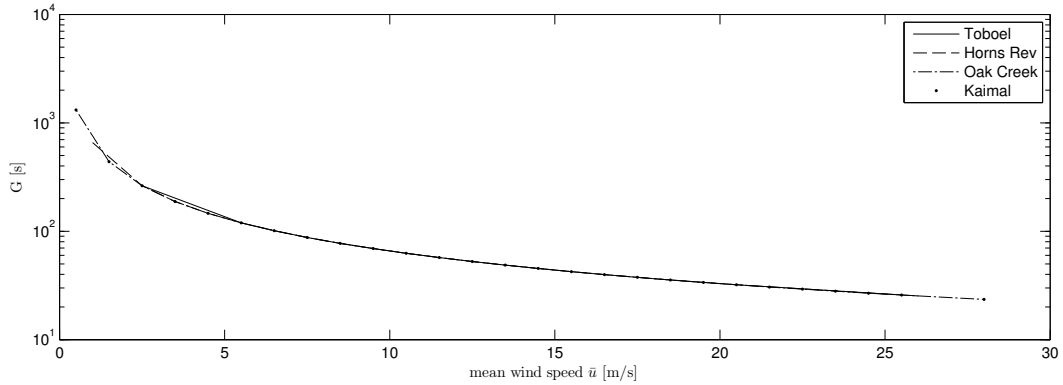

Figure 9.2: Spectrum parameter G, obtained from a fit to the mean spectra.

Despite the applied selection criteria described in section 6.2, several spectra show distortions at high frequencies (cf. appendix G). It appeared to be impossible to remove these distortions, but the fitted spectra are the same as the theoretical ones and can thus be used for the simulations.

The dependence of the spectral moments on the mean wind speed is given in figure 9.4. Note that μ is much larger than λ, which has implications on the *New*Gust expression, as will be explained in section 9.4. The spectral moments depicted in figure 9.4 are normalized as explained in section 3.2.3. The difference in the spectral moments between the sites is explained by the different sampling frequencies. The sampling frequency defines for which frequencies the spectrum is defined. Hence, this plot clearly shows the dependence of the spectral moments on the frequency (cf. also appendix E).

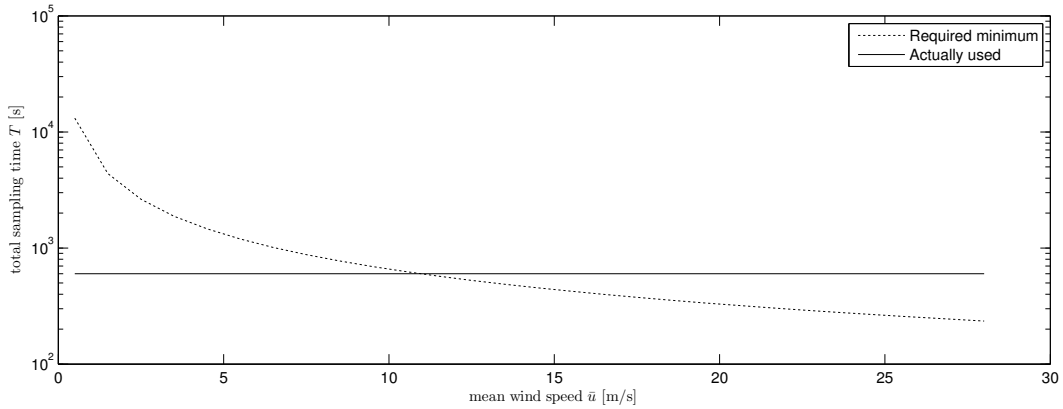

Figure 9.3: Minimum required total sampling time in order to obtain a correct spectrum description.

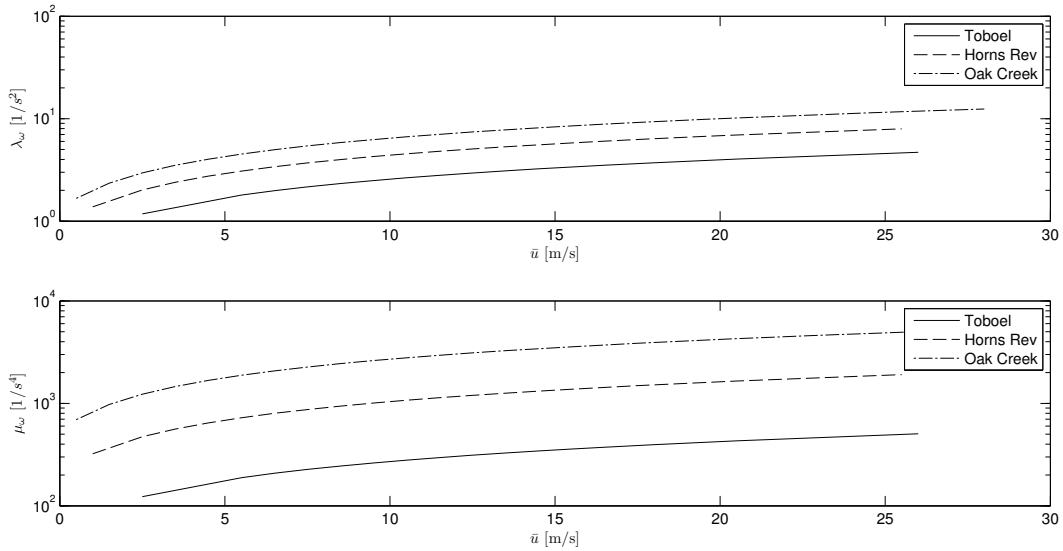

Figure 9.4: Second and fourth order spectral moment. Obtained from the fitted spectra.

9.2 Cumulative density function

An example of an empirical cdf is given in figure 9.5. Both the average empirical cdf of the measured and the simulated non-Gaussian time series is plotted (no fit to a theoretical cdf is used, cf. section 7.1). The figure shows that the resemblance of the cdf resulting from the non-Gaussian simulation is reasonably good. The cdf's show that the turbulent part of the wind speed ranges from $\sim$ -4 – 4 m/s for all three sites (cf. appendix J). The effect of cdf-mapping on a Gaussian time series depends on the difference between the Gaussian and measured cdf. An example is given in figure 3.10.

9.3 Statistical properties of time series and gusts

The mean skewness and kurtosis for each site are given in table 9.1. The skewness and kurtosis for each time series is given for each site in figure 9.6. A fit has been made between skewness

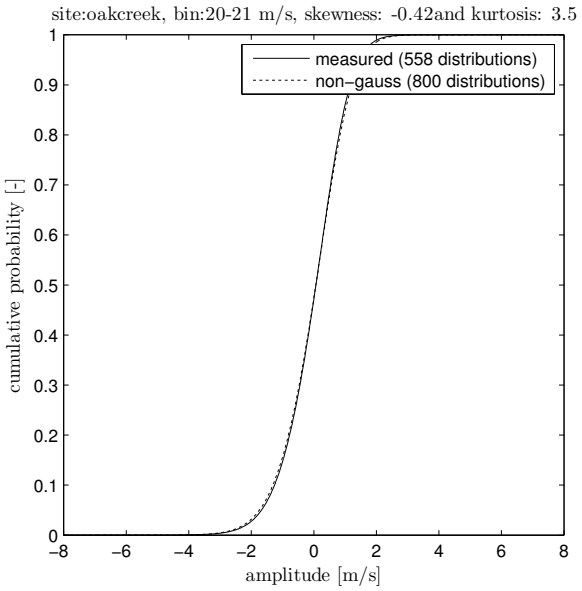

Figure 9.5: Example of a mean cdf estimated from the measured and the corresponding simulated non-Gaussian time series. This plot shows that the resemblance between both cdf's is almost perfect.

and kurtosis with a second order polynomial, which shows that there is a relation between the skewness and kurtosis. The deviation of the statistical properties from being Gaussian is not

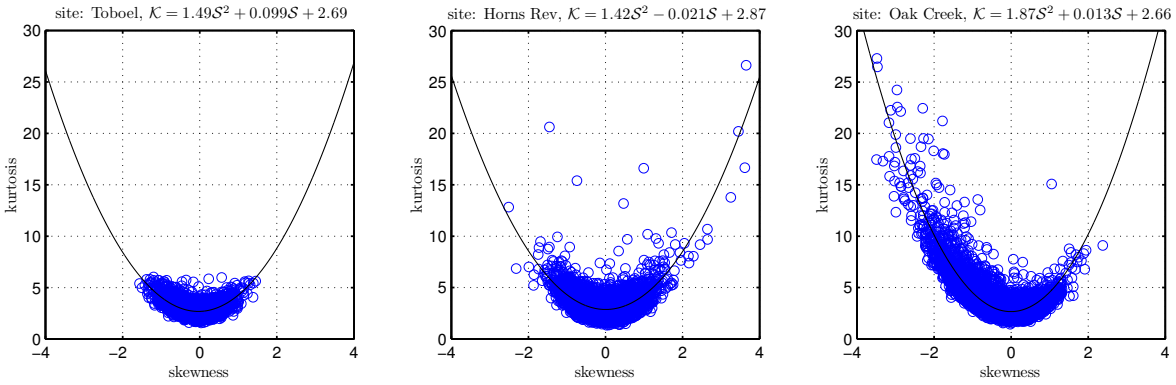

Figure 9.6: Relation between skewness and kurtosis for all three sites, including a second order polynomial fit.

so large for all three sites. Horns Rev shows perfect Gaussian kurtosis. Oak Creek shows the highest deviation from pure Gaussian skewness and kurtosis. For this site the non-Gaussian simulation has been carried out. That Oak Creek shows the highest non-Gaussian behavior is not strange, because it has a much more complex terrain surrounding the measurement mast (cf. section 3.2.4 and 6.1). For all sites the mean skewness is negative for almost all mean wind speeds. This points towards a higher probability for wind speeds lower than the mean wind speed, compared to what would be expected from the Gaussian distribution (cf. figure 3.4). The skewness is in the range given in section 3.2.4. The higher kurtosis of Oak

Creek tells that the mean wind speed occurs more often than expected from the Gaussian distribution. The opposite is true for Toboel.

bin	Toboel		Horns Rev		Oak Creek	
index	$\mathcal{S}$	$\mathcal{K}$	$\mathcal{S}$	$\mathcal{K}$	$\mathcal{S}$	$\mathcal{K}$
1	0.07	2.88	0.06	2.91	0.37	2.90
2	-0.07	2.91	0.02	3.04	0.29	2.95
3	-0.10	2.91	-0.01	3.03	0.22	2.86
4	-0.11	2.85	-0.02	3.01	0.15	3.66
5	-0.11	2.84	-0.05	3.04	0.04	2.93
6	-0.11	2.80	-0.07	3.05	-0.08	2.93
7	-0.04	2.78	-0.11	3.05	-0.18	2.97
8	-0.06	2.76	-0.13	3.06	-0.27	3.12
9	-0.06	2.77	-0.13	3.06	-0.36	3.25
10	-0.06	2.73	-0.15	3.07	-0.45	3.24
11	-0.05	2.77	-0.15	3.05	-0.47	3.46
12	-0.05	2.74	-0.14	3.00	-0.59	3.96
13	-0.01	2.70	-0.12	3.00	-0.53	3.82
14	-0.00	2.74	-0.12	2.99	-0.51	3.73
15	0.01	2.73	-0.15	2.97	-0.53	3.83
16	0.03	2.76	-0.16	2.95	-0.41	3.61
17			-0.16	2.92	-0.44	3.72
18			-0.11	2.97	-0.44	3.66
19			-0.14	2.87	-0.48	3.74
20			-0.18	2.95	-0.46	3.70
21			-0.20	2.97	-0.42	3.50
22					-0.46	3.54
23					-0.47	3.58
24					-0.51	3.70
25					-0.39	3.34
26					-0.38	3.16
27					-0.50	3.27
mean	-0.05	2.79	-0.11	2.98	-0.31	3.41

Table 9.1: Mean skewness and kurtosis for each measurement site.

9.3.1 Probability density function of mean wind speeds

In figure 9.7 the mean wind speed probability $f(\bar{u})$ has been plotted. All ten-minute mean wind speeds have been used to obtain the plot. A fit has been made with the two-parameter Weibull distribution. The coefficients c and k of the Weibull distribution are obtained from a maximum likelihood estimate using the MATLAB function `wblfit`. The fit with the Weibull distribution is only appropriate for Horns Rev. From a search on the internet, comparable values for c and k were found for Horns Rev [$\bar{u} = 9.5$ m/s, $c = 10.71$ and $k = 2.33$; Sommer, 2002, table 4.1]. To get a good estimate of the wind climate at a certain location, a data set which is more equally divided over a year should be used for the fit. See section 6.1 for the

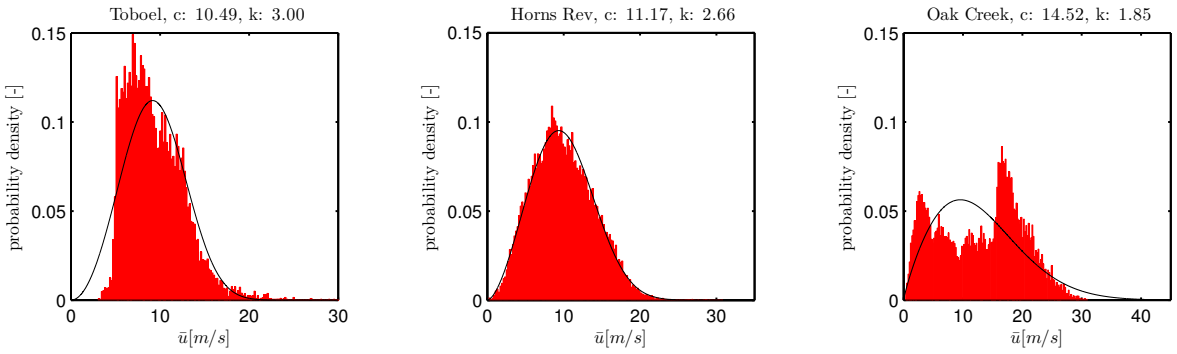

Figure 9.7: Probability density $f(\bar{u})$ of mean wind speed occurrence in the used time series for all three sites.

time span of the data used for the fits.

9.3.2 Statistics of A

In figure 9.8, the probability of gust amplitude occurrence, $f(\bar{u}, A)$ has been visualized for all three sites. The fit to the data has been done in accordance with section 6.4. The non-

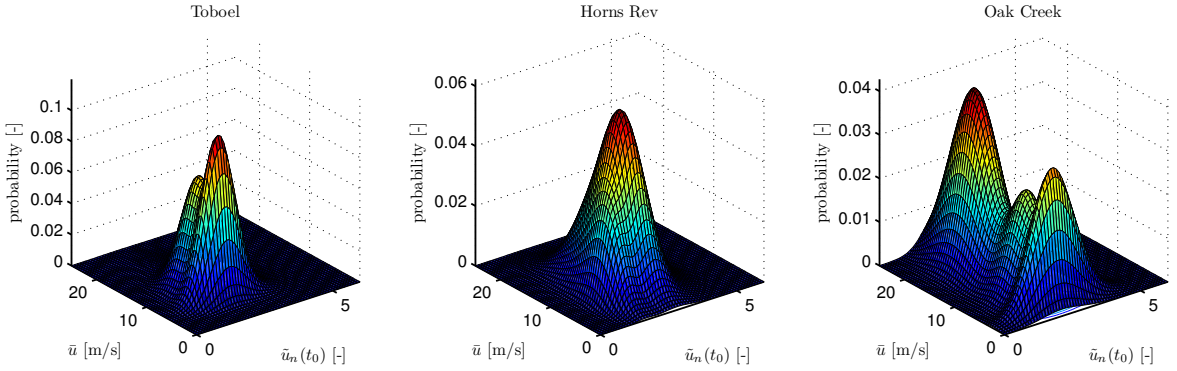

Figure 9.8: Probability of gust occurrence $f(\bar{u}, A)$ for all three sites ($\tilde{u}_n(t_0) = A$).

Gaussian behavior at Oak Creek can clearly be seen in the multi-modal probability density function. The relative gust amplitude is bound by $\sim 5 - 6$ times the standard deviation. The plots also show that the probability of gusts is highest for gusts with a relative amplitude of ~ 2.5. The wind speed probability $f(\bar{u}) = \int_{-\infty}^{\infty} f(\bar{u}, A)dA)$ can clearly be observed in these plots.

9.3.3 Statistics of B

In figure 9.9 the pdf of B is given for all three sites. There is a clear difference between the pdf of B obtained from the measurements and the pdf derived by Bierbooms [2009a] based on the assumption of Gaussian distributed turbulence. The acceleration of the wind speed (B) is indeed bounded by zero. However, the measured B shows a much larger probability of high values compared to the cdf's predicted by the Gaussian theory of B. The difference in B is in agreement with observations on the mean gust shape in section 9.4. This suggests that

in order to obtain correct gusts, the statistics of B should be non-Gaussian. The differences between the three sites are explained by the differences in the spectral moments (cf. figure 9.4), which is where the theoretical pdf of B is based upon. It should be investigated if the

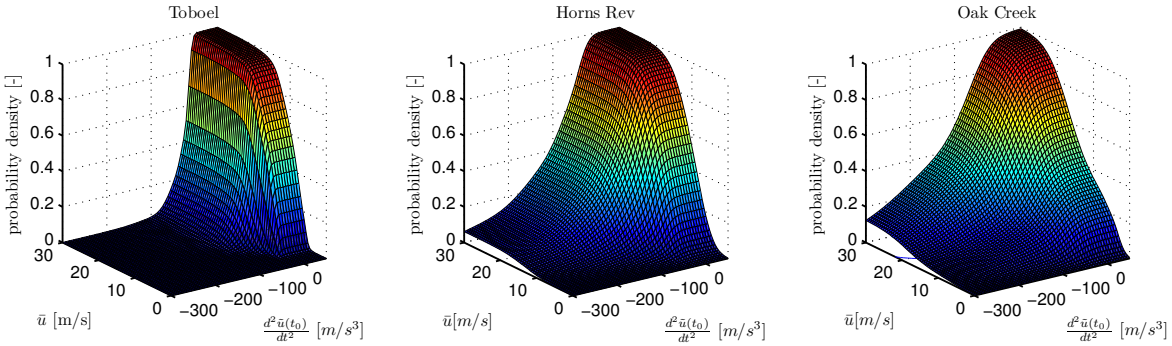

(a) $F(B, \bar{u})$ for measured gusts

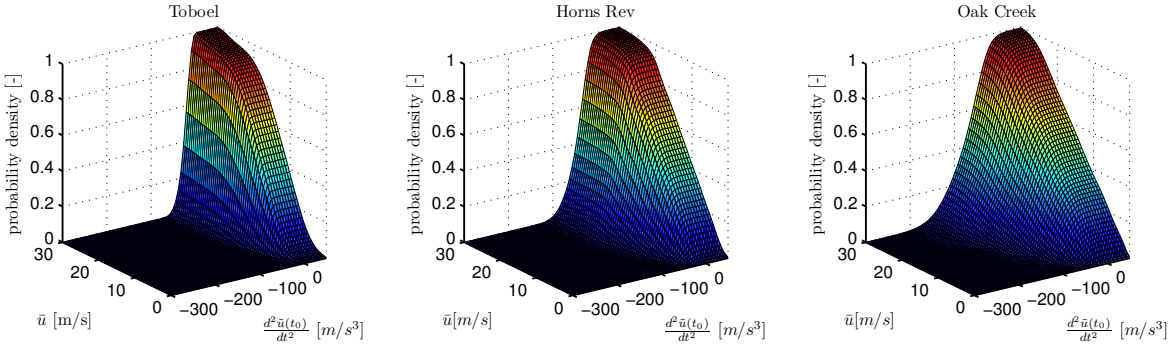

(b) $F(B, \bar{u})$ for *New*Gust gusts derived from Gaussian theory

Figure 9.9: Comparison of cumulative density of wind speed acceleration $F(B, \bar{u})$ for all three sites for measured and *New*Gust gusts

measured statistics of B would give better results when used for the simulation of *New*Gust. In order to do this, *New*Gust has been simulated for Oak Creek, with the measured cdf as input for B. The results are displayed in appendix J. The difference with the *New*Gust gusts with theoretical B is only minor and disappears for higher A. In section 9.4 the mean gust shape resulting from the *New*Gust expression is further analysed.

9.3.4 Correlation between statistical parameters

In table 9.2 the correlation coefficient between several statistical parameters is given. The correlation coefficient ρ has been calculated with the MATLAB function `corrcoef`.

$$\rho(x, y) = \frac{C(x, y)}{\sqrt{C(x, x)C(y, y)}} \tag{9.1}$$

$$C(x, y) = \langle (x - \bar{x})\,(y - \bar{y}) \rangle \tag{9.2}$$

Where $C(x, y)$ is the covariance function of x and y. The MATLAB function also calculates the significance of each correlation coefficient. Although the value of the correlations are different, each correlation is significant, except the ones indicated with a bar. The table clearly shows

		I	$\bar{u}$	$\sigma_{\tilde{u}}$	$\mathcal{S}$	$\mathcal{K}$	A	B
Toboel	I	1.00	0.20	0.62	0.12	-0.36	0.13	-0.20
	$\bar{u}$	0.20	1.00	0.88	0.05	-0.12	0.02	-0.70
	$\sigma_{\tilde{u}}$	0.62	0.88	1.00	0.10	-0.28	-0.05	-0.65
	$\mathcal{S}$	0.12	0.05	0.10	1.00	-0.15	0.15	-0.08
	$\mathcal{K}$	-0.36	-0.12	-0.28	-0.15	1.00	0.05	0.10
	A	0.13	0.02	-0.05	0.15	0.05	1.00	-0.14
	B	-0.20	-0.70	-0.65	-0.08	0.10	-0.14	1.00
Horns Rev	I	1.00	-0.07	0.54	0.15	-0.05	-0.16	-0.25
	$\bar{u}$	-0.07	1.00	0.73	-0.12	-	-	-0.41
	$\sigma_{\tilde{u}}$	0.54	0.73	1.00	-	-0.05	-0.12	-0.50
	$\mathcal{S}$	0.15	-0.12	-	1.00	-0.24	0.16	-0.02
	$\mathcal{K}$	-0.05	-	-0.05	-0.24	1.00	0.07	0.03
	A	-0.16	-	-0.12	0.16	0.07	1.00	-0.17
	B	-0.25	-0.41	-0.50	-0.02	0.03	-0.17	1.00
Oak Creek	I	1.00	-0.72	0.10	0.49	-0.05	0.05	-0.03
	$\bar{u}$	-0.72	1.00	0.37	-0.38	0.04	-0.03	-0.21
	$\sigma_{\tilde{u}}$	0.10	0.37	1.00	-	-0.06	-0.05	-0.40
	$\mathcal{S}$	0.49	-0.38	-	1.00	0.10	0.12	-0.02
	$\mathcal{K}$	-0.05	0.04	-0.06	0.10	1.00	-	0.02
	A	0.05	-0.03	-0.05	0.12	-	1.00	-0.21
	B	-0.03	-0.21	-0.40	-0.02	0.02	-0.21	1.00

Table 9.2: Correlation between several statistical properties of the time series

that the correlation between the turbulence intensity and the standard deviation and mean wind speed depends on the mean skewness (cf. table 9.1). With increasing negative mean skewness, the correlation between skewness and turbulence intensity increases. At the same time, the correlation between standard deviation and turbulence intensity decreases and the correlation between turbulence intensity and the mean wind speed goes from a positive to an increasing negative value. Hence, for large negative mean skewness, the turbulence intensity increases if the mean wind speed decreases. This points towards the application of the rapid distortion theory [Burton et al., 2008, Ch. 2.11]. Another interesting correlation is the one between A and B as well as the one between B and $\bar{u}$ and $\sigma_{\tilde{u}}$, where again the mean skewness and kurtosis are of influence. In section 4.6 it was said that if for random variables z it holds that $\langle g_1(z_1) \cdots g_n(z_n) \rangle$ equals $\langle g_1(z_1) \rangle \cdots \langle g_n(z_n) \rangle$, then they are independent. This holds well for the variables $\bar{u}$ and A, which justifies to say that they are independent.

9.4 Evolution of the mean gust shape with the wind speed

In figure 9.10 the evolution of the *New*Gust mean gust shape has been visualized. The evolution of the mean gust shape as suggested by the *New*Gust expression is clearly not present in the measured mean gust shapes. The measured mean gusts in general have a higher acceleration towards the peak value as suggested by the *New*Gust expression. The deviation

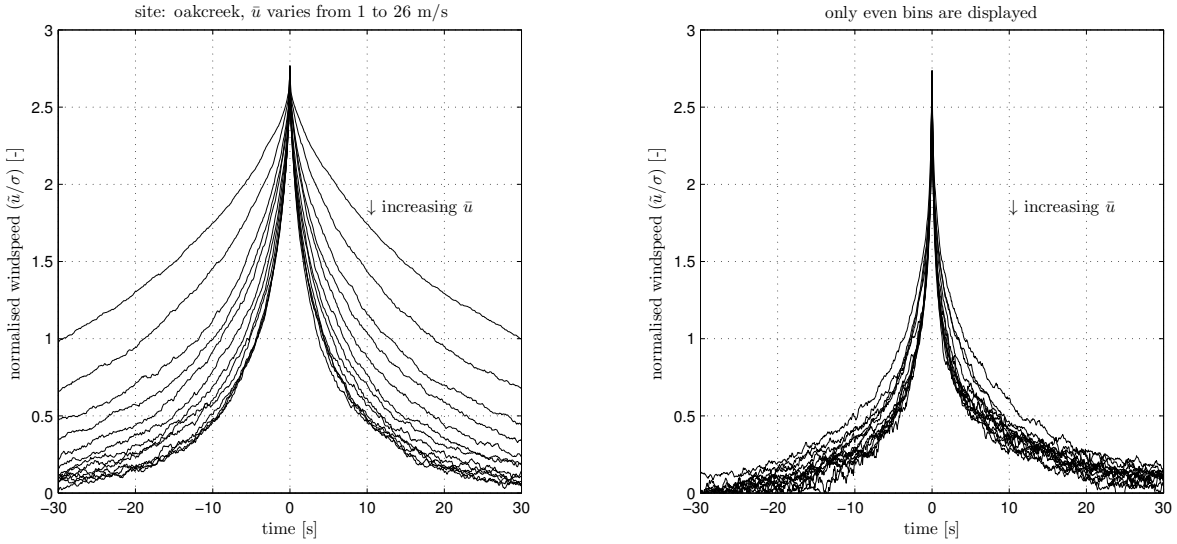

Figure 9.10: Evolution of the mean *New*Gust (left) and mean measured (right) gust shape with mean wind speed for Oak Creek (gust amplitude class 4 is depicted). The same is observed for the other sites (cf. appendix J). The mean *New*Gust shapes are obtained from ensemble averages of the simulated *New*Gust gusts.

between the *New*Gust and measured mean gust shape becomes minor for the higher mean wind speeds. This is the range of mean wind speeds and relative amplitude that *New*Gust was developed for. In figure 9.10, B is the acceleration of the wind speed at the peak value. Note that the acceleration of the wind towards the peak value is not equal to B.

From the plot it is clear that the acceleration of the wind is much higher for the measured as for the *New*Gust gusts. These accelerations can, for example, be quantified by the ratio $\Delta\tilde{u}_n/\Delta t$ for ten seconds before the maximum. The attentive reader might already notice that this relates to the velocity increment detection method described in section 4.3.1. This method is also used in the papers dealing with non-Gaussian turbulence mentioned in section 3.2.4. For small time lags a much higher than expected change in turbulent wind speed is found. This can also be seen in the mean gust shapes in figure 9.10. This would hence mean that the *New*Gust gust does not resemble the physical gust. The question to be answered is if this is a feature of Gaussian gusts or just belongs only to *New*Gust gusts.

As shown in section 9.1, the discrete spectral moments are site dependent. The effect of the spectral moments on the *New*Gust shape is reflected in the three factors in the mean gust shape (eq. 4.18). The evolution of these factors with respect to the mean wind speed is given in figure 9.11. From this graph it becomes clear that the effect of B is small, unless B is large, which is generally not the case as shown in section 9.3.3. Also the effect of adding the second derivative in the term belonging to A is very small. Therefore, it can be concluded that the *New*Gust expression actually is a scaling of the normalized acf. In appendix J the acf resulting from the spectrum can be found. The mean gust shape indeed very much resembles the normalized acf.

In this context the evolution of the mean *New*Gust gust becomes natural, because at lower mean wind speed, the correlation -represented by the acf- will last longer. This causes the acf and hence the gust to have a lower acceleration towards the peak value compared to the physical gusts.

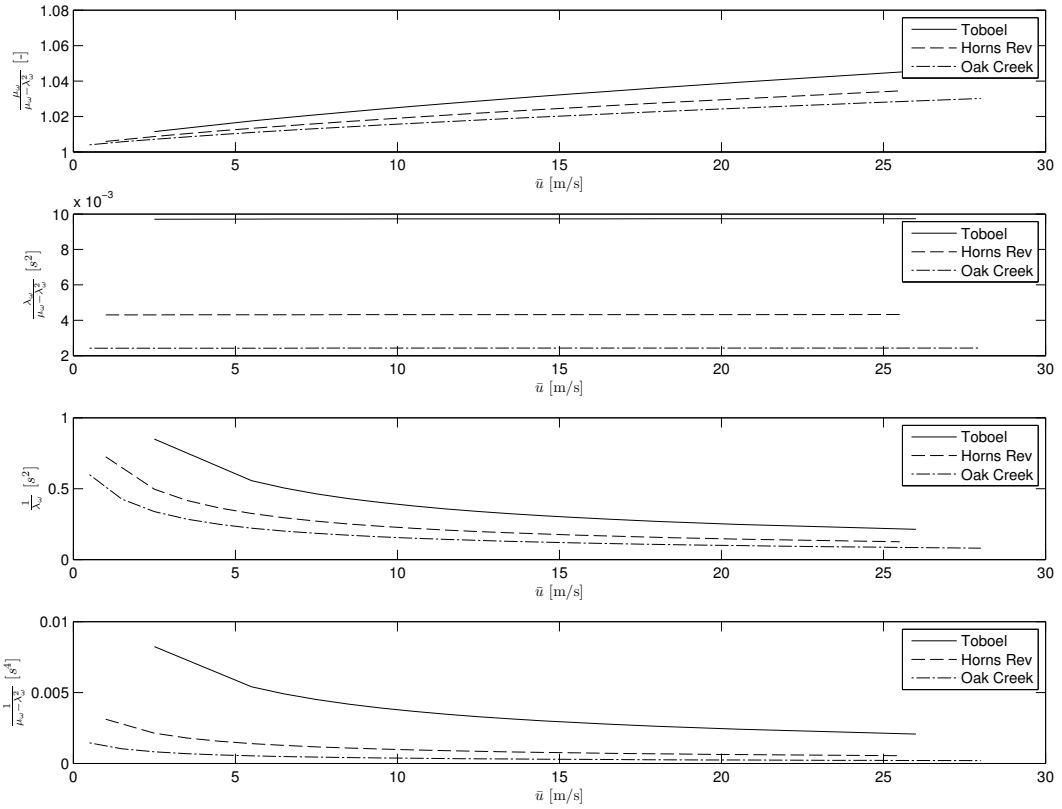

Figure 9.11: Evolution of the three different factors in the mean *New*Gust expression depending on the spectral moments

Although the factors which determine the influence of B in the *New*Gust expression are small, the influence of B can still be observed in the mean gust shapes for the lower mean wind speeds in appendix J. The difference between the mean gust shape resulting from eq. (4.12) and from eq. (4.20) is only minor and indeed disappears at higher relative gust amplitudes (The *New*Gust expression from eq. 4.20 is the asymptotic form of eq. 4.12). The same is observed when the measured cdf of B is used to simulate *New*Gust gusts. The influence of B can thus be neglected.

The difference with measured wind speed gusts becomes much smaller at higher mean wind speeds. This is explained by the autocorrelation function, which represents a much shorter temporal correlation for high mean wind speeds. It hence seems that the *New*Gust expression for higher mean wind speed, applies also to the gusts in wind with a lower velocity. This shows the agreement with the explanation of intermittency (gusts) in turbulence given in section 3.2.4, which said that gusts are part of structures with a much higher velocity than the surrounding turbulence. The Gaussian theory for simulating gusts based upon the acf of turbulence is hence insufficient for the lower mean wind speeds.

From section 9.5 it appears that the resemblance between load responses resulting from several types of gusts is better if the different gust shapes show a better resemblance. Therefore, the theoretical mean gust shape based on non-Gaussian theory (cf. section 4.5) was investigated. Only the evolution of the mean gust shape resulting from the non-Gaussian theory has been simulated (in accordance to section 7.3). The result is shown in figure 9.12.

From the graph it becomes clear that the transformation to non-Gaussian mean gusts does

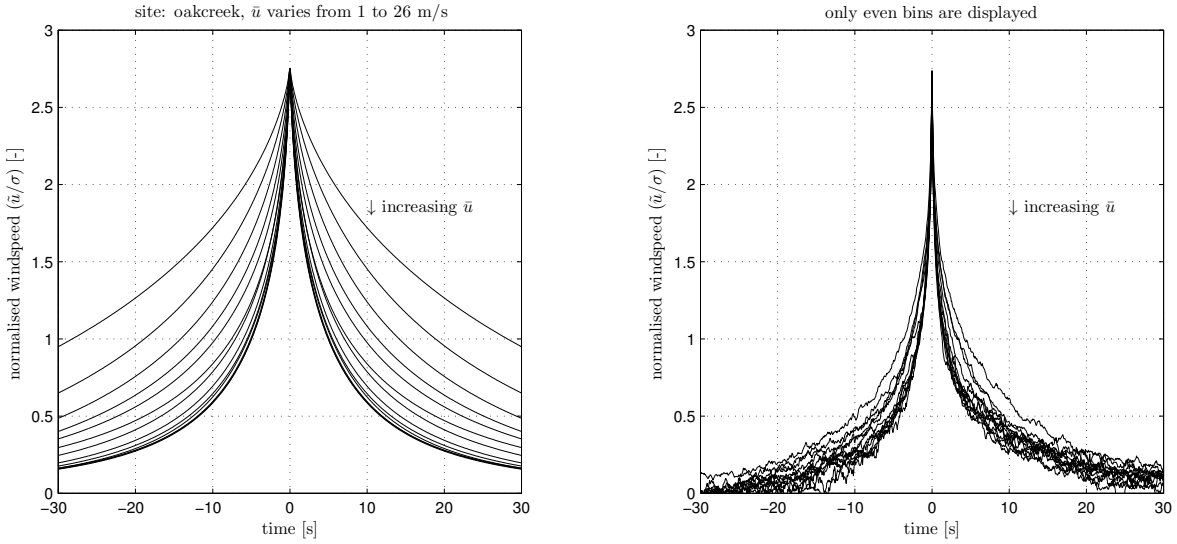

Figure 9.12: Evolution of the mean Risø (left) and mean measured (right) gust shape with mean wind speed for Oak Creek (gust amplitude class 4 is depicted). The mean Risø gust is obtained from eq. (4.24).

not change the scaling behavior of the theoretical mean gust shape. However, another transformation function would probably give other results.

9.5 Mean gust and load response

An example of the mean gust and load response shape for the investigated gust types is given in figure 9.13. In order to be able to quantitatively compare all the mean gust and load shapes, the mean square error (mse) has been calculated for each site, between all gust types.

$$e = \frac{1}{\tau}\sum_{t=1}^{\tau}\left(\tilde{u}_{measured}(t) - \tilde{u}_{NewGust}(t)\right)^2 \tag{9.3}$$

For the calculation of the mse from the load responses, the loads are divided by a factor 10^6, to get a meaningful mse. The results of this comparison are given in the figures 9.14a, 9.14b, 9.14c, 9.15, 9.16, 9.17 and 9.18 and tables J.1, J.2 and J.3 and are discussed below.

Resemblance between measured and *New*Gust gusts

As can be seen from the graphs, the resemblance between the measured and *New*Gust mean gust shape is reasonably good for a large range of mean wind speeds and relative gust amplitudes. The higher mse at both edges of the normalized amplitude range is due to the low number of gusts found for these amplitudes, as well as the larger class width. The worse resemblance at low mean wind speeds can be explained by the sometimes large bin and class width. More important is that the measured gusts at low mean wind speed are actually higher amplitude gusts than expected from their classification. This is because they start at a negative mean wind speed. Hence, the absolute amplitude of the gusts is much higher

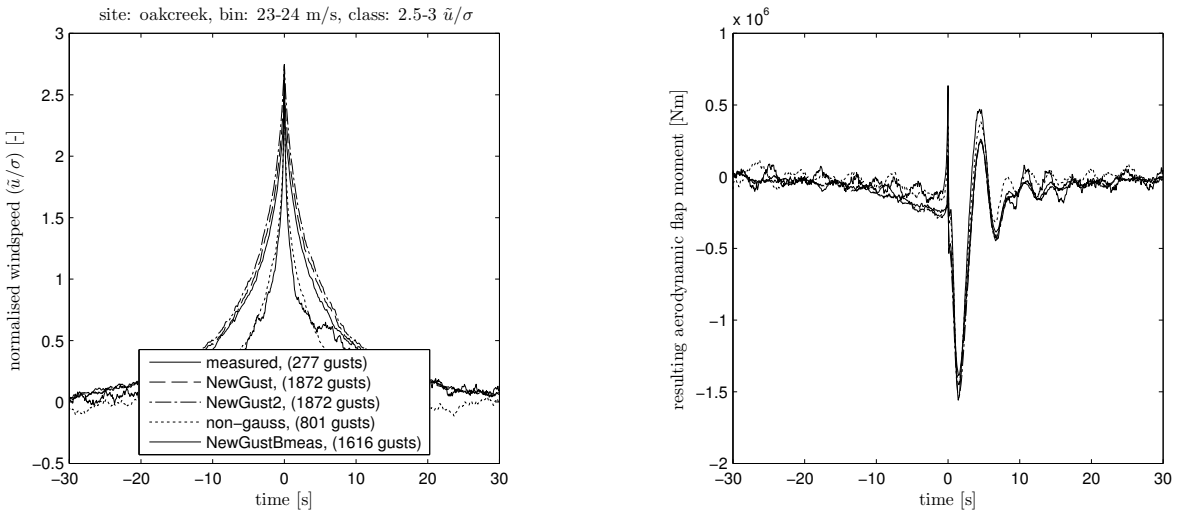

Figure 9.13: Example of a mean gust (left) and load response (right) shape for all simulated gust types

than the class it belongs to. In lower mean wind speed turbulence it thus seems that the wind speed has to go down before a gust is possible; as if the structure takes energy from the surrounding turbulence in order to exist.

The resemblance of the two mean load shapes shows a different character. For most of the bin-class combinations, the resemblance is quite good. However, between $\sim 4 - 13$ m/s the resemblance is much worse. This behavior is partly related to the bad resemblance of both gust types and partly to the cut-in and rated wind speed and thus to the behavior of the turbine pitch-control. As soon as the pitch becomes active, the difference between the load responses of both gust types disappears. The high peak in the $11 - 12$ m/s bin is caused by the calculation of the loads from *New*Gust gusts, because one transfer function is used for the whole bin; whereas for the calculation of the loads from measured gusts a transfer function depending on the mean wind speed of each time series is used.

Resemblance between non-Gaussian, and measured gust

From the graph in figure 9.15 it can be seen that the resemblance between the measured and the non-Gaussian gusts is almost perfect. This can be expected, because both the spectral density function and the distribution function are resolved in the simulation of non-Gaussian gusts. The worse resemblance of the load responses between $13 - 5$ m/s are observed even in this case.

Resemblance between non-Gaussian and *New*Gust gusts

From the graph in figure 9.15 it can be seen that the resemblance between the *New*Gust and the non-Gaussian gusts is almost equal to the resemblance between the measured and the *New*Gust gusts. This is as expected, due to the almost perfect resemblance between the measured and the non-Gaussian gusts.

Resemblance between *New*Gust2 and *New*Gust gusts

From the graph in figure 9.17 it can be seen that there is almost no difference between the *New*Gust2 and the *New*Gust gusts, which is by no means surprising.

Resemblance between *New*Gust2 and measured gusts

From the graph in figure 9.18 it can be seen that the resemblance between the *New*Gust2 and the measured gusts is equal to the resemblance between the measured and the *New*Gust gusts. This is as expected, because of the almost perfect resemblance between the *New*Gust2 and the *New*Gust gusts.

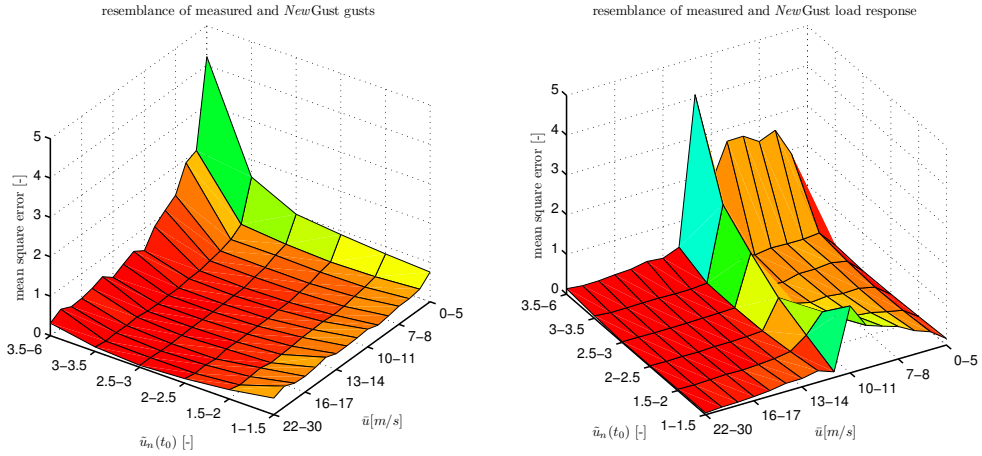

(a) Toboel, left: mean gust, right: mean load response

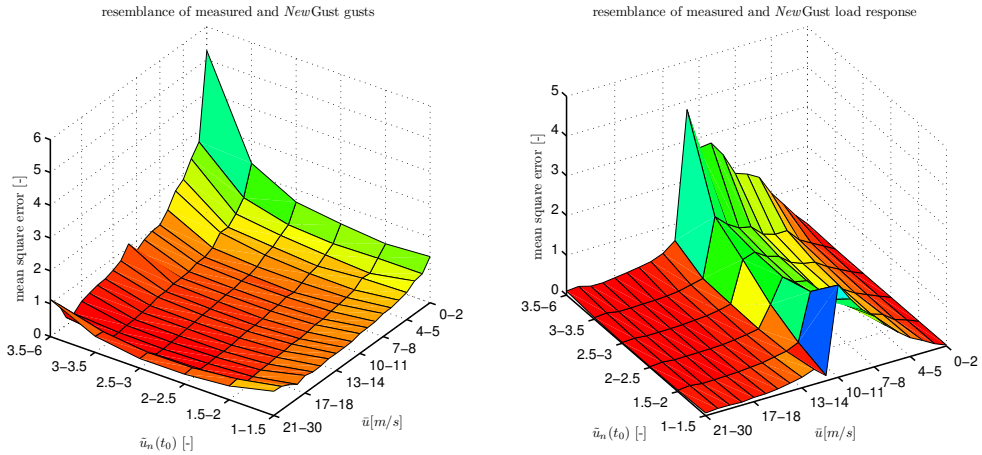

(b) Horns Rev, left: mean gust, right: mean load response

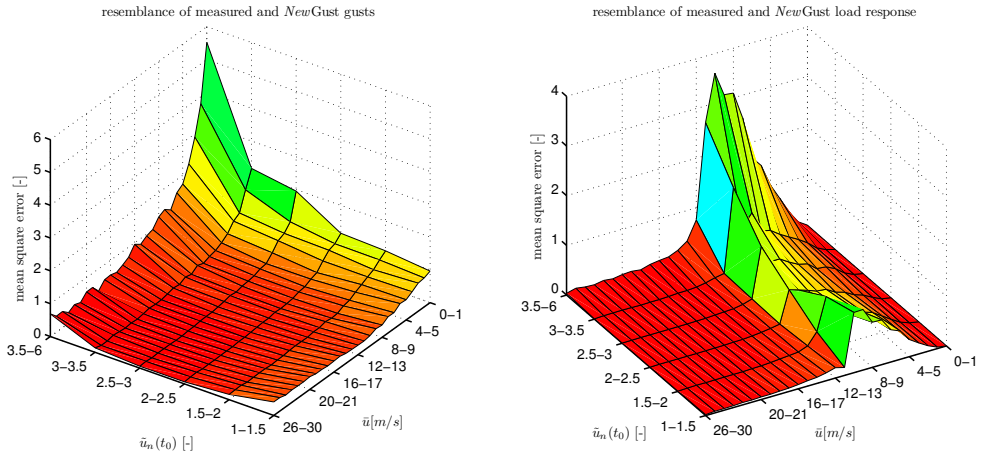

(c) Oak Creek, left: mean gust, right: mean load response

Figure 9.14: Graphical representation of the mse comparison between measured and *New*Gust gusts

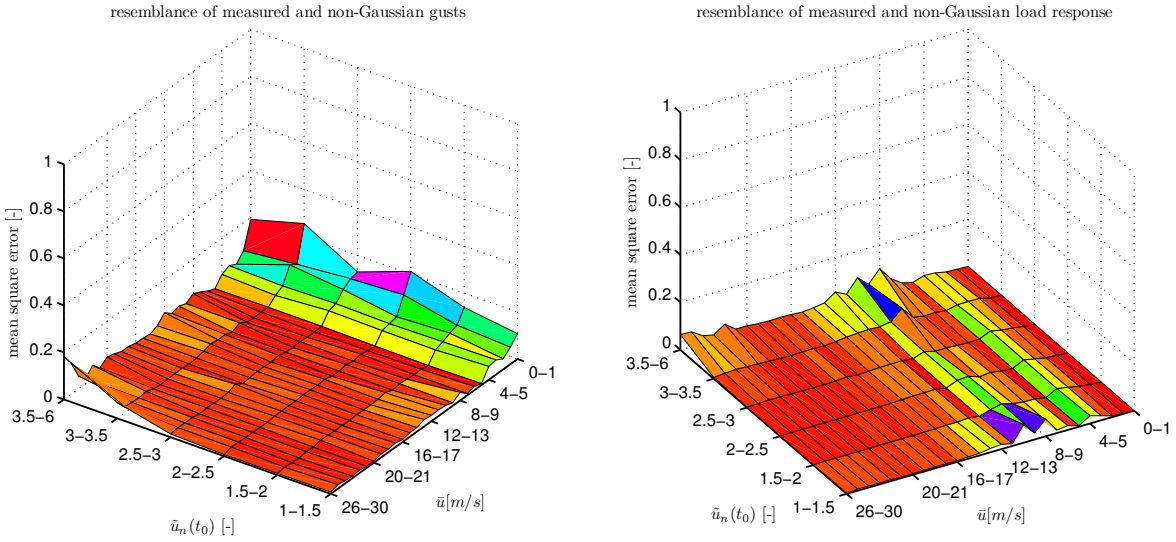

Figure 9.15: Graphical representation of the mse comparison for Oak Creek between measured and non-Gaussian gusts, left: mean gust, right: mean load response.

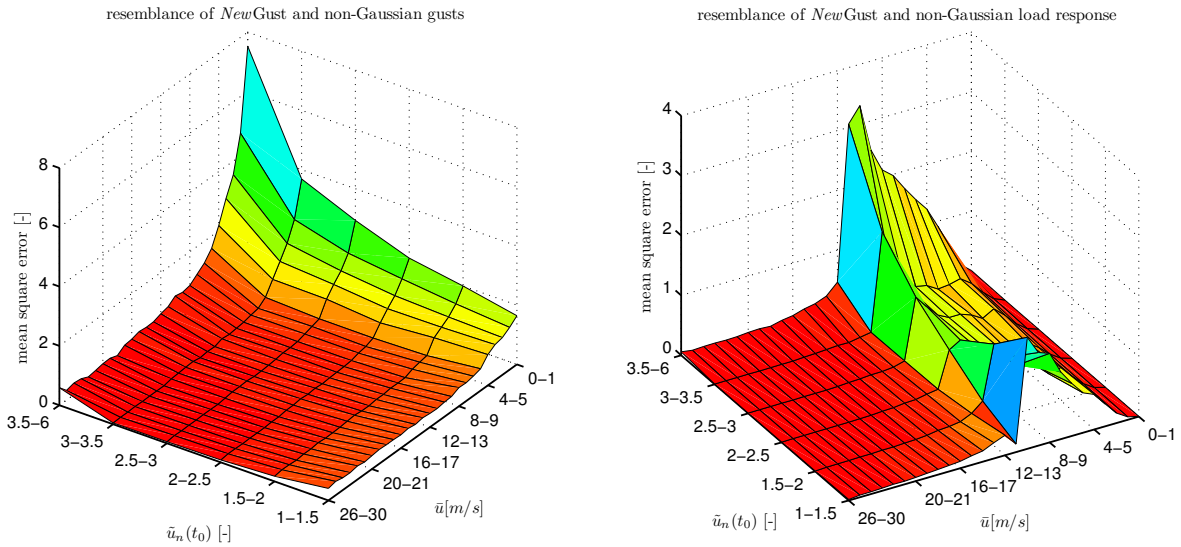

Figure 9.16: Graphical representation of the mse comparison for Oak Creek between *New*Gust and non-Gaussian gusts, left: mean gust, right: mean load response.

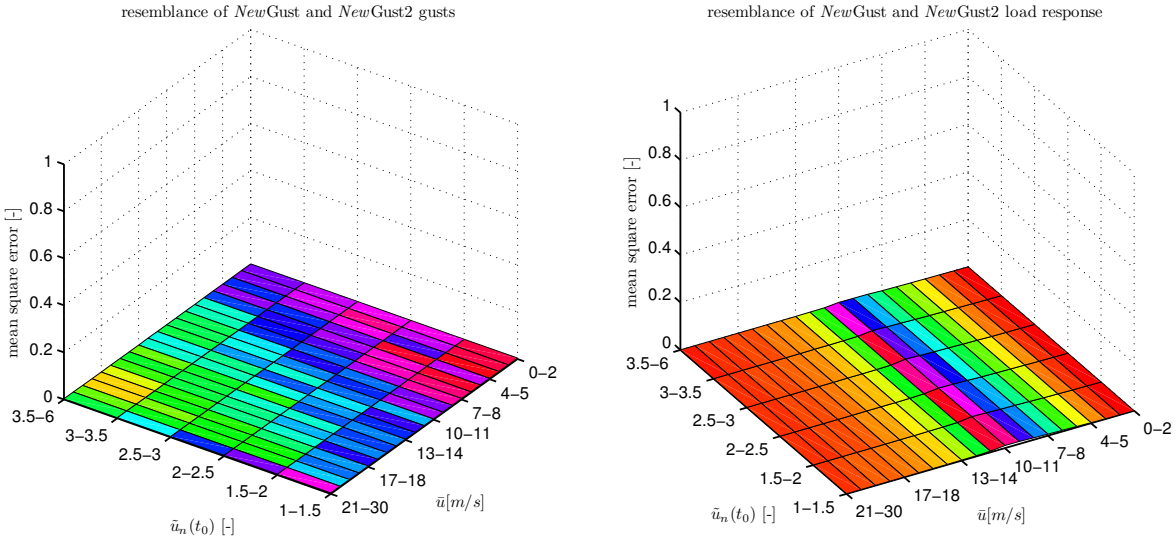

Figure 9.17: Graphical representation of the mse comparison for Hornsrev between *New*Gust2 and *New*Gust gusts, left: mean gust, right: mean load response.

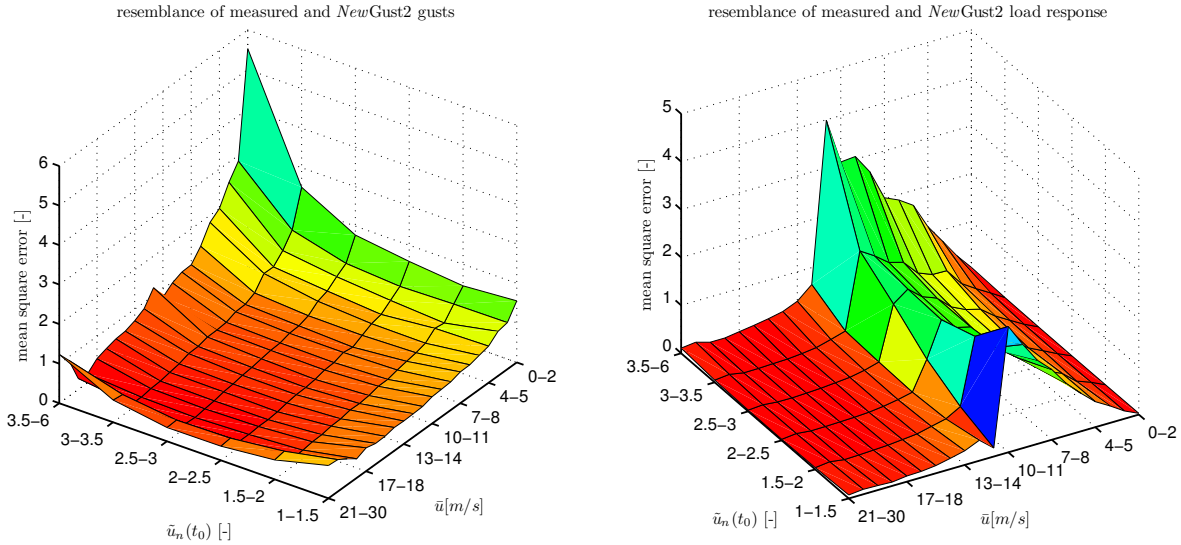

Figure 9.18: Graphical representation of the mse comparison for Hornsrev between *New*Gust2 and measured gusts, left: mean gust, right: mean load response.

Chapter 10

Extremes

The final goal behind analyzing gusts is to find the gust leading to the most extreme load response in the life time of a wind turbine. In this chapter it is investigated (1) which gusts lead to the extreme load response of the wind turbine, (2) how the 50-years' load response compares for several calculation methods and (3) what the influence is of non-Gaussian turbulence on the distribution of extreme loads.

10.1 Extreme load response

From an investigation of the load response of a pitch-regulated wind turbine to extreme rise time gusts done by Bierbooms [2005], the question is postulated which gust type leads to the extreme loading of pitch-regulated wind turbines. In an attempt to answer this question, the load response has been calculated for all time series from all three sites described in section 6.1. From each load response time series $l(t)$, the load response around the extreme response $l(t_0)$ is stored together with the underlying part of the wind speed time series.

$$l(t_0) = \max(l(t)), \quad t \in 0 \ldots 600s \tag{10.1}$$

$$l_{max}(t) = l(t), \quad t \in t_0 \pm 30s \tag{10.2}$$

$$\tilde{u}_{max}(t) = \tilde{u}(t), \quad t \in t_0 \pm 30s \tag{10.3}$$

For each site, all load responses and gusts are normalized and classified as described in section 6.3. Of course, the used classes for the loads differ from the ones given there. The extreme shapes are calculated as the ensemble average of all gusts belonging to a load response in a certain bin-class. In appendix K graphs of all the extreme mean gust and load response shapes are given.

10.1.1 Extreme gust shape

Figure 10.1 shows the development of the extreme gust shape with the mean wind speed, which is equal for all three sites. The graph clearly shows that the extreme gust shape changes from a gust with extreme amplitude to a gust with extreme rise time[1] as soon the the pitch becomes active. The gusts leading to the extreme load response can thus be divided in two regions: (1) pitch inactive and (2) pitch active. Within these two regions, the extreme

mean gust shape shows only minor changes with increasing mean wind speed. The gusts in

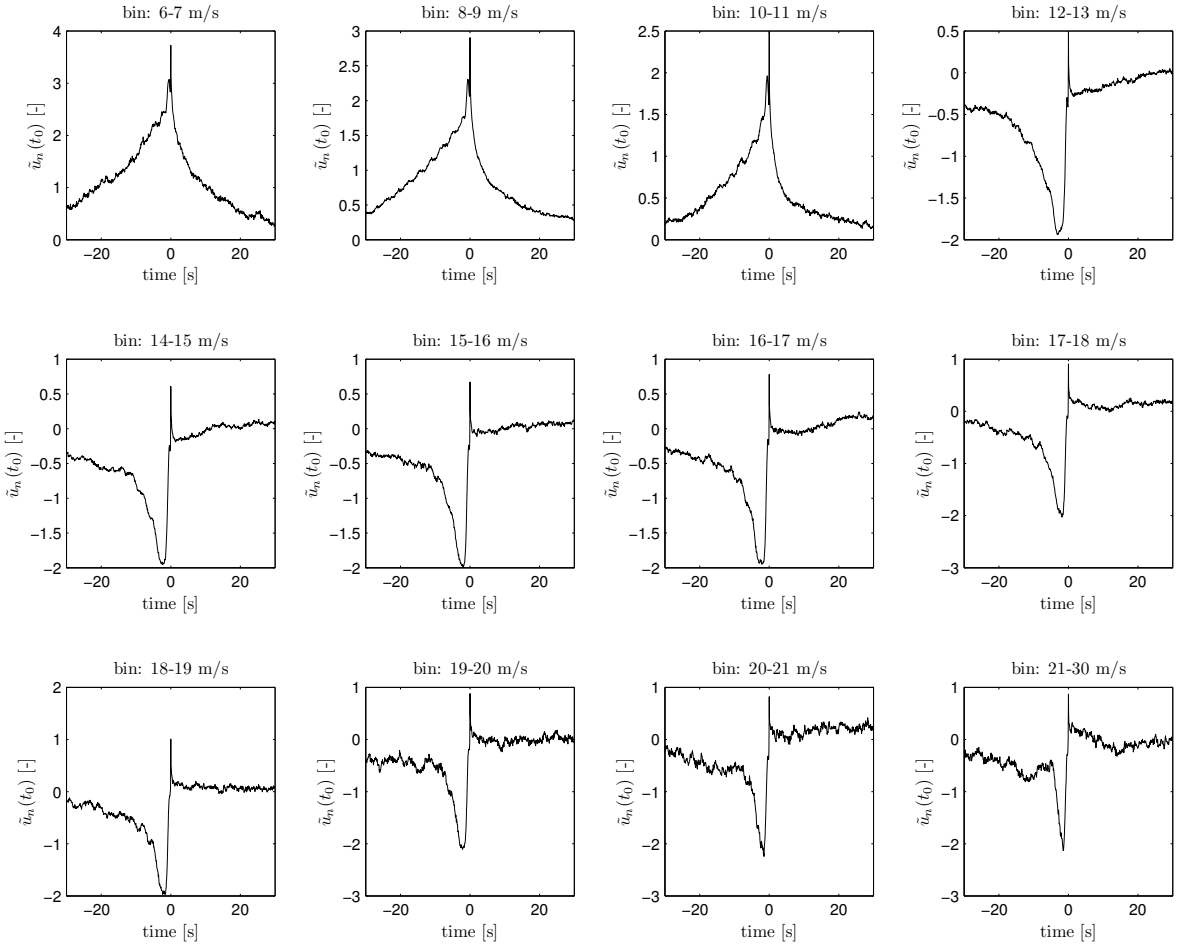

Figure 10.1: Evolution of the average extreme gust shape with the mean wind speed. The results shown here are for Horns Rev, but are similar for Oak Creek and Toboel. The extremes are for load response amplitude class 6 (cf. appendix K)

region 2 are equal to the gust leading to the extreme load response of a pitch-regulated wind turbine as predicted by Nielsen et al. [2004, figure 47]. Note that the gust evolution with the mean wind speed as depicted in figure 10.1 is valid for one load response class. For the higher load amplitude classes, the evolution is the same, although the amplitudes are different (cf. appendix K). The mean gust shape obtained here is quite close to the theoretical extreme rise time gust developed by Bierbooms [2006]. The difference lies in the reduction of the wind speed after the velocity jump. This part of the gust, however, is not so important, as the extreme load response will occur during the jump. The part after the jump hence has no effect on the extreme load response. The extreme gusts all lack symmetry; and in Bierbooms [2007] an expression is given to derive the gust leading to an extreme in the load response. This expression is based upon a combination of the cross- and autocorrelation function of wind speed and load response, which can give rise to non-symmetric extreme gusts.

[1]Extreme amplitude gusts are characterized by their extreme amplitude (first three gusts in figure 10.1), whereas extreme rise time gusts are characterized by their extreme rise time (all other gusts in figure 10.1).

10.1.2 Wind speed range with maximum loads

In figure 10.2 the development of the gust and load amplitude are shown for one load amplitude class. It is interesting to see that even within the width of a load amplitude class the highest load responses are indeed not obtained for the extreme rise time gust, but for extreme amplitude gusts in turbulence with moderate mean wind speeds ($\sim 9 - 12$ m/s). This is the transition between region 1 and 2. From comparison with figure 4.7, the same behavior can be observed. The amplitude of the mean gust leading to the extreme load response in this

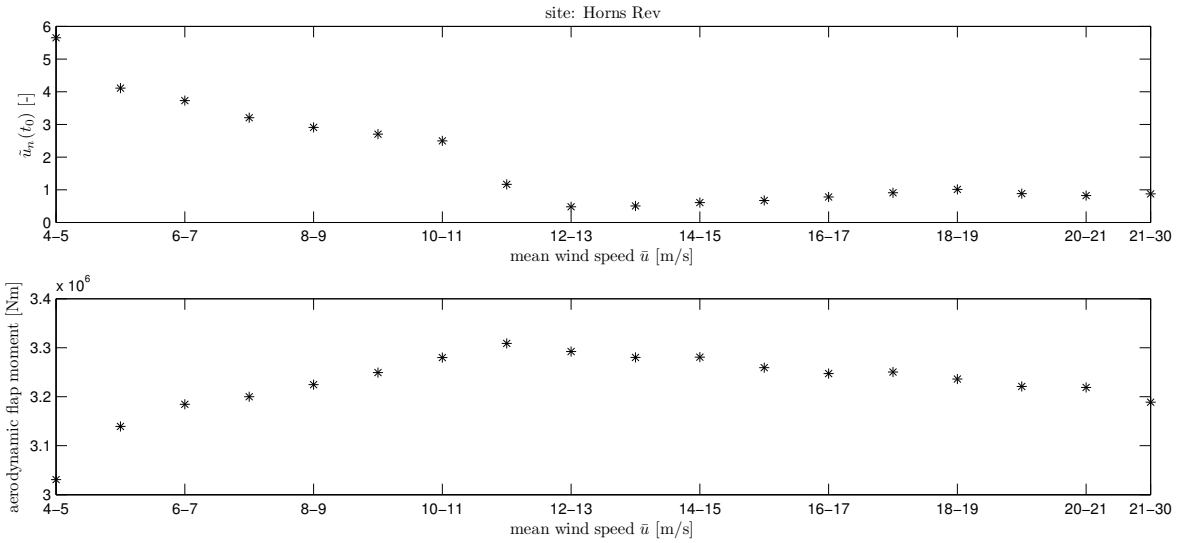

Figure 10.2: Evolution of the average extreme gust and load amplitude with the mean wind speed. The results shown here are for Horns Rev, but are similar for Oak Creek and Toboel. The extremes are for load response amplitude class 6 (cf. appendix K)

class is decreasing with the mean wind speed. This is logical, because the loads are increasing with mean wind speed and hence a smaller gust is required to obtain the same extreme load response amplitude.

In figure 10.3 the evolution of the extreme load response with the mean wind speed is given for all time series of each site. The plot shows that the highest load response from gusts occur in the transition between region 1 and 2, as was already noticed before. In figure 4.7 the evolution of the thrust with the mean wind speed is plotted. The extreme loads are added to these mean ones, which shows that the extreme really happens in the transition between region 1 and 2. This observation explains why negative amplitude gusts in region 2 are most dangerous for pitch-regulated wind turbines, because they lead to a load increase. This in contrast with positive amplitude gusts in region 2, which lead to a decreasing load. When observing the results in appendix K it is noticed that the largest negative gusts (which also cause high loads) are most present for Oak Creek. This site also has the largest negative skewness. Negative skewness indicates that values smaller than the mean one are more often observed as expected from Gaussian theory. This points towards more frequent (large) negative excursions in the wind speed. This can indeed be observed from the time series of Oak Creek (see figure 10.4). For these type of wind regimes, extreme loads will thus be more frequent, as can be observed in figure 10.3.

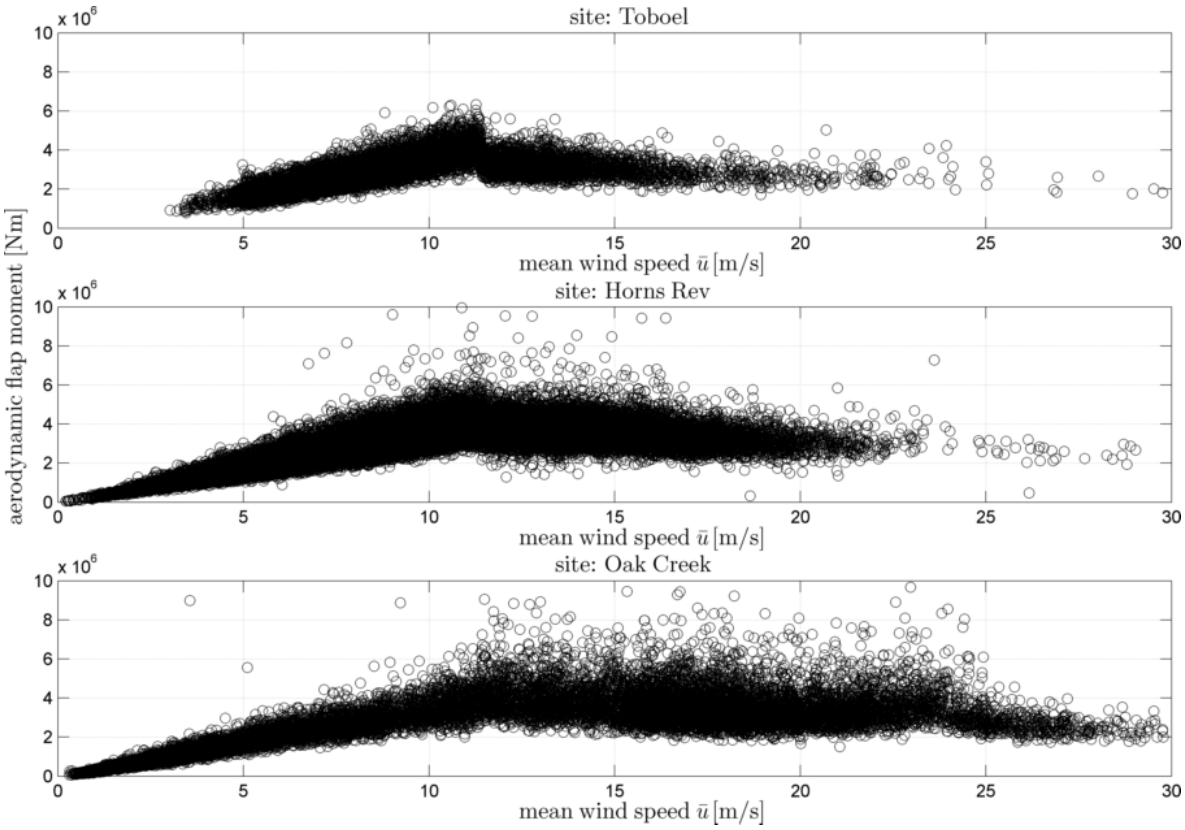

Figure 10.3: Evolution of the extreme load response with the mean wind speed. The extreme is taken as the maximum in a time series of 600 seconds.

10.1.3 50-years' extreme load response

In section 2.4 it was explained that for wind turbine design the 50-years' extreme value is used as the maximum value a wind turbine has to deal with during its life time. In this section the 50-years' extreme load response will be derived from measurements, Gaussian theory and conditional simulations with *New*Gust and *Load*Gust. The results will be compared with each other and with the results from the previous section. It has to be noted that the values obtained here do not represent the values which will be encountered in reality. Here, only a comparison between different methods has been made, with many simplifications included. In appendix E the methods applied here have been checked for Gaussian turbulence which should then compare with Gaussian theory.

50-years' extreme using measurements

The measured ten-minute maximum load responses shown in figure 10.3 can be used to derive a distribution function of the maximum loads. The theory for this is explained in section 2.4. By assuming that below and above a certain wind speed the maximum loads do not contribute to the upper tail of the cdf, a limited range of wind speeds can be used. As a consequence of the amount of data available for the higher and lower wind speeds, a range of 4 – 17, 18 – 20 m/s is chosen for Toboel, a range of 4 – 20 m/s for Horns Rev and 4 – 23 m/s for Oak Creek. For the density $f(\bar{u})$, results from section 9.3.1 are used. In order to obtain good results, a

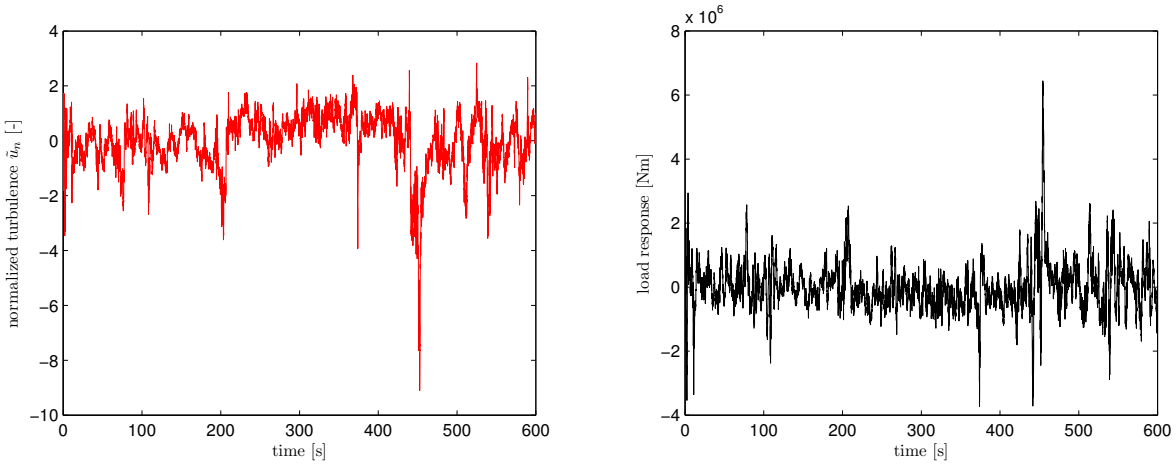

Figure 10.4: Turbulence time series from Oak Creek including a large negative gust. This phenomenon causes the extreme load response in the time series.

small enough bin width should be taken. In this case, that is a bin width of 0.2 m/s because of the limited amount of time series.

Because the empirical cdf exists only for a limited range of load responses, a fit with some theoretical extreme value distribution is required for extrapolation. There are many possible extreme value distributions, but here only a generalized extreme value (GEV) fit has been used (`gevfit` in MATLAB). In figure 10.5 an example is given of an empirical cdf and its fit. For the weighted summation of all conditional cdf's (eq. 2.14) an inter- extrapolation scheme has been used, which uses the empirical cdf up to the 90$^{\text{th}}$ percentile and the GEV fit for above the 90$^{\text{th}}$ percentile.

In figure 10.6 the conditional distributions $F(l_{max}|\bar{u})$ for each mean wind speed are shown for Toboel (with a wind speed bin width of 1 m/s). The thick line is the cdf $F(l_{max})$, obtained via a weighed summation, using eq. (2.14). The lower plot shows the tail of the cdf, with the horizontal line representing the 50-years' return period. Note that the cdf $F(l_{max})$ is shifted upwards to one, to compensate for the probability of wind speeds outside the range taken into account. The graphs for Horns Rev and Oak Creek are similar.

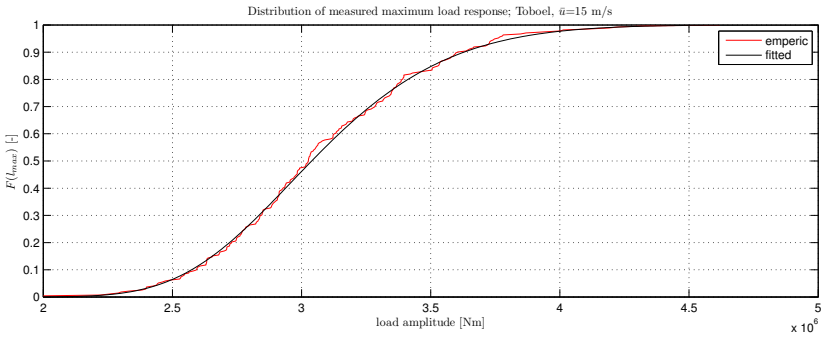

Figure 10.5: Example of an emipirical cdf and its GEV fit.

In order to find out the influence of the different wind speeds on the average results, a comparison was made with the other methods for the wind speeds $\bar{u}$ =6, 11 and 18 m/s. The

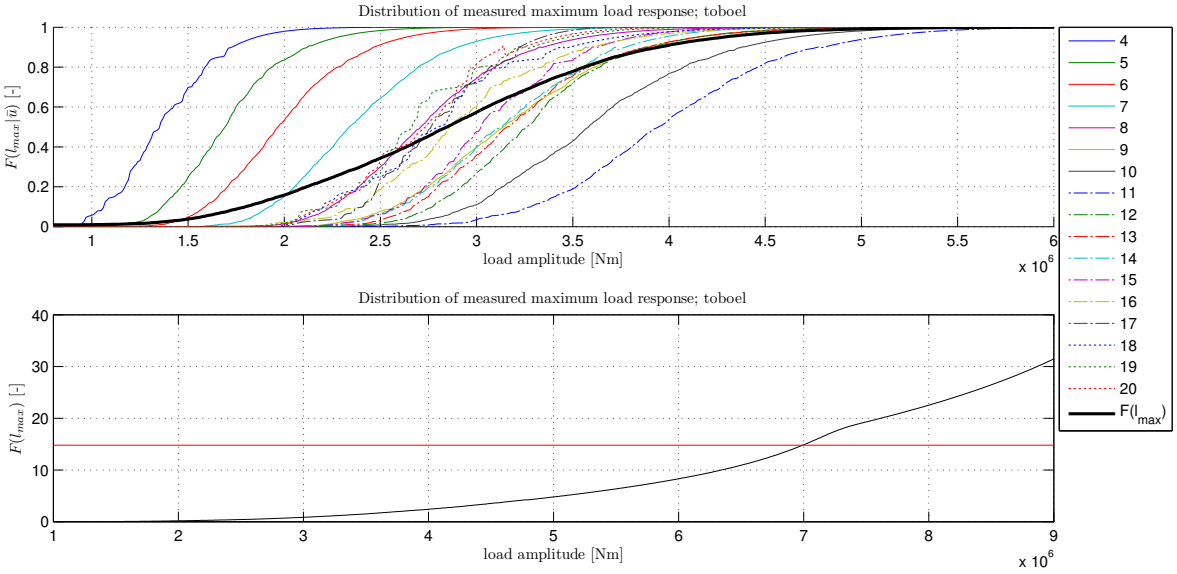

Figure 10.6: Extreme value distribution for Toboel. For the picture a wind speed bin width of 1 m/s has been taken. The upper graph displays the conditional cdf $F(l_{max}|\bar{u})$ and total cdf $F(l_{max})$. The lower graph shows the tail of $F(l_{max})$. The 50-years' return period is indicated by the red line. The corresponding 50-years' extreme load response is 7.00 MNm.

resulting 50-years' extreme load responses are given in table 10.1 (assuming a probability of one for each mean wind speed).

50-years' extreme using Gaussian theory

In section 2.4 a theoretical expression (Rice equation) has been given to obtain the 50-years' response level for a Gaussian random variable. This gives the possibility to compare the extreme values obtained from the measurements with a theoretical value for a Gaussian random variable. The second order spectral moment $\mu_{f,2}$ and standard deviation of the loads σ_l are derived from load calculations for the measured time series with a mean wind speed given in the former paragraph. To obtain the weighed average, the Rice cdf has been used. In table 10.1 the results are shown.

50-years' extreme using conditional simulation

The *New*Gust method for simulating gusts can be used to derive a distribution function of the maximum loads. The theory for this is explained in section 4.6. The simulations to obtain $F(l_{max}|\bar{u}, A)$ have been carried out for the same wind speed range as used for the measurements and an amplitude range of $1 - 7$. For the density $f(\bar{u}, A)$, results from section 9.3.2 are used. The inter- and extrapolation of the cdf have been done in exactly the same way as for the empirical cdf resulting from measurements.

The expression given in Bierbooms [2007] to derive a gust leading to an extreme in the load response can also be used to derive the distribution function of the maximum loads (cf. section 4.6). Because the load response $l(t)$ is defined by a linear system, eq. (4.33) can be used, which has been denoted by *Load*Gust. The simulations have been carried out with the

same wind speed and amplitude range as simulated with the *New*Gust method. The results can be found in table 10.1.

Comparison of 50-years' extreme values

In table 10.1 the results for the 50-years' extreme load response are given for the different methods. There are clear differences between the 50-years' values of the different methods.

		Toboel	Horns Rev	Oak Creek
weighed average	$l_{50} \rightarrow$ meas. [MNm]	8.86	10.38	28.03
	$l_{50} \rightarrow$ Rice cdf [MNm]	9.66	8.54	8.95
	nr. of meas. t-s	11825	38147	11700
	$l_{50} \rightarrow$ cond. sim. with *New*Gust [MNm]	8.86	11.47	10.68
	$l_{50} \rightarrow$ cond. sim. with *Load*Gust [MNm]	12.21	12.67	13.19
	nr. of sim. max.	137800	137800	137800
	$\sum f(\bar{u})$	0.99	0.94	0.79
$\bar{u} = 6^{\pm 0.1}$ m/s	$l_{50} \rightarrow$ meas. [MNm]	4.25	4.36	5.00
	$l_{50} \rightarrow$ Rice eq. [MNm]	5.06	5.11	5.34
	nr. of meas. t-s	324	636	149
	$l_{50} \rightarrow$ cond. sim. with *New*Gust [MNm]	5.13	6.38	6.28
	$l_{50} \rightarrow$ cond. sim. with *Load*Gust [MNm]	6.27	6.65	6.53
	nr. of sim. max.	1300	1300	1300
	$f(\bar{u})$	0.025	0.015	0.007
$\bar{u} = 11^{\pm 0.1}$ m/s	$l_{50} \rightarrow$ meas. [MNm]	7.47	10.28	11.25
	$l_{50} \rightarrow$ Rice eq. [MNm]	10.18	9.54	10.24
	nr. of meas. t-s	218	692	106
	$l_{50} \rightarrow$ cond. sim. with *New*Gust [MNm]	9.39	12.49	11.39
	$l_{50} \rightarrow$ cond. sim. with *Load*Gust [MNm]	10.44	12.63	12.46
	nr. of sim. max.	1300	1300	1300
	$f(\bar{u})$	0.019	0.017	0.006
$\bar{u} = 18^{\pm 0.1}$ m/s	$l_{50} \rightarrow$ meas. [MNm]	4.67	5.65	21.88
	$l_{50} \rightarrow$ Rice eq. [MNm]	4.53	4.85	4.86
	nr. of meas. t-s	14	113	193
	$l_{50} \rightarrow$ cond. sim. with *New*Gust [MNm]	12.61	5.24	7.62
	$l_{50} \rightarrow$ cond. sim. with *Load*Gust [MNm]	12.31	7.59	8.29
	nr. of sim. max.	1300	1300	1300
	$f(\bar{u})$	0.001	0.003	0.012

Table 10.1: Extreme values with a return period of 50-year obtained from measurements, Gaussian distributed turbulence and conditional simulations.

In appendix E (figure E.4) it is shown that each time series has its own extrapolation and corresponding 50-years' value. This large range of possible extrapolations is caused by the limited amount of maxima taken into account. Another reason is the fact that the measured time series show non-Gaussian statistics, whereas the theory assumes Gaussian statistics. In figure 10.7 the empirical cdf of local maxima has been plotted for some time series together

with the Rice cdf of local maxima. The resemblance of the empirical values with the Rice cdf is reasonably good, although there is a large spread in instantaneous cdf's (caused by the limited amount of data in a time series of ten minutes). The average of the GEV fits clearly shows the influence of one cdf with a heavy tail in case of an ensemble average. The most

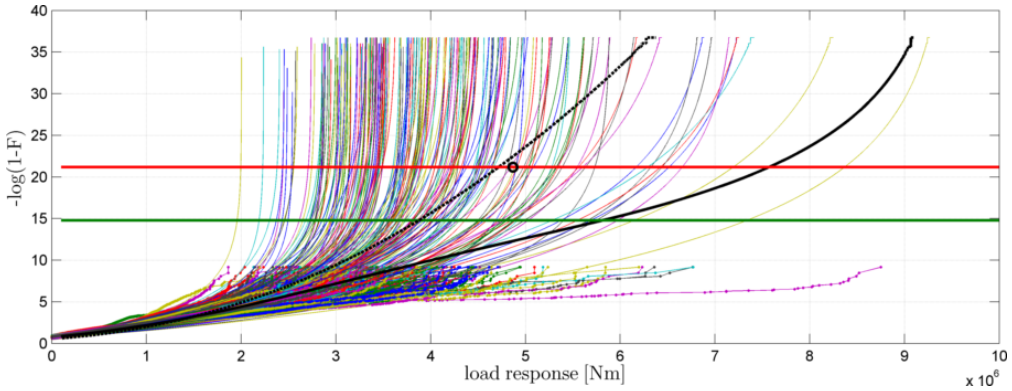

Figure 10.7: Empirical cdf's of local maxima for all the time series from Oak Creek at $\bar{u} = 18$ m/s (dots), together with their corresponding GEV fit (thin solid lines), the Rice cdf (thick dashed line) and Rice equation (circle) from the ensemble average statistics and ensemble average of all GEV fits (black thick solid line).

right empirical cdf with the very heavy tail is a result from the turbulence time series with many negative gusts. In figure 10.8 this time series is shown together with its load response. A third reason for the differences lies in the discreteness of the calculations and the continuous

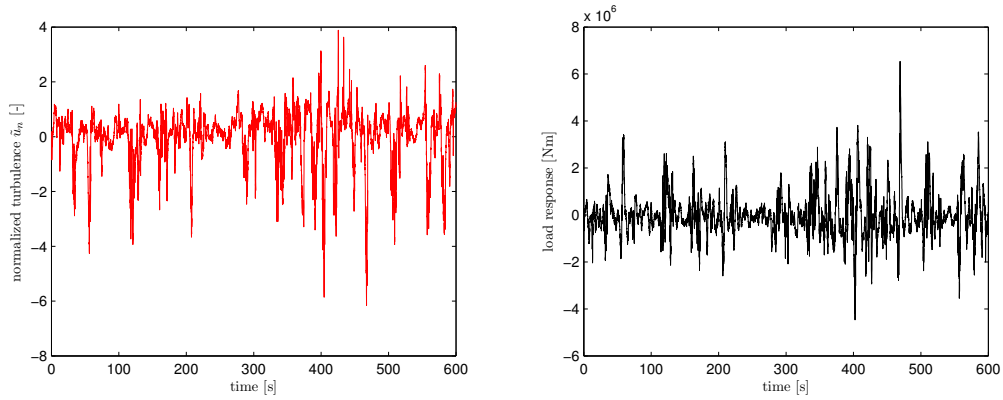

Figure 10.8: Turbulence time series from Oak Creek and its load response, explaining the heavy tail of the resulting cdf. This turbulence time series has a skewness of -1.58 and kurtosis of 6.88, which indicates that this turbulence is highly non-Gaussian distributed.

theory. This is shown in figure 10.9a; a different width of the wind speed bin gives a different 50-years value.

The large 50-years' value from measurements at Oak Creek with a mean wind speed of 18 m/s is explained by its fit, as can be seen in figure 10.9b. The heavy tail of the empirical cdf is explained by figure 10.4 and 10.8. These figures show that the heavy tail is caused by (frequent) large negative gusts, which are not captured by Gaussian theory. However, it should be noted that these negative are also not captured by the applied calculation method

of the load response. A linearized transfer function is used, which has no limit on the pitch angle if the pitch control is active and hence can be a reason for the very high loads.

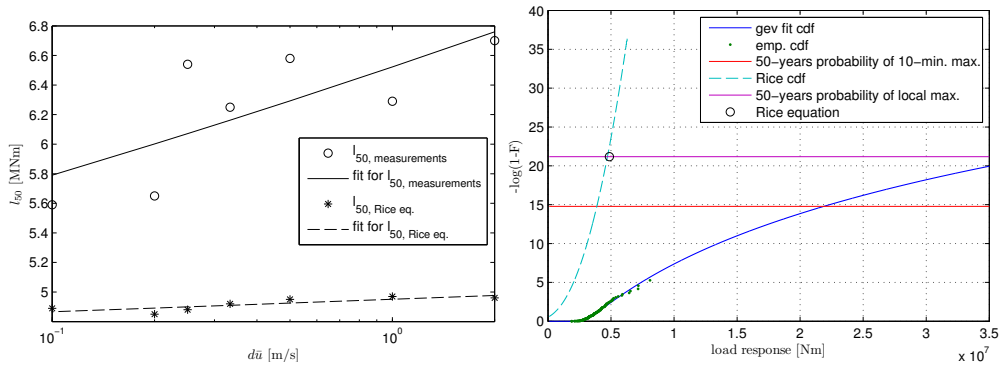

(a) **(b)**

Figure 10.9: a) Effect of discrete calculations visualized by varying the wind speed bin width. b) Extreme value cdf for Oak Creek at $\bar{u} = 18$ m/s.

10.2 Effect of non-Gaussian turbulence

From the investigation of the non-Gaussian behavior of turbulence in section 3.2.4, the question arises what the effect of non-Gaussian turbulence is on the extreme load response. This has been investigated by simulating the load response for measured, Gaussian and non-Gaussian simulated ten-minute time series. For each time series the maximum load response has been stored.

$$l_{max} = \max\left(l(t)\right), \quad t \in 0 \ldots 600s \tag{10.4}$$

For each different type of time series a histogram of the ten-minute maxima has been made. The measured time series are from Oak Creek and Horns Rev for the 16 – 17 m/s mean wind speed bin (1138 and 1261 time series) and from Toboel for the 10 – 11 m/s mean wind speed bin (1132 time series). The number of simulated time series is equal to the number of measured time series. In figure 10.10 the resulting histograms are presented. The plot clearly shows that the distribution of the extremes is much wider for the measured as for the simulated time series. The difference between the distributions of Gaussian and non-Gaussian maxima are only small. Both methods do not resemble the heavy tail of the measured histogram. Together with the results of the former section it can be concluded that the non-Gaussian (measured) behavior of turbulence has significant influence on the extreme loads. Proper non-Gaussian simulation is therefore necessary to obtain a good estimation of the 50-years' extreme load. These results are in agreement with the literature (cf. section 3.2.4).

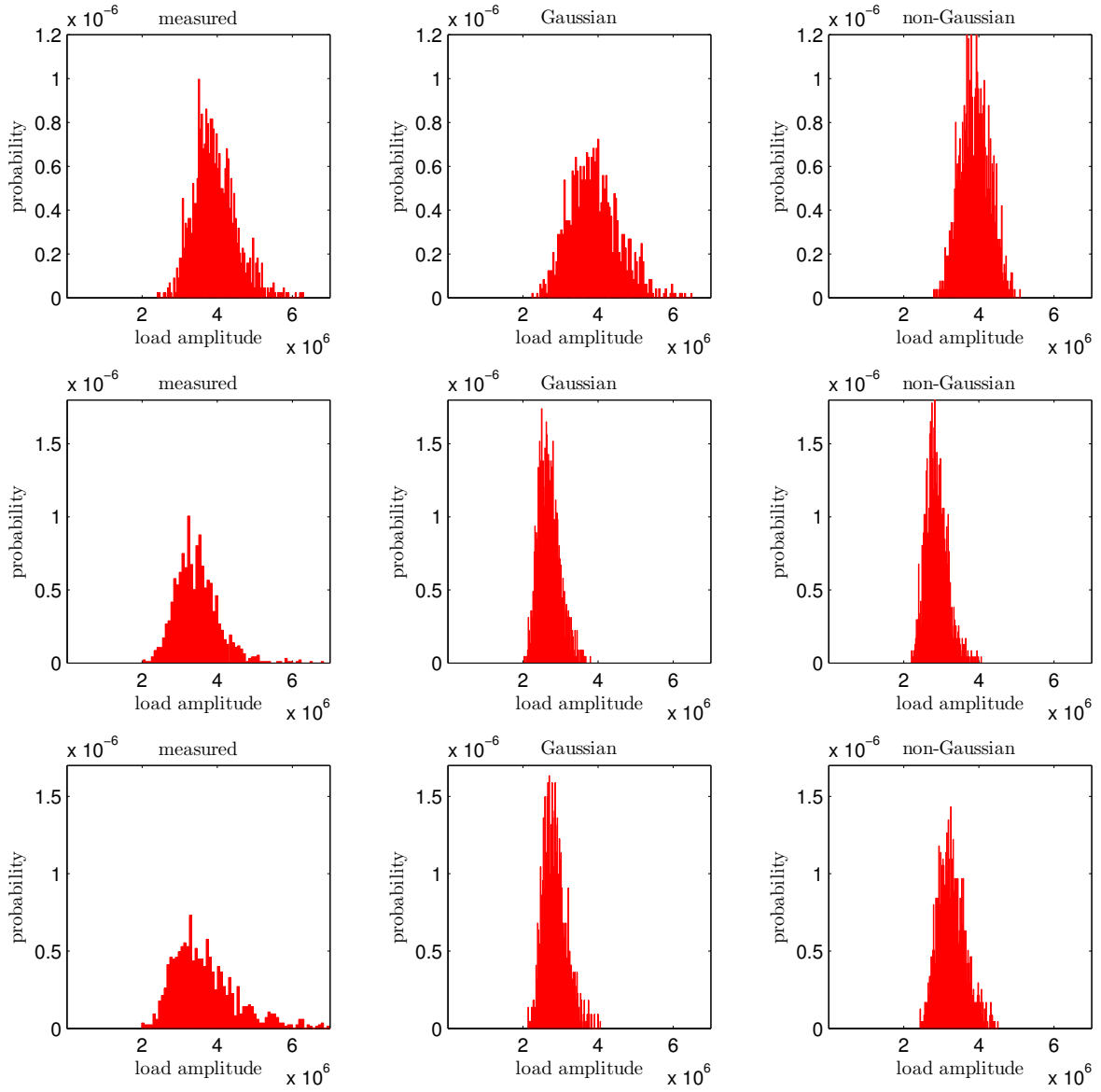

Figure 10.10: Histograms depicting the distribution of the extreme loads for three different types of turbulence time series, for all sites. left: measured turbulence, middle: Gaussian turbulence, right: non-Gaussian turbulence. top: Toboel, middle: Horns Rev, bottom: Oak Creek.

Conclusion

In general it can be concluded that the resemblance between measured and *New*Gust gusts is particularly good in the extreme cases for which *New*Gust has been designed (high mean wind speed, high relative amplitude). In these extreme cases the resemblance of the shape as well as the load responses are comparable with measured gusts. The better the gust shape resemblance, the better the resemblance of the resulting loads. The comparison of the different simulation methods shows that in these extreme cases there is no need for non-Gaussian simulations of gusts. However, in the case of lower mean wind speeds, non-Gaussian theory is required. Furthermore, the influence of B can be neglected and equation 4.20 suffices.

If the control of the blade pitch angle is active, the extreme loading is caused by an extreme rise time gust (this in contrast with stall-regulated wind turbines, where maximum amplitude gusts always cause the extreme load response). However, the extreme loading of a pitch-regulated wind turbine should not be searched for at the extreme wind speeds, but at the wind speeds where the transition of inactive to active pitch control takes place. In this wind speed region the extreme load response is caused by gusts with an extreme amplitude, as can be simulated with the *New*Gust method. When the autocorrelation function is used as a basis to simulate these type of gusts (i.e. with the *New*Gust and Risø method), a higher mean wind speed should be taken, to achieve a better resemblance of the theoretical and physical gust shape and the resulting load response.

In order to assess the 50-years' extreme wind turbine loading, conditional simulation with *New*- or *Load*Gust can be applied if the turbulence statistics are not to much different from Gaussian statistics. If the deviation from Gaussian statistics becomes too large and in particular if many large negative gusts are observed, proper non-Gaussian simulation is required.

From the research performed in this thesis a number of recommendations can de drawn:

- Time series should be long enough for a proper estimation of the spectrum;
- In order to simulate turbulence with the correct statistics, both the spectral density function and the probability density function should be taken into account;
- If a fit has to be made to a certain extreme value distribution, to extrapolate the distribution to a certain extreme value, the amount of data taken into account should be sufficiently large. If too little data is taken into account, the range of possible extrapolations and hence of the extreme value becomes too large;
- In the case of discrete calculations for extreme value analysis, the continuous theory should be approached as much as possible;

To make the validation more universal, other terrain types (wind climates) should be investigated as well. Although the shape of the same type of gusts are independent of terrain type, different terrain types give different gust types.

While only a simplified linear wind turbine model has been taken into account, the validation of *New*Gust, and more importantly, the investigation of extreme gusts and 50-years' load responses, should be extended to a non-linear wind turbine model and three-dimensional gusts.

In the future, it should be investigated how large the effect of negative (extreme rise time) gusts is on the pitch-control of the wind turbine, to see if the resulting high loads can be avoided with another control method; and if so, what type of gusts then cause the extreme loads.

A field of research that also should get attention is the simulation of non-Gaussian turbulence, in order to get a good representation of 'complex terrain turbulence'. In appendix I a work plan is proposed for simulation of turbulence using 'continuous time random walks'.

References

K. Beers. *Numerical methods for chemical engineering*. Cambridge university press, 2007.

H. Bergström. A statistical analysis of gust characteristics. *Boundary layer meteorology*, 39: 153–173, 1987.

W. Bierbooms. Investigation of spatial gusts with extreme rise time on the extreme loads of pitch-regulated wind turbines. *Wind Energy*, 8:17–34, 2005.

W. Bierbooms. Constrained stochastic simulation - generation of time series around some specific event in a normal process. *Extremes*, 8:207–224, 2006.

W. Bierbooms. Specific gust shapes leading to extreme response of pitch-regulated wind turbines. In *The science of making torque from the wind*, volume Journal of Physics: Conference Series 75, 2007.

W. Bierbooms. Determination of the extreme value in the response of wind turbines by means of constrained stochastic simulation. In *27th ASME wind energy symposium, Reno*, 2008.

W. Bierbooms. *Constrained stochastic simulation of wind gusts for wind turbine design*. PhD thesis, Delft University of Technology, 2009a.

W. Bierbooms. Application of constrained stochastic simulation to determine the extreme loads of wind turbines. *Solar Energy Engineering*, 131, 2009b.

W. Bierbooms, J. Dragt, and H. Cleijne. Verification of the mean shape of extreme gusts. *Wind energy*, 2:137–150, 1999.

W. Bierbooms, P. Cheng, G. Larsen, and B. Pedersen. Modelling of extreme gusts for design calculations – *NewGust*. Technical Report FINAL REPORT JOR3-CT98-0239, Delft university of technology, 2001.

F. Böttcher, C. Renner, H.-P. Waldl, and J. Peinke. On the statistics of wind gusts. *Boundary layer meteorology*, 108, July 2003.

F. Böttcher, S. Barth, and J. Peinke. Small and large scale fluctuations in atmospheric wind speeds. *Environmental research and risk assessment*, 21:299–308, 2007.

E. Branlard. Wind energy: on the statistics of gusts and their propagation through a wind farm. Technical report, ECN-Wind-Memo-09-005, 2009.

T. Burton, D. Sharpe, N. Jenkins, and E. Bossanyi. *Wind energy handbook*. John Wiley, April 2008.

B. Castaing, Y. Gagne, and E. Hopfinger. Velocity probability density functions of high reynolds number turbulence. *Physica D*, 46:177–200, 1990.

P. Davidson. *Turbulence, an introduction for scientists and engineers.* Oxford university press, 2007.

G. Deodatis and R. Micaletti. Simulation of highly skewed non-gaussian stochastic processes. *Journal of engineering mechanics*, 127(12):1284–1295, 2001.

O. Ditlevsen, G. Mohr, and P. Hoffmeyer. Integration of non-gaussian fields. *Probabilistic engineering mechanics*, 11:15–23, 1996.

J. A. Dutton. *The Ceaseless Wind, an introduction to the theory of atmospheric motion.* McGraw Hill, New-York, first edition, 1976.

R. Friederichs and D. Kleinhans. Continuous time random walks: Simulation of continuous trajectories. *Physical Review E*, 76, 2007.

H. Gontier, A. P. Schaffarczyk, D. Kleinhans, and R. Friedrich. A comparison of fatigue loads of wind turbine resulting from a non-gaussian turbulence model vs. standard ones. In *Journal of Physics: Conference Series 75*. IOP Publishing, 2007.

M. Grigoriu. *Applied non-Gaussian processes: examples, theory, simulation, linear random vibration, and MATLAB solutions.* Prentice Hall, Inc., 1995.

M. Grigoriu. Existence and construction of translation models for stationary non-gaussian processes. *Probabilistic engineering mechanics*, 24:545–551, 2009.

K. Gurley and A. Kareem. A conditional simulation of non-normal velocity/pressure elds. *Journal of Wind Engineering and Industrial Aerodynamics*, 77 & 78:39–51, 1998.

K. Gurley, A. Kareem, and M. Tognarelli. Simulation of a class of non-normal random processes. *International journal of non-linear mechanics*, 31(5):601–617, 1996.

K. Hansen and G. Larsen. Database on wind characteristics: Structure and philosophy. Technical Report Risø-R-1299(EN), RisøNational Laboratory, November 2001.

K. Hansen and G. Larsen. Full scale experimental analysis of extreme coherent gust with wind direction changes (ecd). In *Journal of Physics: Conference Series 75*. IOP Publishing, 2007.

A. Hense and P. Friederichs. Wind and precipitation extremes in the earth atmosphere. *Extreme Events in Nature and Society*, pages 169–187, 2006.

H. Jokinen, J. Ollila, and O. Aumala. On windowing effects in estimating averaged periodograms of noisy signals. *Measurement*, 28:197–207, 2000.

J. Jonkman, S. Butterfield, W. Musial, and G. Scott. Definition of a 5-mw reference wind turbine for offshore system development. Technical Report NREL/TP-500-38060, National renewable energy laboratory, February 2009.

J. Kaimal, S. Clifford, and R. Lataitis. Effect of finite sampling on atmospheric spectra. *Boundary layer meteorology*, 47:337–347, 1989.

D. Kleinhans, R. Friedrich, A. Schaffarczyk, and J. Peinke. Synthetic turbulence models for wind turbine applications. In *Progress in Turbulence III*, volume 131 of *Springer Proceedings in Physics*, pages 111–114. Springer Berlin Heidelberg, 2009.

P. Kundu and I. Cohen. *Fluid mechanics.* elsevier academis press, 2004.

N. Lagaros, G. Stefanou, and M. Papadrakakis. An enhanced hybrid method for the simulation of highly skewed non-gaussian stochastic fields. *Computer methods in applied mechanics and engineering*, 194:4824 – 4844, 2005.

G. Larsen, W. Bierbooms, and K. Hansen. Mean gust shapes. *Riso-R-1133(EN). Riso national laboratory*, december 2003.

T. Laubrich. *Statistical analysis and stochastic modelling of atmospheric boundary layer wind.* PhD thesis, Bergischen Universität Wuppertal, June 2009.

J. Mann. Simulation of turbulence, gusts and wakes for load calculations. *Wind Energy*, pages 87–92, 2007.

F. Masters and K. Gurley. Non-gaussian simulation: cumulative distribution function map-based spectral correction. *journal of engineering mechanics*, 129:1418–1428, december 2003.

A. Nawroth and J. Peinke. Multiscale reconstruction of time series. *Physical letters A*, 360: 234–237, 2006.

M. Nielsen, G. Larsen, J. Mann, S. Ott, K. Hansen, and B. Pedersen. Wind simulation for extreme and fatigue loads. Technical report, RisøNational Laboratory, Roskilde, Denmark, January 2004.

M. Nielsen, G. Larsen, and K. Hansen. Simulation of inhomogeneous, non-stationary and non-gaussian turbulent winds. In *Journal of Physics: Conference Series 75*, 75, 2007.

H. Olesen, S. Larsen, and J. H/ojstrup. Modelling velocity spectra in the lower part of the planetary boundary layer. *Boundary layer meteorology*, 29:285–312, 1984.

A. Papoulis and S. Pillai. *Probability, random variables and stochastic processes.* McGraw-Hill, fourth edition edition, 2002.

J. Peinke, S. Barth, F. Böttcher, D. Heinemann, and B. Lange. Turbulence, a challenging problem for wind energy. *Physica A*, 338:187–193, 2004.

J. Peinke, E. Anahua, S. Barth, H. Gontier, A. Schaffarcyk, D. Kleinhans, and R. Friedrich. Turbulence a challenging problem for the wind energy conversion. In *EWEC proceedings*, April 2008.

W. Press, S. Teukolsky, W. Vetterling, and B. Flannery. *Numerical recipes in FORTRAN: The art of scientific computing.* Cambridge university press, second edition edition, 1992.

D. Schertzer and S. Lovejoy. Uncertainty and predictability in geophysics: chaos and multi-fractal insights. *State of the Planet, Frontiers and Challenges in Geophysics*, 150:317334, 2004.

F. Schmitt. Gusts in intermittent wind turbulence and the dynamics of their recurrent times. *Wind energy*, pages 73–79, 2007.

Z.-S. She. Intermittency and non-gaussian statistics in turbulence. *Fuid dynamics research*, 8:143–158, 1991.

M. Shinozuka. Simulation of multivariate and multidimensional random processes. *The Journal of the Acoustical Society of America*, 49:357–367, January 1971.

M. Shinozuka and F. Yamazaki. Digital generation of non-gaussian stochastic fields. *Journal of engineering mechanics*, 114(7):1183–1197, 1988.

S. Smith. *The Scientist and Engineer's Guide to Digital Signal Processing*. California Technical Publishing, 1997.

A. Sommer. Wind resources at horns rev. Technical Report D-160949, Tech-wise, December 2002.

R. Stull. *An introduction to boundary layer meteorology*. Atmospheric science library. kluwer academic publishers, 1988.

R. Stull. *Meteorology for Scientists and Engineers*. Brooks/Cole, second edition edition, 2000.

H. Tieleman. Universality of velocity spectra. *Journal of wind engineering and industrials aerodynamics*, 56:55–69, 1995.

P. Veers. Three-dimensional wind simulation. *Sandia Report – SAND88 0152. Sandia National Laboratories*, 1988.

E. Weisstein. "hermite polynomial" from mathworld – a wolfram web resource. Online, 2009. URL `http://mathworld.wolfram.com/HermitePolynomial.html`. Accessed 01-Oktober-2009.

Wikipedia. Bartlett's method – wikipedia, the free encyclopedia. Online, July 2009a. URL `http://en.wikipedia.org/w/index.php?title=Bartlett%27s_method&oldid=301308281`. Accessed 30-September-2009.

Wikipedia. Hermite polynomials – wikipedia, the free encyclopedia. Online, November 2009b. URL `http://en.wikipedia.org/w/index.php?title=Hermite_polynomials&oldid=324953126`. Accessed 12-November-2009.

Wikipedia. Ionosphere – wikipedia, the free encyclopedia. Online, October 2009c. URL `http://en.wikipedia.org/w/index.php?title=Ionosphere&oldid=318672995`. Accessed 10-October-2009.

Wikipedia. Welch's method – wikipedia, the free encyclopedia. Online, July 2009d. URL `http://en.wikipedia.org/w/index.php?title=Welch%27s_method&oldid=303326703`. Accessed 30-September-2009.

S. Winterstein. Non-normal responses and fatigue damage. *Journal of engineering mechanics*, 111(10):1291–1295, October 1985.

S. Winterstein. Nonlinear vibration models for extremes and fatigue. *Journal of engineering mechanics*, 114(10):1772–1790, October 1988.

Part III

Appendices

Appendix A

Pitch controller

For the operation of a wind turbine it is important that the power can be controlled. The power output should be as high and 'flat' as possible, while the turbine is protected against high loads. For operation under full load conditions (wind speed equal to or higher than the nominal wind speed), this means that the power should be maintained at the nominal level, especially during wind speed disturbances (e.g. wind gusts). In a pitch controlled turbine this is achieved by continuously adjusting the blade pitch angle, to compensate for a change in power resulting from a change in wind speed.

The specifications of the NREL 5 MW turbine can be found in table 8.1. The mean wind speed of a turbulent wind speed time series is used to determine the transfer function of the system as described in section 8.2. The transfer function translates the wind speed and blade pitch angle (input) into the power (output) and defines the operating point around which the control system works.

The requirements for the operation of the imposed control system are:

- Reach steady state as fast as possible;
- Power fluctuations as small as possible;
- No steady state error.

The imposed control system has the configuration depicted in figure 8.1, where transfer function and control system are in parallel. In this way, the controller will be able to return the generated power to its nominal value by changing the pitch angle. This in contrast with the series configuration, which is not capable of eliminating the effect of a disturbance on the input signal. The series configuration is however useful in setting the control parameters, because it makes the steady state error visible (in contrast with the parallel configuration).

As the applied controller is a PI-controller, two control parameters need to be determined, the gain factor K and integral time factor T. The parameters K and T are determined as follows:

1. Determine the DC gain G_{DC} of the uncontrolled system to a step in the pitch angle;
2. Use the DC gain to calculate the starting point for searching the optimal K of the P-control to a step in wind speed. $K_{start} = 1/G_{DC}$;
3. Search for the K with optimal behavior (fast response, little oscillations, small steady state error);
4. Search for the optimal T of the PI-control together with the former found K (fast response, little overshoot).

Repeat these steps for a number of mean wind speeds, in order to obtain the relation between mean wind speed and K and T. This procedure has been done for the NREL 5 MW turbine, with help of MATLAB. An example of the procedure for one mean wind speed is given below.

```
%% initialize parameters
V0=16;     %mean wind speed
%Transfer function of the wind turbine
windturbine='NREL_5MW';
sys=transfer(windturbine,V0);

%% Open loop control action to obtain the DC-gain
%first an open loop system will be used to determine the DC-gain of the
%system. Herefore a hard step on the blade pitch angle is used.
Tfinal=60;
% a step action, the effect of output 4 (Pg) to input 1 (theta).
[y,t] = step(sys(4,1),Tfinal);
%the final value is approx. equal to the DC-gain:
DCgain = y(length(y)); %= -809,5 kW
timeConstantDCgain = DCgain * 0.63; %= -510 kW, which happens
%at t=3.16 s (time constant is obtained with use of interpolation).

%Set the value for K, which is defined as the change in pitch angle applied
%upon a change in power of 1 W
K = 1/DCgain; %=  -1.24e-6 deg/W
```

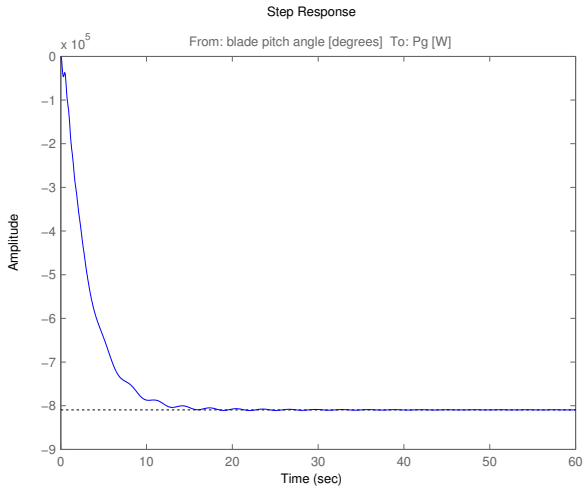

Figure A.1: Open loop control, determine DC gain

```
%% Total system with P-controller('closed loop'); instability check
Tfinal=60;
%check when instability occurs
K = [-1e-7 -1e-6 -1e-5 -1e-4];
for j = 1:length(K)
% Transfer function of the P-controller
syscp=tf(K(j),1);
%transfer function of the total system with Proportional control
%here feedin=1 means that we are connecting the output of the syscp to the
```

```
%input 1 of the system sys and feedout=4 means output 4 of sys is
%connected to the input of the controller syscp
feedin=1;
feedout=4;
sysclp=feedback(series(sys,syscp),1,feedin,feedout);
%sysclp=feedback(sys,syscp,feedin,feedout);
figure('color','none');
step(sysclp(4,2),Tfinal); shg
end
```

```
%% Total system with P-controller('closed loop'); optimization
Tfinal=60;
%optimize K
K = [-9e-7 -1e-6 -1.5e-6 -2e-6 -2.5e-6 -3e-6 -4.5e-6];
for j = 1:length(K)
% Transfer function of the P-controller
syscp=tf(K(j),1);
%transfer function of the total system with Proportional control
%here feedin=1 means that we are connecting the output of the syscp to the
%input 1 of the system sys and feedout=4 means output 4 of sys is
%connected to the input of the controller syscp
feedin=1;
feedout=4;
sysclp=feedback(series(sys,syscp),1,feedin,feedout);
%sysclp=feedback(sys,syscp,feedin,feedout);
figure('color','none');
step(sysclp(4,2),Tfinal); shg
end
%desired behavior is achieved at K=-2e-6.
```

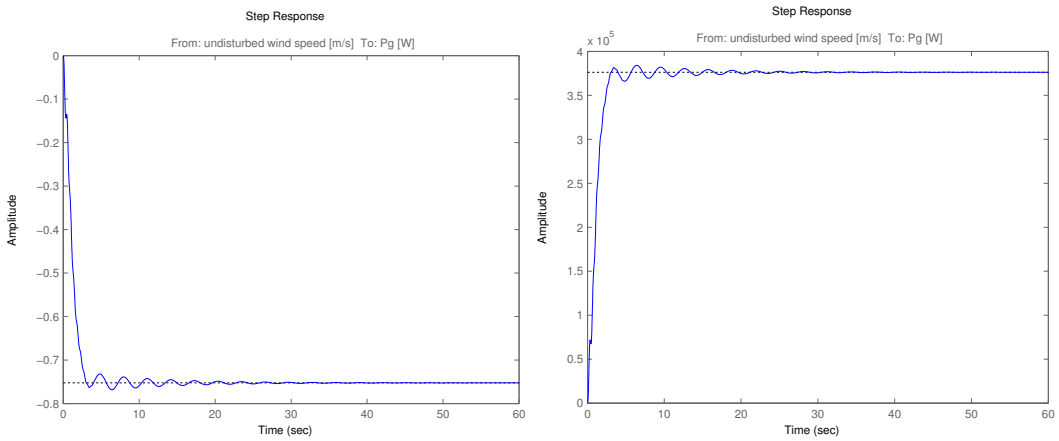

(a) series configuration **(b)** parallel configuration

Figure A.2: Closed loop proportional control, determine optimal K. In this case only proportional control is applied

```
%% Total system with PI controller ('closed loop'); instability check
Tfinal=60;
```

```
K = -2e-6;
%check when instability occurs
T = [20 10 5 4 3 2 1 0.5 0.2 0.1];
for j = 1:length(T)
% transfer function of the PI-controller
syscpi=tf([K*T(j) K], [T(j) 0]);
feedin=1;
feedout=4;
sysclpi=feedback(series(sys,syscpi),1,feedin,feedout);
%sysclpi=feedback(sys,syscpi,feedin,feedout);
figure('color','none');
step(sysclpi(4,2)); shg
end
```

```
%% Total system with PI controller ('closed loop'); optimization
Tfinal=60;
K = -2e-6;
T = [2.8 2.7 2.6 2.5 2.4 2.3 2.2];
for j = 1:length(T)
% transfer function of the PI-controller
syscpi=tf([K*T(j) K], [T(j) 0]);
feedin=1;
feedout=4;
sysclpi=feedback(series(sys,syscpi),1,feedin,feedout);
%sysclpi=feedback(sys,syscpi,feedin,feedout);
figure('color','none');
step(sysclpi(4,2)); shg
end
```

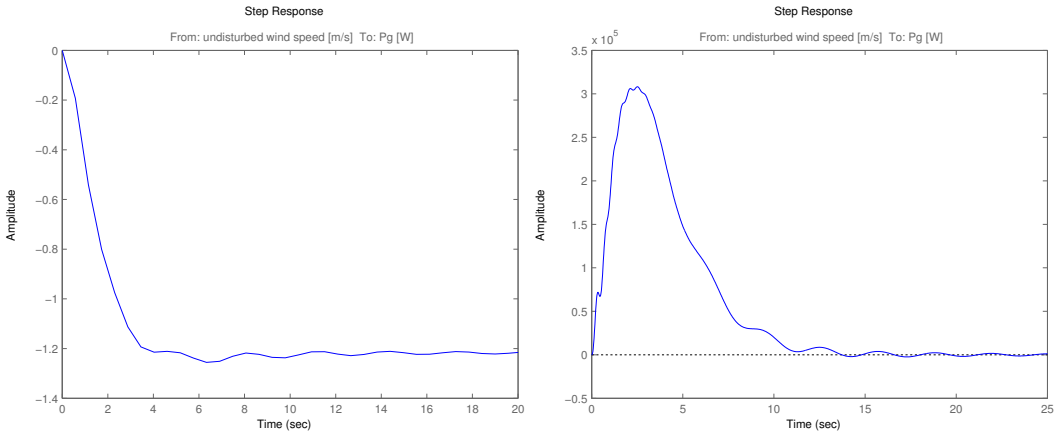

(a) series configuration **(b)** parallel configuration

Figure A.3: Closed loop proportional and integral control, determine optimal T. In this case both proportional and integral control is applied.

If this procedure is repeated for a number of mean wind speeds, the dependence of the control parameters is obtained. In figure A.4 the results for T and K including a fit are given. In figure A.5 the difference in the response of the generator power to a wind speed step for the controlled and uncontrolled wind turbine is illustrated.

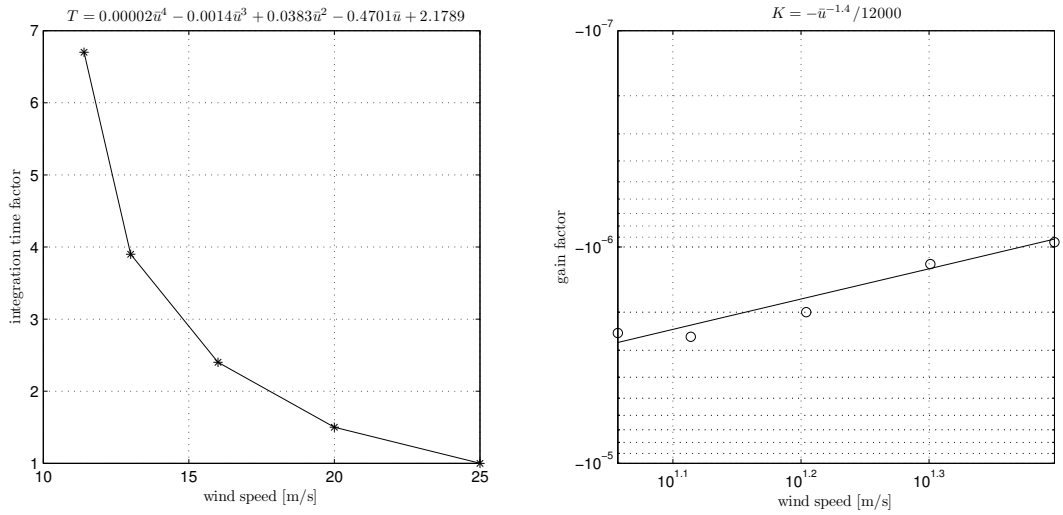

Figure A.4: Dependence of the control parameters on the wind speed. These parameters are for the PI-controller of the NREL 5 MW wind turbine

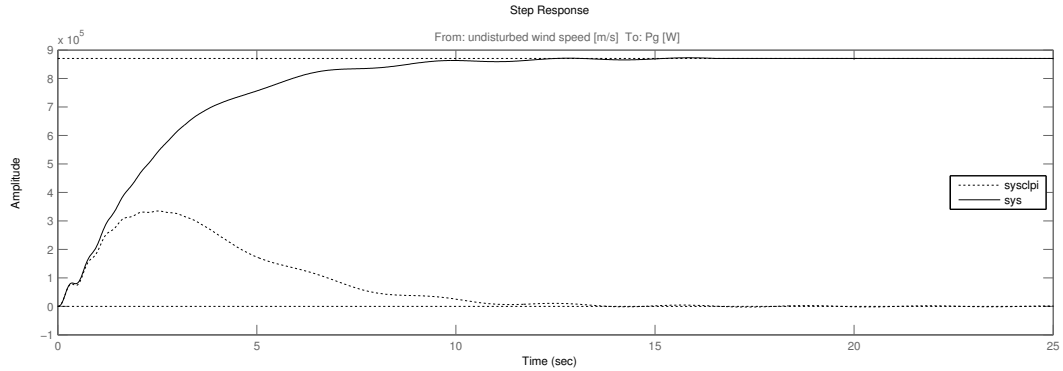

(a) Response to a step in wind speed, with (sysclpi) and without (sys) controller

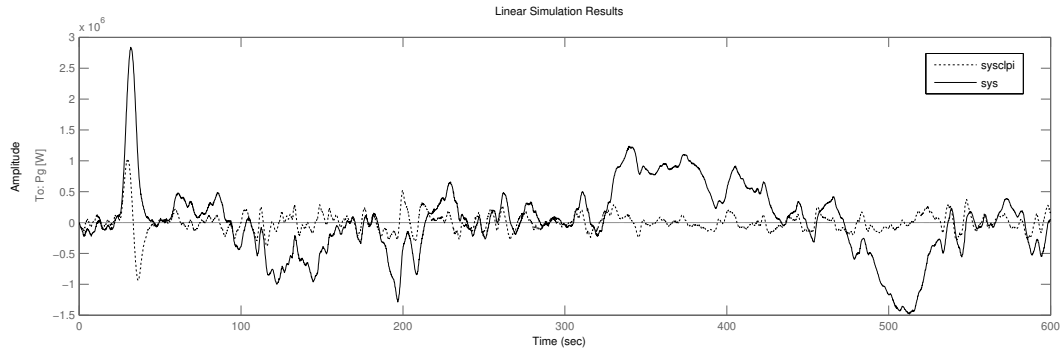

(b) Response to a time series of turbulence, with (sysclpi) and without (sys) controller

Figure A.5: Illustration of the effect of PI-control on the generator output of the wind turbine.

Appendix B

Spectra descriptions

In this appendix several theoretical descriptions of atmospheric spectra are given. For convenience, also a table with roughness-length is given.

In the IEC 61400-1 wind turbine design standard, the following definition of the Kaimal spectrum (neutral atmosphere) is given

$$\text{Kaimal:} \quad \frac{fS_n(f)}{\sigma_n^2} = \frac{4fL_n/\bar{u}}{(1+6fL_n/\bar{u})^{5/3}} \tag{B.1}$$

Where f is the frequency in Hz, n denotes the velocity component (u,v,w), S_n is the single-sided spectrum, σ_n is the standard deviation, $\bar{u}$ is the mean wind speed and L_n is the integral scale parameter. For n is 1,2,3, σ_n is respectively σ_1, $0.8\sigma_1$, $0.5\sigma_1$ and L_n is respectively $8.1\Lambda_1$, $2.7\Lambda_1$, $0.66\Lambda_1$. Where $\Lambda_1 = \min(0.7z, 42)$, z denotes the height above the ground.

In Veers [1988] the following definitions are given for the Frost (stable atmosphere), von Karman (neutral atmosphere) and Solari (neutral atmosphere) spectra:

$$\text{Frost:} \quad S(f) = \frac{12.3\bar{u}_{10}/\left[\ln\left(\frac{10}{z_0}+1\right)\ln\left(\frac{z}{z_0}+1\right)\right]}{1+192\left[(fz/\bar{u}_{10})\ln\left(\frac{10}{z_0}+1\right)\ln\left(\frac{z}{z_0}+1\right)\right]^{5/3}} \tag{B.2}$$

$$\text{von Karman:} \quad S(f) = \frac{22.8u_*^2L_1/\bar{u}}{1.339\left(1+39.48\left(fL_1/\bar{u}\right)^2\right)^{5/6}} \tag{B.3}$$

$$\text{Solari:} \quad S(f) = \frac{2.21u_*^2\beta^{2.5}z/\bar{u}}{\left(1+3.31\left(f\beta^{1.5}z/\bar{u}\right)\right)^{5/3}} \tag{B.4}$$

Where u_* is the friction velocity, $u_* = 0.4\bar{u}/\ln(z/z_0)$, in the von Karman spectrum $\sigma_1^2 = 5.7u_*^2$. To represent the scatter found in measured turbulence spectra, β should be varied by $\beta = \beta_m + \mu_\beta\Delta\beta$, where μ_β is a uniformly distributed random variable in the interval $[-1, 1]$ and β_m and $\Delta\beta$ are

$$\beta_m = \begin{cases} 7.5 & z_0 \le 0.03 \\ 4.5 - 0.856\ln(z_0) & 0.03 \le z_0 \le 1.0 \\ 4.5 & 1.0 \le z_0 \end{cases} \tag{B.5}$$

$$\Delta\beta = \begin{cases} 2.5 & z_0 \le 0.03 \\ 2.0 - 0.143\ln(z_0) & 0.03 \le z_0 \le 1.0 \\ 2.0 & 1.0 \le z_0 \end{cases} \tag{B.6}$$

z_0	classifiction	landscape
0.0002	sea	sea, paved areas, snow covered flat plain, tide flat, smooth desert
0.005	smooth	beaches, pack ice, morass, snow-covered fields
0.03	open	grass prairie or farm fields, tundra, airports, heather
0.1	roughly open	cultivated area with low crops and occasional obstacles (single bushes)
0.25	rough	high crops, crops of varied height, scattered obstacles such as trees or hedgerows, vineyards
0.5	very rough	mixed farm fields and forest clumps, orchards, scattered buildings
1.0	closed	regular coverage with large size obstacles with open spaces roughly equal to obstacle heights, suburban houses, villages, mature forests
≥ 2	chaotic	centers of large towns and cities, irregular forests with scattered clearings

Table B.1: The Davenport-Wieringa roughness-length classification. Taken from [Stull, 2000]

In this way, the low frequency part of the spectrum is a random variable, where the high frequency part matches the Kaimal and von Karman spectrum.

Another description of the von Karman spectrum together with its autocorrelation function given by Nielsen et al. [2004], is

$$S_{\tilde{u}}(f) = \frac{9}{55}\alpha\varepsilon^{2/3}\frac{1}{L_{\tilde{u}}^{-2} + (2\pi f/\bar{u})^2}^{5/6} \tag{B.7}$$

$$R_{\tilde{u}}(\tau) = \frac{2^{2/3}9}{55\sqrt{\pi}\Gamma(\frac{5}{6})}\alpha\varepsilon^{2/3}(\tau\bar{u}L)^{1/3}K_{\frac{1}{3}}(\tau\bar{u}/L_{\tilde{u}}) \tag{B.8}$$

Where $\Gamma(\cdot)$ denotes the Gamma function, and $K_{\frac{1}{3}}(\cdot)$ is the Bessel function of second kind of order 1/3. Typical atmospheric parameters are $L_{\tilde{u}} = 100$ m and $\alpha\varepsilon^{2/3} = 0.1$.

To describe the stochastic behavior of turbulence in space, coherence functions are required. Some possible coherence functions are found in the IEC standard and Veers [1988];

$$\text{Kaimal:} \quad Coh(r,f) = e^{-12\sqrt{(fr/\bar{u})^2 + (0.12r/8.1\Lambda_1)^2}} \tag{B.9}$$

$$\text{Solari:} \quad Coh(r,f) = e^{\frac{-(12+5\mu_b)(r/z_m)^{1/4}rf}{\bar{u}}} \tag{B.10}$$

Where r is the magnitude of the separation vector between two points in space onto a plane normal to the average wind direction, z_m is the mean height between the two points and μ_b is a random variable uniformly distributed on the interval $[-1, 1]$.

Appendix C

Relation between different spectral moments and the autocorrelation function

In this thesis, $S_f(f)$ and $S_\omega(\omega)$ are the spectral density function of the turbulent wind speed $\tilde{u}(t)$. The mathematical formulation of frequency is either the cyclic frequency f in cycles per second (Hz) or the angular frequency ω in radians per second (rad/s). The spectral density function represents the variance of $\tilde{u}(t)$ as it is distributed over the frequencies in $\tilde{u}(t)$. Because the total variance is clearly independent of its distribution over ω or f, it holds that

$$\int_0^\infty S_f(f)\,df = \int_0^\infty S_\omega(\omega)\,d\omega \tag{C.1}$$

Because $S_f(f)$ and $S_\omega(\omega)$ represent a real physical process, they are only defined for positive frequencies. Because $\omega = 2\pi f$, the relation between both spectra is

$$\int_0^\infty S_f(f)\,df = \int_0^\infty S_\omega(\omega)\,d2\pi f \tag{C.2}$$

$$S_f(f) = 2\pi S_\omega(\omega) \tag{C.3}$$

The spectral moments are defined for both spectra as

$$m_{f,n} = \int_0^\infty (f)^n\, S_f(f)\,df \tag{C.4}$$

$$m_{\omega,n} = \int_0^\infty (\omega)^n\, S_\omega(\omega)\,d\omega \tag{C.5}$$

By inserting the relation between both spectra, the relation between both definitions of the spectral moments is obtained

$$m_{f,n} = \int_0^\infty (f)^n\, S_f(f)\,df \tag{C.6}$$

$$m_{f,n} = \int_0^\infty \left(\frac{\omega}{2\pi}\right)^n 2\pi S_\omega(\omega)\,d\frac{\omega}{2\pi} \tag{C.7}$$

$$m_{f,n} = (2\pi)^{-n} \int_0^\infty (\omega)^n\, S_\omega(\omega)\,d\omega \tag{C.8}$$

$$m_{f,n} = (2\pi)^{-n}\, m_{\omega,n} \tag{C.9}$$

The derivatives of the autocorrelation function are obtained with help of the inverse Fourier transformation. By using the relation between both spectra just like for the spectral moments, the relation between the acf and both definitions of the spectral moments is found.

$$\frac{d^n}{d\tau^n}R(\tau) = \int_0^\infty (i2\pi f)^n \, S_f(f) e^{2\pi i \tau f} \, df \tag{C.10}$$

$$\frac{d^n}{d\tau^n}R(\tau) = \int_0^\infty (i\omega)^n \, S_\omega(\omega) e^{i\tau\omega} \, d\omega \tag{C.11}$$

For the case $\tau = 0$, this becomes

$$\frac{d^n}{d\tau^n}R(0) = (i2\pi)^n \int_0^\infty (f)^n \, S_f(f) df = (i2\pi)^n \, m_{f,n} \tag{C.12}$$

$$\frac{d^n}{d\tau^n}R(0) = (i)^n \int_0^\infty (\omega)^n \, S_\omega(\omega) d\omega = (i)^n \, m_{\omega,n} \tag{C.13}$$

By its definition, $i^n = (-1)^{n/2}$, which gives

$$\frac{d^n}{d\tau^n}R(0) = (-1)^{n/2}(2\pi)^n m_{f,n} = (-1)^{n/2} m_{\omega,n}, \qquad n = 0, 1, 2, \ldots \tag{C.14}$$

And again,

$$(2\pi)^n m_{f,n} = m_{\omega,n} \tag{C.15}$$

This theory has been checked with the theoretical Fourier pair

$$r(\tau) = e^{-\frac{|\tau|}{\mathcal{T}}} \tag{C.16}$$

$$S_f(f) = \frac{2\mathcal{T}}{1 + (2\pi f \mathcal{T})^2} \tag{C.17}$$

Where $\mathcal{T}$ is the integral time scale. It has been checked whether the MATLAB routine to derive the acf from the spectrum gives the same results as the theoretical spectrum. In figure C.1 the results are shown. It is clear that the resemblance is almost perfect.

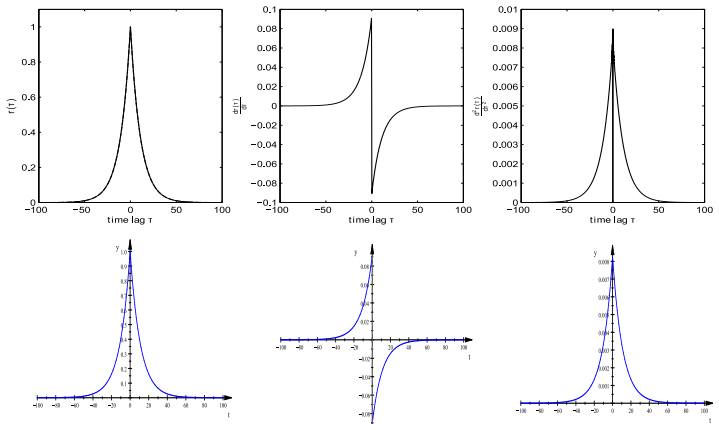

Figure C.1: Comparison of the acf and its first and second derivative (from left to right). Upper row: discrete acf dirived with help of MATLAB; lower row: continuous acf and its derivatives derived with help of MuPad (part of the symbolic math toolbox in MATLAB).

Appendix D

Example of Veers method

Discrete fluctuating wind speed time series are obtained with the Veers method by first generating Fourier coefficients with proper statistics and next perform an inverse FFT to convert them from frequency to time domain. The following example for $N = 1$ point in space, $M = 8$ points in time with a time step $\Delta t = 1$ and $\bar{u} = 8$, $\sigma_u = 1$, illustrates the principle:

The Fourier Transform is used to transform the Fourier coefficients from frequency to time domain. In order to obtain the correct coefficients, first the correct frequency components should be derived. The total period $T = M\Delta t$ contains the frequency components $f = \Delta f(1, \ldots, M/2 - 1)$, with $\Delta f = 1/T$. In FFT, the number of frequency components should be exactly equal to M, to get time series of length M. By using the same amount neg. and positive frequencies, the IFFT of the Fourier coefficients will sum up cosines and sines. This results in a time series with only real values. Because we are dealing with a physical one-sided spectrum, only the positive half of frequencies is taken into account. This is corrected in the inverse Fourier transform below, to get a time series of length M.

$$f = \begin{bmatrix} 0.1250 & 0.2500 & 0.3750 \end{bmatrix}$$

With the above information known, it's possible to compute the PSD from a specified spectrum $S(f)$ for each frequency. For example the Kaimal description can be used (cf. appendix B). In order to get the correct variance, $S(f)$ should be multiplied with the width of the frequency bins Δf and divided by 2 (for a reason explained below). Because we are dealing with one point, there's no CSD and $S(f)$ is a 1x1 matrix. With Cholesky factorization, the matrix $H(f)$ is obtained. This matrix H contains all the information about the wind field which has to be simulated.

$$S = \begin{bmatrix} 0.1939 & 0.0643 & 0.0333 \end{bmatrix}$$
$$H = \begin{bmatrix} 0.4403 & 0.2536 & 0.1824 \end{bmatrix}$$

The starting point for generating the time series are white noise inputs, which are generated for each frequency component by $X(f) = e^{i\theta(f)}$. Where θ is a random phase, uniformly distributed within $0 - 2\pi$. Another possibility is to generate standard Gaussian distributed

random variables a_k and b_k as in eq. (3.31).

$$X = \begin{bmatrix} -0.3721 - 0.9807i \\ 0.6165 + 0.4671i \\ -0.1800 + 2.4215i \end{bmatrix}$$

With the multiplication $V(f) = X(f)H(f)$, the random phases become correlated according to the information stored in $H(f)$.

$$V = \begin{bmatrix} -0.1517 - 0.3999i \\ 0.1448 + 0.1097i \\ -0.0304 + 0.4092i \end{bmatrix}$$

To obtain the full time series with M time points for each spatial point N, the following operation should be done;

$$T = M * IFFT(\begin{bmatrix} 0 & V & 0 & \text{rot90}(V^T) \end{bmatrix})$$

$$T = \begin{matrix} -0.0747 \\ -0.4041 \\ 1.3286 \\ 0.3778 \\ 0.6538 \\ -0.0347 \\ -1.9077 \\ 0.0610 \end{matrix}$$

The first Fourier coefficient is set to zero, to get a zero mean. Next the computed Fourier coefficients for the positive frequencies are placed. The first of the Fourier coefficients for the negative frequencies is also set to zero, to avoid imaginary values. Finally, the (imaginary) Fourier coefficients for the positive frequencies are rotated ninety degrees in the imaginary plane, to create the Fourier coefficients for the negative frequencies, assuming an artificial double-sided symmetric spectrum. In order to keep the area below the spectrum equal to the variance, the discrete values $S(f)$ obtained from the spectrum should be multiplied with $\Delta f/2$. From the inverse fast Fourier transform, a similar result as in figure D.1 should be obtained.

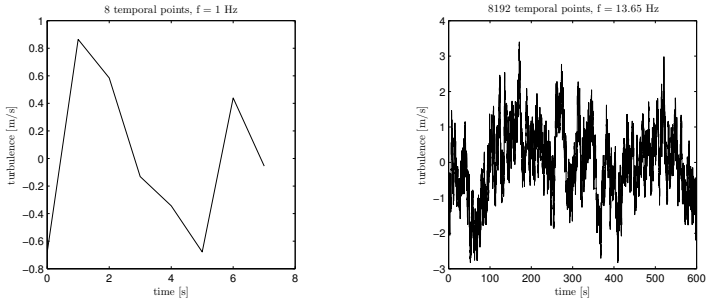

Figure D.1: Example of a time series simulated according to Veers method with 8 temporal points and 2^{13} temporal points ($\bar{u} = 8, \sigma_u = 1$).

Appendix E

Check of extreme value routines

For the extreme value analysis in section 10.1.3 the there applied methods have to be checked. A comparison between the several theories is made for one mean wind speed ($\bar{u} = 6$ m/s). For this purpose a number of Gaussian time series have been simulated with the Kaimal spectrum as an input. For each time series the loads have been calculated. These time series have been used to check the following quantities.

Check of ν_0

The zero up-crossing frequency ν_0 is used in the Rice equation (cf. section 2.4). It has been checked if ν_0 obtained via direct counting from the load calculations is the same as the one obtained via the spectrum of the load response. for each load response time series the spectrum is estimated. From this spectrum the second order spectral moment can be calculated. Together with the variance of the load response, ν_0 can be obtained. The results can be seen in figure E.1. The magnitude of ν_0 from the time series depends on the sampling

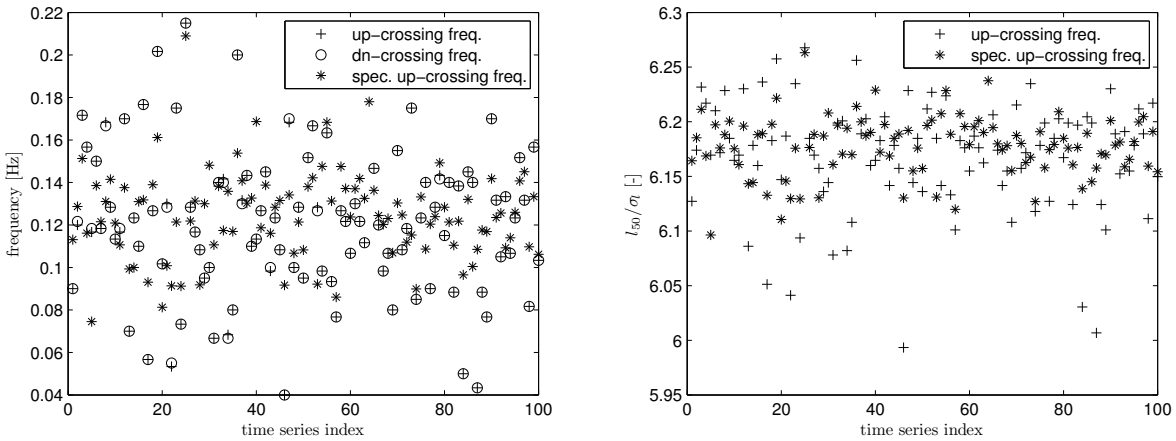

Figure E.1: Frequency of zero-crossings. The up- and down-crossings are almost always equal. The up-crossing rate from the spectrum seems to be more averaged out. The mean of the different zero-crossings is equal. The effect of the scatter of ν_0 on the Rice equation is clearly small. The final scatter in the Rice equation is determined by the scatter in the standard deviation of each time series.

rate and the level of discretization of the spectrum; the higher the sampling rate (sampling

frequency), the higher ν_0. This dependency is caused by the spectral moment $m_{f,2}$ (cf. section 3.2.3). In figure E.2 the dependency of $m_{f,2}$ on f and df is visualized. For the continuous case, where the frequency goes from zero to infinity, $m_{f,2}$ will be infinitely large (cf. figure C.1).

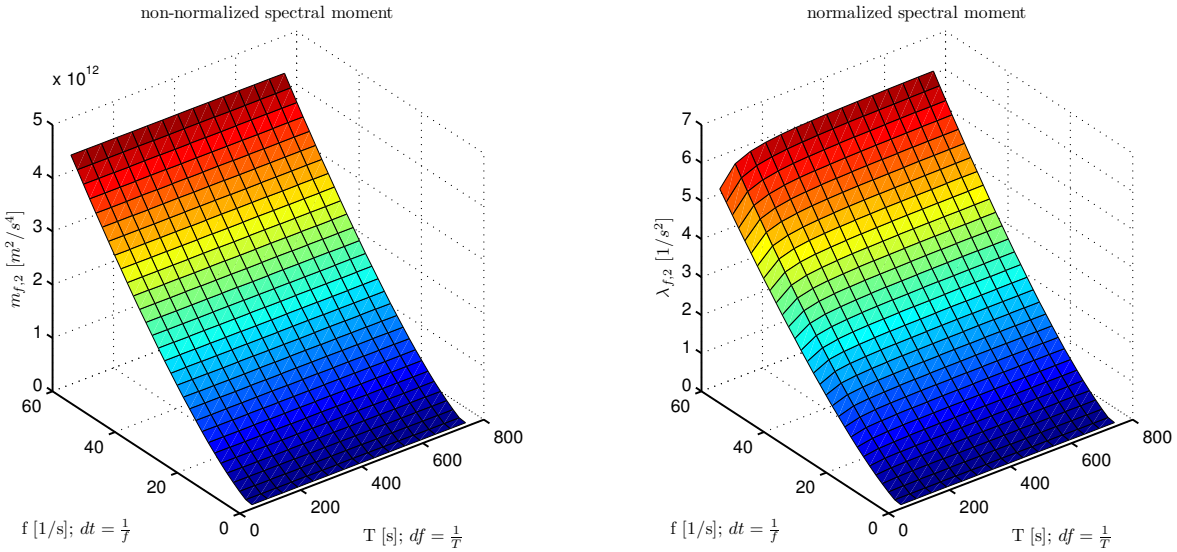

Figure E.2: Dependency of $m_{f,2}$ (left) and $\lambda_{f,2}$ (right) on f and df. It is clear that $\lambda_{f,2}$ depends on the level of discretization, for small df, $\lambda_{f,2}$ will approach a limit.

Check of spectrum estimation

The estimation procedure of the spectrum can be verified by checking the relation $S_{rr}(f) = |H(f)|^2 S_{uu}(f)$. The spectra $S_{uu}(f)$ and $S_{rr}(f)$ are known from respectively the input spectrum for the simulation of Gaussian wind speed time series and the spectrum of the resulting load response. $H(f)$ is obtained from the transfer function with as input the wind speed and as output the blade root bending moment. The frequency response can be obtained with use of the MATLAB function `bode`. With $H(f)$ known, $S_{rr}(f)$ can be obtained from the equation given above and should then coincide with the one obtained from the simulated load time series. In figure E.3 the results are shown.

Check of different 50-years extreme values

In section 2.4 the Gaussian theory is given with respect to extreme loads. eq. (2.16) and cdf (2.17) have been used to calculate the 50-years extreme load response. For each load response time series the maximum has been stored, so a cdf can be constructed. This cdf is extrapolated with help of MATLAB function `gevfit`. The average has been taken from 100 simulation of each 1000 time series. The time series have a length of ten minutes. The obtained average results for each method are given in table E.1 and figure E.4.

The zero up-crossing frequency from the spectral moments differs a bit from the direct counting, which can be explained by the spectra shown in figure E.3. For the estimation of the load spectrum a window is used to smooth the time series edges. This results in a little

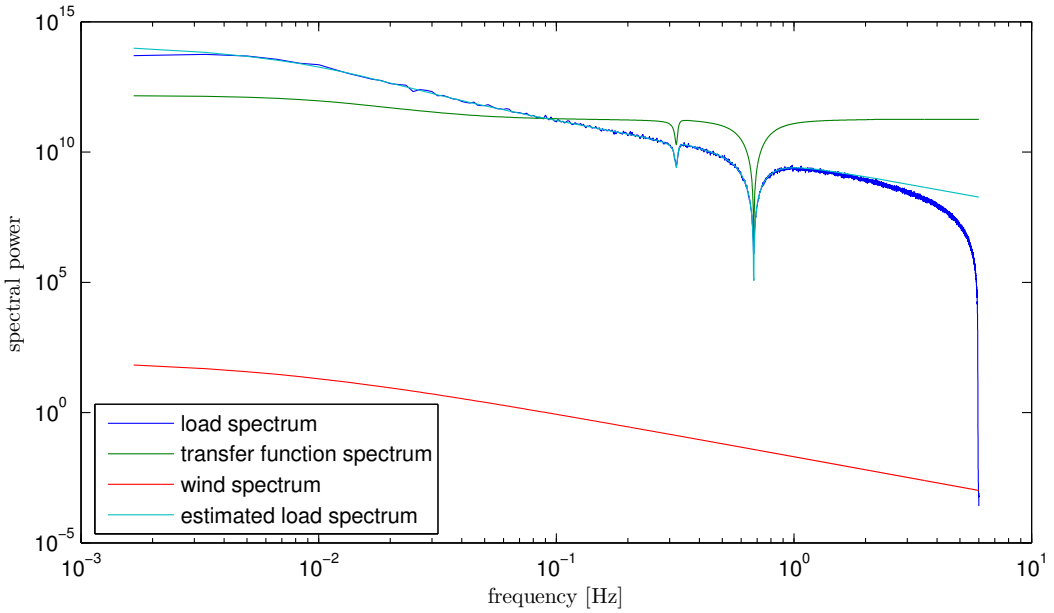

Figure E.3: The different obtained spectra. It is clear that the two spectra of the load response coincide very well. The difference lies in the use of a window to smooth the time series edges in the estimation procedure.

	Value
ν_0 counted	0.121 Hz
ν_0 from spectrum	0.125 Hz
l_{50} Rice eq. – counted	4.67 MNm
l_{50} Rice eq. – from spectrum	4.67 MNm
l_{50} empirical 10-min max.	4.66 MNm
l_{50} Rice cdf	4.64 MNm
$\langle \sigma_l \rangle$ (ensemble average)	0.78 MNm

Table E.1: Comparison of the different values for the 50-years extreme load response

different spectral amplitude at low frequencies, which gives the difference in zero up-crossing frequency.

The difference between the Rice cdf and the empirical cdf is explained by the fact that the Rice cdf is defined for local maxima, which are assumed to be independent to enable the extrapolation to the 50-years value. The local maxima in the load response time series may not be completely independent. The empirical cdf is made for the 10-minute maxima which can reasonably well be assumed to be independent. This explains why the value for F_{50} differs for both methods. The value φ used in the Rice cdf is almost one, which means that the resulting cdf is (almost) Gaussian.

The 50-years extreme values from the empirical cdf is close to the value obtained from the Rice equation and cdf. Note that a sufficient large amount of maxima is needed to get a good estimate of (extrapolation to) the empirical 50-years value.

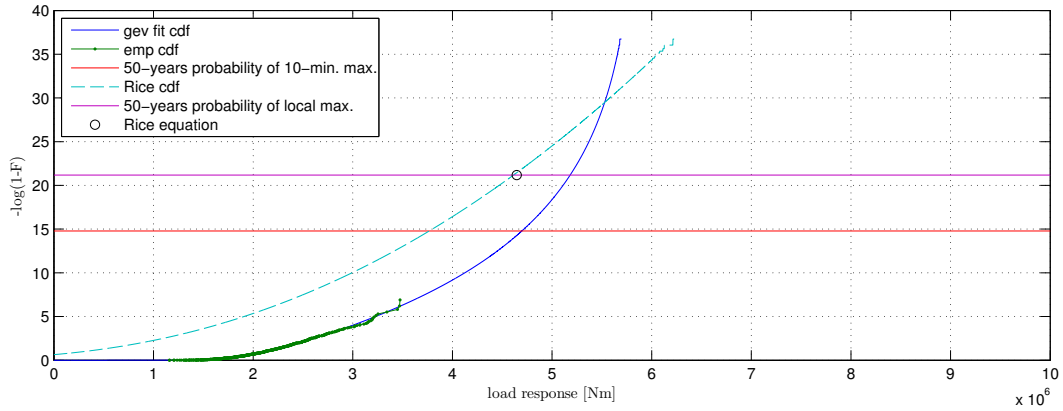

(a)

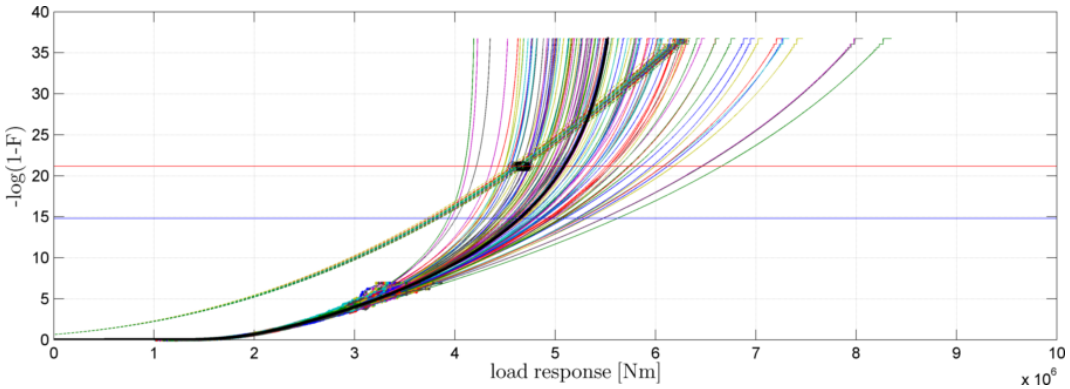

(b)

Figure E.4: a) Example of one realization of the extreme cdf's. b) 100 realizations of the extreme cdf's, each based upon 1000 maxima. For each realization a different extrapolation of the tail is obtained, which shows the difficulty of extreme value analysis. The thick solid line is the GEV fit for all the 100000 maxima.

Appendix F

Information about met-masts

In this appendix, the set up of the met-masts of each measurement site described in section 6.1 is given graphically. The pictures are taken from "http://www.winddata.com".

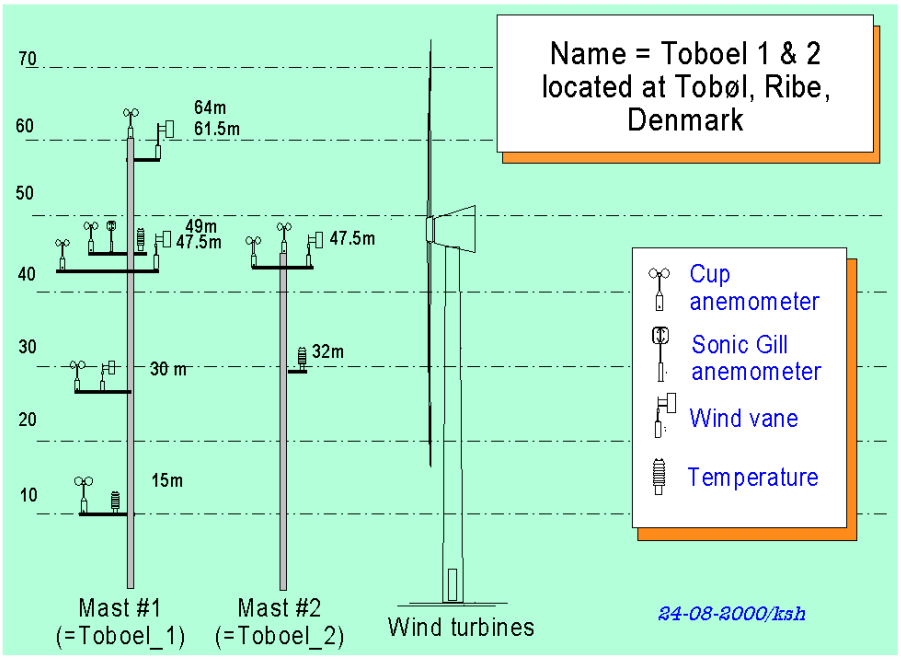

Figure F.1: layout of Toboel met-mast

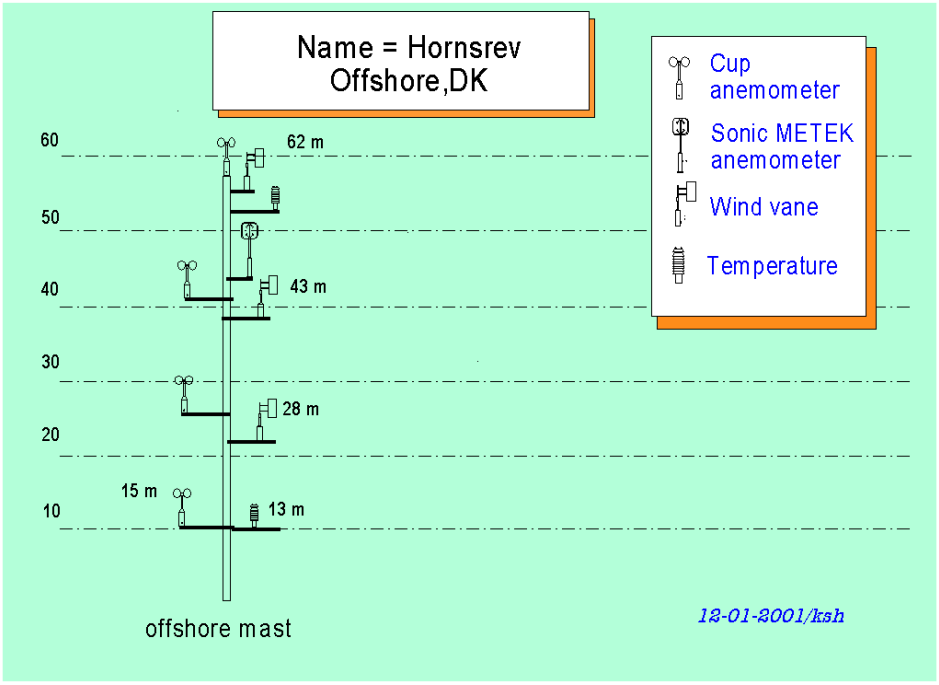

Figure F.2: layout of Hornsrev met-mast

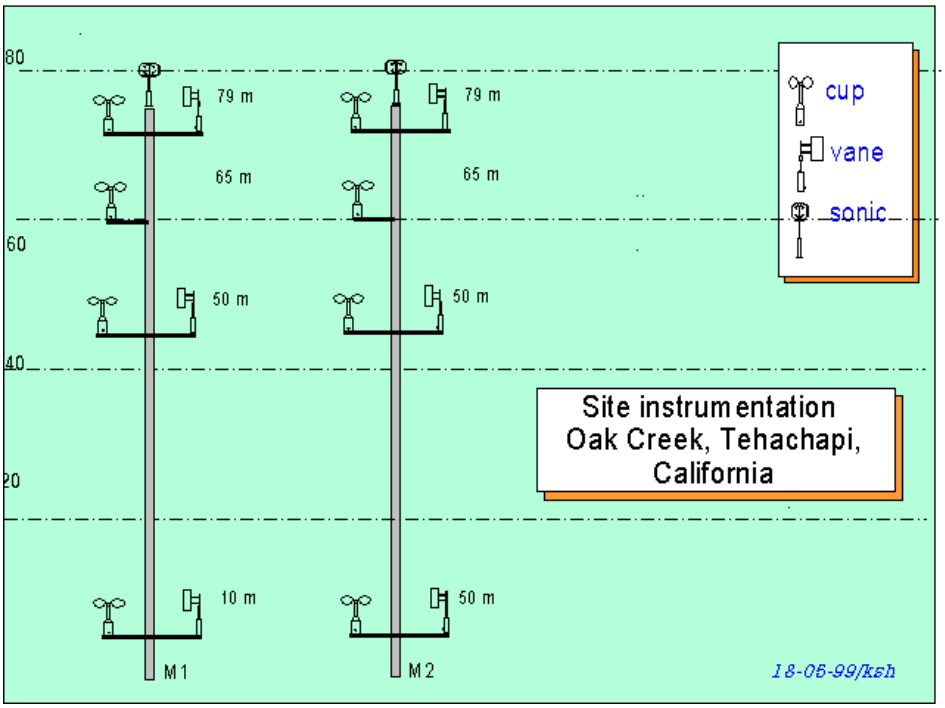

Figure F.3: layout of Oak Creek met-mast

Appendix G

Distorted spectra

In figure G.1 examples of the distorted spectra are given for each site. It appears that each site shows its own type of distortions in the spectra. The spectra from Toboel show a wide peak around one frequency, which according to Stull [1988], can be explained by blue noise which points to high frequency noise imposed on the data by e.g. instrumental error due to data conversion steps. The spectra from Oak Creek show several smaller peaks at high frequencies. Its not known what the reason of this noise can be. The spectra for Hornsrev (12 Hz) show a distinct peak at 0.6 Hz. The spectra for Hornsrev (20 Hz) show a lot of noise at the high frequency tail.

A possible explanation for spectral distortion is aliasing, because the true signal of atmospheric turbulence always have frequencies higher than the sampling rate of the measuring instrument. If the data is filtered by an analog electronic filter prior to the digitizing, frequencies higher than the Nyquist frequency can be removed. If this is not done, it is impossible to digitally filter the data, because its not known which portion of the amplitude at the resolved frequency is real and what is aliased into it.

The spectra for Hornsrev (20 Hz) show an extreme round-of behavior at the high frequencies, together with large peaks. The reason for this can be found in the description of the measurement. It appeared that the METEK software had a bug at a sampling rate of 20 Hz. At this frequency large peaks were introduced in the data, although these were as much as possible removed by "Database on wind characteristics" it still can be seen in the spectra.

The distortions only appear at the lower wind speeds and disappear (or become small) for Toboel at 8 m/s, for Hornsrev at 9 m/s and for Oak Creek at 5 m/s.

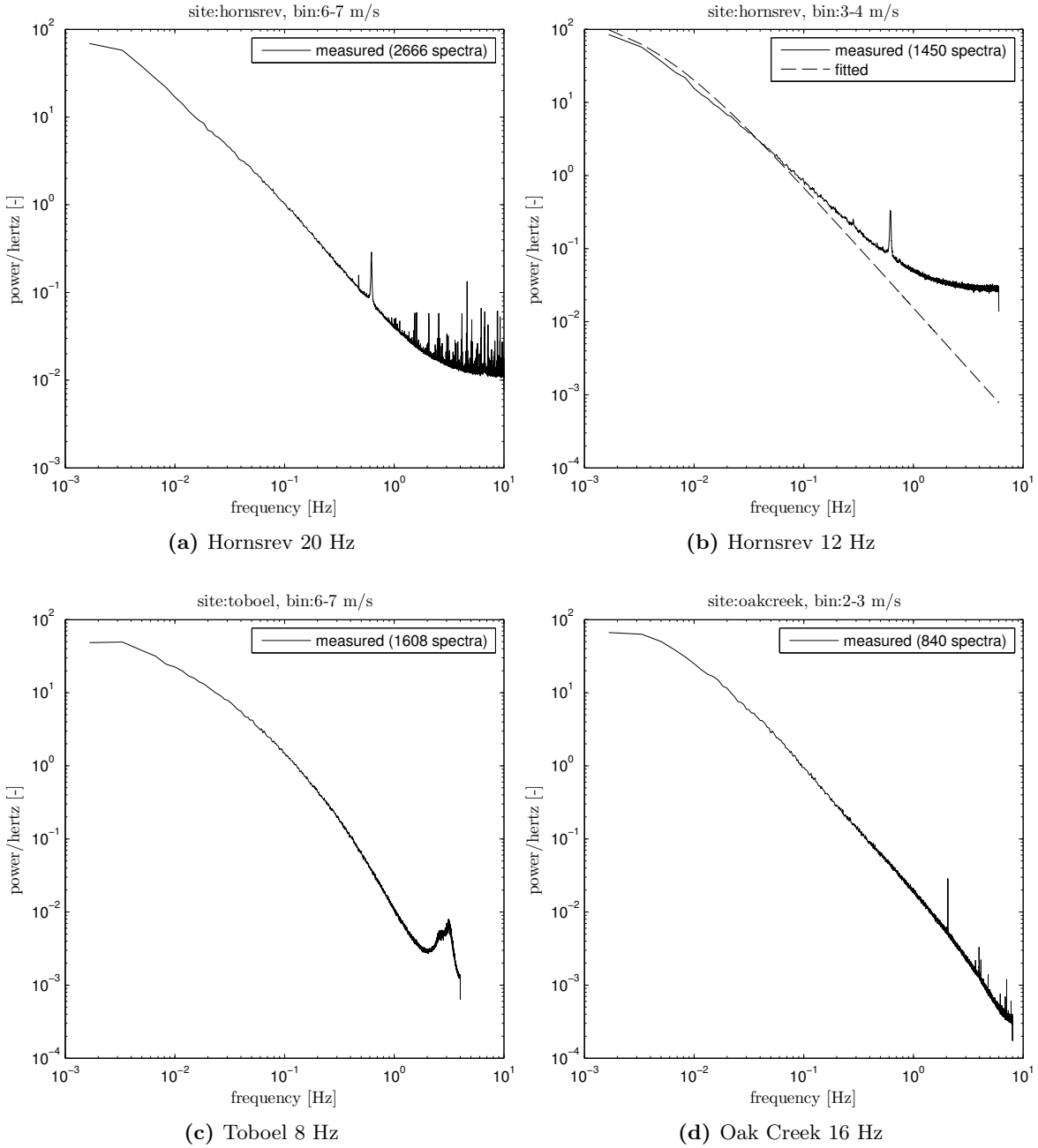

(a) Hornsrev 20 Hz

(b) Hornsrev 12 Hz

(c) Toboel 8 Hz

(d) Oak Creek 16 Hz

Figure G.1: Examples of spectra containing distorted high frequency behavior

Appendix H

Flowcharts of the analysis process

The flowcharts showed here correspond to the MATLAB files used for the analysis of the data. The flowcharts don't show the details of each m-file, but are meant to tell where each m-file is used for and what globally is done in each m-file. In the file `mainprocess.m` all the main steps in the analysis and simulations can be invoked. The global variables `meetplaats` and `vlaagtype` are defined in `dataDirectory.m`. Other files which contain important input are:

- `dataDirectory.m`, which contains the information about the file paths and general properties of the different gust types and measurements;
- `binClassDef.m`, which contains the information about the bin and class definitions. (`extremebinClassDef.m` for the analysis of the 'extreme gust shape');
- `turbinemodel.m`, which contains the information about the used turbine and the controller;
- `extrafiguresresults.m`, which contains the code to generate all the figures not generated with `comparison.m`.

For more details, the reader is directed to the m-files, which contain a description of their content.

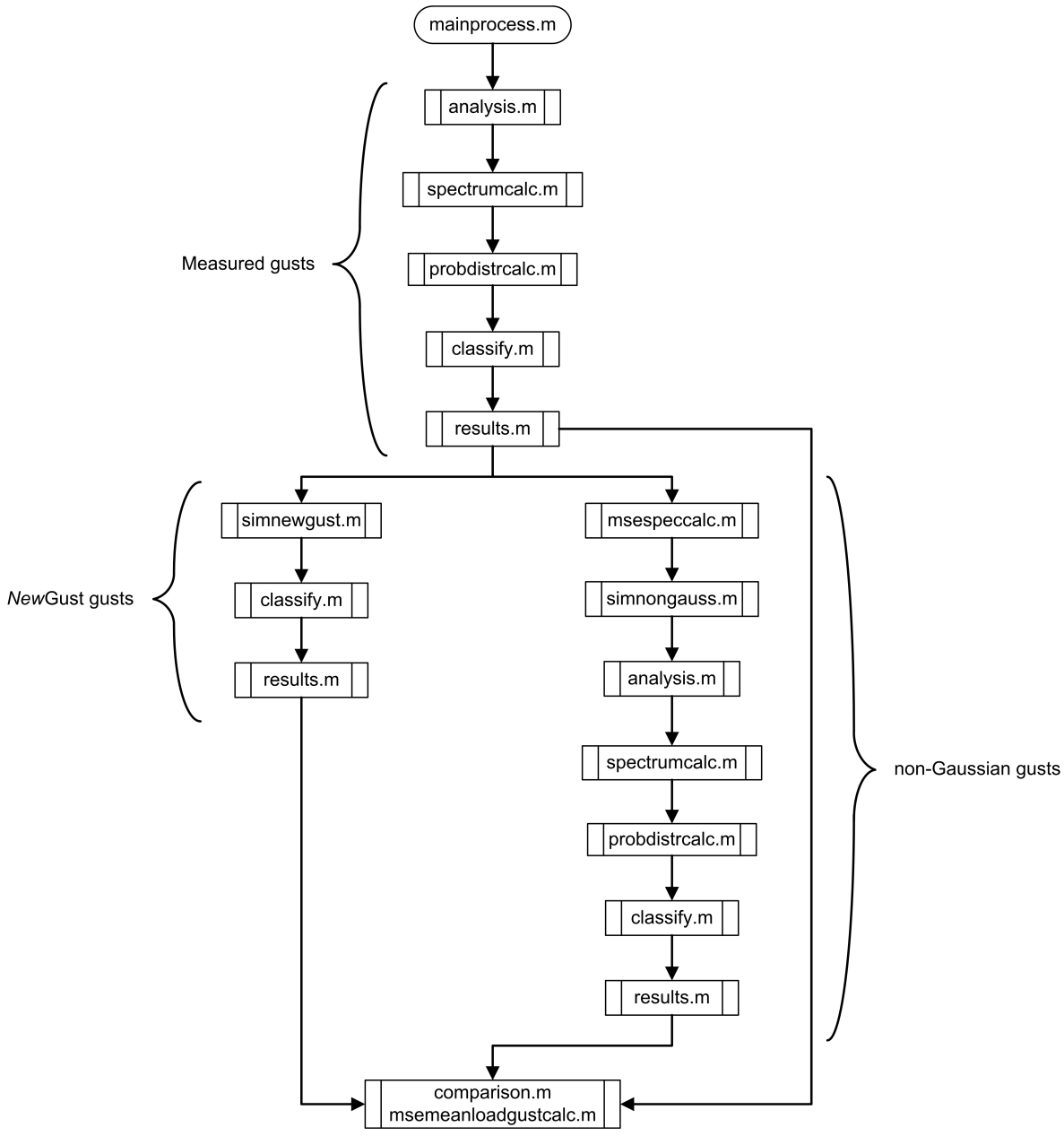

Figure H.1: Steps taken for the validation of *New*Gust

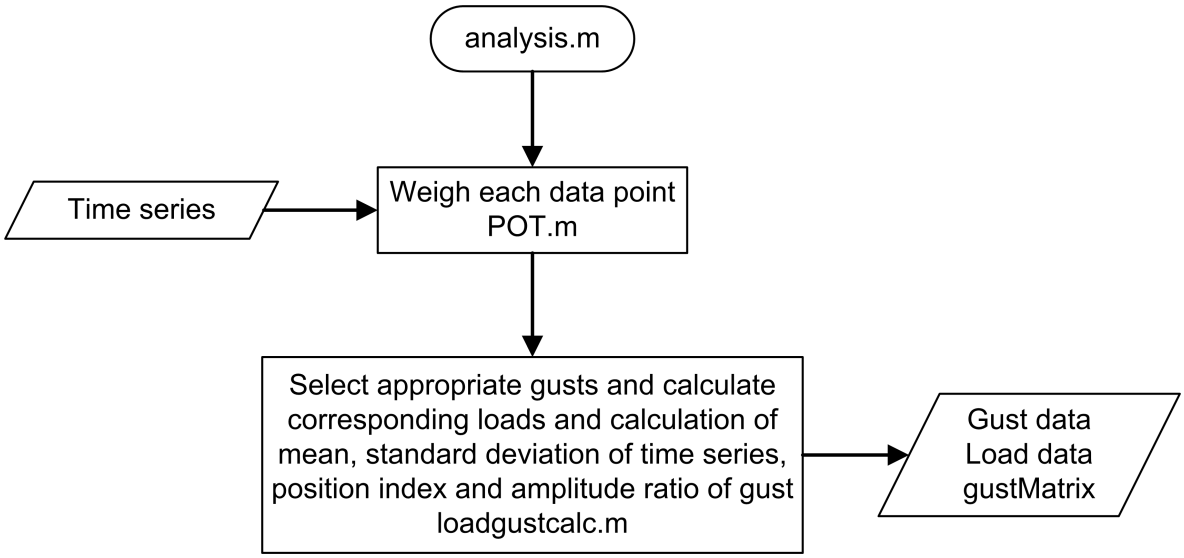

Figure H.2: Steps taken in the analysis m-file

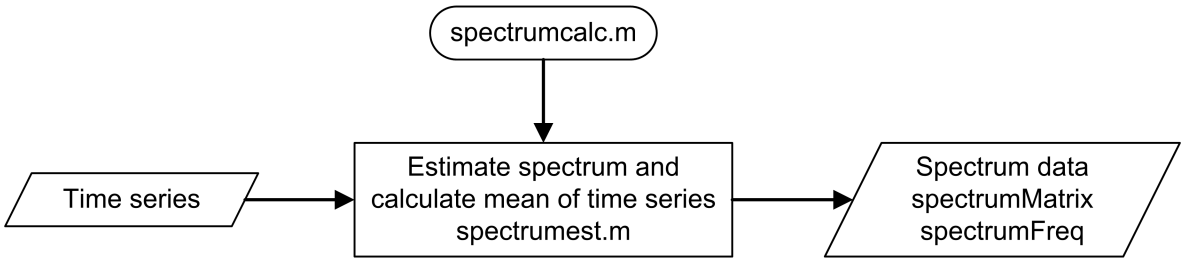

Figure H.3: Steps taken in the spectrumcalc m-file

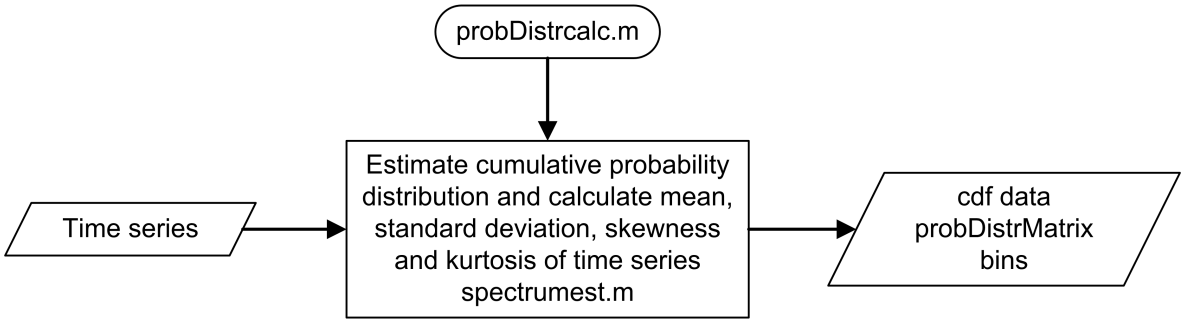

Figure H.4: Steps taken in the probdistrcalc m-file

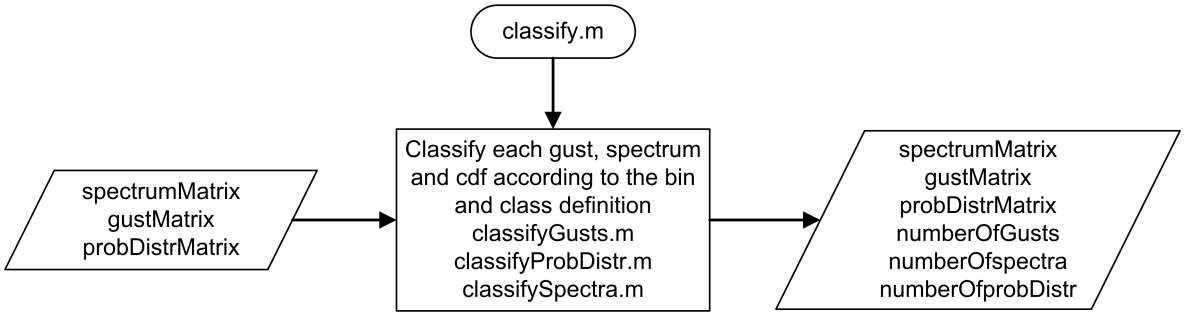

Figure H.5: Steps taken in the classify m-file

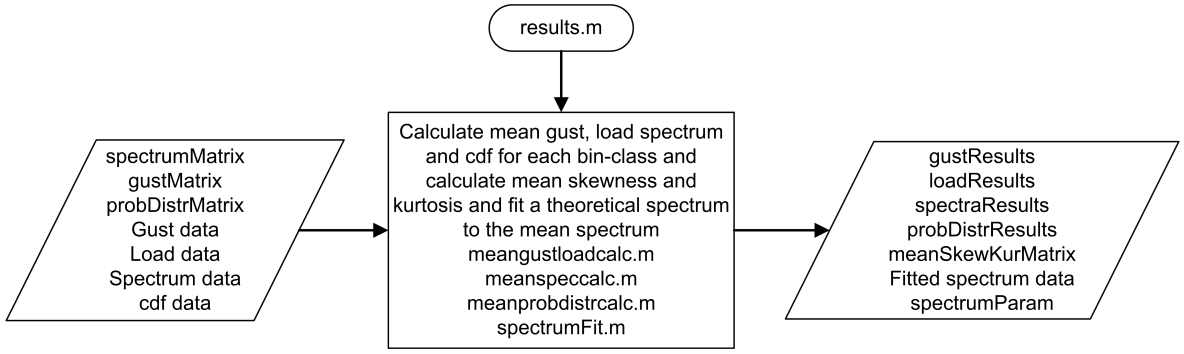

Figure H.6: Steps taken in the results m-file

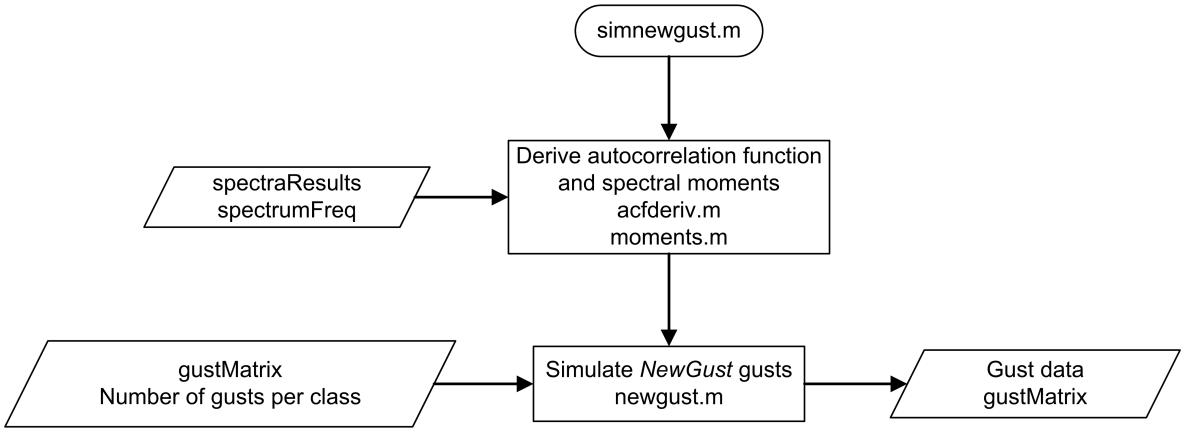

Figure H.7: Steps taken in the simnewgust m-file

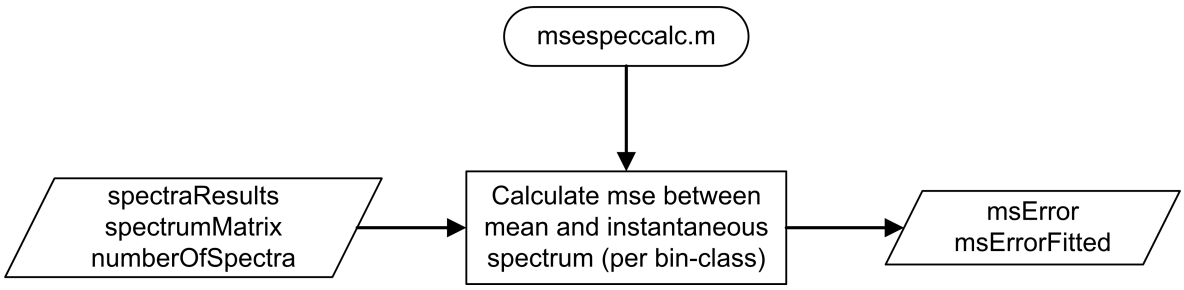

Figure H.8: Steps taken in the msespeccalc m-file

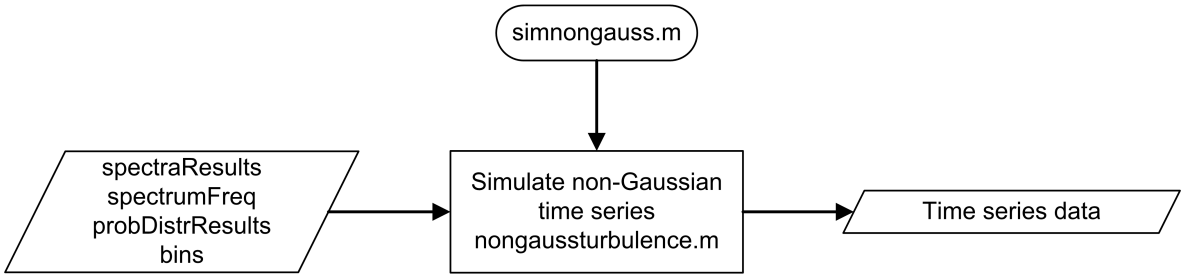

Figure H.9: Steps taken in the simnongauss m-file

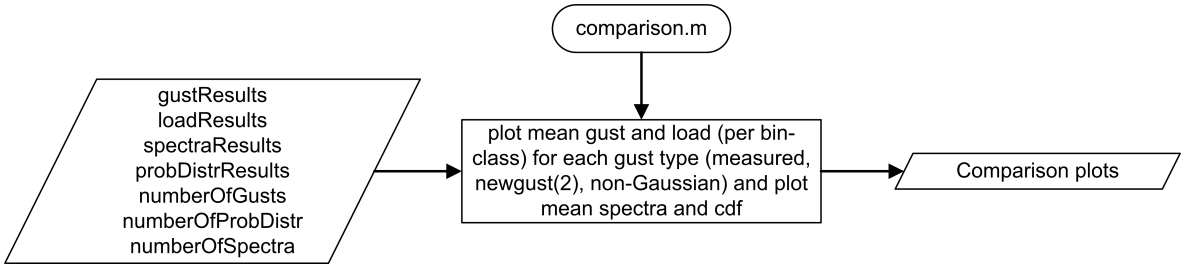

Figure H.10: Steps taken in the comparison m-file

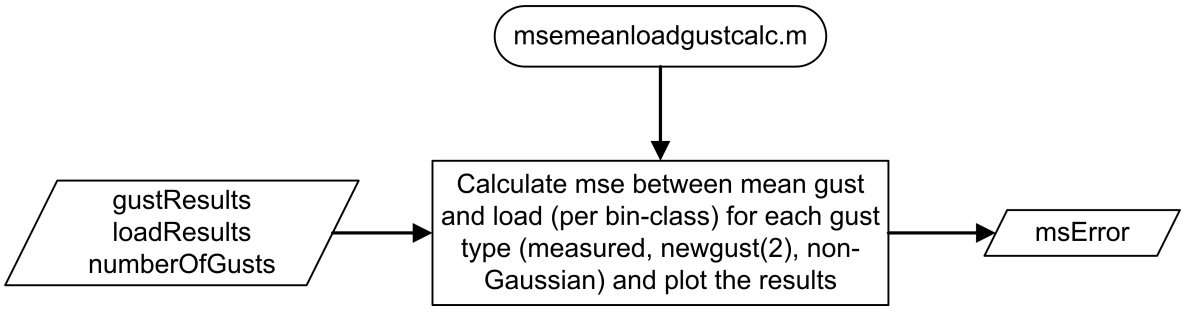

Figure H.11: Steps taken in the msemeanloadgustcalc m-file

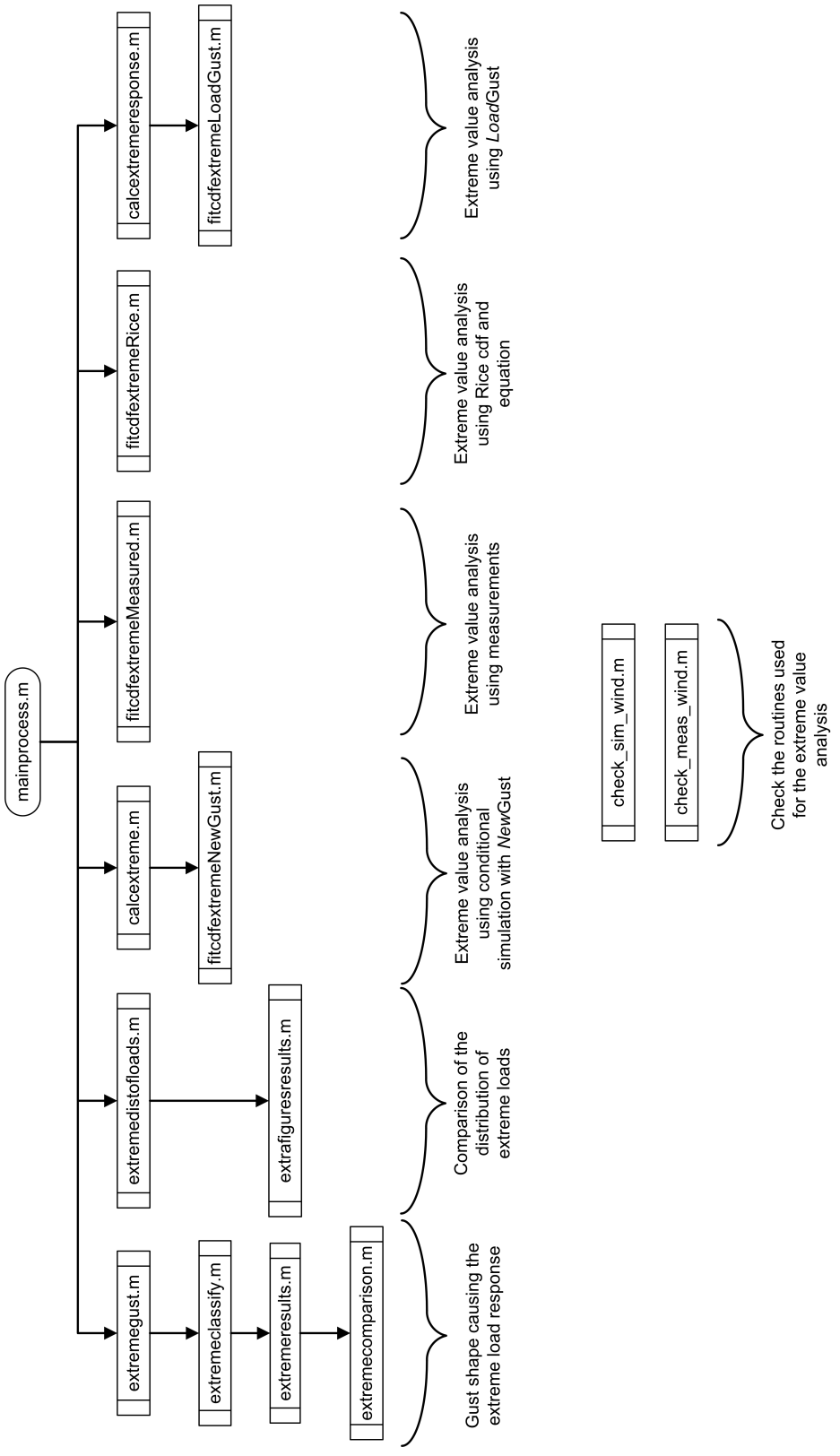

Figure H.12: Steps taken for the analysis of extremes

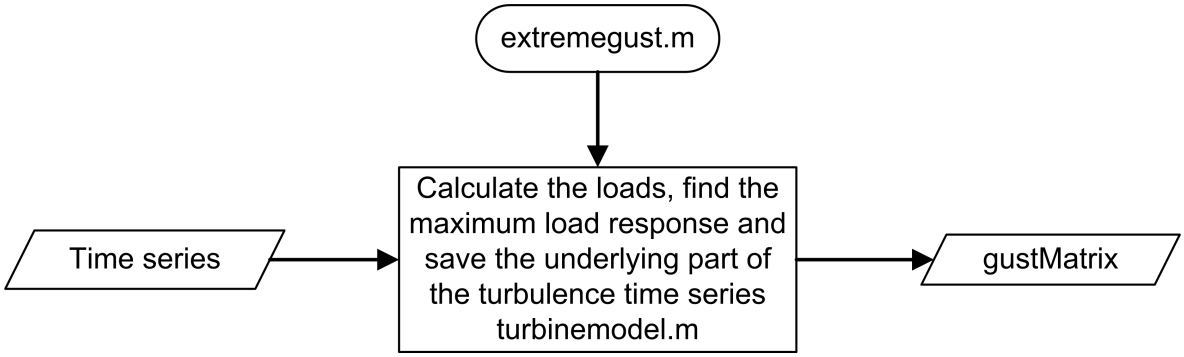

Figure H.13: Steps taken in the extremegust m-file

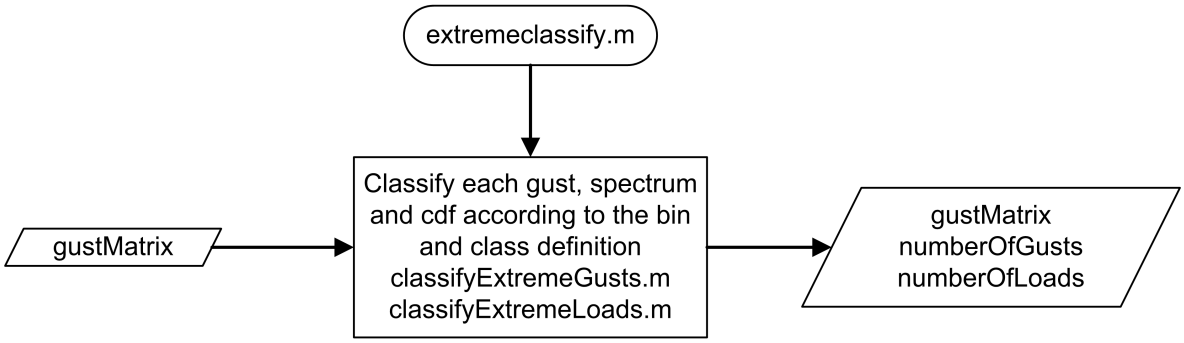

Figure H.14: Steps taken in the extremeclassify m-file

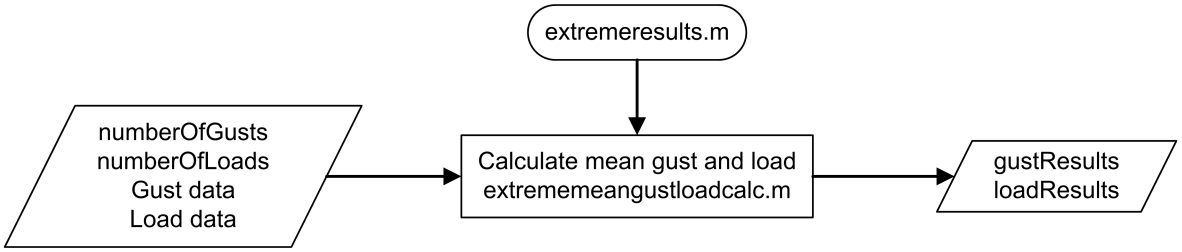

Figure H.15: Steps taken in the extremeresults m-file

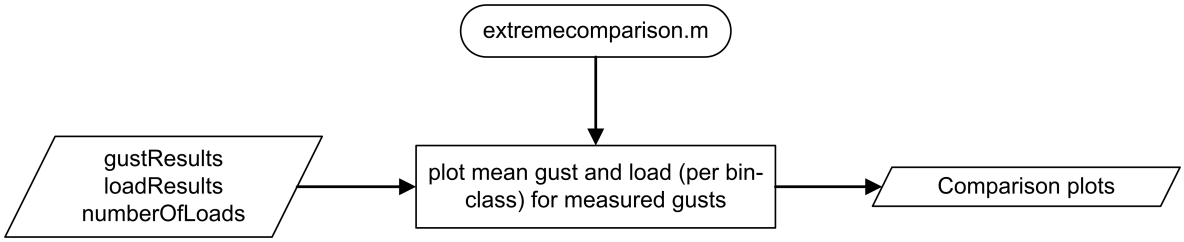

Figure H.16: Steps taken in the extremecomparison m-file

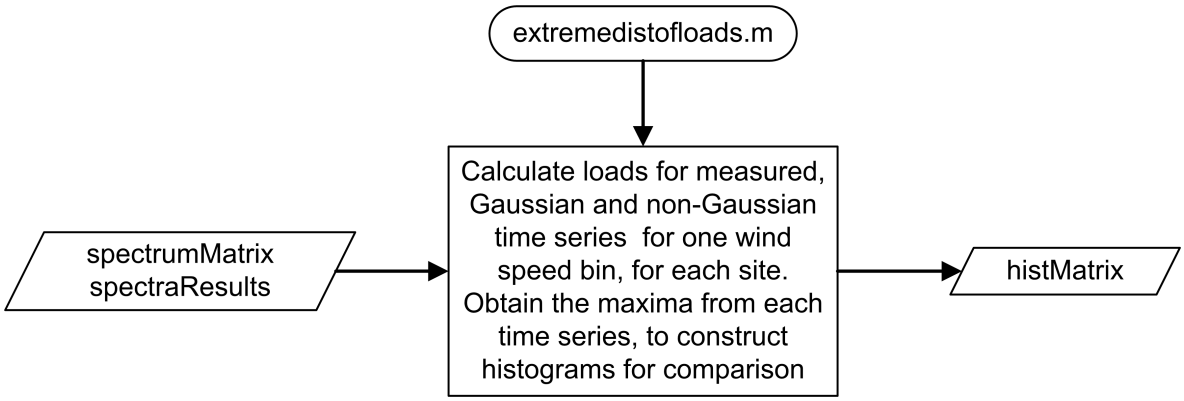

Figure H.17: Steps taken in the extremedistofloads m-file

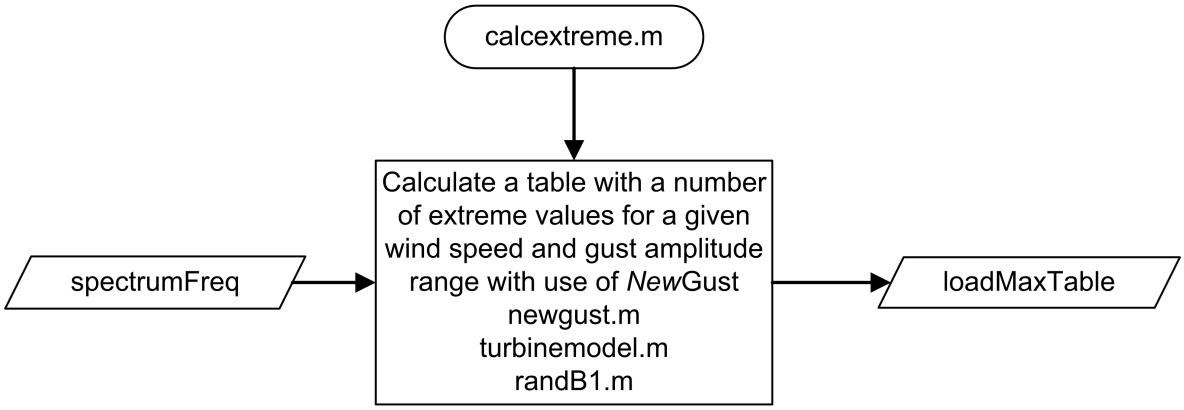

Figure H.18: Steps taken in the calcextreme m-file

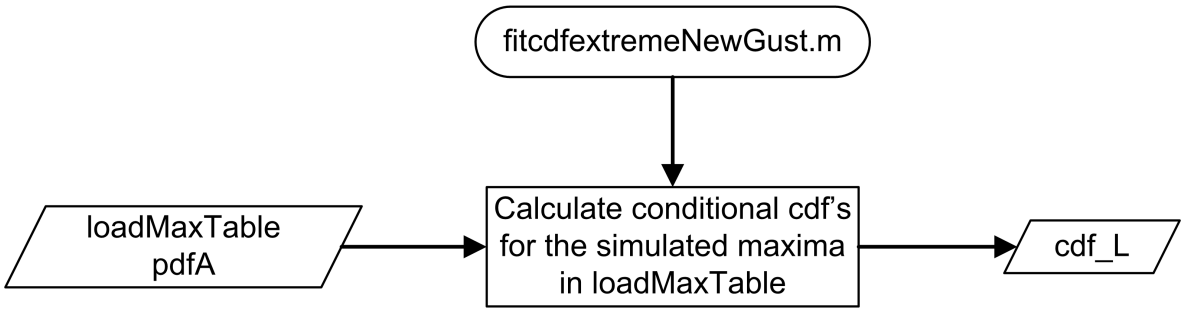

Figure H.19: Steps taken in the fitcdfExtremeNewGust m-file

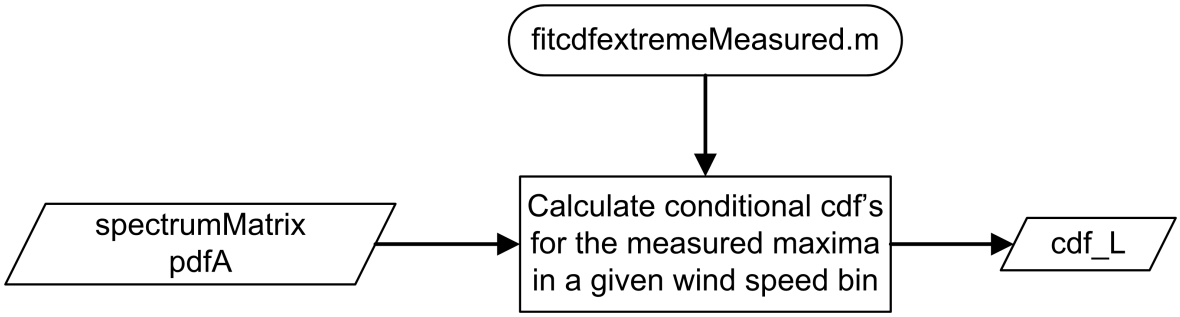

Figure H.20: Steps taken in the fitcdfextremeMeasured m-file

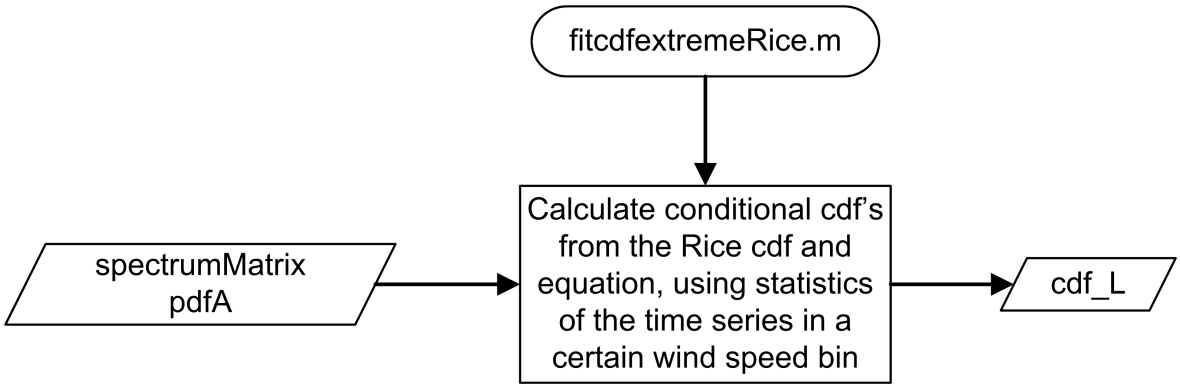

Figure H.21: Steps taken in the fitcdfextremeRice m-file

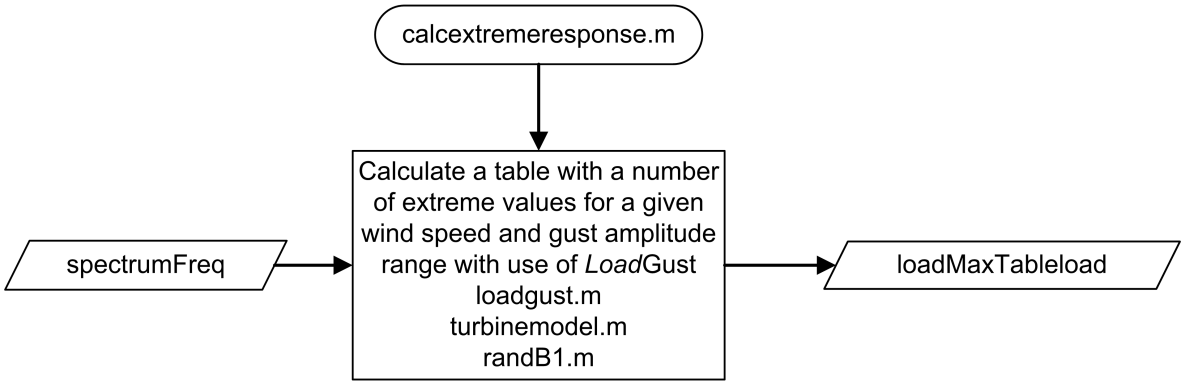

Figure H.22: Steps taken in the calcextremeresponse m-file

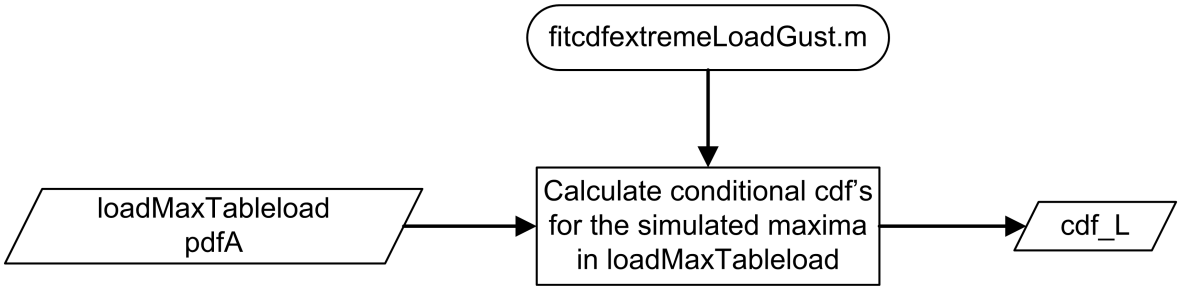

Figure H.23: Steps taken in the fitcdfextremeLoadGust m-file

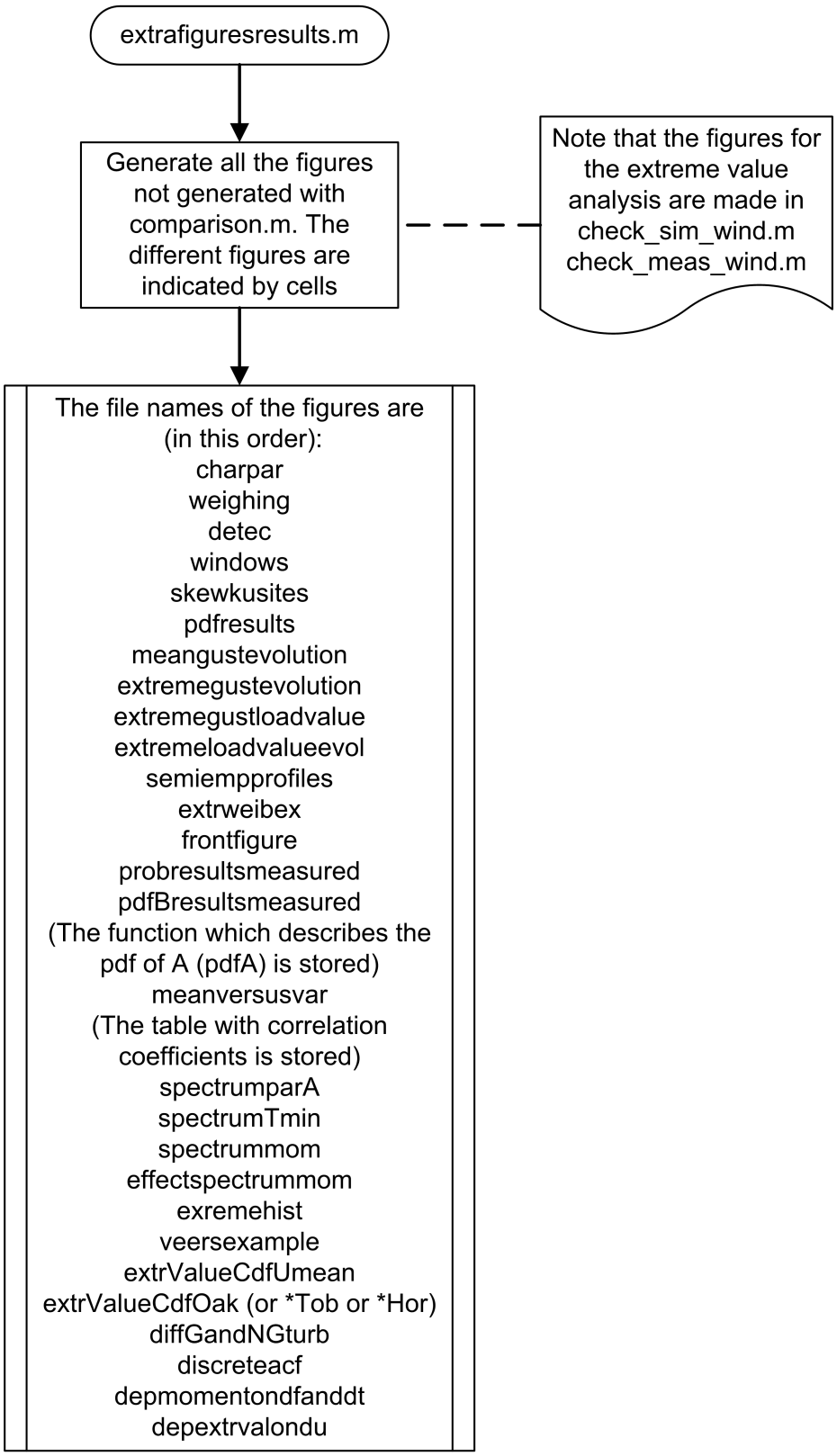

Figure H.24: Steps taken in the extrafiguresresults m-file

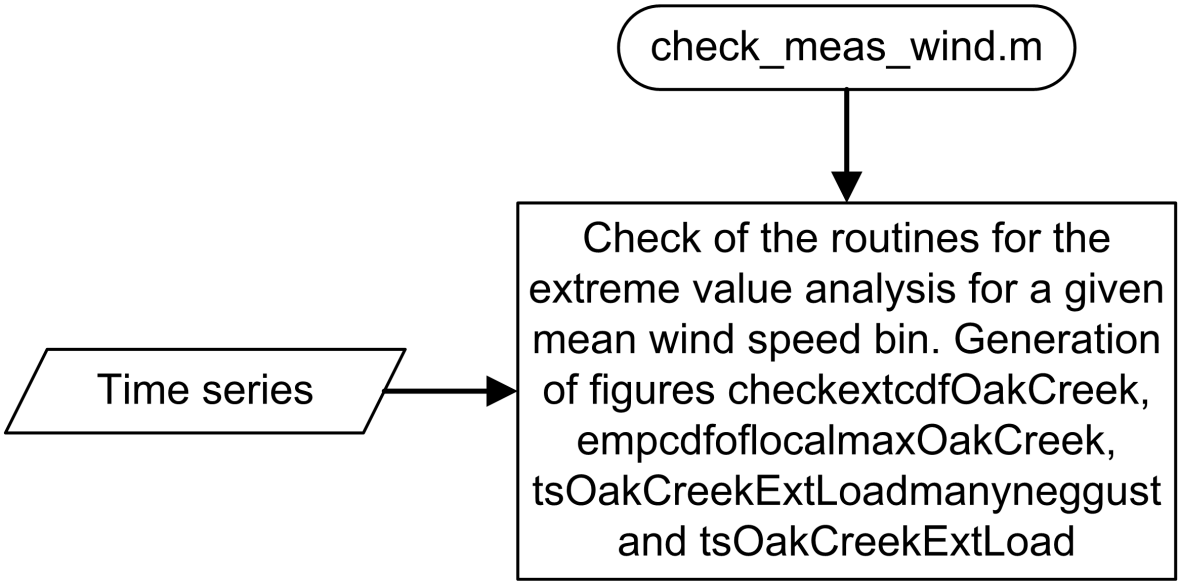

Figure H.25: Steps taken in the check_meas_wind m-file

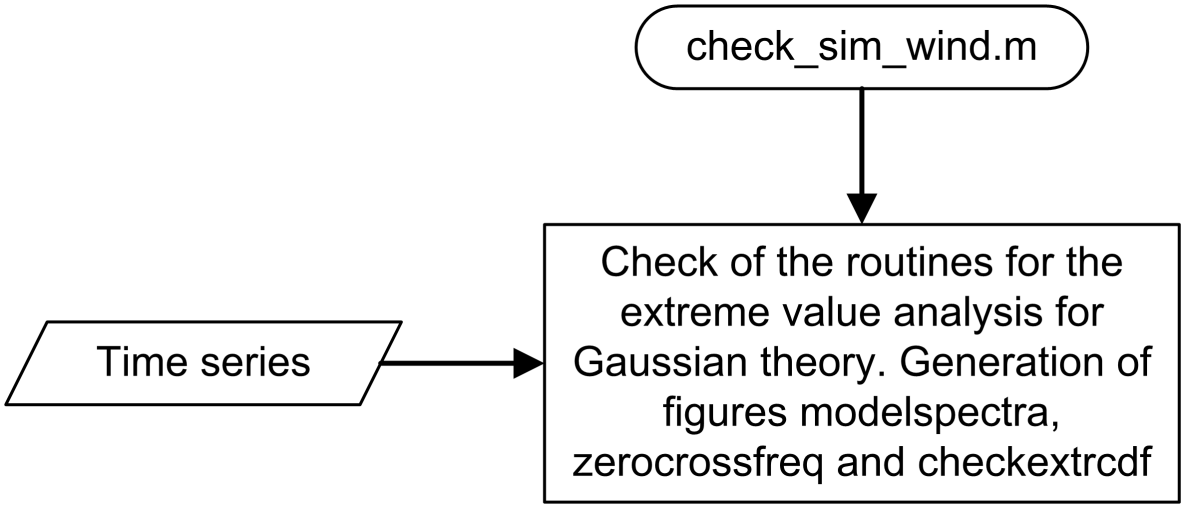

Figure H.26: Steps taken in the check_sim_wind m-file

Appendix I

Work plan to use CTRW for turbulence simulation

In order to include non-Gaussian behavior of turbulence in numerical simulations, a method based on continuous time random walks (CTRW) has been developed by Friederichs and Kleinhans [2007]. This method is especially developed to represent the non-Gaussian behavior of atmospheric turbulence. It is therefore interesting to investigate if this method gives a better representation of atmospheric turbulence when compared to the spectral representation method. The following steps are proposed in order to do this:

1. Literature review in order to find enough information about this method;
2. Describe the theory;
3. Program the method in MATLAB;
4. Perform simulations of turbulence based on Gaussian and non-Gaussian (from measurements) pdf's, both with the CTRW and spectral representation method;
5. Compare the results with respect to the mean statistics (mean, standard deviation, skewness, kurtosis) as well as the spectra and probability distributions.

Literature to be read:

- Gontier et al. [2007, Ch. 4];
- Peinke et al. [2008];
- Peinke et al. [2004];
- Friederichs and Kleinhans [2007];
- Nawroth and Peinke [2006];
- Laubrich [2009] (a reference material);
- Papoulis and Pillai [2002] (theory of random walks).

Appendix J

Graphs of gusts and load responses for each site

For each site only a small selection is displayed. The digital version contains all graphs.

J.1 Results for Toboel

$\tilde{u}_n(t_0) \rightarrow$	1-1.5		1.5-2		2-2.5		2.5-3		3-3.5		3.5-6		
$\bar{u} \downarrow$	gust	load	gust	load	gust	load	gust	load	gust	load	gust	load	type
0-5	0.76	0.16	0.81	0.11	0.90	0.07	1.02	0.05	1.56	0.09	4.22	0.29	m,n
5-6	0.51	0.45	0.43	0.39	0.40	0.36	0.45	0.41	0.55	0.51	2.02	1.90	m,n
6-7	0.46	0.60	0.35	0.47	0.33	0.45	0.36	0.49	0.36	0.47	1.91	2.61	m,n
7-8	0.46	0.82	0.31	0.56	0.23	0.43	0.24	0.45	0.26	0.47	1.27	2.44	m,n
8-9	0.40	0.94	0.25	0.60	0.20	0.48	0.18	0.45	0.20	0.49	1.08	2.69	m,n
9-10	0.36	1.08	0.22	0.68	0.14	0.44	0.11	0.34	0.14	0.43	0.86	2.68	m,n
10-11	0.45	1.69	0.24	0.93	0.14	0.54	0.10	0.38	0.13	0.49	0.44	1.73	m,n
11-12	0.42	0.14	0.23	0.46	0.11	0.79	0.08	1.32	0.08	1.93	0.61	4.08	m,n
12-13	0.41	0.29	0.22	0.17	0.11	0.08	0.07	0.05	0.08	0.07	0.48	0.36	m,n
13-14	0.40	0.21	0.19	0.10	0.10	0.05	0.06	0.04	0.06	0.04	0.33	0.20	m,n
14-15	0.50	0.20	0.17	0.07	0.09	0.04	0.06	0.03	0.07	0.03	0.54	0.24	m,n
15-16	0.44	0.14	0.15	0.05	0.10	0.03	0.04	0.01	0.11	0.04	0.43	0.16	m,n
16-17	0.40	0.10	0.21	0.06	0.04	0.01	0.03	0.01	0.08	0.04	0.37	0.14	m,n
17-19	0.42	0.08	0.18	0.04	0.08	0.02	0.03	0.01	0.09	0.03	0.35	0.10	m,n
19-22	0.53	0.07	0.16	0.03	0.05	0.01	0.05	0.01	0.07	0.02	0.48	0.10	m,n
22-30	0.42	0.04	0.23	0.03	0.11	0.02	0.05	0.02	0.11	0.06	0.32	0.14	m,n

Table J.1: mse between gusts for Toboel, 'm' denotes 'measured' and 'n' denotes 'newgust'

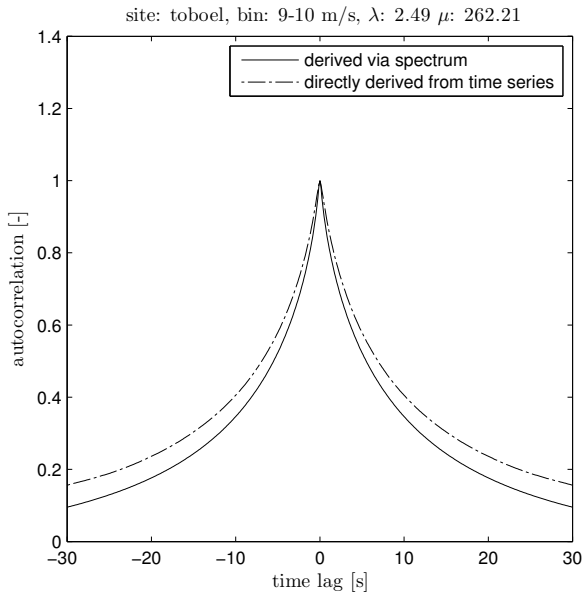
site: toboel, bin: 9-10 m/s, λ: 2.49 μ: 262.21
derived via spectrum
directly derived from time series
autocorrelation [-]
time lag [s]

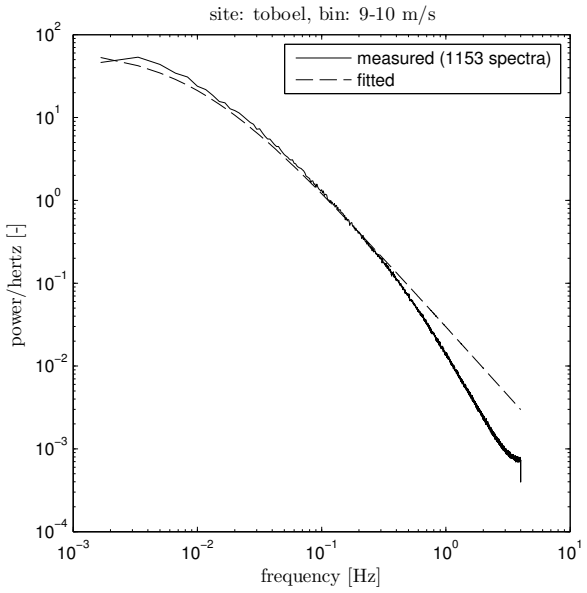
site: toboel, bin: 9-10 m/s
measured (1153 spectra)
fitted
power/hertz [-]
frequency [Hz]

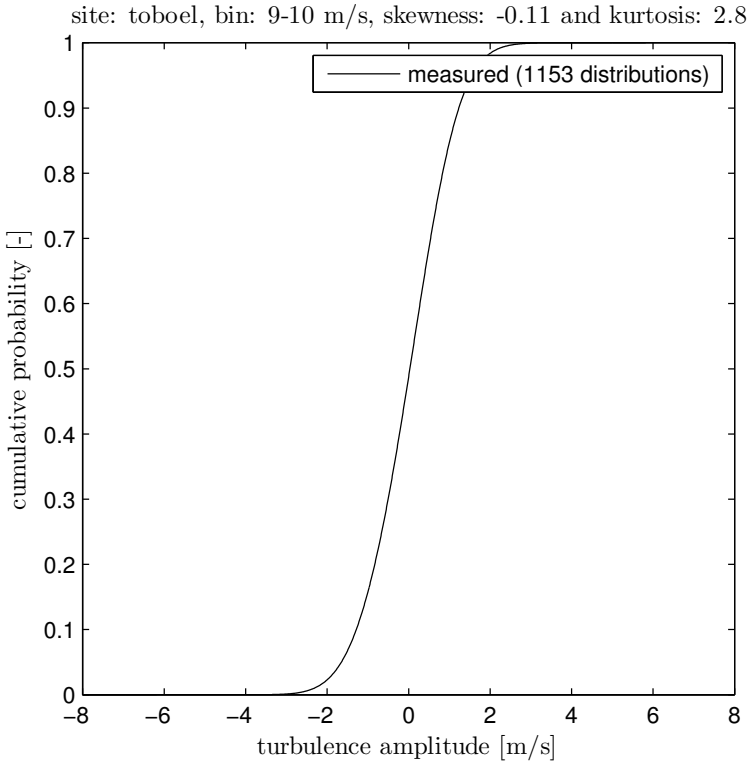
site: toboel, bin: 9-10 m/s, skewness: -0.11 and kurtosis: 2.8
measured (1153 distributions)
cumulative probability [-]
turbulence amplitude [m/s]

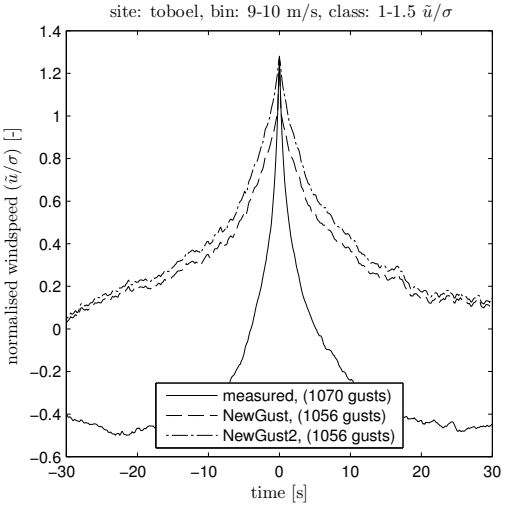
site: toboel, bin: 9-10 m/s, class: 1-1.5 $\tilde{u}/\sigma$
normalised windspeed $(\tilde{u}/\sigma)$ [-]
time [s]
measured, (1070 gusts)
NewGust, (1056 gusts)
NewGust2, (1056 gusts)

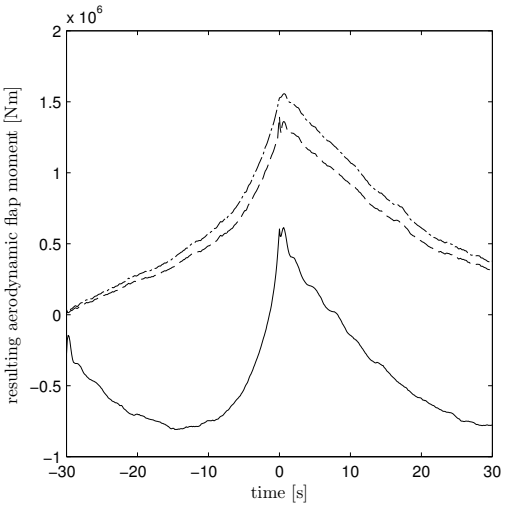
x 10^6
resulting aerodynamic flap moment [Nm]
time [s]

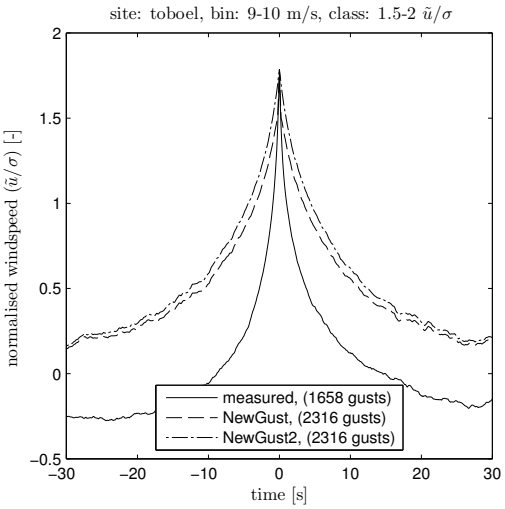
site: toboel, bin: 9-10 m/s, class: 1.5-2 $\tilde{u}/\sigma$
normalised windspeed $(\tilde{u}/\sigma)$ [-]
time [s]
measured, (1658 gusts)
NewGust, (2316 gusts)
NewGust2, (2316 gusts)

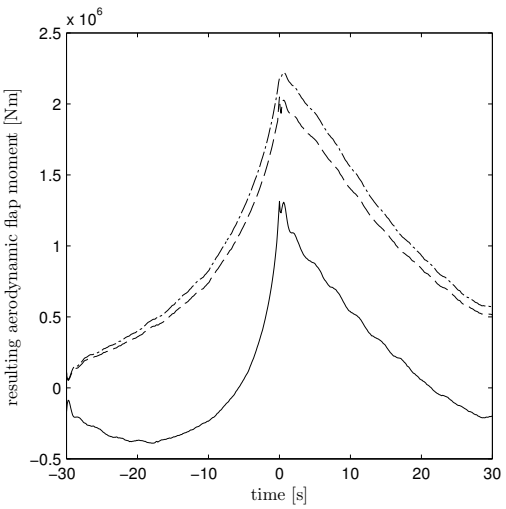
x 10^6
resulting aerodynamic flap moment [Nm]
time [s]

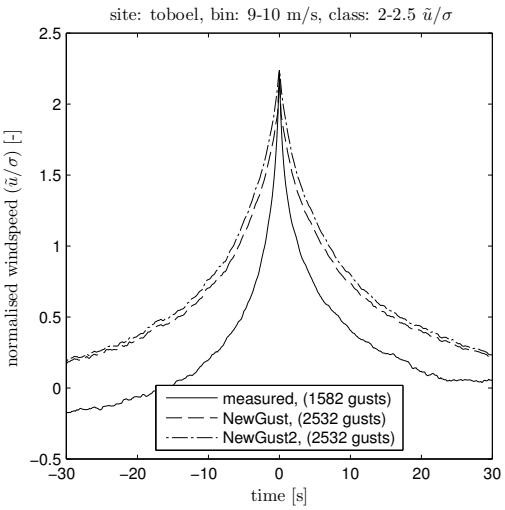
site: toboel, bin: 9-10 m/s, class: 2-2.5 $\tilde{u}/\sigma$
normalised windspeed $(\tilde{u}/\sigma)$ [-]
time [s]
measured, (1582 gusts)
NewGust, (2532 gusts)
NewGust2, (2532 gusts)

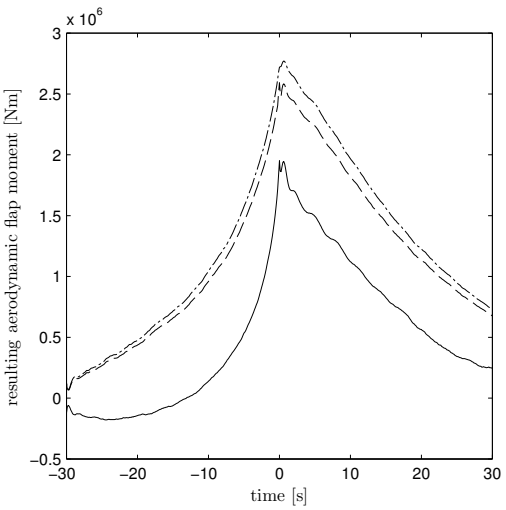
x 10^6
resulting aerodynamic flap moment [Nm]
time [s]

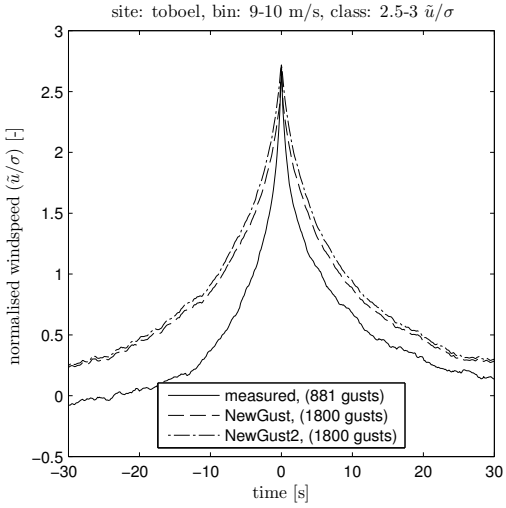
site: toboel, bin: 9-10 m/s, class: 2.5-3 $\tilde{u}/\sigma$
normalised windspeed $(\tilde{u}/\sigma)$ [-]
time [s]
measured, (881 gusts)
NewGust, (1800 gusts)
NewGust2, (1800 gusts)

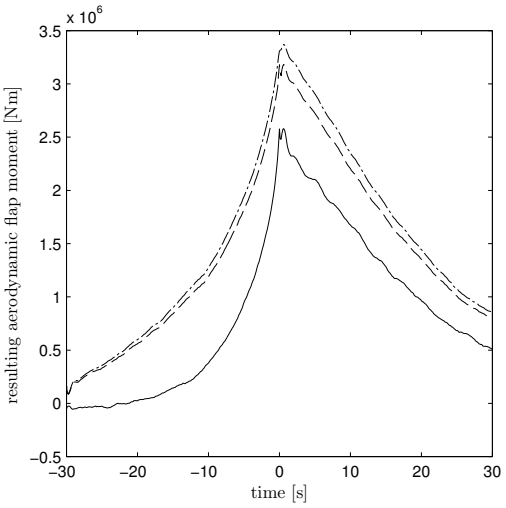
x 10^6
resulting aerodynamic flap moment [Nm]
time [s]

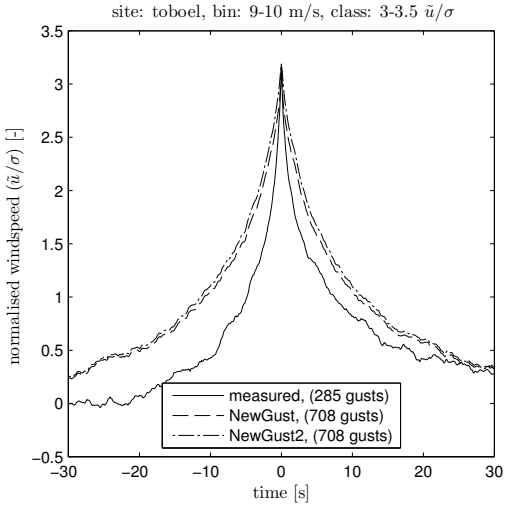
site: toboel, bin: 9-10 m/s, class: 3-3.5 $\tilde{u}/\sigma$
normalised windspeed $(\tilde{u}/\sigma)$ [-]
time [s]
measured, (285 gusts)
NewGust, (708 gusts)
NewGust2, (708 gusts)

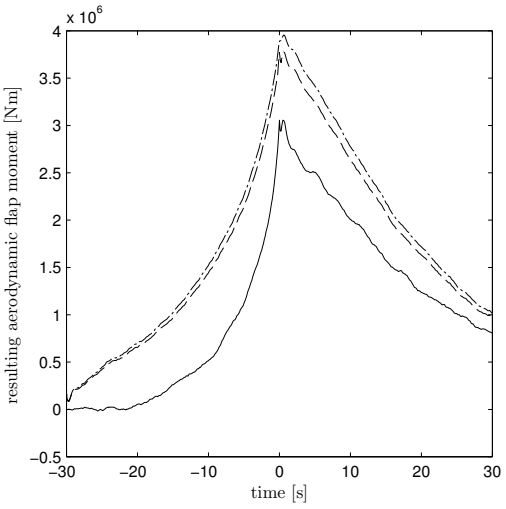
x 10^6
resulting aerodynamic flap moment [Nm]
time [s]

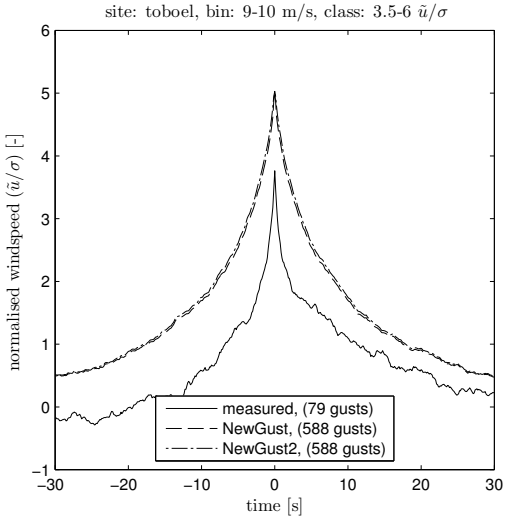
site: toboel, bin: 9-10 m/s, class: 3.5-6 $\tilde{u}/\sigma$
normalised windspeed $(\tilde{u}/\sigma)$ [-]
time [s]
measured, (79 gusts)
NewGust, (588 gusts)
NewGust2, (588 gusts)

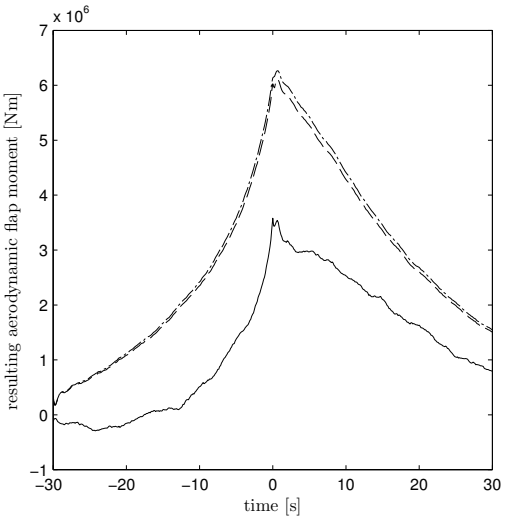
x 10^6
resulting aerodynamic flap moment [Nm]
time [s]

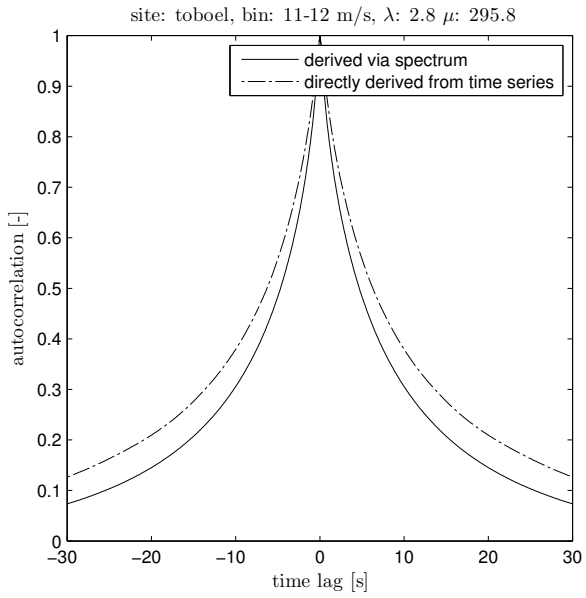
site: toboel, bin: 11-12 m/s, λ: 2.8 μ: 295.8
derived via spectrum
directly derived from time series
autocorrelation [-]
time lag [s]

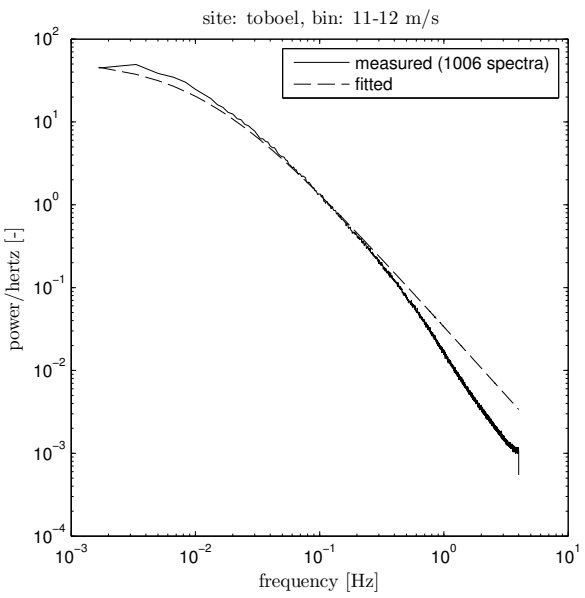
site: toboel, bin: 11-12 m/s
measured (1006 spectra)
fitted
power/hertz [-]
frequency [Hz]

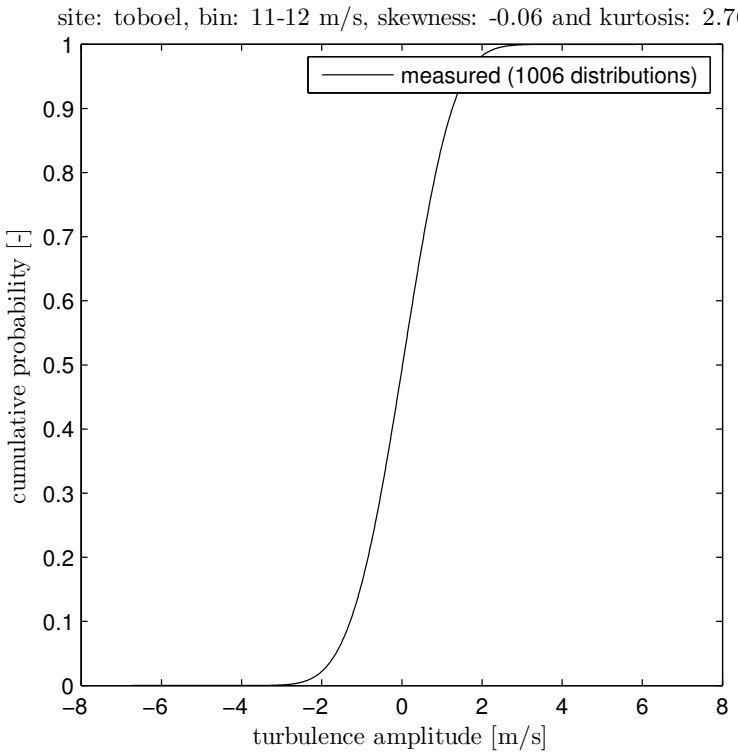
site: toboel, bin: 11-12 m/s, skewness: -0.06 and kurtosis: 2.76
measured (1006 distributions)
cumulative probability [-]
turbulence amplitude [m/s]

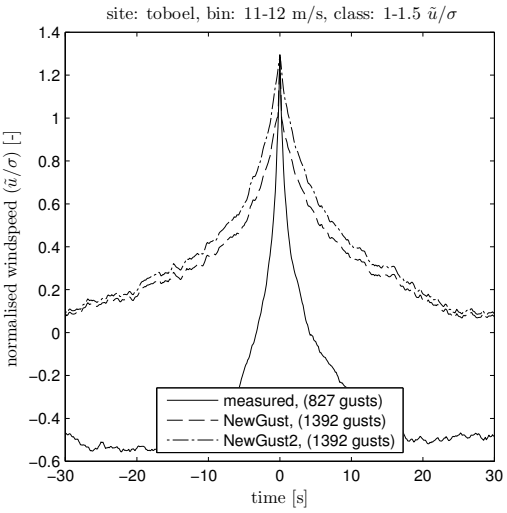
site: toboel, bin: 11-12 m/s, class: 1-1.5 $\tilde{u}/\sigma$
normalised windspeed ($\tilde{u}/\sigma$) [-]
time [s]
measured, (827 gusts)
NewGust, (1392 gusts)
NewGust2, (1392 gusts)

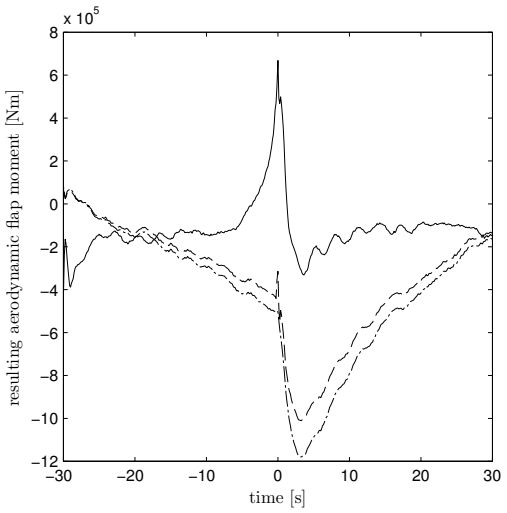
x 10^5
resulting aerodynamic flap moment [Nm]
time [s]

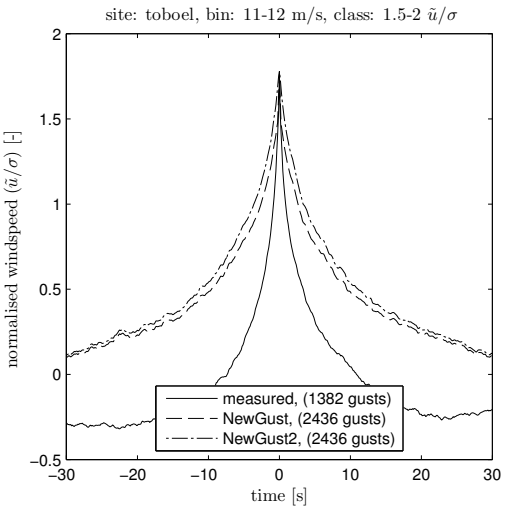
site: toboel, bin: 11-12 m/s, class: 1.5-2 $\tilde{u}/\sigma$
normalised windspeed ($\tilde{u}/\sigma$) [-]
time [s]
measured, (1382 gusts)
NewGust, (2436 gusts)
NewGust2, (2436 gusts)

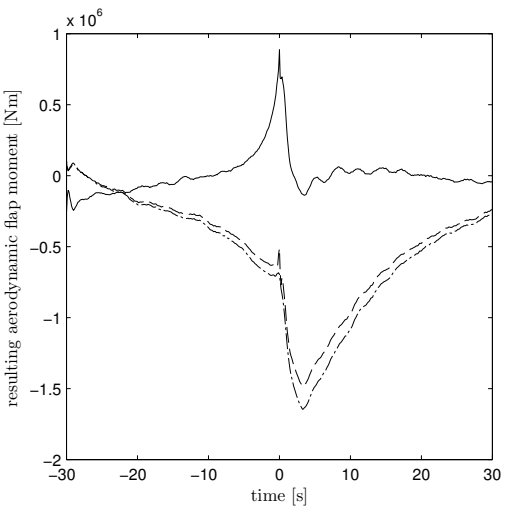
x 10^6
resulting aerodynamic flap moment [Nm]
time [s]

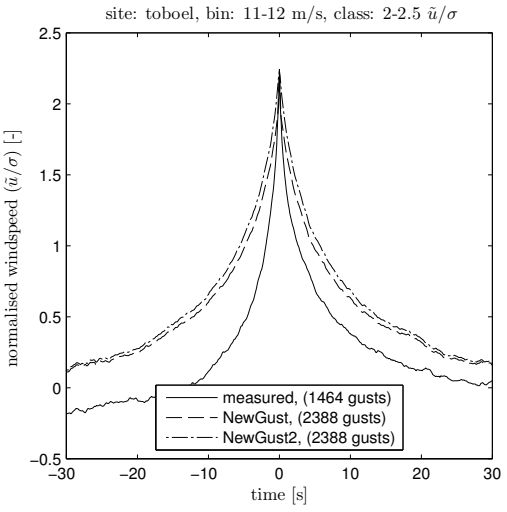
site: toboel, bin: 11-12 m/s, class: 2-2.5 $\tilde{u}/\sigma$
normalised windspeed ($\tilde{u}/\sigma$) [-]
time [s]
measured, (1464 gusts)
NewGust, (2388 gusts)
NewGust2, (2388 gusts)

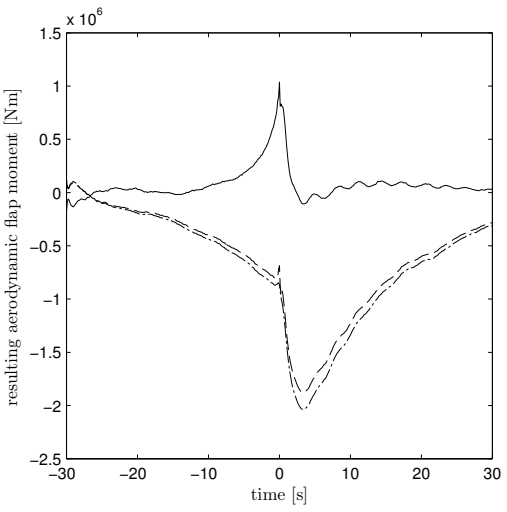
x 10^6
resulting aerodynamic flap moment [Nm]
time [s]

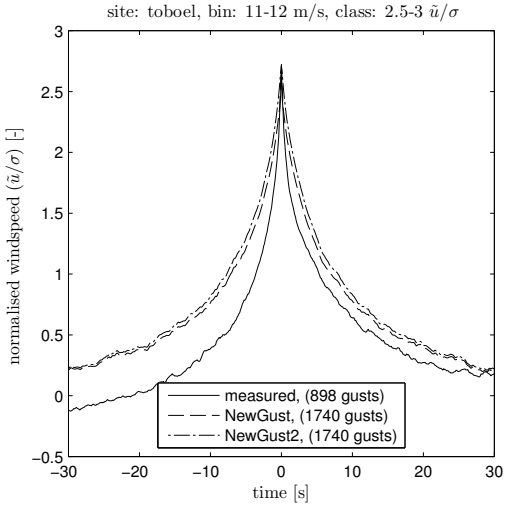
site: toboel, bin: 11-12 m/s, class: 2.5-3 $\tilde{u}/\sigma$
normalised windspeed $(\tilde{u}/\sigma)$ [-]
time [s]
measured, (898 gusts)
NewGust, (1740 gusts)
NewGust2, (1740 gusts)

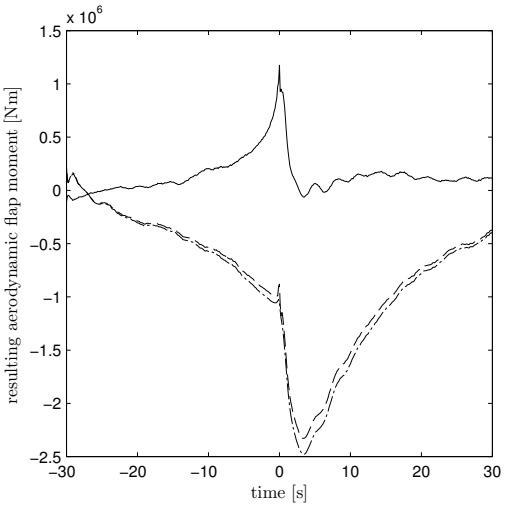
x 10^6
resulting aerodynamic flap moment [Nm]
time [s]

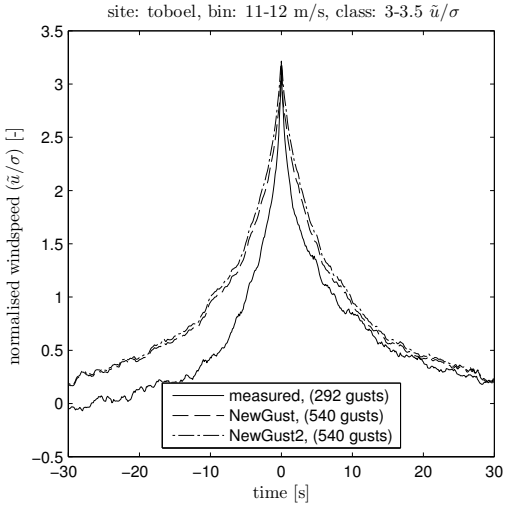
site: toboel, bin: 11-12 m/s, class: 3-3.5 $\tilde{u}/\sigma$
normalised windspeed $(\tilde{u}/\sigma)$ [-]
time [s]
measured, (292 gusts)
NewGust, (540 gusts)
NewGust2, (540 gusts)

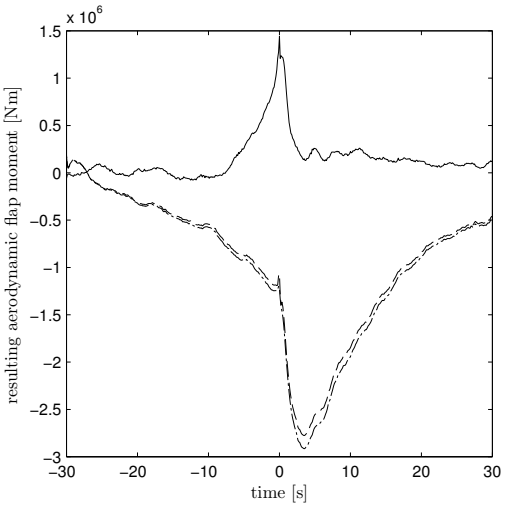
x 10^6
resulting aerodynamic flap moment [Nm]
time [s]

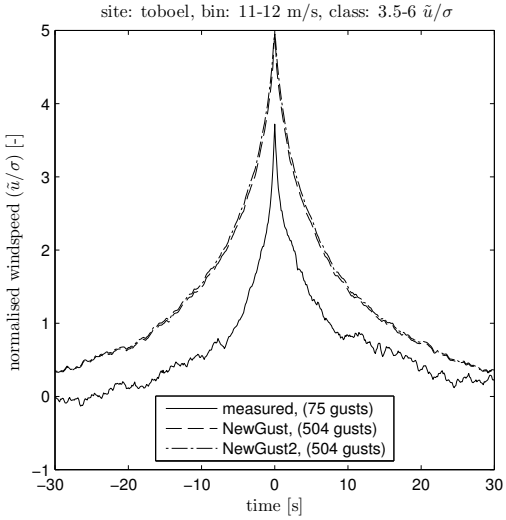
site: toboel, bin: 11-12 m/s, class: 3.5-6 $\tilde{u}/\sigma$
normalised windspeed $(\tilde{u}/\sigma)$ [-]
time [s]
measured, (75 gusts)
NewGust, (504 gusts)
NewGust2, (504 gusts)

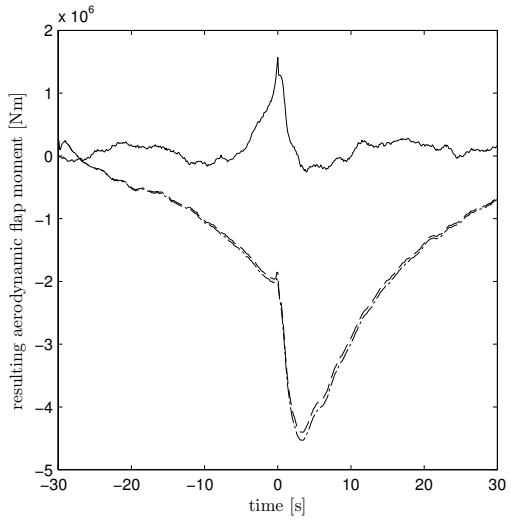
x 10^6
resulting aerodynamic flap moment [Nm]
time [s]

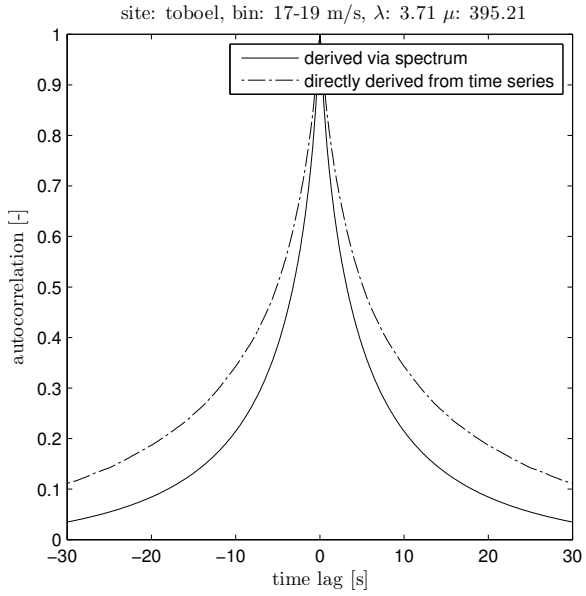
site: toboel, bin: 17-19 m/s, λ: 3.71 μ: 395.21
derived via spectrum
directly derived from time series
autocorrelation [-]
time lag [s]

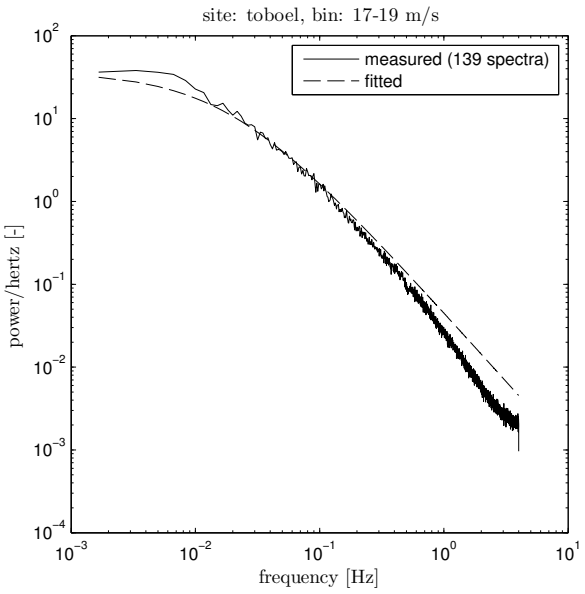
site: toboel, bin: 17-19 m/s
measured (139 spectra)
fitted
power/hertz [-]
frequency [Hz]

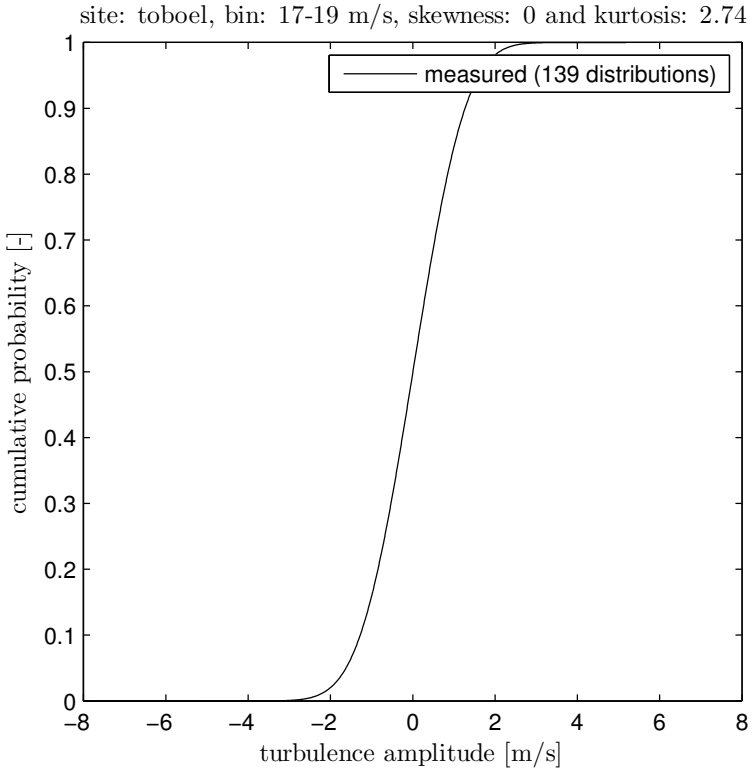
site: toboel, bin: 17-19 m/s, skewness: 0 and kurtosis: 2.74
measured (139 distributions)
cumulative probability [-]
turbulence amplitude [m/s]

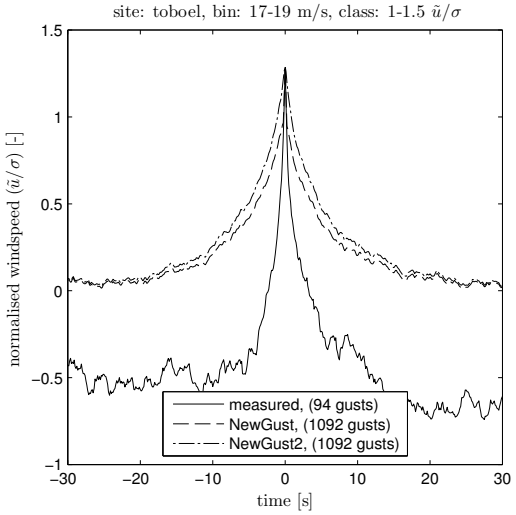
site: toboel, bin: 17-19 m/s, class: 1-1.5 $\tilde{u}/\sigma$
normalised windspeed ($\tilde{u}/\sigma$) [-]
time [s]
measured, (94 gusts)
NewGust, (1092 gusts)
NewGust2, (1092 gusts)

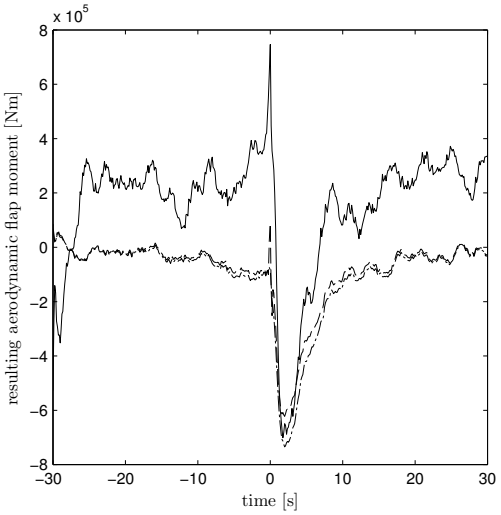
x 10^5
resulting aerodynamic flap moment [Nm]
time [s]

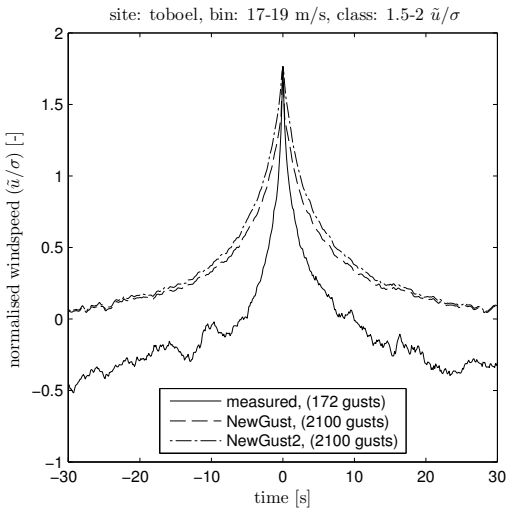
site: toboel, bin: 17-19 m/s, class: 1.5-2 $\tilde{u}/\sigma$
normalised windspeed ($\tilde{u}/\sigma$) [-]
time [s]
measured, (172 gusts)
NewGust, (2100 gusts)
NewGust2, (2100 gusts)

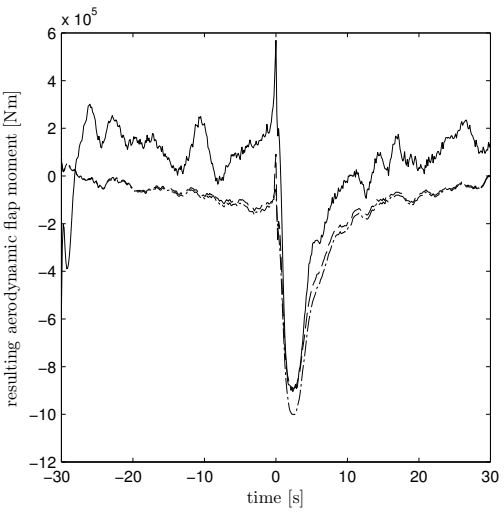
x 10^5
resulting aerodynamic flap moment [Nm]
time [s]

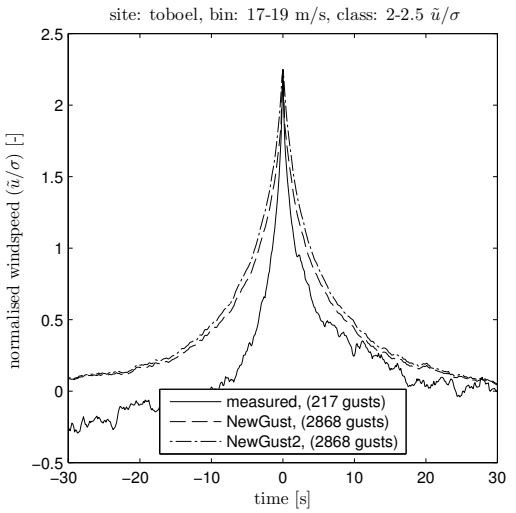
site: toboel, bin: 17-19 m/s, class: 2-2.5 $\tilde{u}/\sigma$
normalised windspeed ($\tilde{u}/\sigma$) [-]
time [s]
measured, (217 gusts)
NewGust, (2868 gusts)
NewGust2, (2868 gusts)

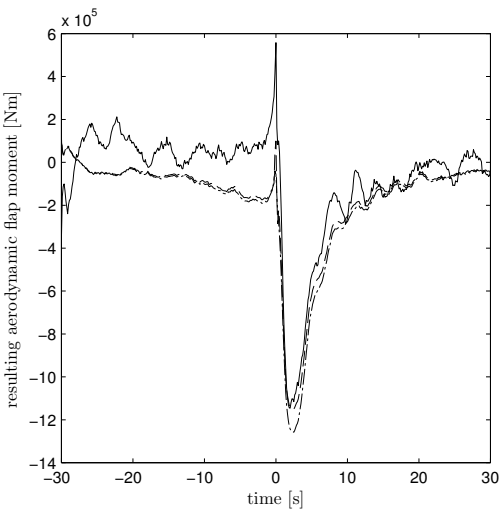
x 10^5
resulting aerodynamic flap moment [Nm]
time [s]

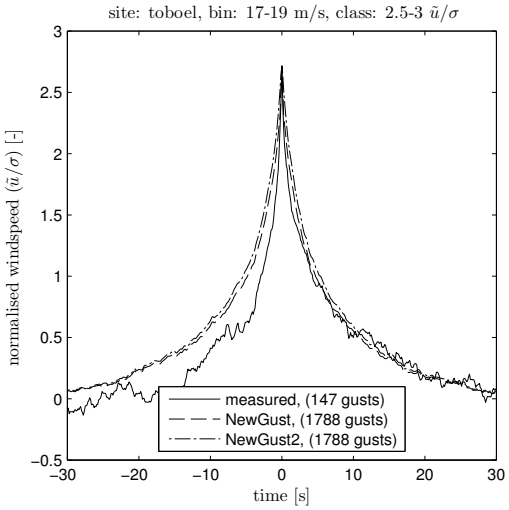
site: toboel, bin: 17-19 m/s, class: 2.5-3 $\tilde{u}/\sigma$
normalised windspeed ($\tilde{u}/\sigma$) [-]
time [s]
measured, (147 gusts)
NewGust, (1788 gusts)
NewGust2, (1788 gusts)

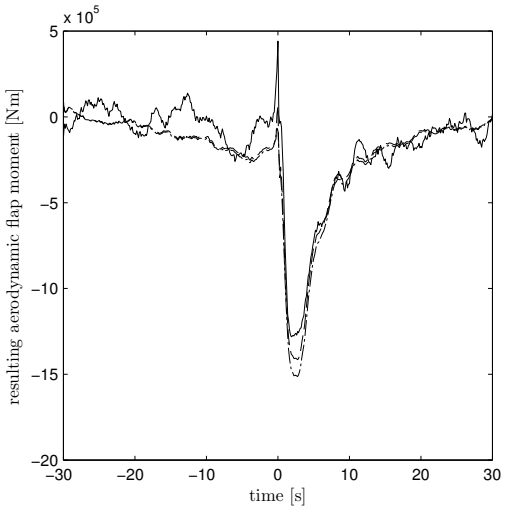
x 10^5
resulting aerodynamic flap moment [Nm]
time [s]

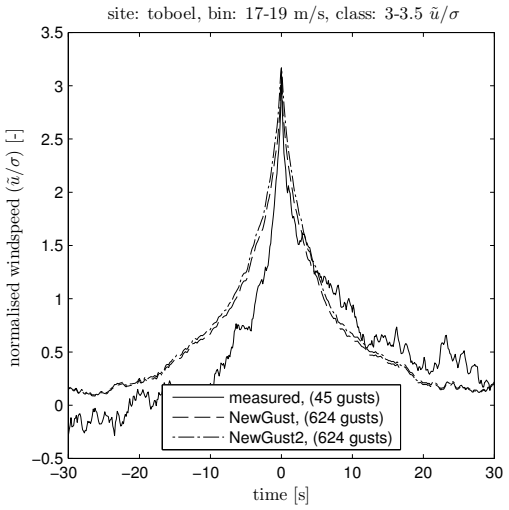
site: toboel, bin: 17-19 m/s, class: 3-3.5 $\tilde{u}/\sigma$
normalised windspeed ($\tilde{u}/\sigma$) [-]
time [s]
measured, (45 gusts)
NewGust, (624 gusts)
NewGust2, (624 gusts)

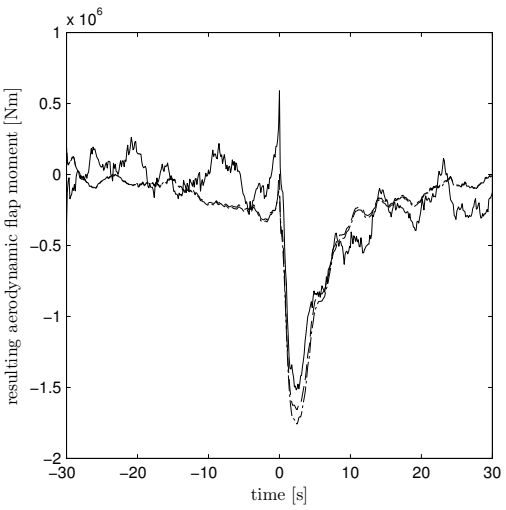
x 10^6
resulting aerodynamic flap moment [Nm]
time [s]

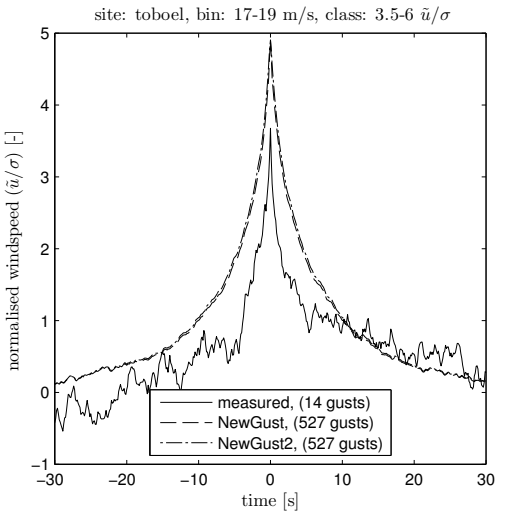
site: toboel, bin: 17-19 m/s, class: 3.5-6 $\tilde{u}/\sigma$
normalised windspeed ($\tilde{u}/\sigma$) [-]
time [s]
measured, (14 gusts)
NewGust, (527 gusts)
NewGust2, (527 gusts)

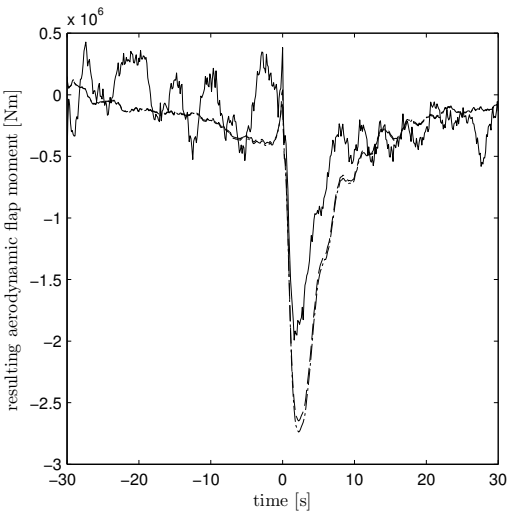
x 10^6
resulting aerodynamic flap moment [Nm]
time [s]

J.2 Results for Oak Creek

$\tilde{u}_n(t_0) \rightarrow$	1-1.5		1.5-2		2-2.5		2.5-3		3-3.5		3.5-6		
$\bar{u} \downarrow$	gust	load	gust	load	gust	load	gust	load	gust	load	gust	load	type
	0.96	0.00	1.10	0.00	1.15	0.00	1.95	0.00	2.16	0.00	5.53	0.01	m,n
0-1	0.11	0.00	0.14	0.00	0.21	0.00	0.13	0.00	0.26	0.00	0.19	0.00	m,ng
	1.64	0.00	2.00	0.00	2.30	0.00	2.93	0.01	3.69	0.01	7.52	0.02	n,ng
	0.88	0.03	0.95	0.03	0.96	0.03	1.15	0.04	1.64	0.05	3.79	0.13	m,n
1-2	0.07	0.00	0.09	0.00	0.13	0.00	0.12	0.00	0.10	0.00	0.08	0.00	m,ng
	1.43	0.05	1.58	0.06	1.78	0.06	2.00	0.07	2.50	0.09	4.77	0.17	n,ng
	0.86	0.11	0.79	0.10	0.90	0.12	0.93	0.12	1.07	0.14	2.90	0.39	m,n
2-3	0.04	0.01	0.07	0.01	0.06	0.01	0.10	0.01	0.12	0.02	0.05	0.01	m,ng
	1.26	0.17	1.31	0.18	1.39	0.18	1.58	0.21	1.87	0.25	3.54	0.47	n,ng
	0.73	0.22	0.70	0.21	0.70	0.22	0.84	0.27	0.95	0.30	2.22	0.71	m,n
3-4	0.06	0.02	0.06	0.02	0.06	0.02	0.06	0.02	0.06	0.02	0.06	0.01	m,ng
	1.20	0.37	1.14	0.36	1.12	0.35	1.30	0.40	1.43	0.45	2.91	0.92	n,ng
	0.62	0.35	0.60	0.34	0.48	0.28	0.60	0.35	0.70	0.42	1.73	1.03	m,n
4-5	0.06	0.03	0.05	0.03	0.05	0.03	0.05	0.03	0.04	0.02	0.05	0.02	m,ng
	1.03	0.59	0.96	0.55	0.82	0.47	0.98	0.56	1.00	0.58	2.18	1.26	n,ng
	0.63	0.57	0.50	0.46	0.42	0.38	0.40	0.37	0.56	0.52	1.60	1.48	m,n
5-6	0.01	0.00	0.00	0.00	0.00	0.00	0.01	0.01	0.01	0.00	0.01	0.00	m,ng
	0.74	0.67	0.54	0.49	0.49	0.45	0.49	0.46	0.57	0.53	1.58	1.47	n,ng
	0.49	0.65	0.39	0.52	0.32	0.44	0.38	0.52	0.46	0.63	1.21	1.69	m,n
6-7	0.02	0.02	0.01	0.01	0.01	0.01	0.01	0.00	0.01	0.01	0.02	0.01	m,ng
	0.66	0.88	0.49	0.66	0.38	0.52	0.41	0.57	0.38	0.52	1.26	1.71	n,ng
	0.50	0.90	0.35	0.65	0.29	0.55	0.30	0.57	0.41	0.76	1.35	2.55	m,n
7-8	0.01	0.01	0.01	0.01	0.01	0.01	0.01	0.01	0.01	0.01	0.04	0.05	m,ng
	0.62	1.12	0.43	0.81	0.33	0.63	0.34	0.63	0.33	0.63	1.06	1.98	n,ng
	0.38	0.91	0.25	0.62	0.23	0.57	0.27	0.67	0.33	0.80	1.26	3.10	m,n
8-9	0.03	0.07	0.01	0.02	0.01	0.01	0.01	0.01	0.01	0.02	0.05	0.10	m,ng
	0.62	1.49	0.33	0.80	0.26	0.65	0.25	0.63	0.27	0.67	0.86	2.13	n,ng
	0.40	1.22	0.23	0.73	0.20	0.63	0.25	0.78	0.40	1.22	1.01	3.12	m,n
9-10	0.01	0.03	0.01	0.03	0.01	0.02	0.01	0.01	0.03	0.07	0.03	0.05	m,ng
	0.51	1.56	0.32	0.99	0.23	0.74	0.23	0.73	0.24	0.75	0.81	2.52	n,ng
	0.32	1.21	0.26	1.05	0.18	0.70	0.20	0.78	0.26	0.99	0.95	3.60	m,n
10-11	0.02	0.08	0.01	0.02	0.01	0.02	0.01	0.02	0.01	0.02	0.04	0.09	m,ng
	0.49	1.86	0.32	1.26	0.21	0.85	0.23	0.92	0.21	0.81	0.86	3.31	n,ng
	0.28	0.16	0.21	0.39	0.20	0.75	0.23	1.14	0.31	1.84	0.82	2.66	m,n
11-12	0.03	0.01	0.02	0.00	0.01	0.00	0.02	0.00	0.03	0.02	0.03	0.03	m,ng
	0.45	0.13	0.29	0.37	0.20	0.74	0.19	1.14	0.24	1.74	0.68	3.06	n,ng
	0.29	0.21	0.22	0.16	0.15	0.12	0.18	0.14	0.22	0.17	0.95	0.76	m,n
12-13	0.02	0.02	0.01	0.01	0.02	0.01	0.01	0.01	0.02	0.02	0.06	0.05	m,ng
	0.46	0.33	0.29	0.22	0.18	0.13	0.16	0.12	0.15	0.11	0.61	0.47	n,ng
	0.30	0.16	0.18	0.09	0.15	0.08	0.15	0.08	0.24	0.13	0.69	0.38	m,n
13-14	0.03	0.02	0.01	0.01	0.01	0.01	0.01	0.01	0.03	0.02	0.03	0.02	m,ng
	0.49	0.26	0.26	0.13	0.20	0.10	0.14	0.07	0.16	0.08	0.52	0.29	n,ng

$\tilde{u}_n(t_0) \rightarrow$	1-1.5		1.5-2		2-2.5		2.5-3		3-3.5		3.5-6		
$\bar{u} \downarrow$	gust	load	gust	load	gust	load	gust	load	gust	load	gust	load	type
	0.30	0.12	0.18	0.08	0.13	0.06	0.11	0.05	0.19	0.08	0.59	0.25	m,n
14-15	0.02	0.01	0.01	0.01	0.02	0.01	0.02	0.01	0.02	0.01	0.01	0.02	m,ng
	0.44	0.18	0.26	0.10	0.18	0.07	0.14	0.05	0.13	0.05	0.51	0.22	n,ng
	0.35	0.11	0.19	0.06	0.12	0.04	0.12	0.04	0.15	0.05	0.50	0.18	m,n
15-16	0.02	0.01	0.01	0.01	0.02	0.01	0.01	0.00	0.01	0.01	0.02	0.01	m,ng
	0.48	0.15	0.29	0.09	0.20	0.06	0.16	0.05	0.17	0.06	0.54	0.18	n,ng
	0.33	0.08	0.18	0.04	0.10	0.03	0.11	0.03	0.14	0.04	0.55	0.16	m,n
16-17	0.01	0.00	0.01	0.00	0.01	0.00	0.01	0.00	0.01	0.00	0.02	0.01	m,ng
	0.45	0.11	0.26	0.07	0.16	0.04	0.15	0.04	0.16	0.04	0.46	0.12	n,ng
	0.32	0.07	0.15	0.03	0.10	0.02	0.08	0.02	0.16	0.04	0.54	0.13	m,n
17-18	0.02	0.01	0.01	0.00	0.02	0.00	0.03	0.01	0.01	0.01	0.03	0.02	m,ng
	0.46	0.10	0.23	0.05	0.17	0.03	0.15	0.03	0.14	0.03	0.44	0.10	n,ng
	0.35	0.06	0.15	0.03	0.08	0.01	0.07	0.02	0.12	0.03	0.33	0.08	m,n
18-19	0.01	0.01	0.01	0.00	0.01	0.00	0.01	0.00	0.01	0.00	0.03	0.01	m,ng
	0.46	0.09	0.23	0.04	0.13	0.02	0.11	0.02	0.12	0.02	0.26	0.05	n,ng
	0.35	0.05	0.14	0.02	0.08	0.01	0.05	0.01	0.08	0.02	0.57	0.10	m,n
19-20	0.01	0.00	0.02	0.00	0.02	0.00	0.01	0.00	0.01	0.00	0.04	0.02	m,ng
	0.48	0.07	0.22	0.03	0.13	0.02	0.08	0.01	0.06	0.01	0.35	0.06	n,ng
	0.39	0.05	0.15	0.02	0.07	0.01	0.05	0.01	0.10	0.02	0.56	0.09	m,n
20-21	0.01	0.00	0.02	0.00	0.01	0.00	0.01	0.00	0.01	0.00	0.05	0.02	m,ng
	0.45	0.06	0.25	0.03	0.11	0.01	0.08	0.01	0.07	0.01	0.34	0.06	n,ng
	0.37	0.04	0.16	0.02	0.07	0.01	0.06	0.01	0.08	0.01	0.37	0.06	m,n
21-22	0.01	0.00	0.01	0.00	0.01	0.00	0.01	0.00	0.01	0.01	0.02	0.02	m,ng
	0.41	0.05	0.21	0.03	0.11	0.01	0.09	0.01	0.07	0.01	0.29	0.04	n,ng
	0.37	0.05	0.15	0.02	0.07	0.01	0.06	0.01	0.10	0.02	0.44	0.08	m,n
22-23	0.01	0.01	0.01	0.00	0.01	0.00	0.01	0.00	0.03	0.01	0.06	0.06	m,ng
	0.46	0.05	0.22	0.02	0.11	0.01	0.07	0.01	0.06	0.01	0.25	0.04	n,ng
	0.38	0.04	0.14	0.02	0.06	0.01	0.06	0.01	0.12	0.02	0.33	0.05	m,n
23-24	0.01	0.01	0.01	0.00	0.01	0.00	0.02	0.01	0.02	0.01	0.02	0.02	m,ng
	0.40	0.04	0.19	0.02	0.10	0.01	0.08	0.01	0.07	0.01	0.36	0.04	n,ng
	0.36	0.03	0.18	0.02	0.09	0.01	0.05	0.01	0.08	0.02	0.50	0.05	m,n
24-25	0.01	0.01	0.01	0.00	0.02	0.00	0.02	0.00	0.02	0.01	0.06	0.03	m,ng
	0.41	0.04	0.21	0.02	0.11	0.01	0.07	0.01	0.06	0.01	0.39	0.04	n,ng
	0.41	0.03	0.17	0.01	0.08	0.01	0.07	0.01	0.08	0.02	0.49	0.08	m,n
25-26	0.02	0.01	0.01	0.00	0.02	0.00	0.02	0.00	0.03	0.01	0.13	0.06	m,ng
	0.46	0.03	0.21	0.02	0.11	0.01	0.09	0.01	0.06	0.01	0.32	0.03	n,ng
	0.42	0.02	0.16	0.01	0.06	0.00	0.06	0.00	0.14	0.01	0.69	0.03	m,n
26-30	0.01	0.00	0.01	0.00	0.01	0.00	0.01	0.00	0.07	0.01	0.18	0.06	m,ng
	0.40	0.02	0.18	0.01	0.08	0.00	0.05	0.00	0.04	0.00	0.59	0.06	n,ng

Table J.2: mse between gusts for Oak Creek, 'm' denotes 'measured', 'ng' denotes 'non-Gaussian' and 'n' denotes 'newgust'

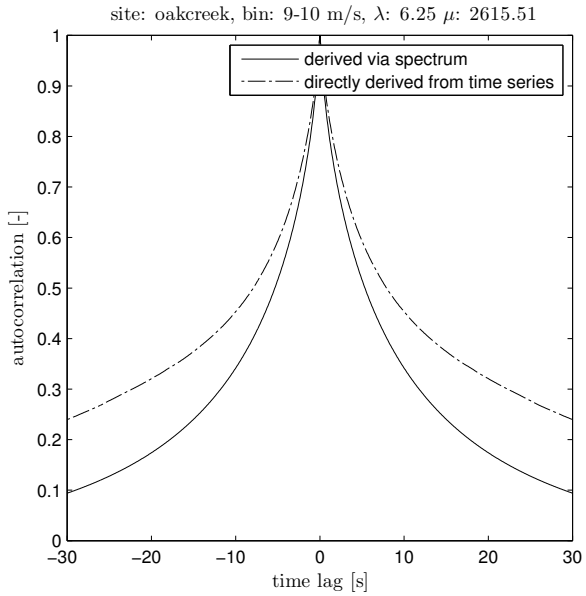
site: oakcreek, bin: 9-10 m/s, λ: 6.25 μ: 2615.51
derived via spectrum
directly derived from time series
autocorrelation [-]
time lag [s]

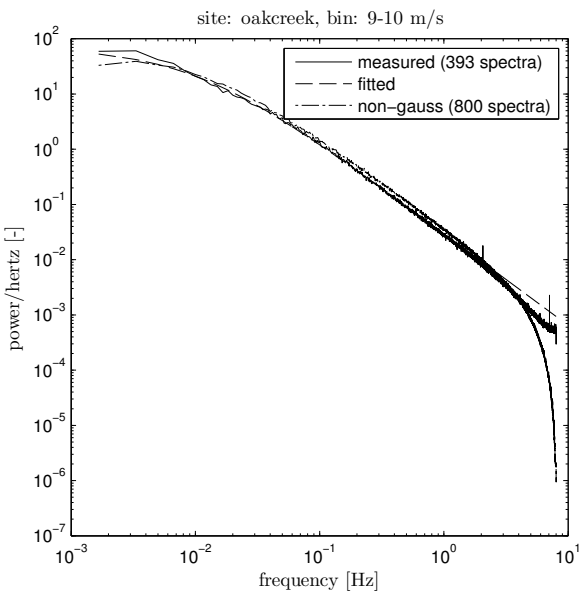
site: oakcreek, bin: 9-10 m/s
measured (393 spectra)
fitted
non−gauss (800 spectra)
power/hertz [-]
frequency [Hz]

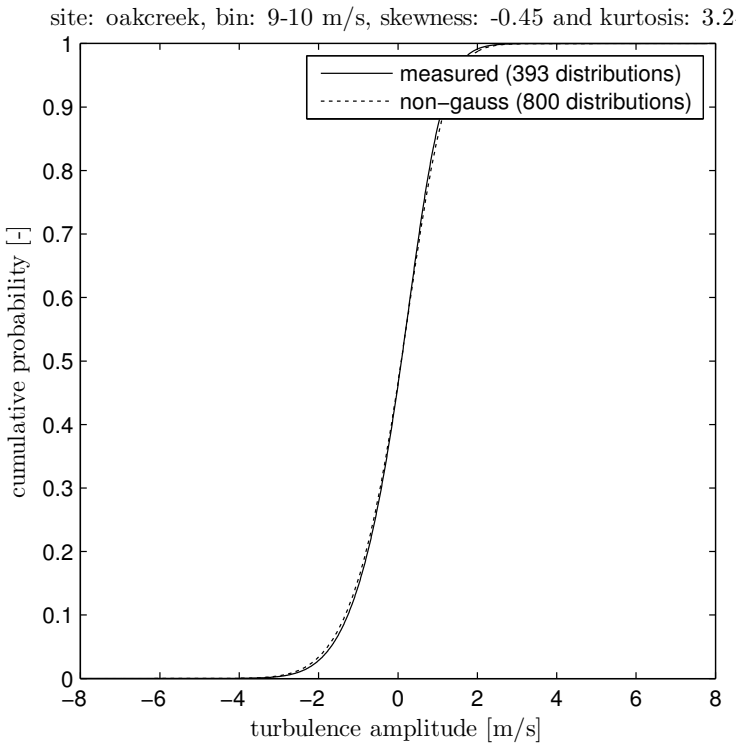
site: oakcreek, bin: 9-10 m/s, skewness: -0.45 and kurtosis: 3.24
measured (393 distributions)
non−gauss (800 distributions)
cumulative probability [-]
turbulence amplitude [m/s]

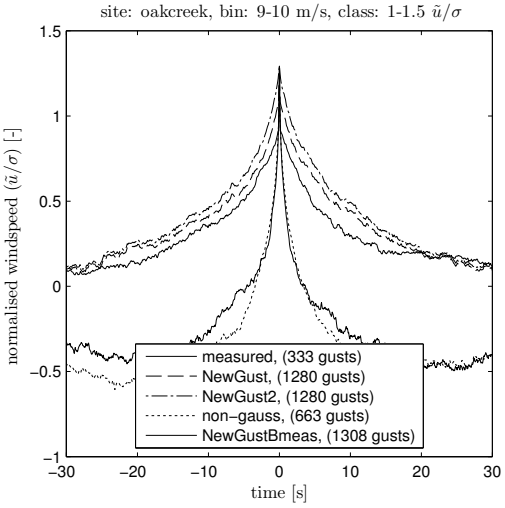
site: oakcreek, bin: 9-10 m/s, class: 1-1.5 $\tilde{u}/\sigma$
normalised windspeed $(\tilde{u}/\sigma)$ [-]
time [s]
measured, (333 gusts)
NewGust, (1280 gusts)
NewGust2, (1280 gusts)
non−gauss, (663 gusts)
NewGustBmeas, (1308 gusts)

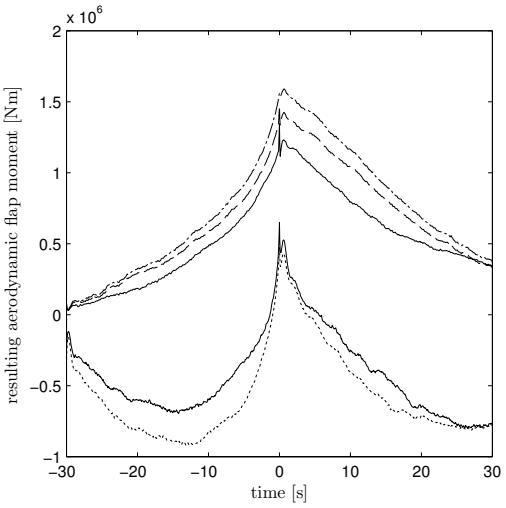
x 10^6
resulting aerodynamic flap moment [Nm]
time [s]

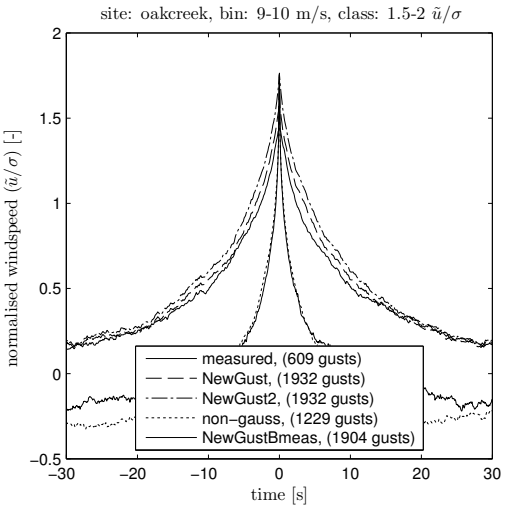
site: oakcreek, bin: 9-10 m/s, class: 1.5-2 $\tilde{u}/\sigma$
normalised windspeed $(\tilde{u}/\sigma)$ [-]
time [s]
measured, (609 gusts)
NewGust, (1932 gusts)
NewGust2, (1932 gusts)
non−gauss, (1229 gusts)
NewGustBmeas, (1904 gusts)

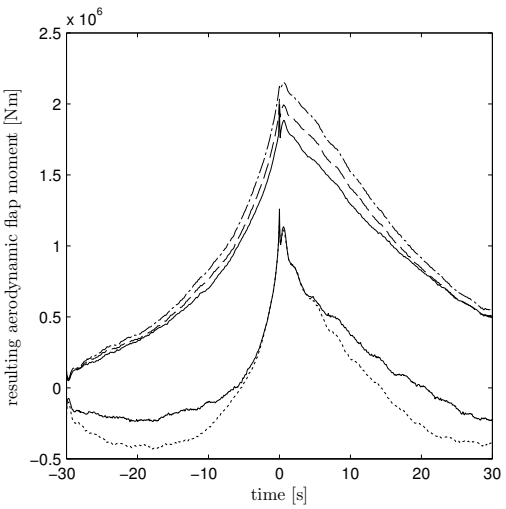
x 10^6
resulting aerodynamic flap moment [Nm]
time [s]

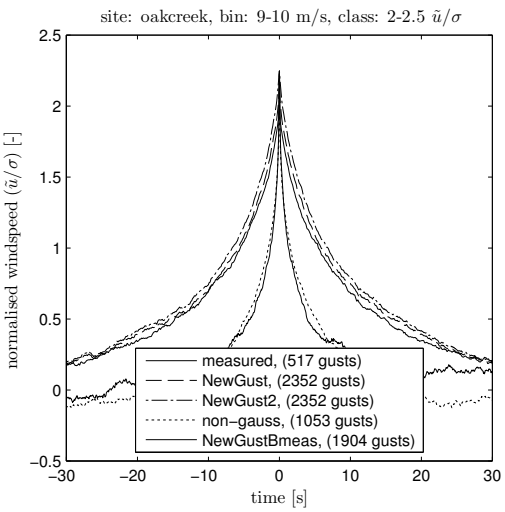
site: oakcreek, bin: 9-10 m/s, class: 2-2.5 $\tilde{u}/\sigma$
normalised windspeed $(\tilde{u}/\sigma)$ [-]
time [s]
measured, (517 gusts)
NewGust, (2352 gusts)
NewGust2, (2352 gusts)
non−gauss, (1053 gusts)
NewGustBmeas, (1904 gusts)

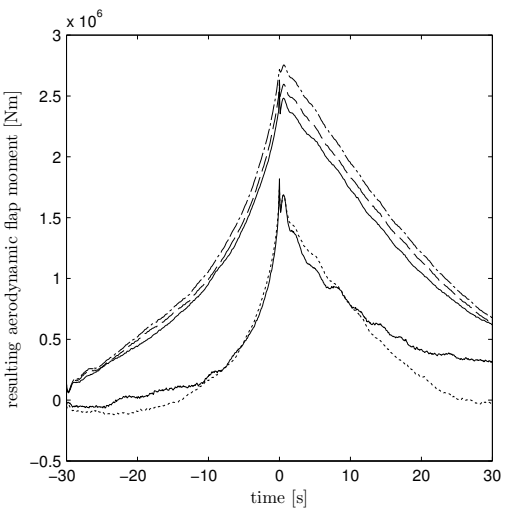
x 10^6
resulting aerodynamic flap moment [Nm]
time [s]

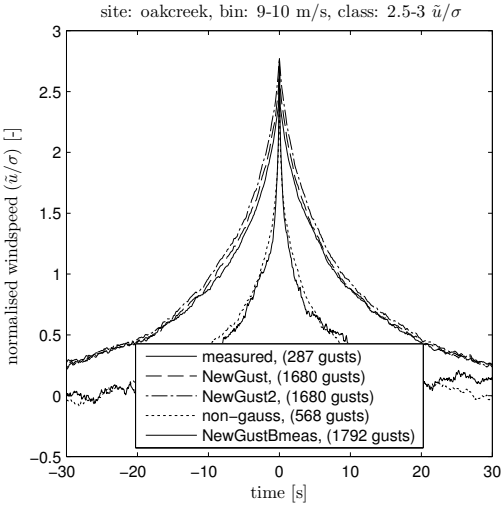
site: oakcreek, bin: 9-10 m/s, class: 2.5-3 $\tilde{u}/\sigma$
normalised windspeed $(\tilde{u}/\sigma)$ [-]
time [s]
measured, (287 gusts)
NewGust, (1680 gusts)
NewGust2, (1680 gusts)
non−gauss, (568 gusts)
NewGustBmeas, (1792 gusts)

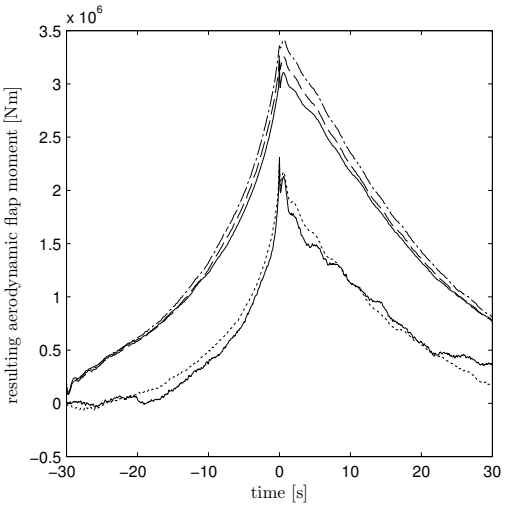
x 10^6
resulting aerodynamic flap moment [Nm]
time [s]

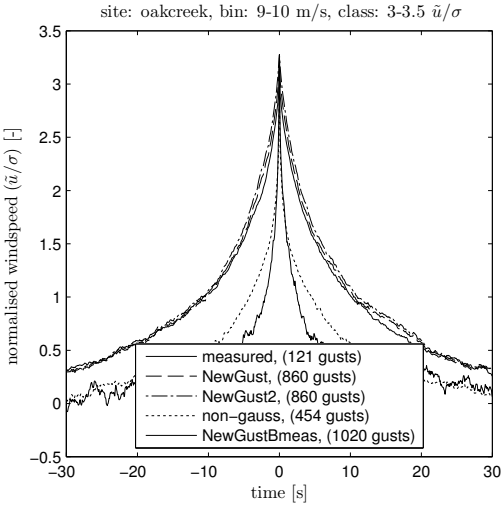
site: oakcreek, bin: 9-10 m/s, class: 3-3.5 $\tilde{u}/\sigma$
normalised windspeed $(\tilde{u}/\sigma)$ [-]
time [s]
measured, (121 gusts)
NewGust, (860 gusts)
NewGust2, (860 gusts)
non−gauss, (454 gusts)
NewGustBmeas, (1020 gusts)

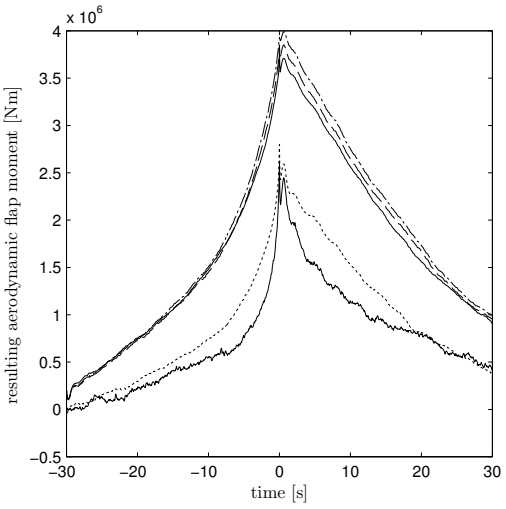
x 10^6
resulting aerodynamic flap moment [Nm]
time [s]

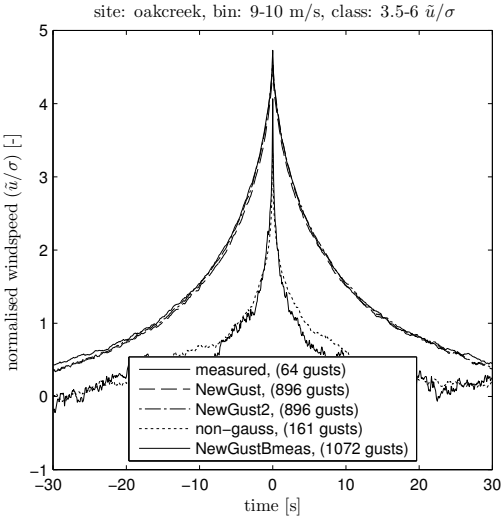
site: oakcreek, bin: 9-10 m/s, class: 3.5-6 $\tilde{u}/\sigma$
normalised windspeed $(\tilde{u}/\sigma)$ [-]
time [s]
measured, (64 gusts)
NewGust, (896 gusts)
NewGust2, (896 gusts)
non−gauss, (161 gusts)
NewGustBmeas, (1072 gusts)

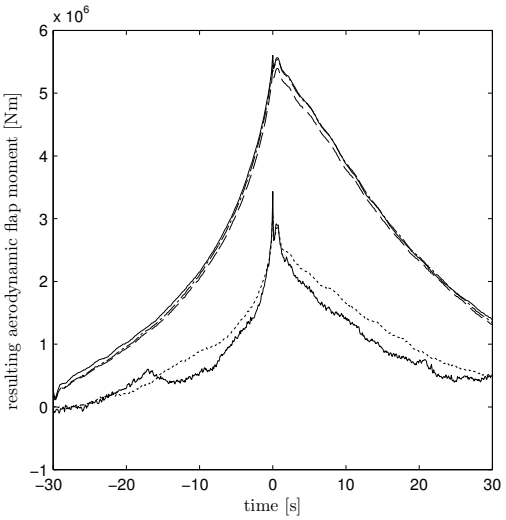
x 10^6
resulting aerodynamic flap moment [Nm]
time [s]

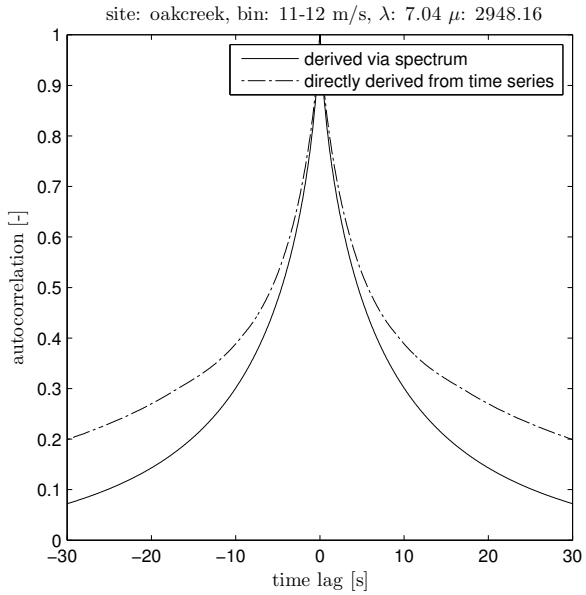
site: oakcreek, bin: 11-12 m/s, λ: 7.04 μ: 2948.16
derived via spectrum
directly derived from time series
autocorrelation [-]
time lag [s]

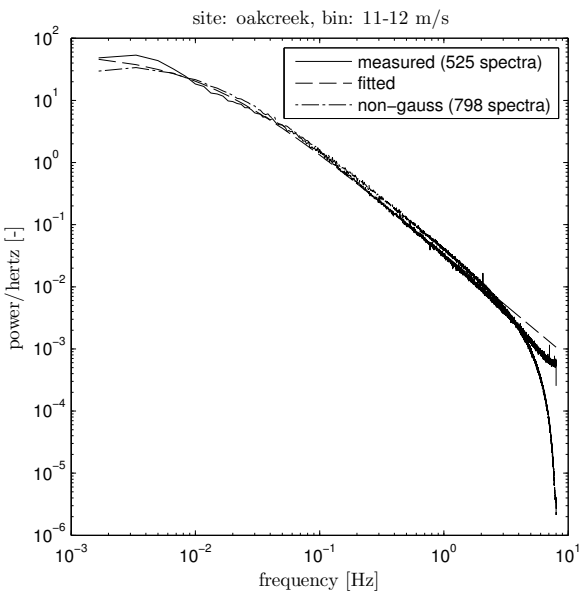
site: oakcreek, bin: 11-12 m/s
measured (525 spectra)
fitted
non−gauss (798 spectra)
power/hertz [-]
frequency [Hz]

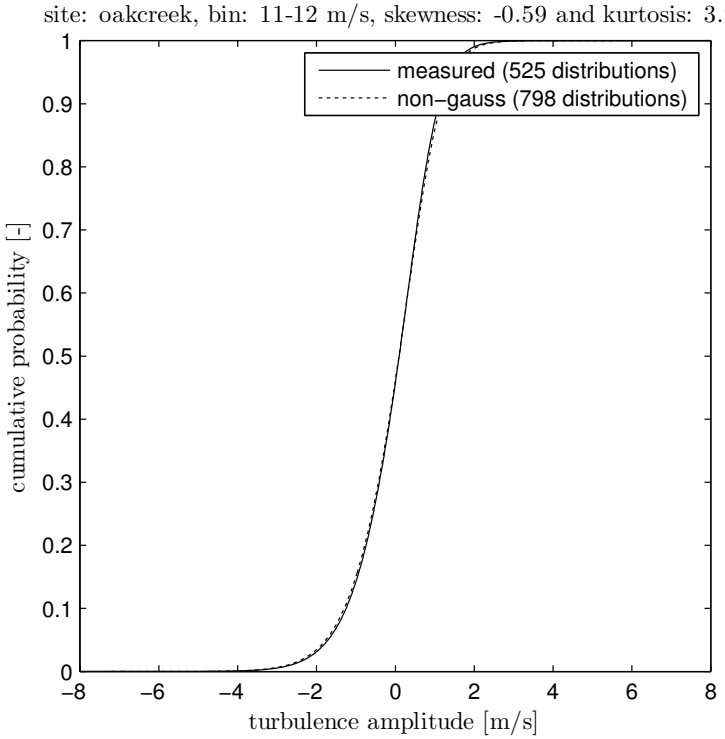
site: oakcreek, bin: 11-12 m/s, skewness: -0.59 and kurtosis: 3.96
measured (525 distributions)
non−gauss (798 distributions)
cumulative probability [-]
turbulence amplitude [m/s]

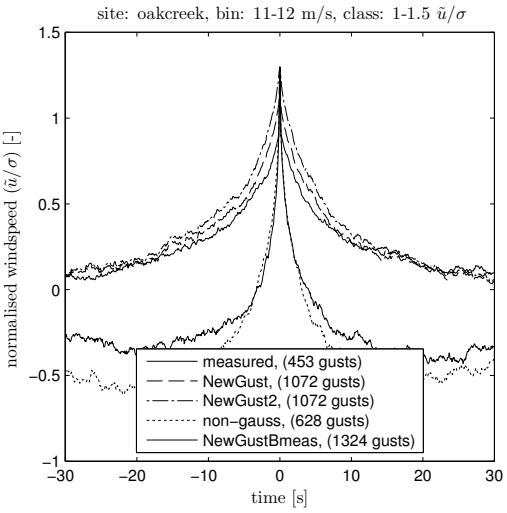
site: oakcreek, bin: 11-12 m/s, class: 1-1.5 $\tilde{u}/\sigma$
normalised windspeed $(\tilde{u}/\sigma)$ [-]
time [s]
measured, (453 gusts)
NewGust, (1072 gusts)
NewGust2, (1072 gusts)
non−gauss, (628 gusts)
NewGustBmeas, (1324 gusts)

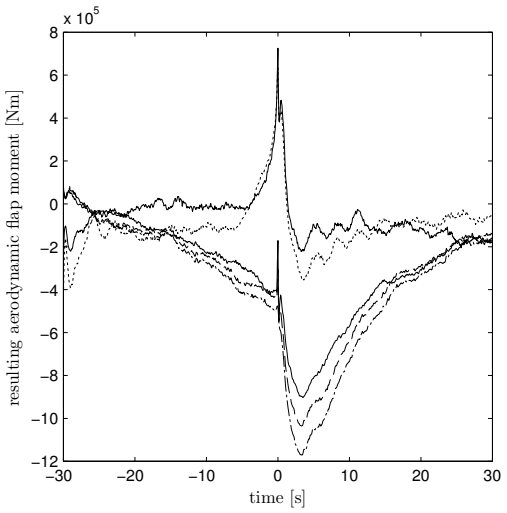
x 10^5
resulting aerodynamic flap moment [Nm]
time [s]

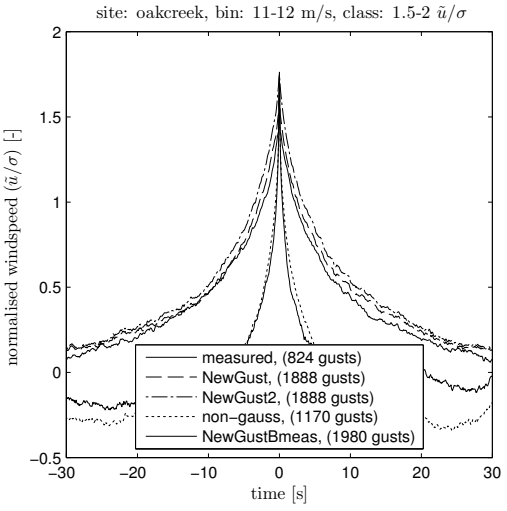
site: oakcreek, bin: 11-12 m/s, class: 1.5-2 $\tilde{u}/\sigma$
normalised windspeed $(\tilde{u}/\sigma)$ [-]
time [s]
measured, (824 gusts)
NewGust, (1888 gusts)
NewGust2, (1888 gusts)
non−gauss, (1170 gusts)
NewGustBmeas, (1980 gusts)

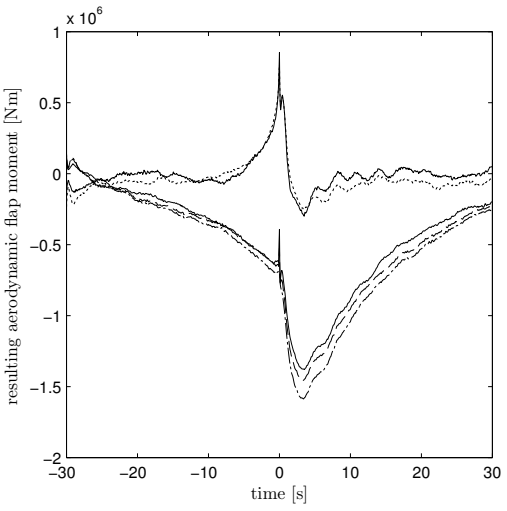
x 10^6
resulting aerodynamic flap moment [Nm]
time [s]

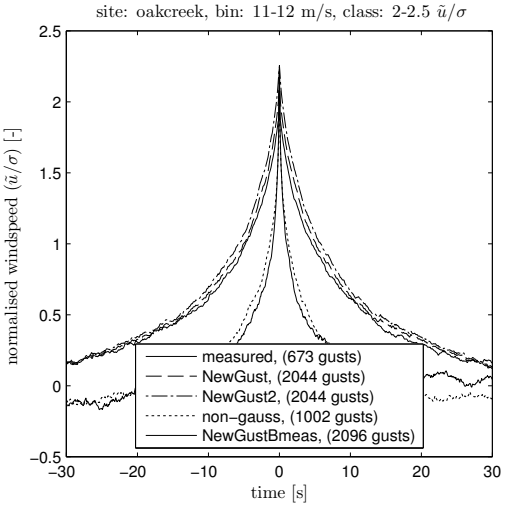
site: oakcreek, bin: 11-12 m/s, class: 2-2.5 $\tilde{u}/\sigma$
normalised windspeed $(\tilde{u}/\sigma)$ [-]
time [s]
measured, (673 gusts)
NewGust, (2044 gusts)
NewGust2, (2044 gusts)
non−gauss, (1002 gusts)
NewGustBmeas, (2096 gusts)

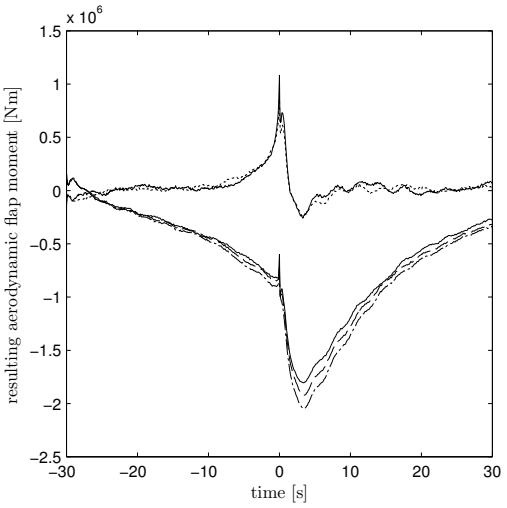
x 10^6
resulting aerodynamic flap moment [Nm]
time [s]

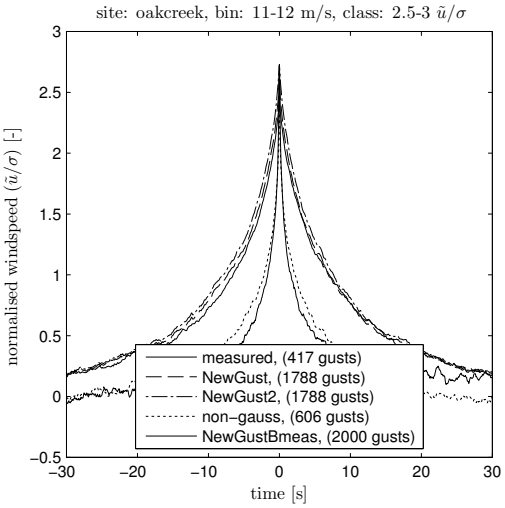
site: oakcreek, bin: 11-12 m/s, class: 2.5-3 $\tilde{u}/\sigma$
normalised windspeed ($\tilde{u}/\sigma$) [-]
time [s]
measured, (417 gusts)
NewGust, (1788 gusts)
NewGust2, (1788 gusts)
non−gauss, (606 gusts)
NewGustBmeas, (2000 gusts)

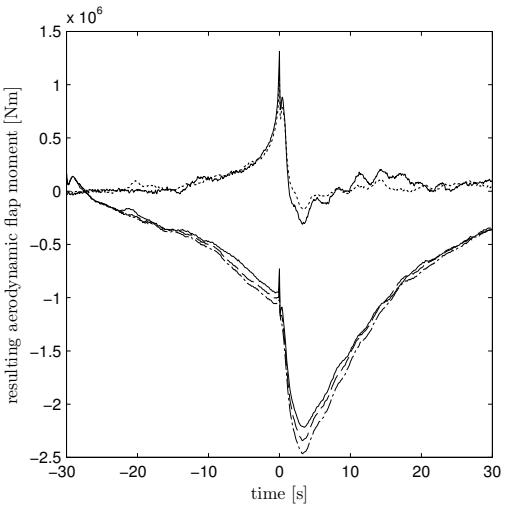
x 10^6
resulting aerodynamic flap moment [Nm]
time [s]

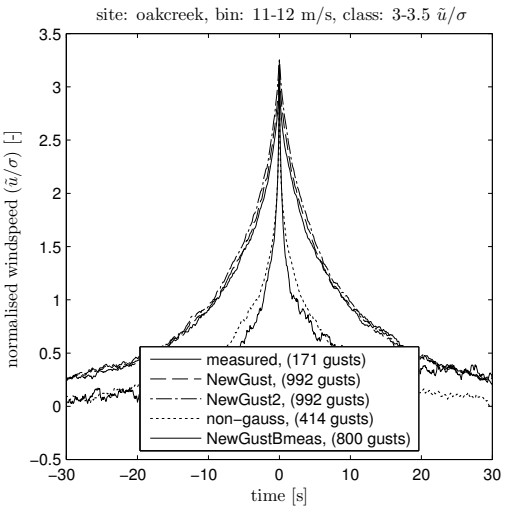
site: oakcreek, bin: 11-12 m/s, class: 3-3.5 $\tilde{u}/\sigma$
normalised windspeed ($\tilde{u}/\sigma$) [-]
time [s]
measured, (171 gusts)
NewGust, (992 gusts)
NewGust2, (992 gusts)
non−gauss, (414 gusts)
NewGustBmeas, (800 gusts)

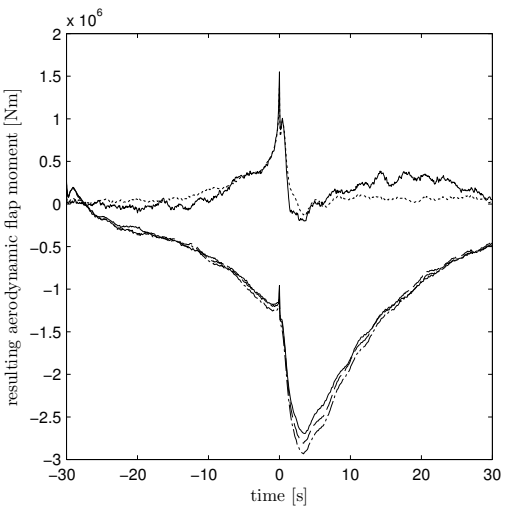
x 10^6
resulting aerodynamic flap moment [Nm]
time [s]

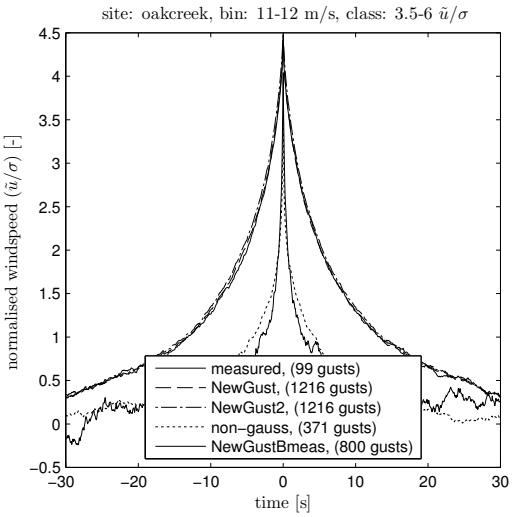
site: oakcreek, bin: 11-12 m/s, class: 3.5-6 $\tilde{u}/\sigma$
normalised windspeed ($\tilde{u}/\sigma$) [-]
time [s]
measured, (99 gusts)
NewGust, (1216 gusts)
NewGust2, (1216 gusts)
non−gauss, (371 gusts)
NewGustBmeas, (800 gusts)

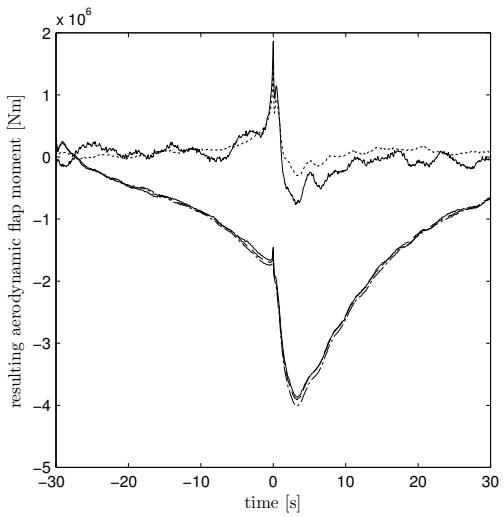
x 10^6
resulting aerodynamic flap moment [Nm]
time [s]

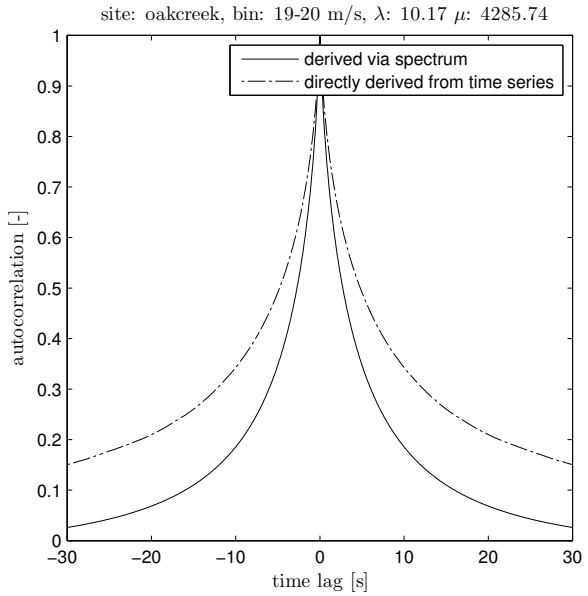
site: oakcreek, bin: 19-20 m/s, λ: 10.17 μ: 4285.74
derived via spectrum
directly derived from time series
autocorrelation [-]
time lag [s]

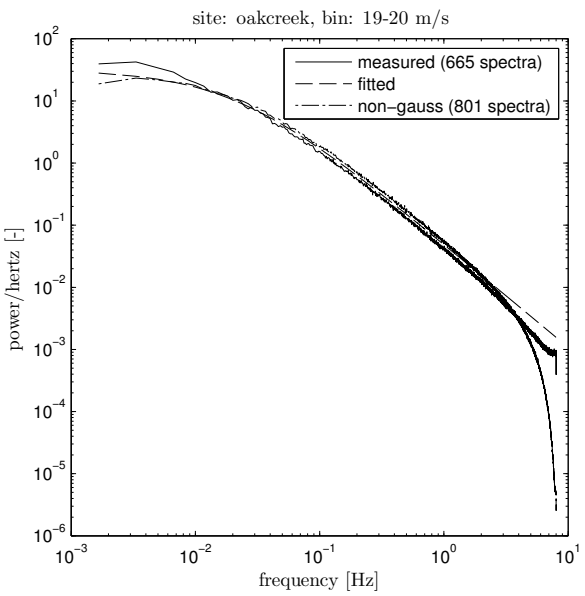
site: oakcreek, bin: 19-20 m/s
measured (665 spectra)
fitted
non−gauss (801 spectra)
power/hertz [-]
frequency [Hz]

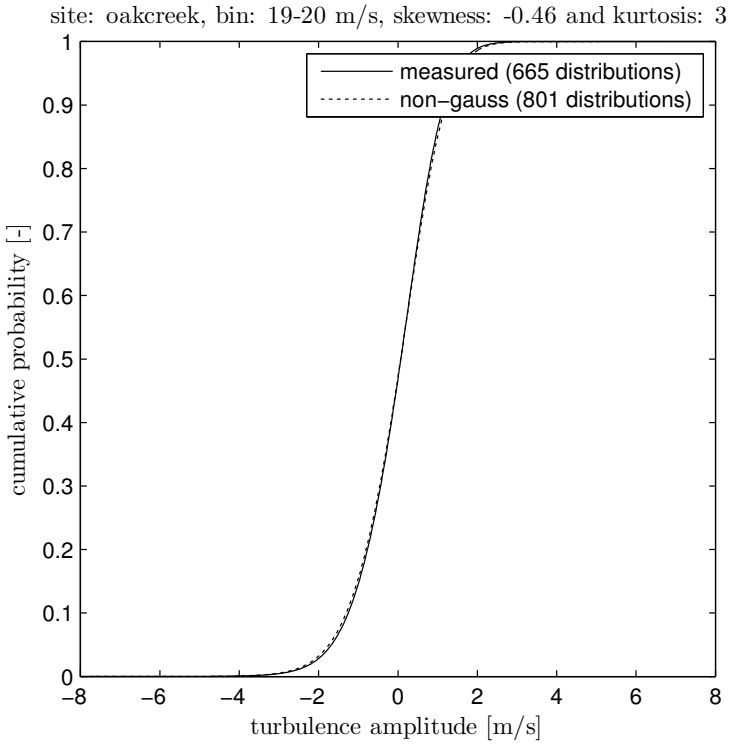
site: oakcreek, bin: 19-20 m/s, skewness: -0.46 and kurtosis: 3.7
measured (665 distributions)
non−gauss (801 distributions)
cumulative probability [-]
turbulence amplitude [m/s]

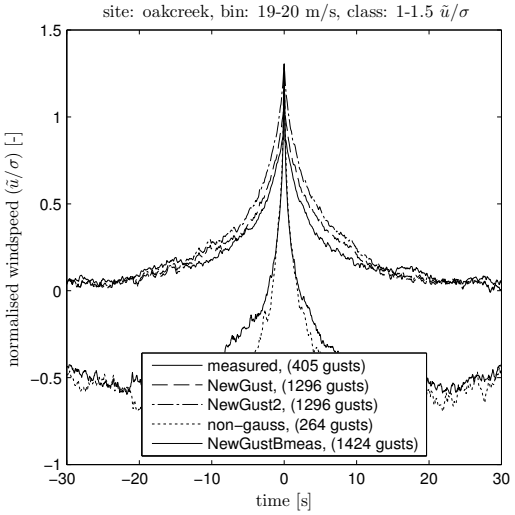
site: oakcreek, bin: 19-20 m/s, class: 1-1.5 $\tilde{u}/\sigma$
normalised windspeed $(\tilde{u}/\sigma)$ [-]
time [s]
measured, (405 gusts)
NewGust, (1296 gusts)
NewGust2, (1296 gusts)
non−gauss, (264 gusts)
NewGustBmeas, (1424 gusts)

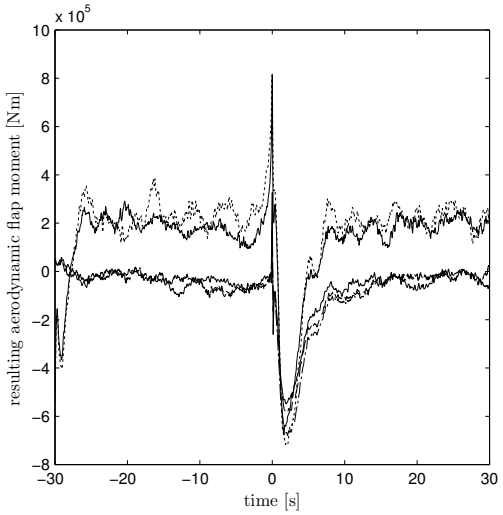
x 10^5
resulting aerodynamic flap moment [Nm]
time [s]

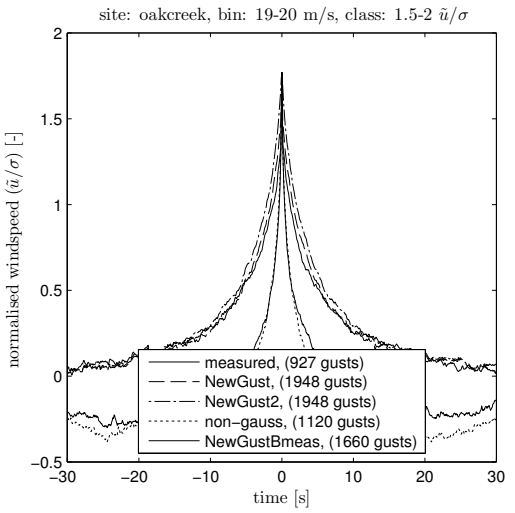
site: oakcreek, bin: 19-20 m/s, class: 1.5-2 $\tilde{u}/\sigma$
normalised windspeed $(\tilde{u}/\sigma)$ [-]
time [s]
measured, (927 gusts)
NewGust, (1948 gusts)
NewGust2, (1948 gusts)
non−gauss, (1120 gusts)
NewGustBmeas, (1660 gusts)

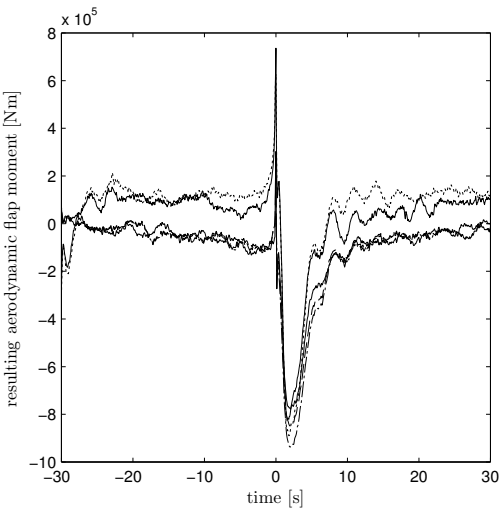
x 10^5
resulting aerodynamic flap moment [Nm]
time [s]

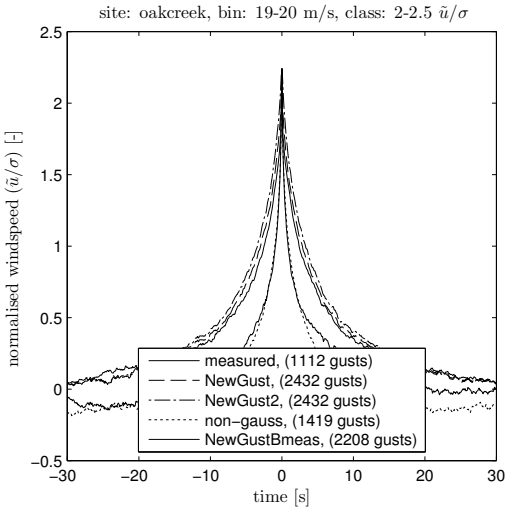
site: oakcreek, bin: 19-20 m/s, class: 2-2.5 $\tilde{u}/\sigma$
normalised windspeed $(\tilde{u}/\sigma)$ [-]
time [s]
measured, (1112 gusts)
NewGust, (2432 gusts)
NewGust2, (2432 gusts)
non−gauss, (1419 gusts)
NewGustBmeas, (2208 gusts)

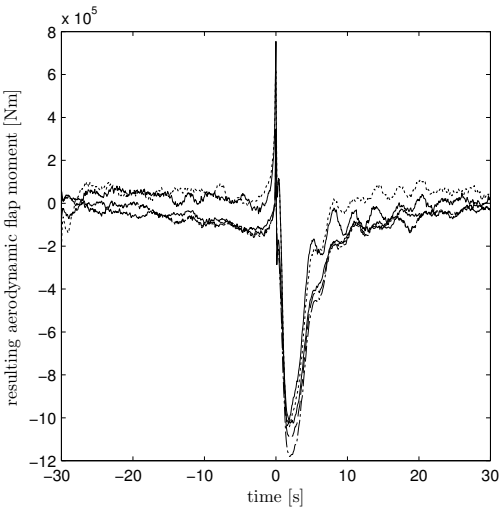
x 10^5
resulting aerodynamic flap moment [Nm]
time [s]

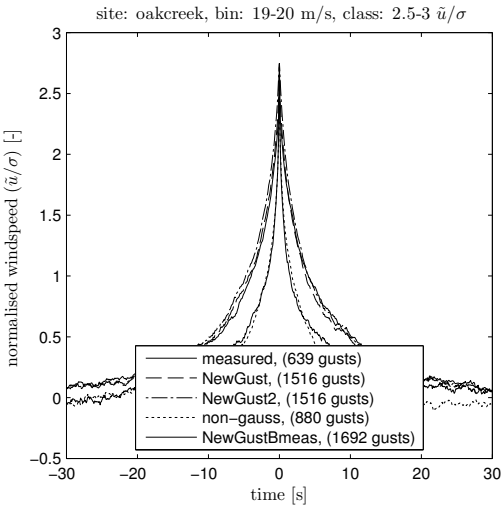
site: oakcreek, bin: 19-20 m/s, class: 2.5-3 $\tilde{u}/\sigma$
normalised windspeed $(\tilde{u}/\sigma)$ [-]
time [s]
measured, (639 gusts)
NewGust, (1516 gusts)
NewGust2, (1516 gusts)
non−gauss, (880 gusts)
NewGustBmeas, (1692 gusts)

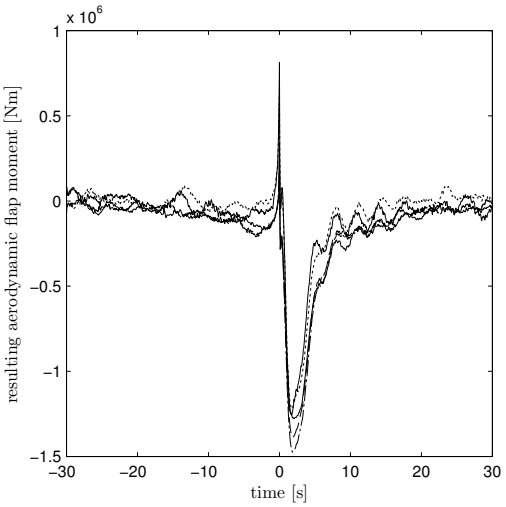
x 10^6
resulting aerodynamic flap moment [Nm]
time [s]

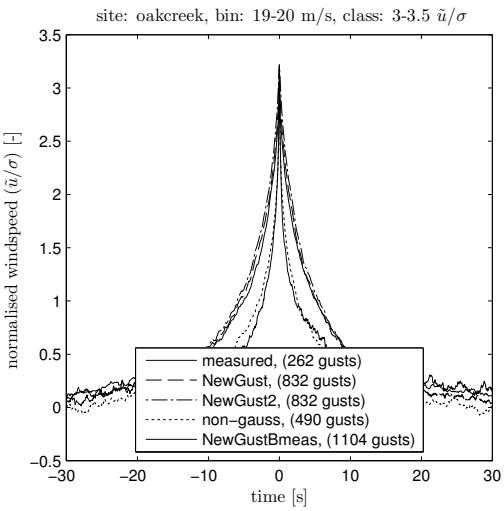
site: oakcreek, bin: 19-20 m/s, class: 3-3.5 $\tilde{u}/\sigma$
normalised windspeed $(\tilde{u}/\sigma)$ [-]
time [s]
measured, (262 gusts)
NewGust, (832 gusts)
NewGust2, (832 gusts)
non−gauss, (490 gusts)
NewGustBmeas, (1104 gusts)

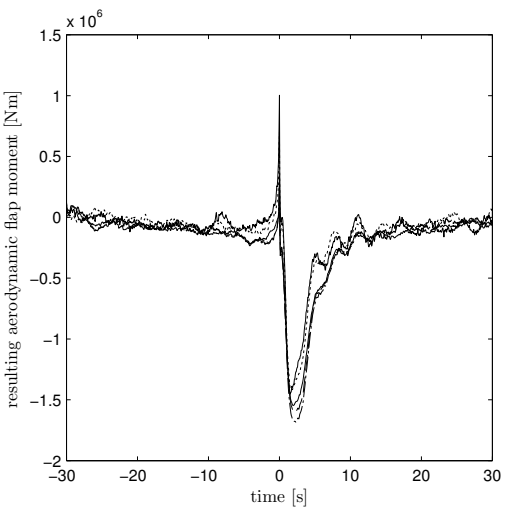
x 10^6
resulting aerodynamic flap moment [Nm]
time [s]

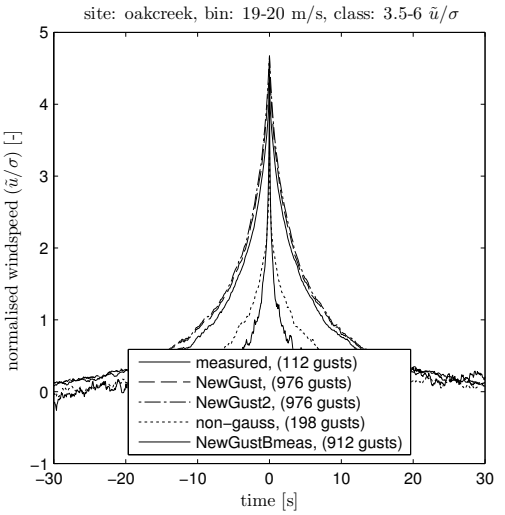
site: oakcreek, bin: 19-20 m/s, class: 3.5-6 $\tilde{u}/\sigma$
normalised windspeed $(\tilde{u}/\sigma)$ [-]
time [s]
measured, (112 gusts)
NewGust, (976 gusts)
NewGust2, (976 gusts)
non−gauss, (198 gusts)
NewGustBmeas, (912 gusts)

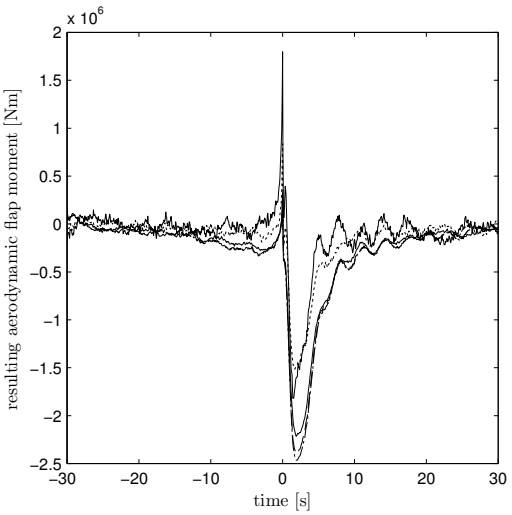
x 10^6
resulting aerodynamic flap moment [Nm]
time [s]

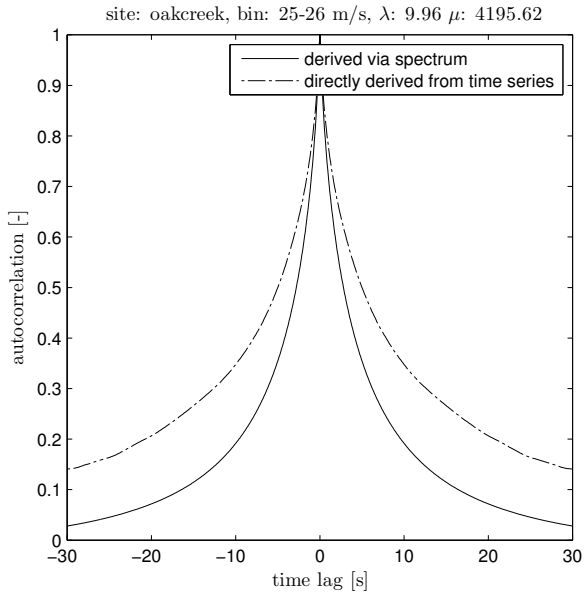
site: oakcreek, bin: 25-26 m/s, λ: 9.96 μ: 4195.62
derived via spectrum
directly derived from time series
autocorrelation [-]
time lag [s]

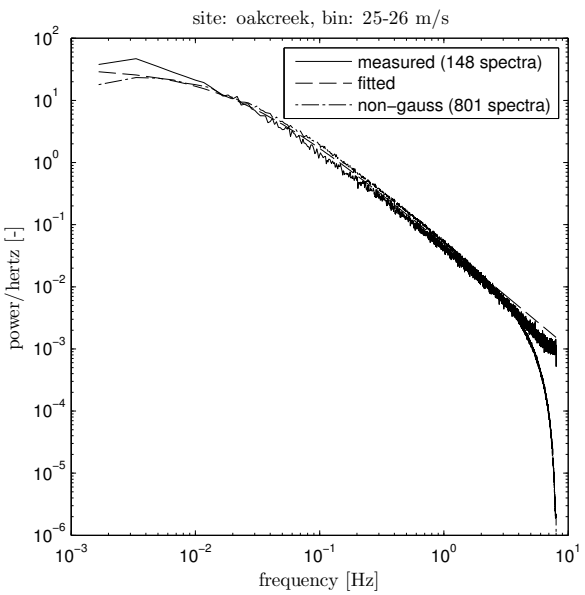
site: oakcreek, bin: 25-26 m/s
measured (148 spectra)
fitted
non−gauss (801 spectra)
power/hertz [-]
frequency [Hz]

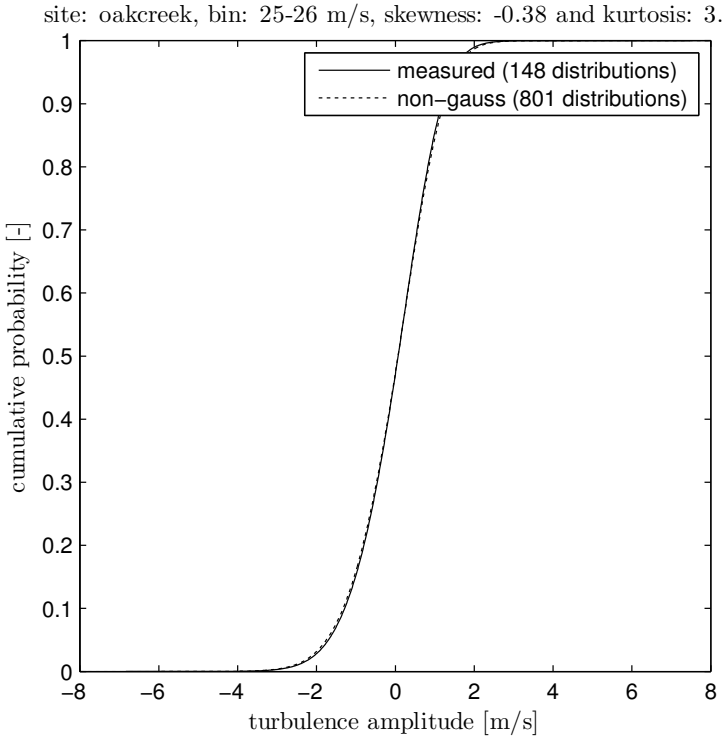
site: oakcreek, bin: 25-26 m/s, skewness: -0.38 and kurtosis: 3.16
measured (148 distributions)
non−gauss (801 distributions)
cumulative probability [-]
turbulence amplitude [m/s]

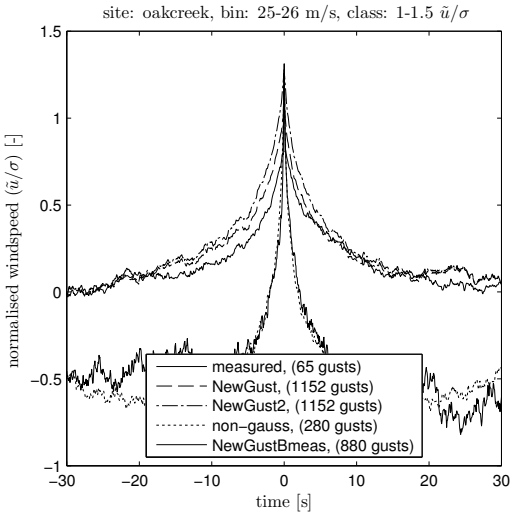
site: oakcreek, bin: 25-26 m/s, class: 1-1.5 $\tilde{u}/\sigma$
normalised windspeed ($\tilde{u}/\sigma$) [-]
time [s]
measured, (65 gusts)
NewGust, (1152 gusts)
NewGust2, (1152 gusts)
non−gauss, (280 gusts)
NewGustBmeas, (880 gusts)

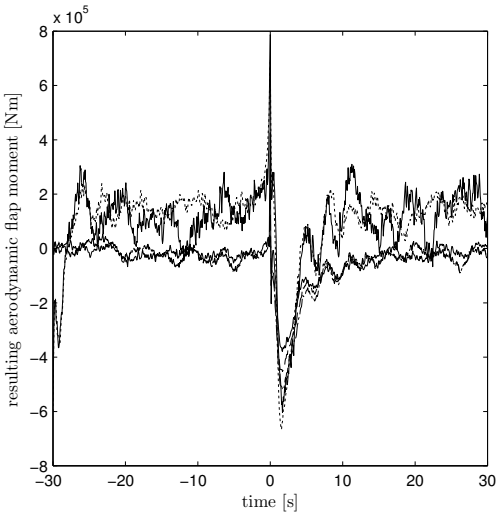
x 10^5
resulting aerodynamic flap moment [Nm]
time [s]

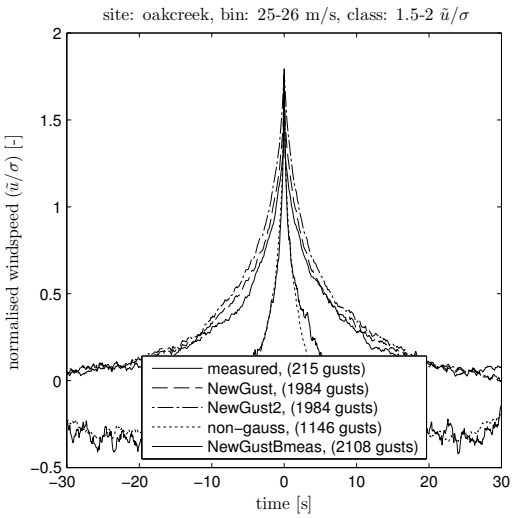
site: oakcreek, bin: 25-26 m/s, class: 1.5-2 $\tilde{u}/\sigma$
normalised windspeed ($\tilde{u}/\sigma$) [-]
time [s]
measured, (215 gusts)
NewGust, (1984 gusts)
NewGust2, (1984 gusts)
non−gauss, (1146 gusts)
NewGustBmeas, (2108 gusts)

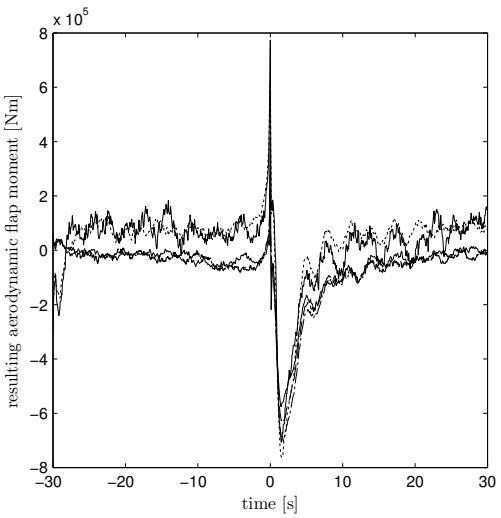
x 10^5
resulting aerodynamic flap moment [Nm]
time [s]

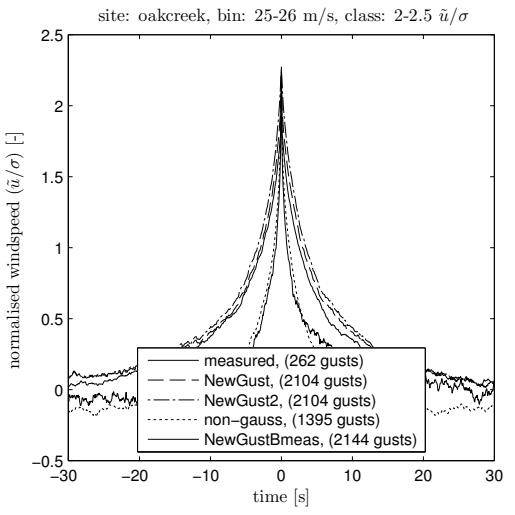
site: oakcreek, bin: 25-26 m/s, class: 2-2.5 $\tilde{u}/\sigma$
normalised windspeed ($\tilde{u}/\sigma$) [-]
time [s]
measured, (262 gusts)
NewGust, (2104 gusts)
NewGust2, (2104 gusts)
non−gauss, (1395 gusts)
NewGustBmeas, (2144 gusts)

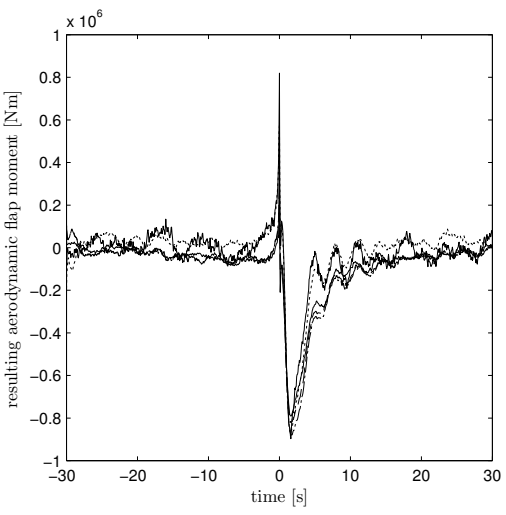
x 10^6
resulting aerodynamic flap moment [Nm]
time [s]

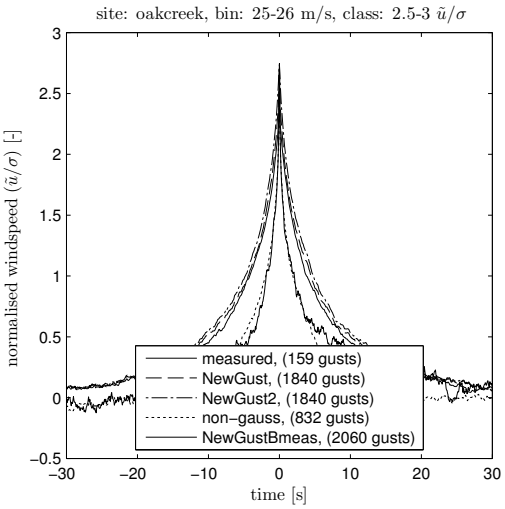
site: oakcreek, bin: 25-26 m/s, class: 2.5-3 $\tilde{u}/\sigma$
normalised windspeed ($\tilde{u}/\sigma$) [-]
time [s]
measured, (159 gusts)
NewGust, (1840 gusts)
NewGust2, (1840 gusts)
non−gauss, (832 gusts)
NewGustBmeas, (2060 gusts)

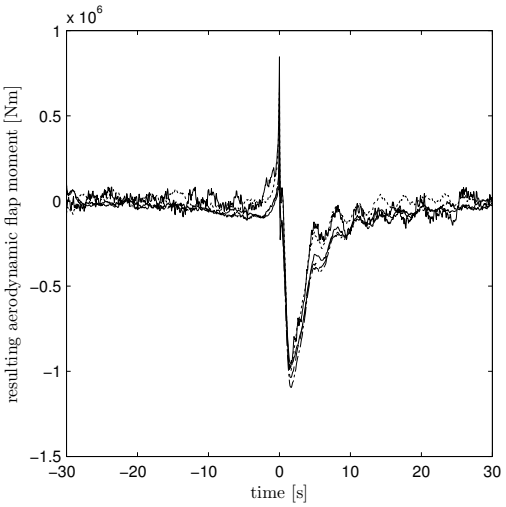
x 10^6
resulting aerodynamic flap moment [Nm]
time [s]

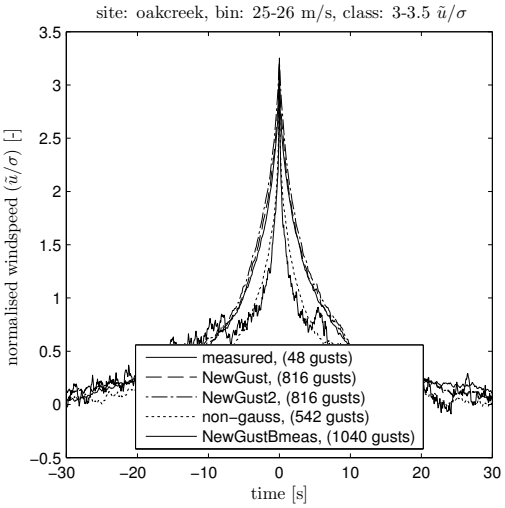
site: oakcreek, bin: 25-26 m/s, class: 3-3.5 $\tilde{u}/\sigma$
normalised windspeed ($\tilde{u}/\sigma$) [-]
time [s]
measured, (48 gusts)
NewGust, (816 gusts)
NewGust2, (816 gusts)
non−gauss, (542 gusts)
NewGustBmeas, (1040 gusts)

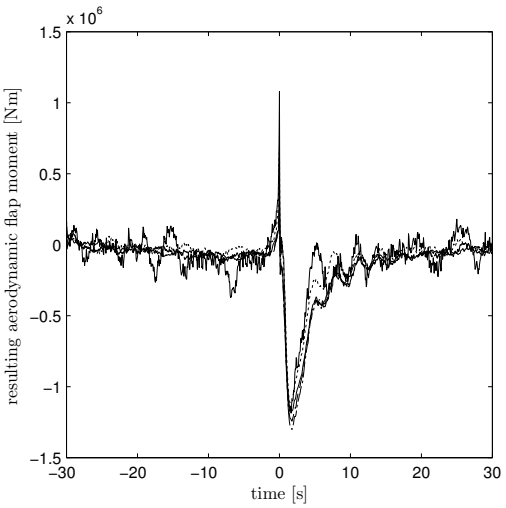
x 10^6
resulting aerodynamic flap moment [Nm]
time [s]

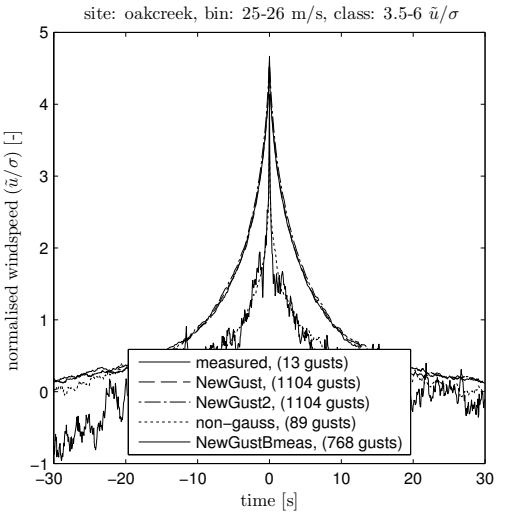
site: oakcreek, bin: 25-26 m/s, class: 3.5-6 $\tilde{u}/\sigma$
normalised windspeed ($\tilde{u}/\sigma$) [-]
time [s]
measured, (13 gusts)
NewGust, (1104 gusts)
NewGust2, (1104 gusts)
non−gauss, (89 gusts)
NewGustBmeas, (768 gusts)

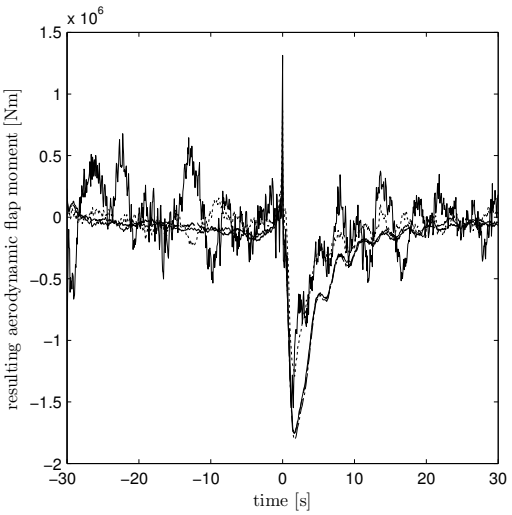
x 10^6
resulting aerodynamic flap moment [Nm]
time [s]

J.3 Results for Horns Rev

$\tilde{u}_n(t_0) \rightarrow$	1-1.5		1.5-2		2-2.5		2.5-3		3-3.5		3.5-6		
$\bar{u} \downarrow$	gust	load	gust	load	gust	load	gust	load	gust	load	gust	load	type
	1.41	0.02	1.31	0.02	1.44	0.01	1.62	0.01	2.32	0.02	5.27	0.04	m,n
0-2	1.56	0.03	1.46	0.02	1.59	0.02	1.78	0.01	2.51	0.02	5.53	0.05	m,n2
	0.00	0.00	0.00	0.00	0.00	0.00	0.00	0.00	0.00	0.00	0.00	0.00	n,n2
	1.05	0.15	1.04	0.14	1.01	0.13	1.10	0.14	1.45	0.19	2.66	0.35	m,n
2-3	1.18	0.16	1.17	0.16	1.13	0.15	1.23	0.16	1.59	0.20	2.86	0.37	m,n2
	0.00	0.00	0.00	0.00	0.00	0.00	0.00	0.00	0.00	0.00	0.00	0.00	n,n2
	1.00	0.32	0.76	0.24	0.84	0.26	0.95	0.29	1.12	0.35	2.32	0.72	m,n
3-4	1.13	0.36	0.86	0.27	0.95	0.30	1.07	0.33	1.25	0.38	2.49	0.77	m,n2
	0.00	0.00	0.00	0.00	0.00	0.00	0.00	0.00	0.00	0.00	0.00	0.00	n,n2
	0.82	0.47	0.78	0.45	0.67	0.39	0.77	0.45	0.89	0.51	1.87	1.08	m,n
4-5	0.93	0.53	0.89	0.52	0.76	0.45	0.87	0.50	1.00	0.58	2.00	1.16	m,n2
	0.00	0.00	0.00	0.00	0.00	0.00	0.00	0.00	0.00	0.00	0.00	0.00	n,n2
	0.76	0.70	0.60	0.56	0.61	0.57	0.69	0.64	0.90	0.83	1.69	1.56	m,n
5-6	0.86	0.80	0.69	0.64	0.70	0.66	0.79	0.73	1.01	0.93	1.82	1.69	m,n2
	0.00	0.00	0.00	0.00	0.00	0.00	0.00	0.00	0.00	0.00	0.00	0.00	n,n2
	0.70	0.95	0.54	0.73	0.50	0.69	0.51	0.70	0.61	0.83	1.27	1.73	m,n
6-7	0.80	1.09	0.62	0.85	0.58	0.80	0.60	0.81	0.69	0.94	1.39	1.89	m,n2
	0.00	0.01	0.00	0.00	0.00	0.00	0.00	0.00	0.00	0.00	0.00	0.00	n,n2
	0.70	1.28	0.50	0.94	0.38	0.73	0.43	0.81	0.50	0.92	0.99	1.84	m,n
7-8	0.79	1.47	0.58	1.10	0.45	0.86	0.51	0.96	0.57	1.06	1.09	2.02	m,n2
	0.00	0.01	0.00	0.01	0.00	0.01	0.00	0.01	0.00	0.01	0.00	0.00	n,n2
	0.63	1.53	0.46	1.14	0.42	1.05	0.42	1.05	0.49	1.19	0.98	2.39	m,n
8-9	0.71	1.75	0.53	1.33	0.49	1.23	0.50	1.23	0.56	1.37	1.08	2.65	m,n2
	0.00	0.01	0.00	0.01	0.00	0.01	0.00	0.01	0.00	0.01	0.00	0.01	n,n2
	0.61	1.89	0.40	1.26	0.34	1.10	0.36	1.14	0.40	1.25	0.89	2.78	m,n
9-10	0.69	2.16	0.46	1.48	0.41	1.31	0.43	1.34	0.46	1.45	0.98	3.06	m,n2
	0.00	0.01	0.00	0.01	0.00	0.01	0.00	0.01	0.00	0.01	0.00	0.01	n,n2
	0.60	2.32	0.40	1.55	0.33	1.32	0.34	1.34	0.38	1.44	0.71	2.74	m,n
10-11	0.68	2.63	0.46	1.82	0.39	1.56	0.41	1.59	0.44	1.68	0.79	3.03	m,n2
	0.00	0.01	0.00	0.01	0.00	0.01	0.00	0.01	0.00	0.01	0.00	0.01	n,n2
	0.53	0.13	0.34	0.36	0.27	0.71	0.31	1.23	0.37	1.71	1.10	3.79	m,n
11-12	0.61	0.18	0.40	0.44	0.33	0.82	0.37	1.37	0.43	1.87	1.20	3.99	m,n2
	0.00	0.00	0.00	0.00	0.00	0.00	0.00	0.00	0.00	0.00	0.00	0.00	n,n2
	0.53	0.38	0.31	0.23	0.24	0.18	0.26	0.20	0.31	0.24	0.76	0.58	m,n
12-13	0.59	0.43	0.37	0.27	0.29	0.22	0.32	0.24	0.37	0.28	0.84	0.65	m,n2
	0.00	0.00	0.00	0.00	0.00	0.00	0.00	0.00	0.00	0.00	0.00	0.00	n,n2
	0.52	0.26	0.32	0.17	0.24	0.13	0.24	0.13	0.31	0.17	0.64	0.35	m,n
13-14	0.58	0.29	0.38	0.20	0.28	0.15	0.29	0.16	0.36	0.20	0.71	0.39	m,n2
	0.00	0.00	0.00	0.00	0.00	0.00	0.00	0.00	0.00	0.00	0.00	0.00	n,n2
	0.52	0.20	0.28	0.11	0.20	0.08	0.20	0.08	0.22	0.09	0.55	0.23	m,n
14-15	0.59	0.23	0.33	0.13	0.25	0.10	0.24	0.10	0.27	0.11	0.62	0.26	m,n2
	0.00	0.00	0.00	0.00	0.00	0.00	0.00	0.00	0.00	0.00	0.00	0.00	n,n2

$\tilde{u}_n(t_0) \rightarrow$	1-1.5		1.5-2		2-2.5		2.5-3		3-3.5		3.5-6		
$\bar{u} \downarrow$	gust	load	gust	load	gust	load	gust	load	gust	load	gust	load	type
	0.48	0.14	0.27	0.08	0.15	0.05	0.17	0.06	0.18	0.06	0.53	0.17	m,n
15-16	0.54	0.16	0.32	0.10	0.19	0.06	0.22	0.07	0.23	0.08	0.60	0.20	m,n2
	0.00	0.00	0.00	0.00	0.00	0.00	0.00	0.00	0.00	0.00	0.00	0.00	n,n2
	0.47	0.11	0.23	0.06	0.13	0.03	0.13	0.03	0.14	0.04	0.46	0.13	m,n
16-17	0.53	0.13	0.27	0.07	0.17	0.04	0.16	0.04	0.18	0.05	0.52	0.14	m,n2
	0.00	0.00	0.00	0.00	0.00	0.00	0.00	0.00	0.00	0.00	0.00	0.00	n,n2
	0.53	0.11	0.22	0.04	0.13	0.03	0.10	0.02	0.13	0.03	0.39	0.09	m,n
17-18	0.59	0.12	0.26	0.05	0.17	0.03	0.13	0.03	0.17	0.04	0.44	0.10	m,n2
	0.00	0.00	0.00	0.00	0.00	0.00	0.00	0.00	0.00	0.00	0.00	0.00	n,n2
	0.43	0.07	0.19	0.03	0.11	0.02	0.06	0.01	0.09	0.02	0.19	0.05	m,n
18-19	0.48	0.08	0.23	0.04	0.14	0.02	0.09	0.02	0.12	0.03	0.23	0.06	m,n2
	0.00	0.00	0.00	0.00	0.00	0.00	0.00	0.00	0.00	0.00	0.00	0.00	n,n2
	0.60	0.09	0.17	0.03	0.11	0.02	0.08	0.01	0.09	0.02	0.24	0.05	m,n
19-20	0.66	0.09	0.21	0.03	0.14	0.02	0.10	0.02	0.12	0.02	0.28	0.06	m,n2
	0.00	0.00	0.00	0.00	0.00	0.00	0.00	0.00	0.00	0.00	0.00	0.00	n,n2
	0.72	0.09	0.46	0.06	0.33	0.05	0.31	0.04	0.46	0.07	0.82	0.13	m,n
20-21	0.81	0.10	0.54	0.07	0.39	0.05	0.37	0.05	0.53	0.08	0.91	0.14	m,n2
	0.00	0.00	0.00	0.00	0.00	0.00	0.00	0.00	0.00	0.00	0.00	0.00	n,n2
	0.74	0.07	0.42	0.03	0.30	0.02	0.29	0.02	0.49	0.04	1.13	0.10	m,n
21-30	0.83	0.07	0.49	0.04	0.36	0.02	0.35	0.02	0.56	0.04	1.23	0.11	m,n2
	0.00	0.00	0.00	0.00	0.00	0.00	0.00	0.00	0.00	0.00	0.00	0.00	n,n2

Table J.3: mse between gusts for Hornsrev, 'm' denotes 'measured', 'n' denotes '*NewGust*' and 'n2' denotes the second *NewGust* equation

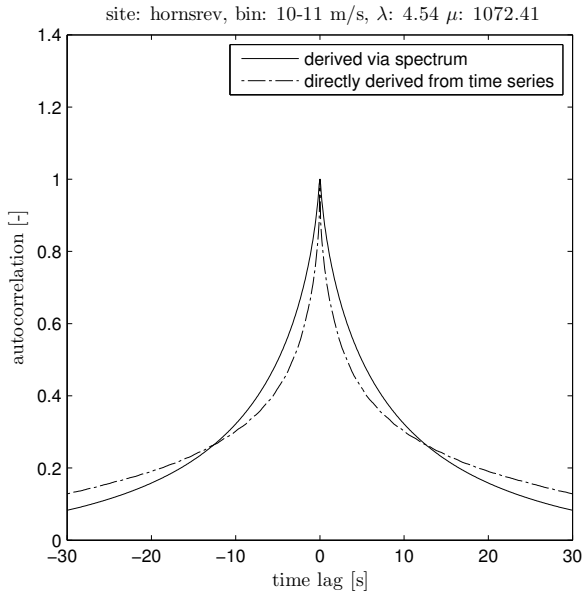
site: hornsrev, bin: 10-11 m/s, λ: 4.54 μ: 1072.41
derived via spectrum
directly derived from time series
autocorrelation [-]
time lag [s]

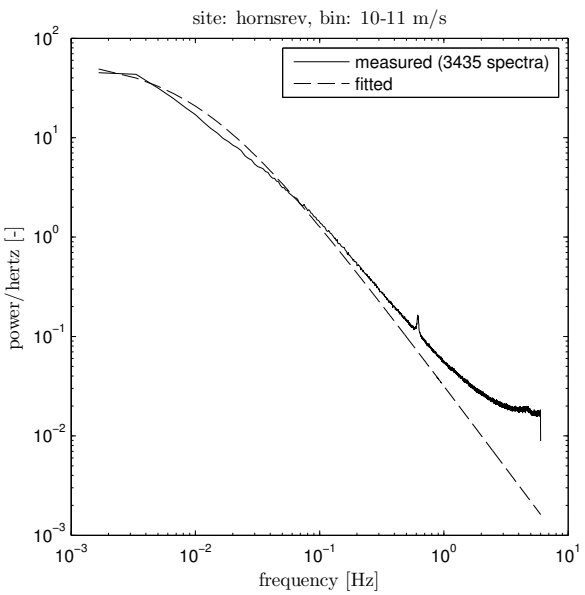
site: hornsrev, bin: 10-11 m/s
measured (3435 spectra)
fitted
power/hertz [-]
frequency [Hz]

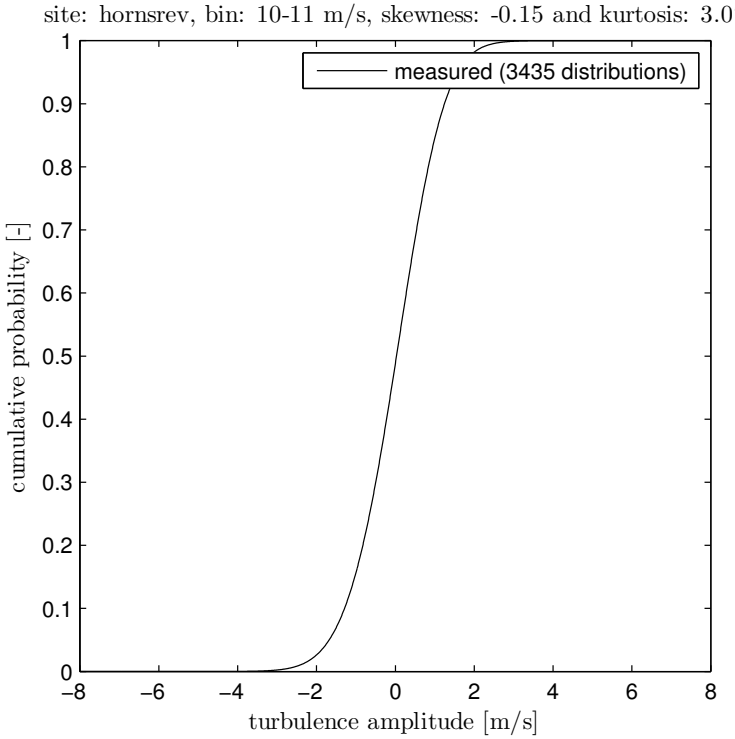
site: hornsrev, bin: 10-11 m/s, skewness: -0.15 and kurtosis: 3.07
measured (3435 distributions)
cumulative probability [-]
turbulence amplitude [m/s]

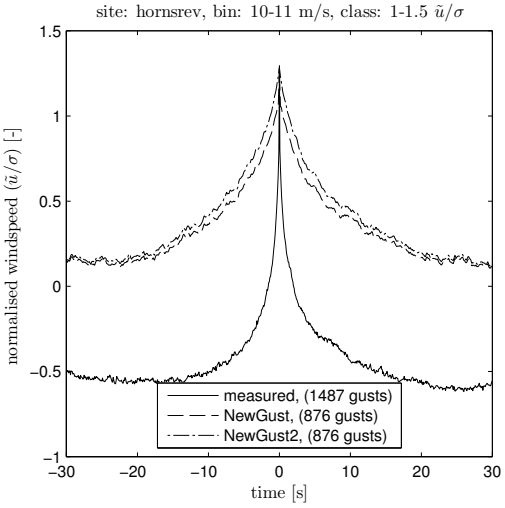
site: hornsrev, bin: 10-11 m/s, class: 1-1.5 $\tilde{u}/\sigma$
normalised windspeed $(\tilde{u}/\sigma)$ [-]
time [s]
measured, (1487 gusts)
NewGust, (876 gusts)
NewGust2, (876 gusts)

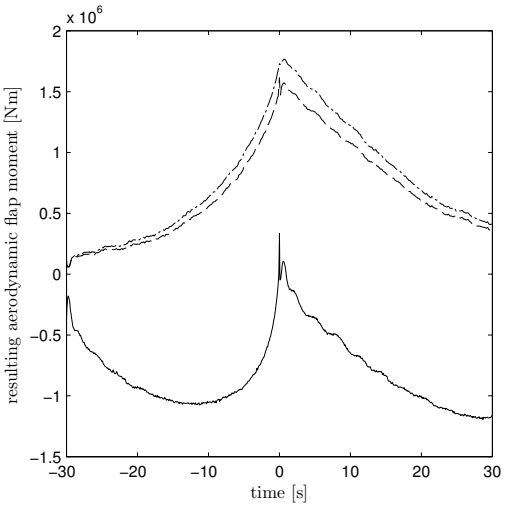
x 10^6
resulting aerodynamic flap moment [Nm]
time [s]

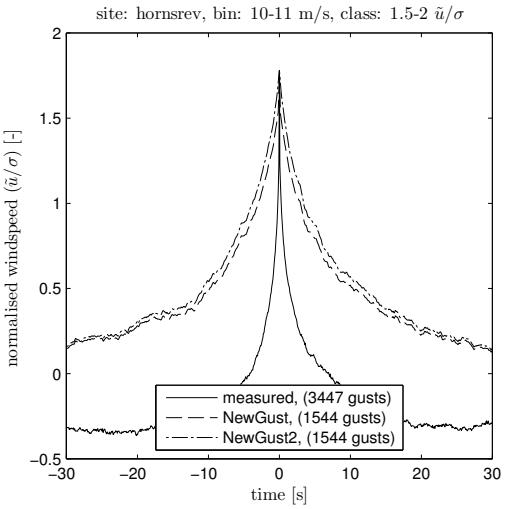
site: hornsrev, bin: 10-11 m/s, class: 1.5-2 $\tilde{u}/\sigma$
normalised windspeed $(\tilde{u}/\sigma)$ [-]
time [s]
measured, (3447 gusts)
NewGust, (1544 gusts)
NewGust2, (1544 gusts)

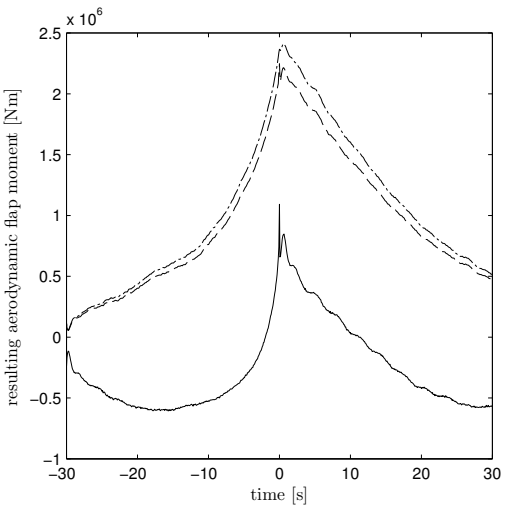
x 10^6
resulting aerodynamic flap moment [Nm]
time [s]

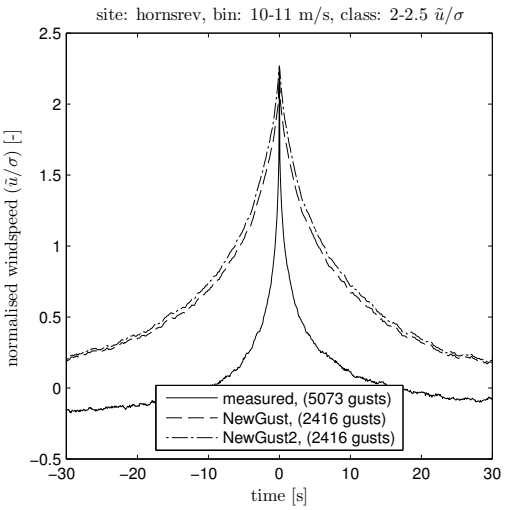
site: hornsrev, bin: 10-11 m/s, class: 2-2.5 $\tilde{u}/\sigma$
normalised windspeed $(\tilde{u}/\sigma)$ [-]
time [s]
measured, (5073 gusts)
NewGust, (2416 gusts)
NewGust2, (2416 gusts)

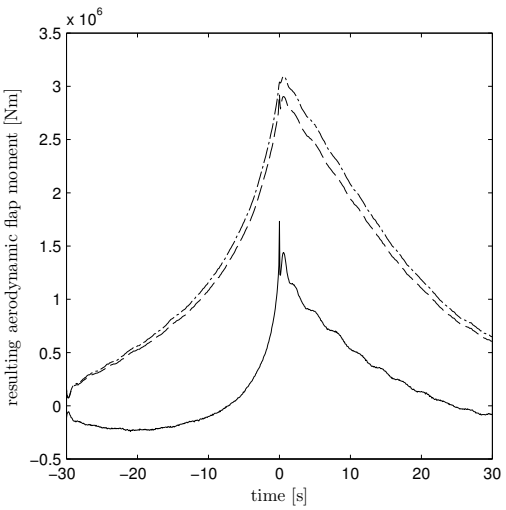
x 10^6
resulting aerodynamic flap moment [Nm]
time [s]

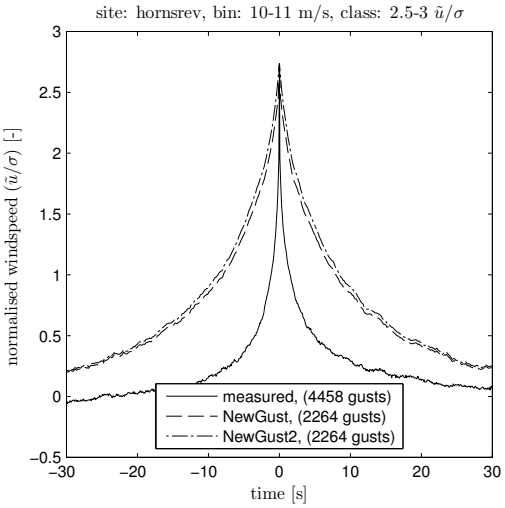
site: hornsrev, bin: 10-11 m/s, class: 2.5-3 $\tilde{u}/\sigma$
normalised windspeed ($\tilde{u}/\sigma$) [-]
time [s]
measured, (4458 gusts)
NewGust, (2264 gusts)
NewGust2, (2264 gusts)

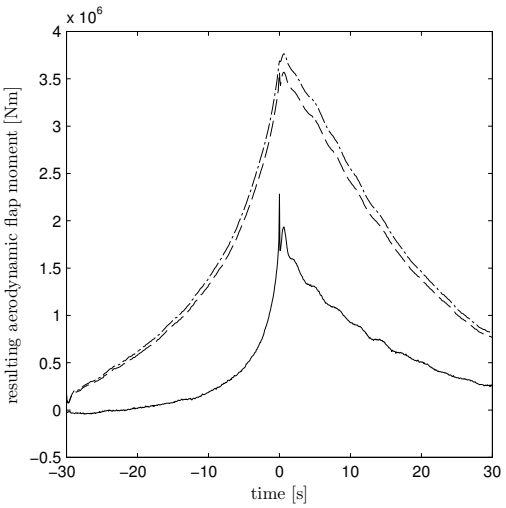
x 10^6
resulting aerodynamic flap moment [Nm]
time [s]

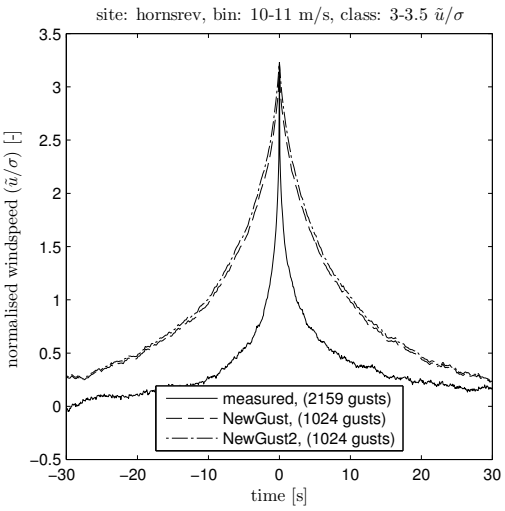
site: hornsrev, bin: 10-11 m/s, class: 3-3.5 $\tilde{u}/\sigma$
normalised windspeed ($\tilde{u}/\sigma$) [-]
time [s]
measured, (2159 gusts)
NewGust, (1024 gusts)
NewGust2, (1024 gusts)

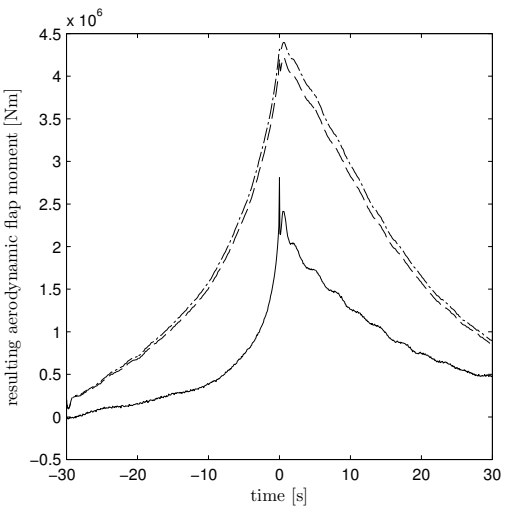
x 10^6
resulting aerodynamic flap moment [Nm]
time [s]

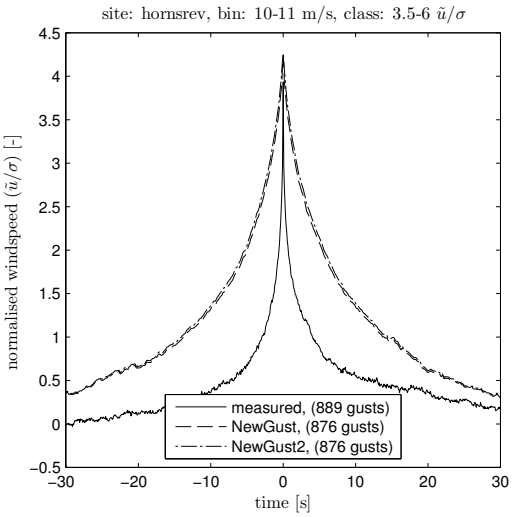
site: hornsrev, bin: 10-11 m/s, class: 3.5-6 $\tilde{u}/\sigma$
normalised windspeed ($\tilde{u}/\sigma$) [-]
time [s]
measured, (889 gusts)
NewGust, (876 gusts)
NewGust2, (876 gusts)

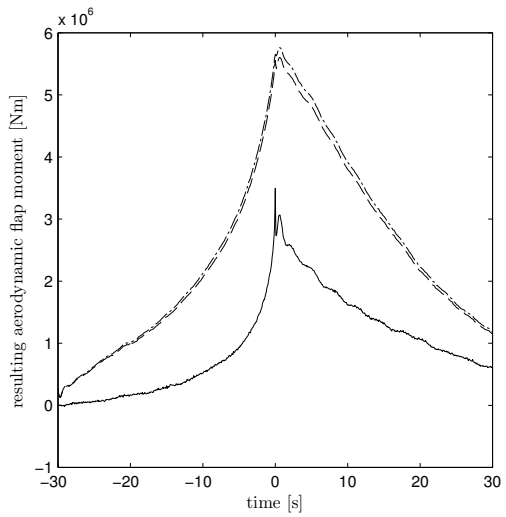
x 10^6
resulting aerodynamic flap moment [Nm]
time [s]

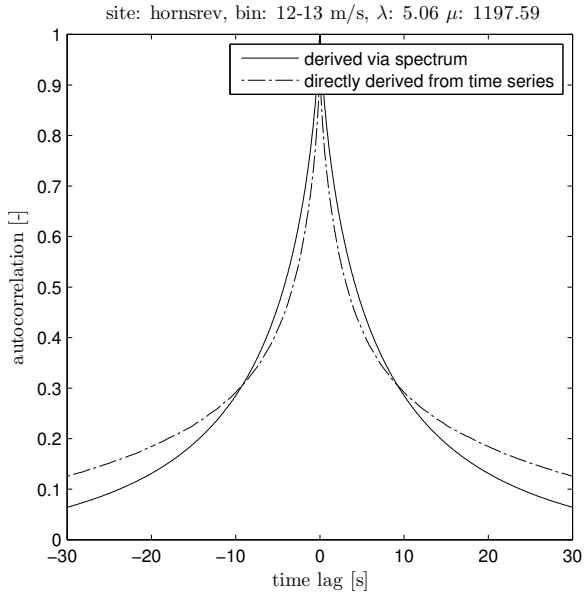
site: hornsrev, bin: 12-13 m/s, λ: 5.06 μ: 1197.59
derived via spectrum
directly derived from time series
autocorrelation [-]
time lag [s]

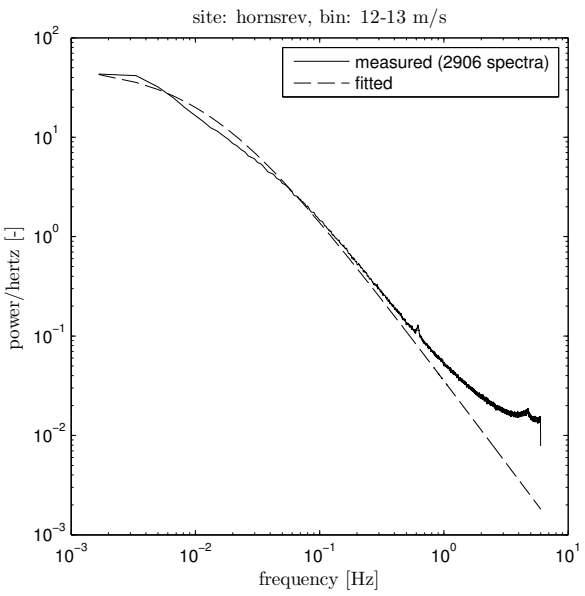
site: hornsrev, bin: 12-13 m/s
measured (2906 spectra)
fitted
power/hertz [-]
frequency [Hz]

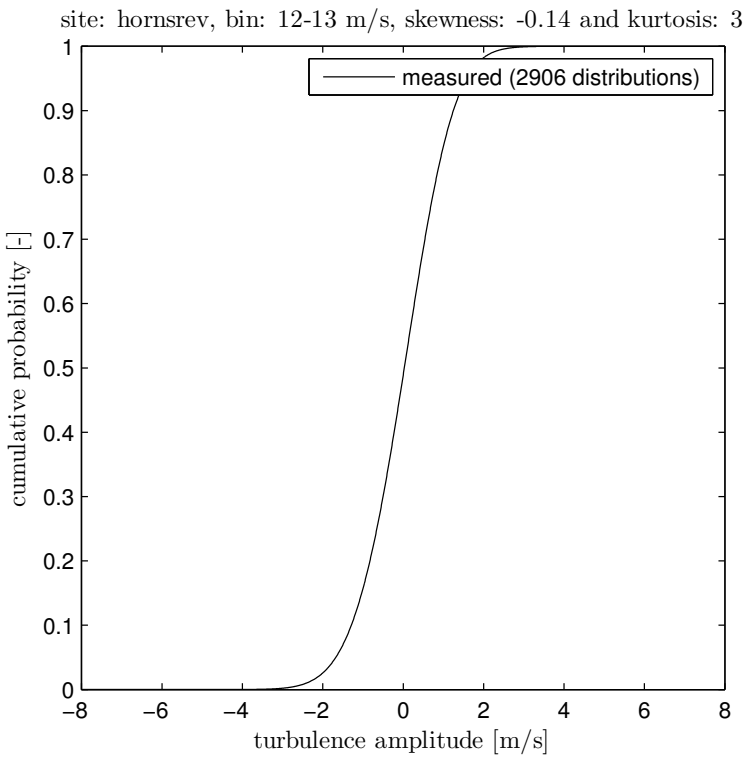
site: hornsrev, bin: 12-13 m/s, skewness: -0.14 and kurtosis: 3
measured (2906 distributions)
cumulative probability [-]
turbulence amplitude [m/s]

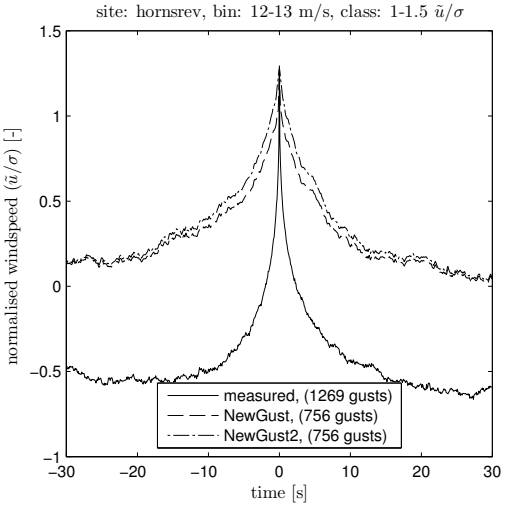
site: hornsrev, bin: 12-13 m/s, class: 1-1.5 $\tilde{u}/\sigma$
normalised windspeed $(\tilde{u}/\sigma)$ [-]
time [s]
measured, (1269 gusts)
NewGust, (756 gusts)
NewGust2, (756 gusts)

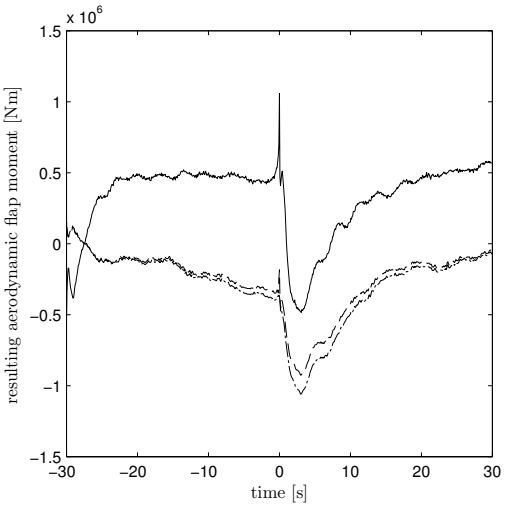
x 10^6
resulting aerodynamic flap moment [Nm]
time [s]

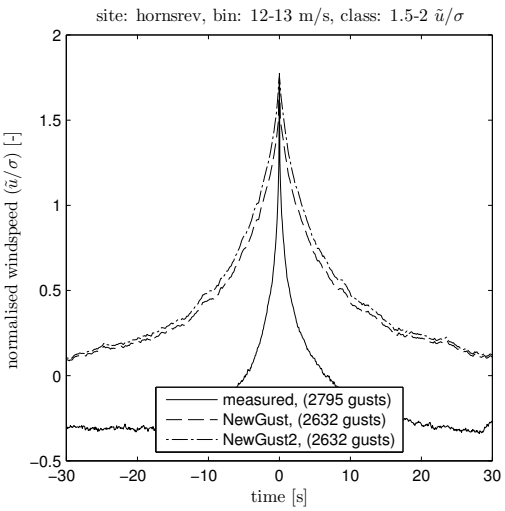
site: hornsrev, bin: 12-13 m/s, class: 1.5-2 $\tilde{u}/\sigma$
normalised windspeed $(\tilde{u}/\sigma)$ [-]
time [s]
measured, (2795 gusts)
NewGust, (2632 gusts)
NewGust2, (2632 gusts)

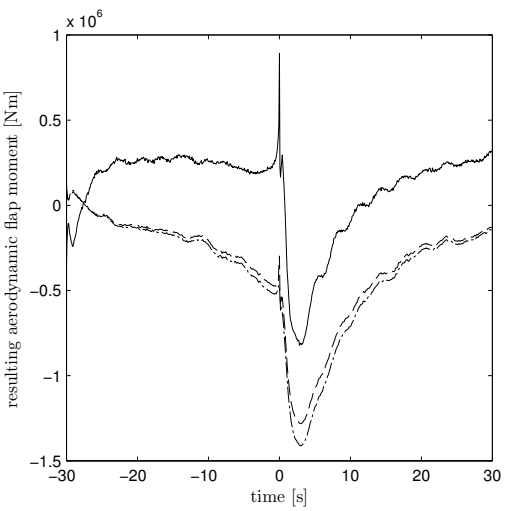
x 10^6
resulting aerodynamic flap moment [Nm]
time [s]

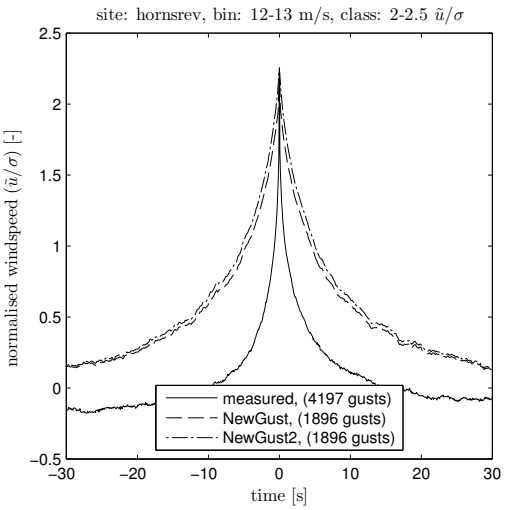
site: hornsrev, bin: 12-13 m/s, class: 2-2.5 $\tilde{u}/\sigma$
normalised windspeed $(\tilde{u}/\sigma)$ [-]
time [s]
measured, (4197 gusts)
NewGust, (1896 gusts)
NewGust2, (1896 gusts)

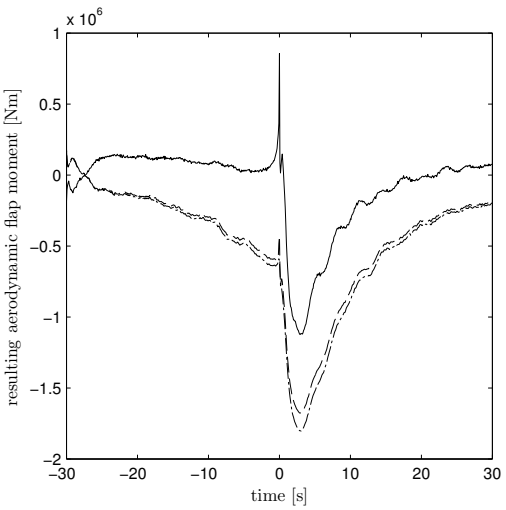
x 10^6
resulting aerodynamic flap moment [Nm]
time [s]

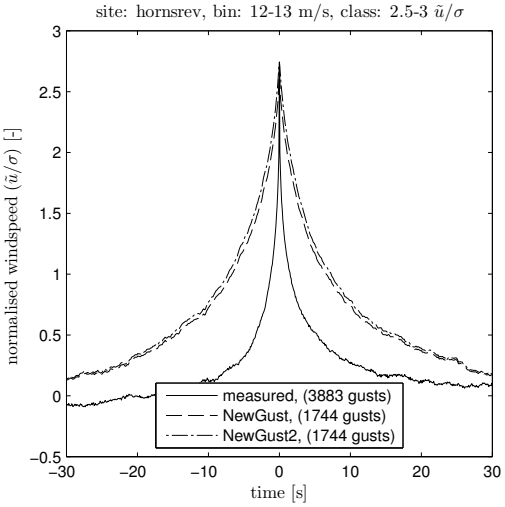
site: hornsrev, bin: 12-13 m/s, class: 2.5-3 $\tilde{u}/\sigma$
normalised windspeed ($\tilde{u}/\sigma$) [-]
time [s]
measured, (3883 gusts)
NewGust, (1744 gusts)
NewGust2, (1744 gusts)

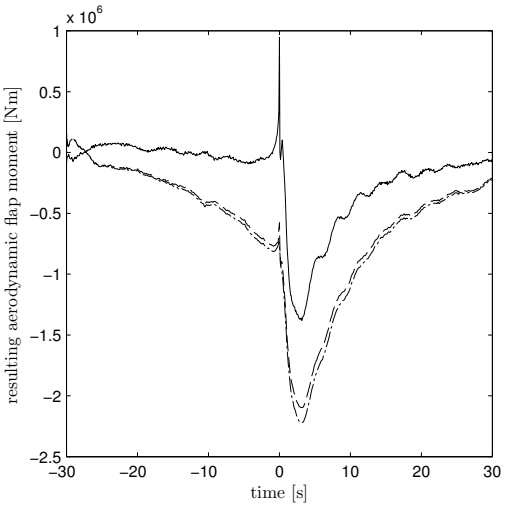
x 10^6
resulting aerodynamic flap moment [Nm]
time [s]

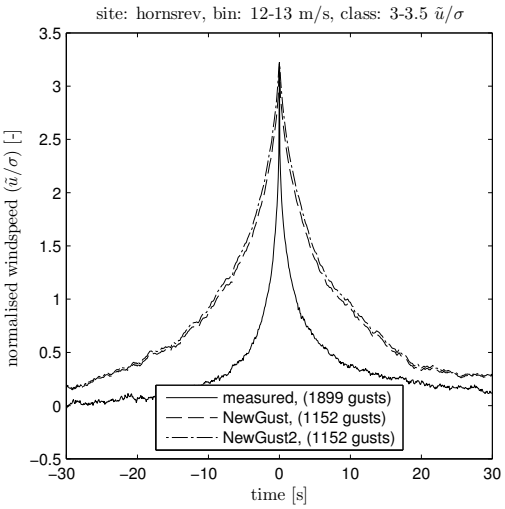
site: hornsrev, bin: 12-13 m/s, class: 3-3.5 $\tilde{u}/\sigma$
normalised windspeed ($\tilde{u}/\sigma$) [-]
time [s]
measured, (1899 gusts)
NewGust, (1152 gusts)
NewGust2, (1152 gusts)

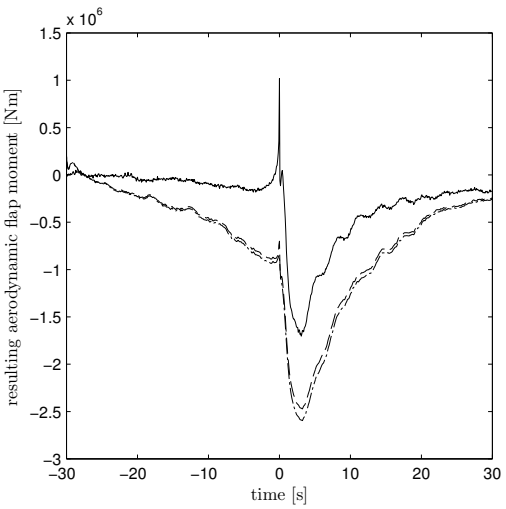
x 10^6
resulting aerodynamic flap moment [Nm]
time [s]

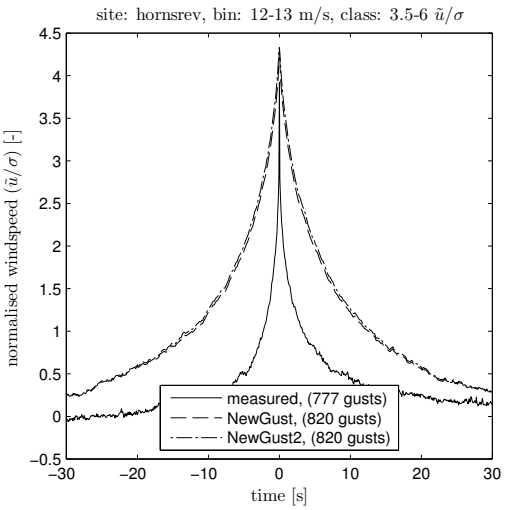
site: hornsrev, bin: 12-13 m/s, class: 3.5-6 $\tilde{u}/\sigma$
normalised windspeed ($\tilde{u}/\sigma$) [-]
time [s]
measured, (777 gusts)
NewGust, (820 gusts)
NewGust2, (820 gusts)

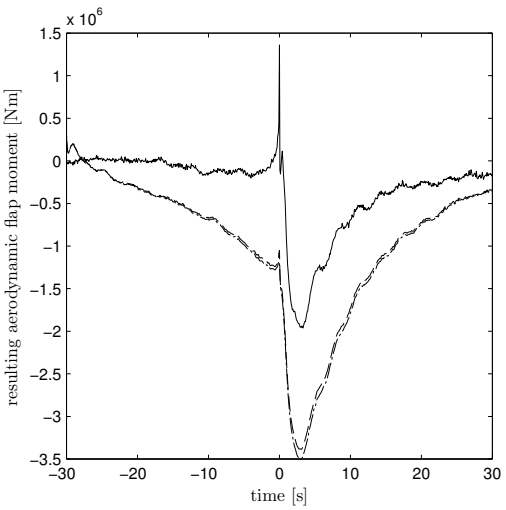
x 10^6
resulting aerodynamic flap moment [Nm]
time [s]

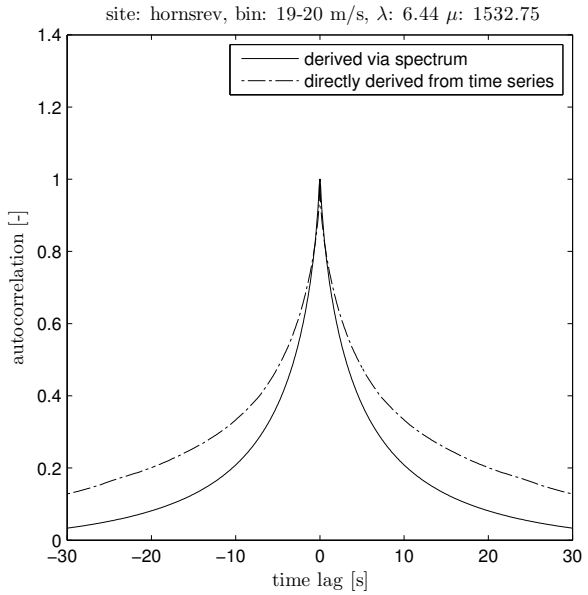
site: hornsrev, bin: 19-20 m/s, λ: 6.44 μ: 1532.75
derived via spectrum
directly derived from time series
autocorrelation [-]
time lag [s]

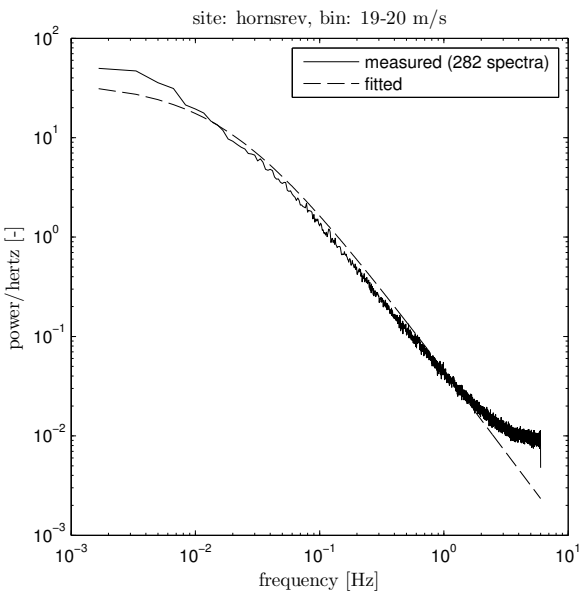
site: hornsrev, bin: 19-20 m/s
measured (282 spectra)
fitted
power/hertz [-]
frequency [Hz]

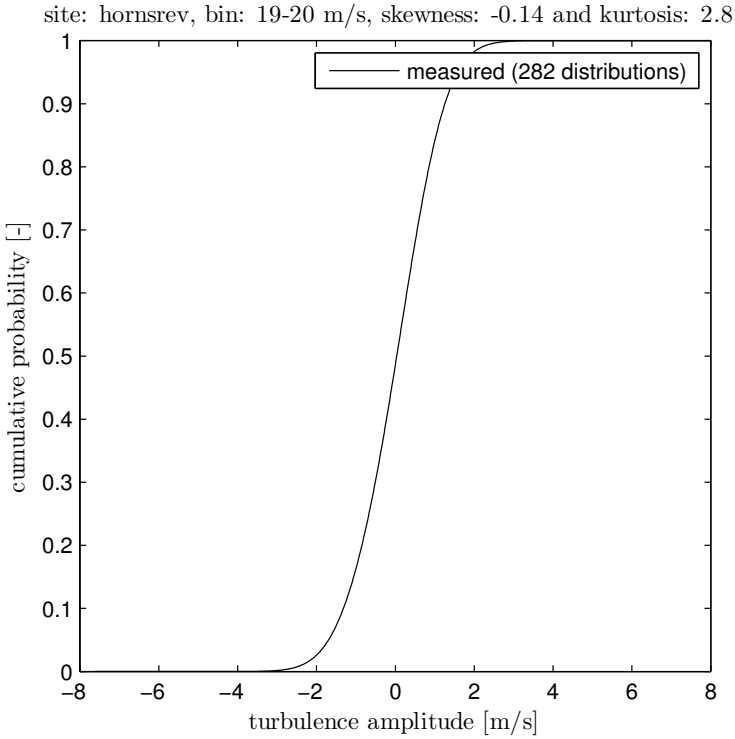
site: hornsrev, bin: 19-20 m/s, skewness: -0.14 and kurtosis: 2.87
measured (282 distributions)
cumulative probability [-]
turbulence amplitude [m/s]

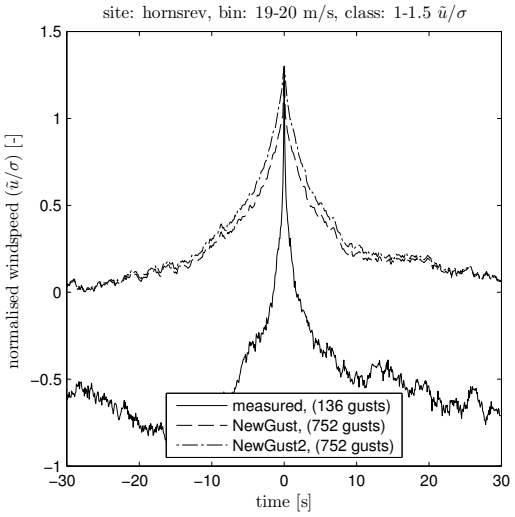
site: hornsrev, bin: 19-20 m/s, class: 1-1.5 $\tilde{u}/\sigma$
normalised windspeed ($\tilde{u}/\sigma$) [-]
time [s]
measured, (136 gusts)
NewGust, (752 gusts)
NewGust2, (752 gusts)

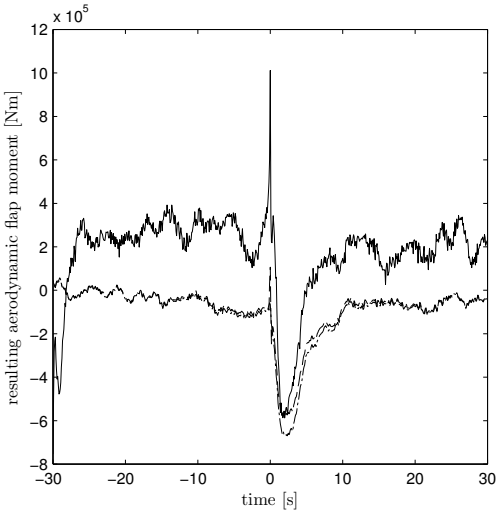
x 10^5
resulting aerodynamic flap moment [Nm]
time [s]

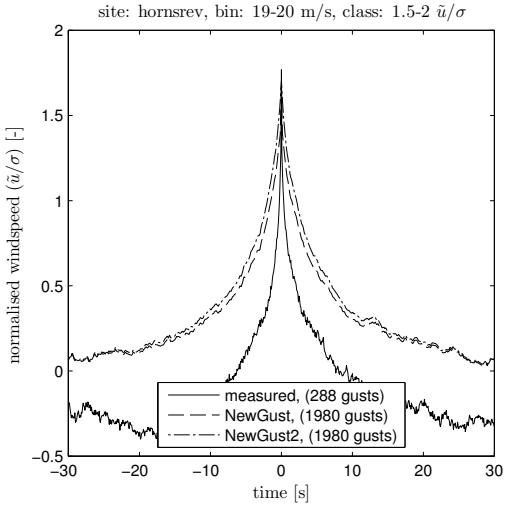
site: hornsrev, bin: 19-20 m/s, class: 1.5-2 $\tilde{u}/\sigma$
normalised windspeed ($\tilde{u}/\sigma$) [-]
time [s]
measured, (288 gusts)
NewGust, (1980 gusts)
NewGust2, (1980 gusts)

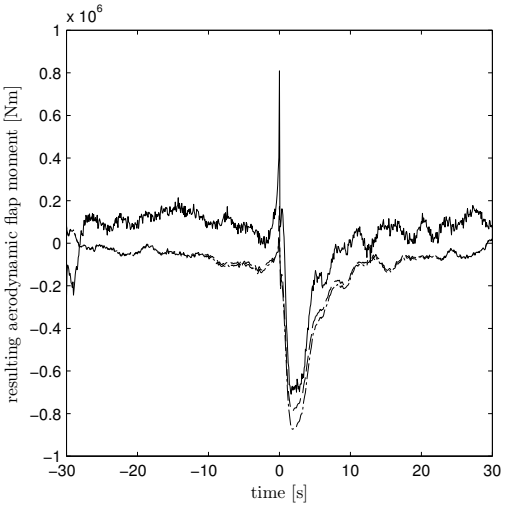
x 10^6
resulting aerodynamic flap moment [Nm]
time [s]

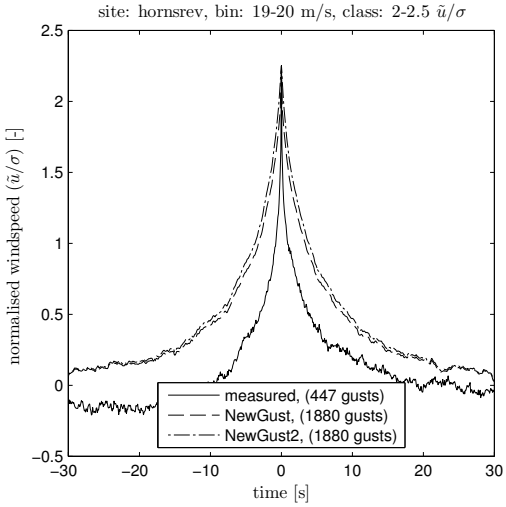
site: hornsrev, bin: 19-20 m/s, class: 2-2.5 $\tilde{u}/\sigma$
normalised windspeed ($\tilde{u}/\sigma$) [-]
time [s]
measured, (447 gusts)
NewGust, (1880 gusts)
NewGust2, (1880 gusts)

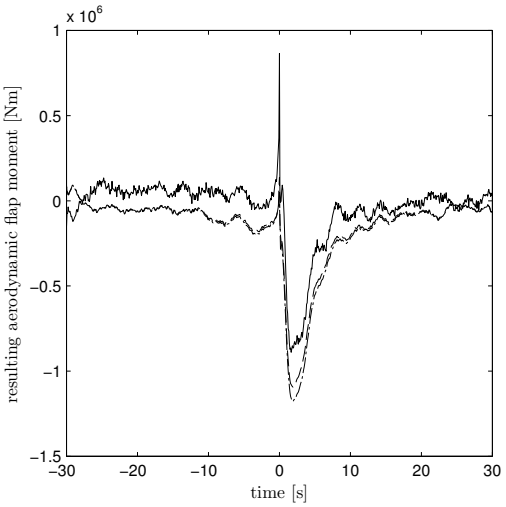
x 10^6
resulting aerodynamic flap moment [Nm]
time [s]

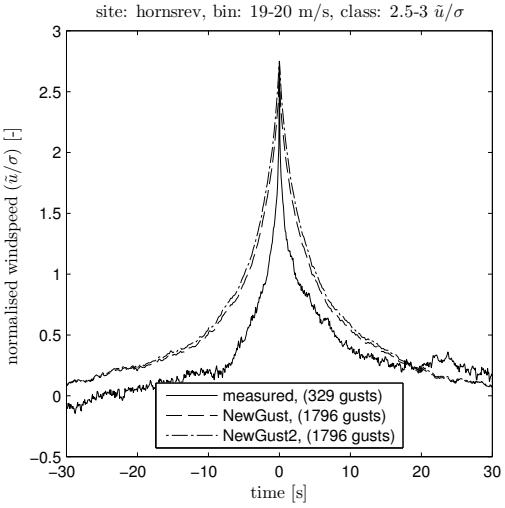
site: hornsrev, bin: 19-20 m/s, class: 2.5-3 $\tilde{u}/\sigma$
normalised windspeed ($\tilde{u}/\sigma$) [-]
time [s]
measured, (329 gusts)
NewGust, (1796 gusts)
NewGust2, (1796 gusts)

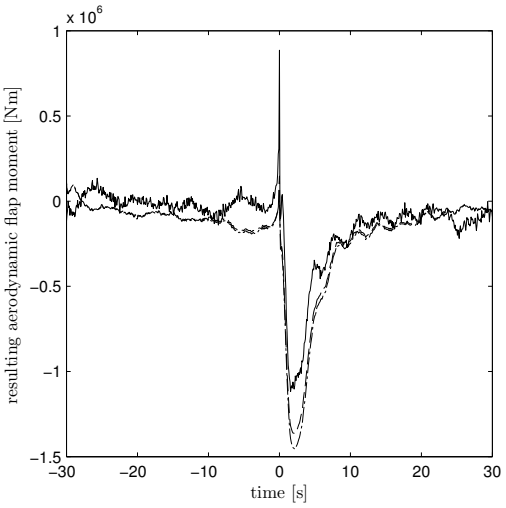
x 10^6
resulting aerodynamic flap moment [Nm]
time [s]

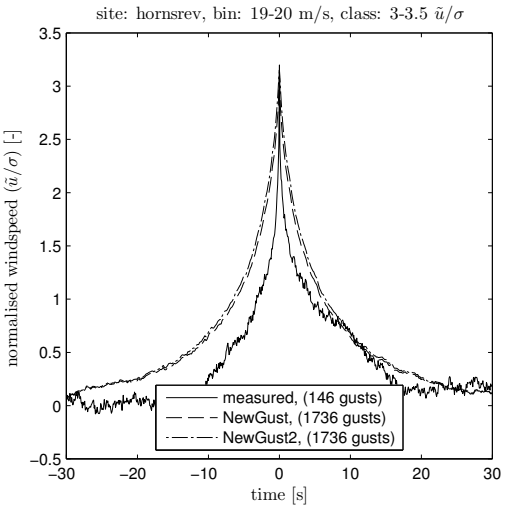
site: hornsrev, bin: 19-20 m/s, class: 3-3.5 $\tilde{u}/\sigma$
normalised windspeed ($\tilde{u}/\sigma$) [-]
time [s]
measured, (146 gusts)
NewGust, (1736 gusts)
NewGust2, (1736 gusts)

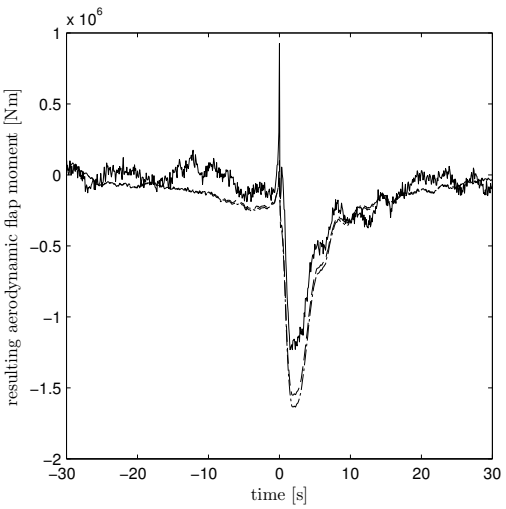
x 10^6
resulting aerodynamic flap moment [Nm]
time [s]

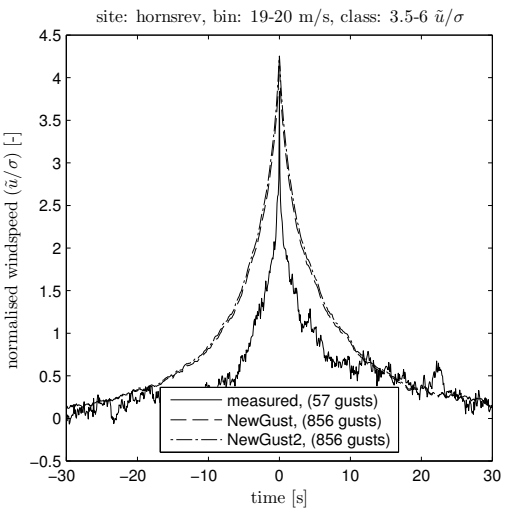
site: hornsrev, bin: 19-20 m/s, class: 3.5-6 $\tilde{u}/\sigma$
normalised windspeed ($\tilde{u}/\sigma$) [-]
time [s]
measured, (57 gusts)
NewGust, (856 gusts)
NewGust2, (856 gusts)

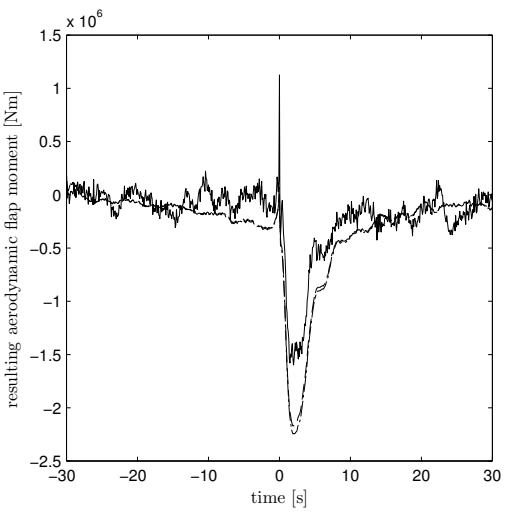
x 10^6
resulting aerodynamic flap moment [Nm]
time [s]

Appendix K

Graphs of extreme gusts for each site

K.1 Results for Toboel

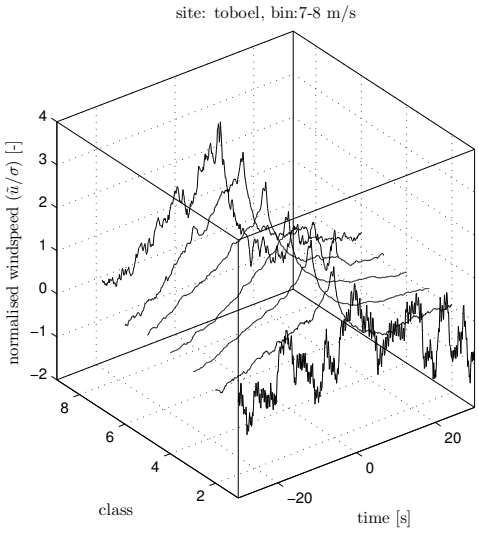
site: toboel, bin:7-8 m/s
normalised windspeed ($\tilde{u}/\sigma$) [-]
class
time [s]

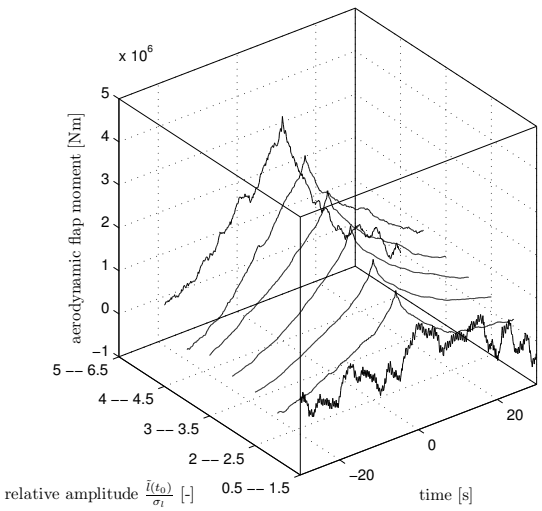
x 10^6
aerodynamic flap moment [Nm]
relative amplitude $\frac{\tilde{l}(t_0)}{\sigma_l}$ [-]
time [s]

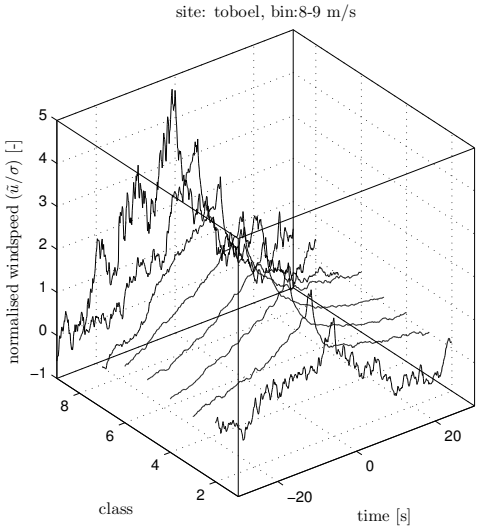
site: toboel, bin:8-9 m/s
normalised windspeed ($\tilde{u}/\sigma$) [-]
class
time [s]

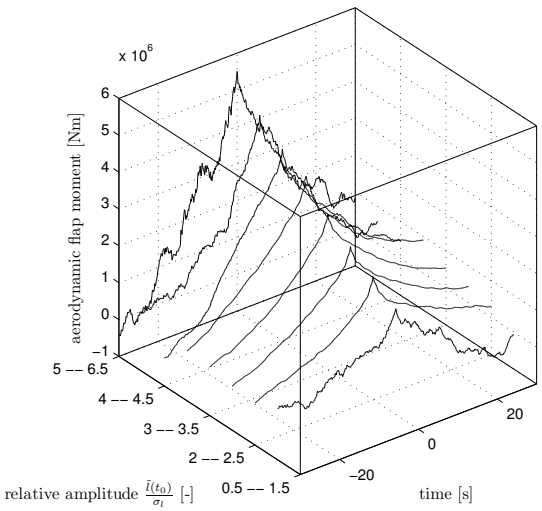
x 10^6
aerodynamic flap moment [Nm]
relative amplitude $\frac{\tilde{l}(t_0)}{\sigma_l}$ [-]
time [s]

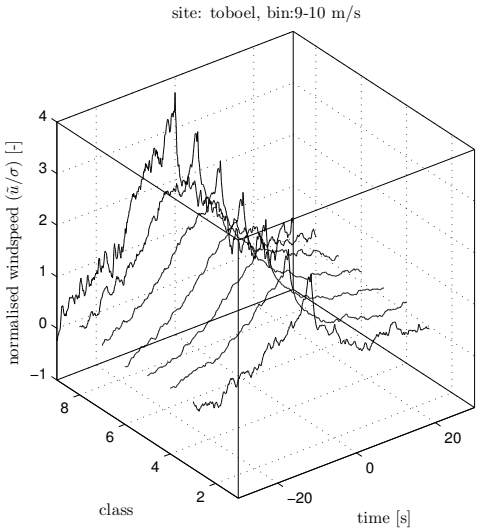
site: toboel, bin:9-10 m/s
normalised windspeed ($\tilde{u}/\sigma$) [-]
class
time [s]

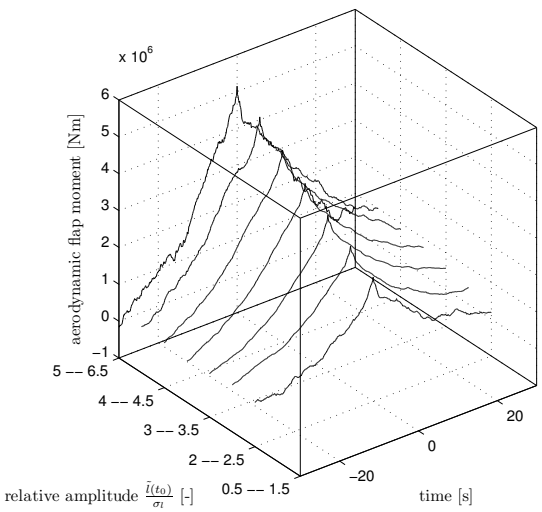
x 10^6
aerodynamic flap moment [Nm]
relative amplitude $\frac{\tilde{l}(t_0)}{\sigma_l}$ [-]
time [s]

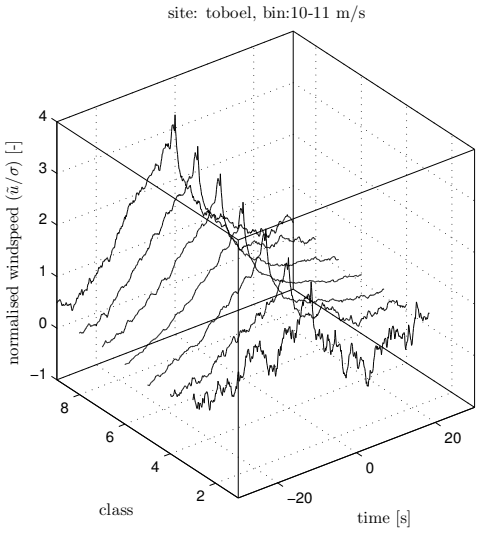
site: toboel, bin:10-11 m/s
normalised windspeed $(\tilde{u}/\sigma)$ [-]
class
time [s]

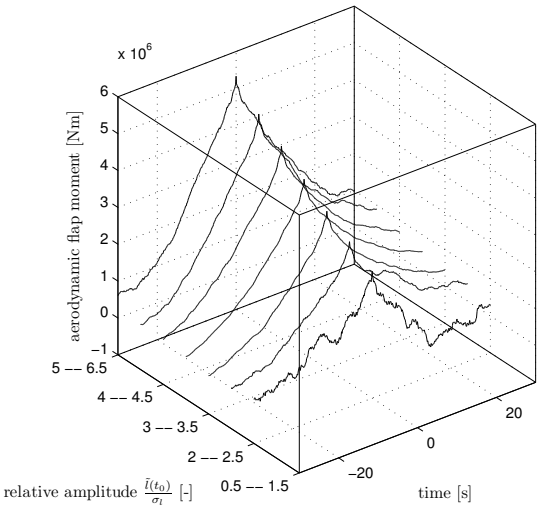
x 10^6
aerodynamic flap moment [Nm]
relative amplitude $\frac{\tilde{l}(t_0)}{\sigma_l}$ [-]
time [s]

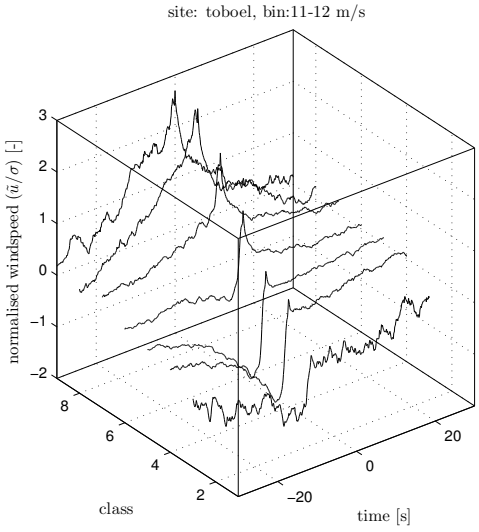
site: toboel, bin:11-12 m/s
normalised windspeed $(\tilde{u}/\sigma)$ [-]
class
time [s]

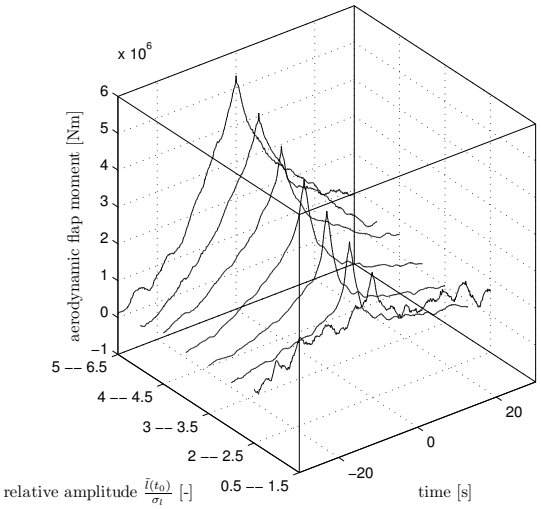
x 10^6
aerodynamic flap moment [Nm]
relative amplitude $\frac{\tilde{l}(t_0)}{\sigma_l}$ [-]
time [s]

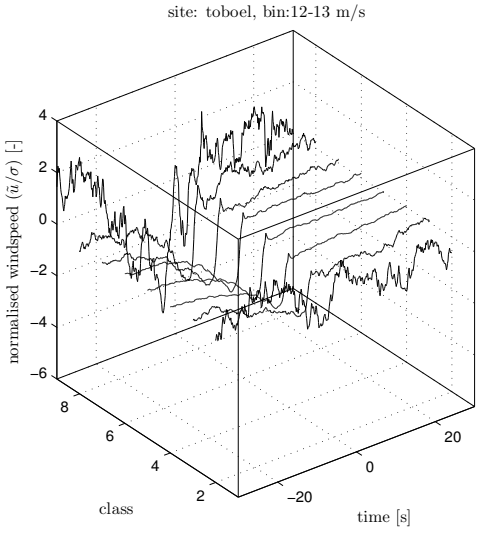
site: toboel, bin:12-13 m/s
normalised windspeed $(\tilde{u}/\sigma)$ [-]
class
time [s]

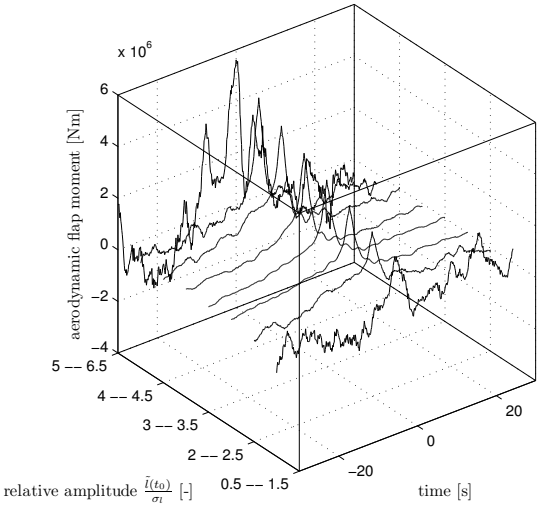
x 10^6
aerodynamic flap moment [Nm]
relative amplitude $\frac{\tilde{l}(t_0)}{\sigma_l}$ [-]
time [s]

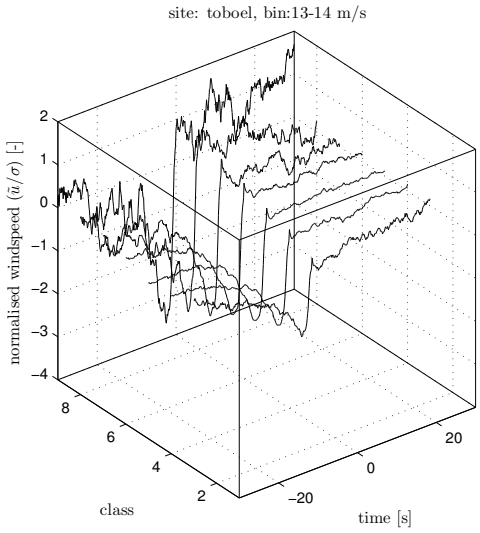
site: toboel, bin:13-14 m/s
normalised windspeed ($\tilde{u}/\sigma$) [-]
class
time [s]

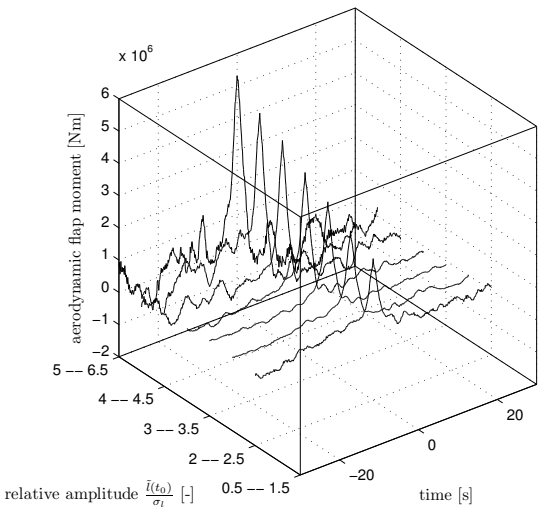
x 10^6
aerodynamic flap moment [Nm]
relative amplitude $\frac{\tilde{l}(t_0)}{\sigma_l}$ [-]
time [s]

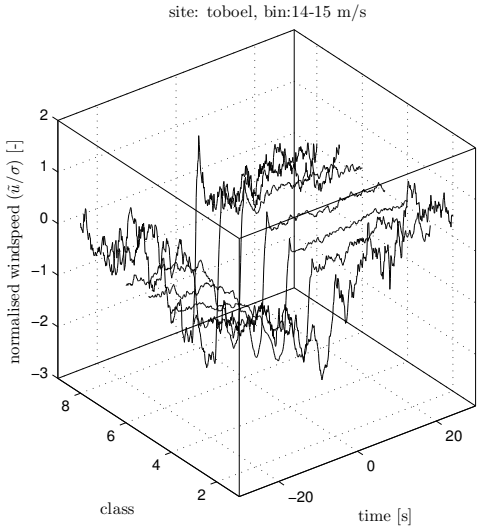
site: toboel, bin:14-15 m/s
normalised windspeed ($\tilde{u}/\sigma$) [-]
class
time [s]

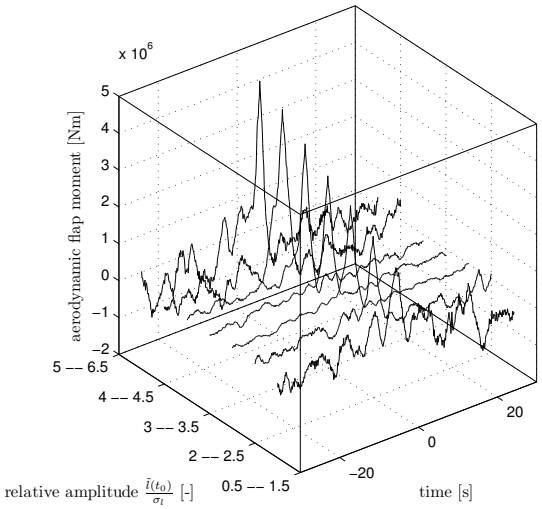
x 10^6
aerodynamic flap moment [Nm]
relative amplitude $\frac{\tilde{l}(t_0)}{\sigma_l}$ [-]
time [s]

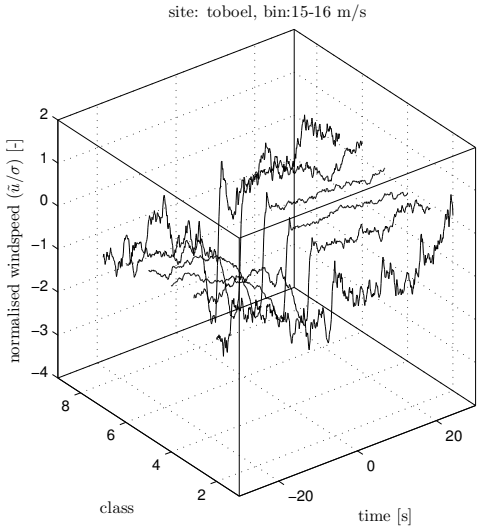
site: toboel, bin:15-16 m/s
normalised windspeed ($\tilde{u}/\sigma$) [-]
class
time [s]

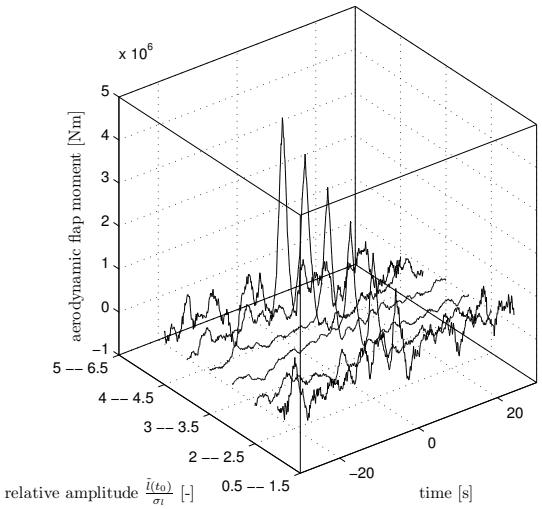
x 10^6
aerodynamic flap moment [Nm]
relative amplitude $\frac{\tilde{l}(t_0)}{\sigma_l}$ [-]
time [s]

K.2 Results for Horns Rev

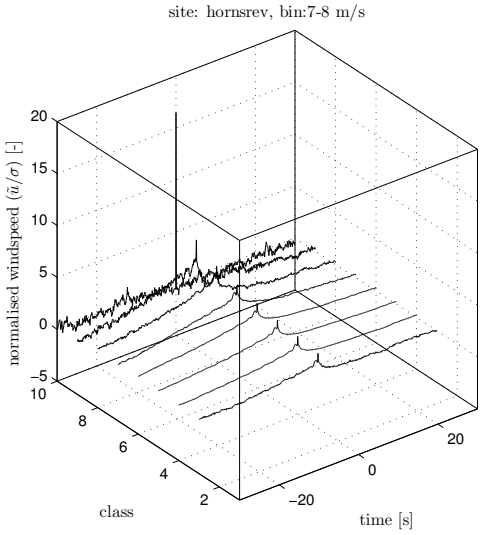
site: hornsrev, bin:7-8 m/s
normalised windspeed $(\tilde{u}/\sigma)$ [-]
class
time [s]

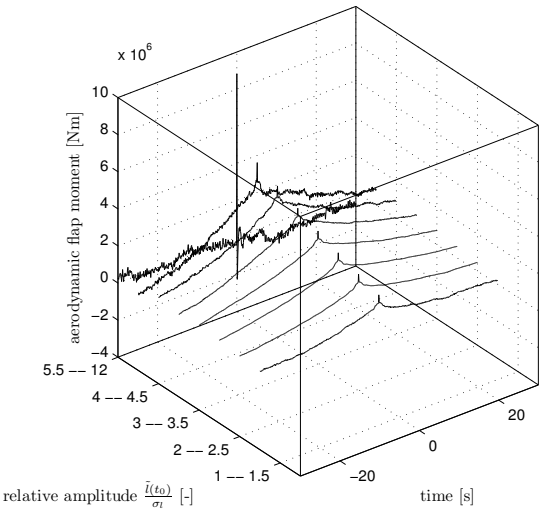
x 10^6
aerodynamic flap moment [Nm]
5.5 — 12
4 — 4.5
3 — 3.5
2 — 2.5
1 — 1.5
relative amplitude $\frac{\tilde{l}(t_0)}{\sigma_l}$ [-]
time [s]

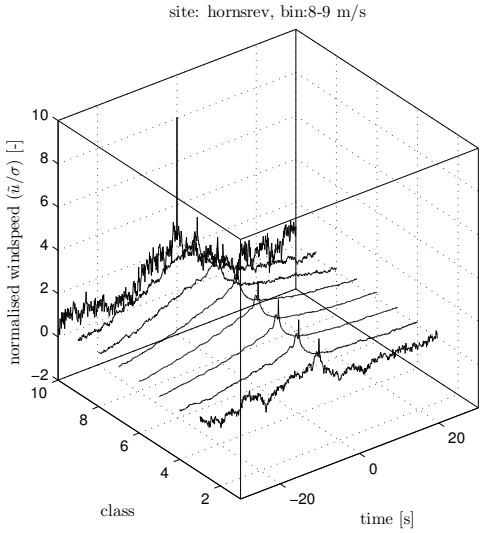
site: hornsrev, bin:8-9 m/s
normalised windspeed $(\tilde{u}/\sigma)$ [-]
class
time [s]

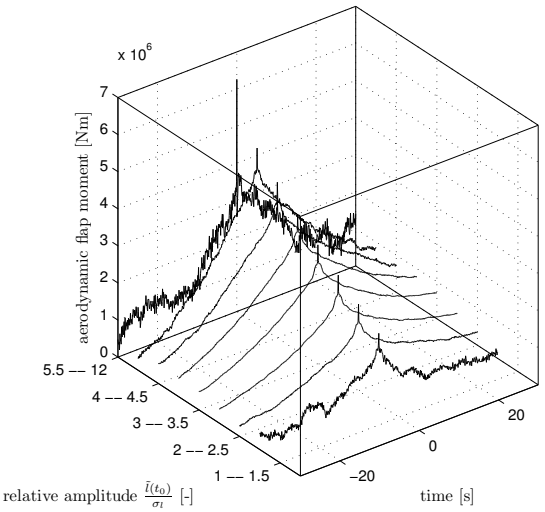
x 10^6
aerodynamic flap moment [Nm]
5.5 — 12
4 — 4.5
3 — 3.5
2 — 2.5
1 — 1.5
relative amplitude $\frac{\tilde{l}(t_0)}{\sigma_l}$ [-]
time [s]

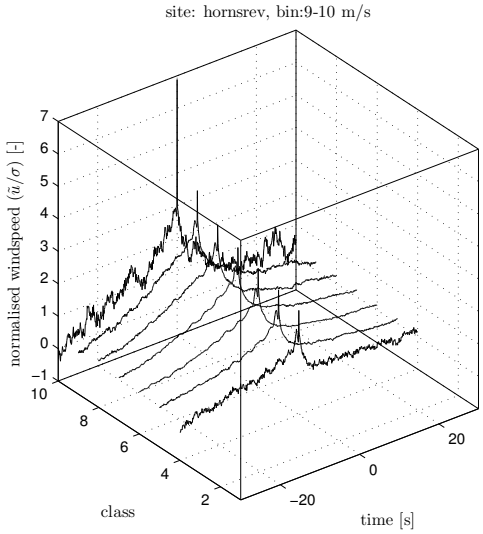
site: hornsrev, bin:9-10 m/s
normalised windspeed $(\tilde{u}/\sigma)$ [-]
class
time [s]

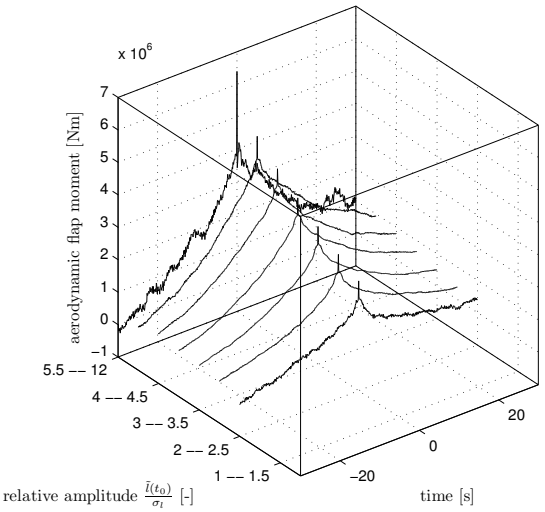
x 10^6
aerodynamic flap moment [Nm]
5.5 — 12
4 — 4.5
3 — 3.5
2 — 2.5
1 — 1.5
relative amplitude $\frac{\tilde{l}(t_0)}{\sigma_l}$ [-]
time [s]

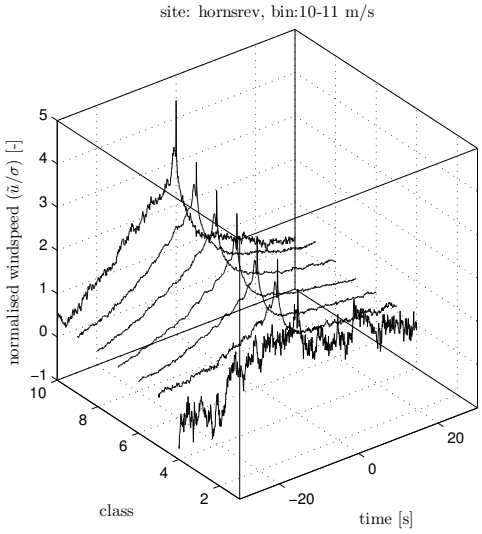
site: hornsrev, bin:10-11 m/s
normalised windspeed $(\tilde{u}/\sigma)$ [-]
class
time [s]

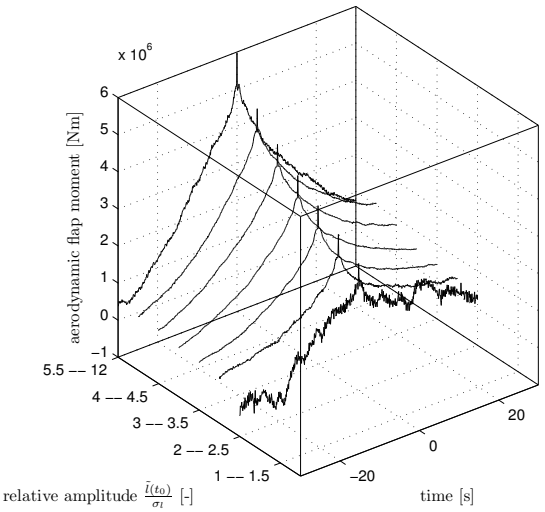
x 10^6
aerodynamic flap moment [Nm]
relative amplitude $\frac{\tilde{l}(t_0)}{\sigma_l}$ [-]
time [s]

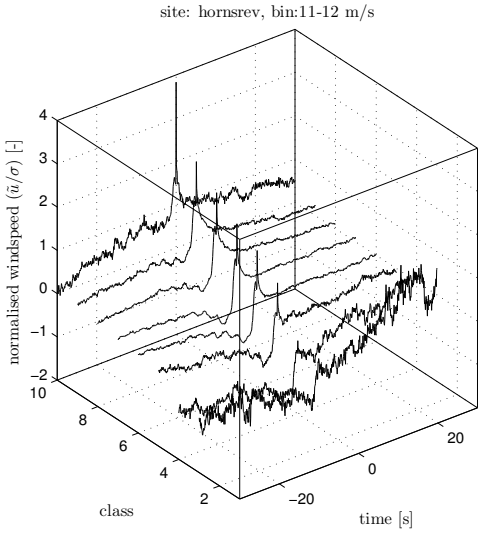
site: hornsrev, bin:11-12 m/s
normalised windspeed $(\tilde{u}/\sigma)$ [-]
class
time [s]

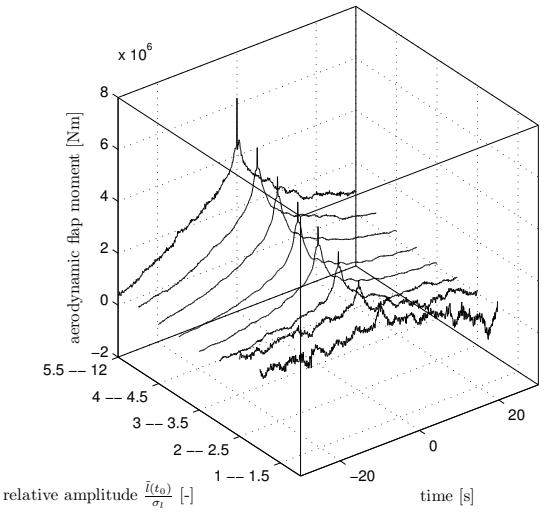
x 10^6
aerodynamic flap moment [Nm]
relative amplitude $\frac{\tilde{l}(t_0)}{\sigma_l}$ [-]
time [s]

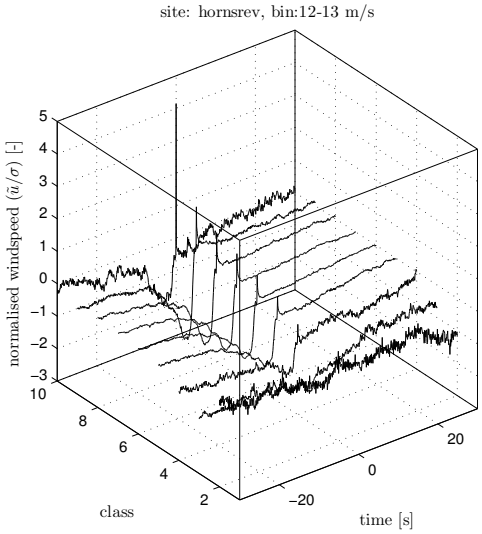
site: hornsrev, bin:12-13 m/s
normalised windspeed $(\tilde{u}/\sigma)$ [-]
class
time [s]

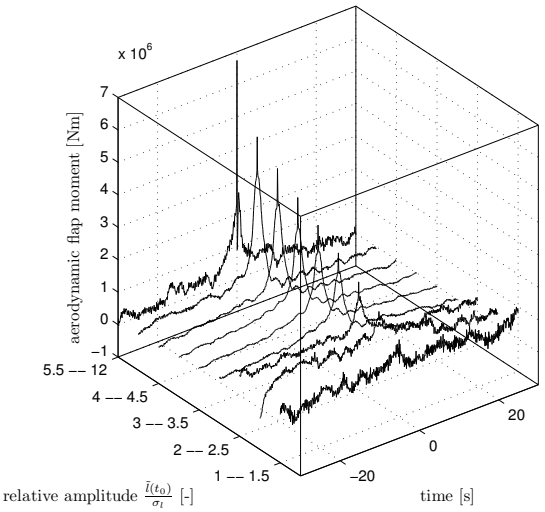
x 10^6
aerodynamic flap moment [Nm]
relative amplitude $\frac{\tilde{l}(t_0)}{\sigma_l}$ [-]
time [s]

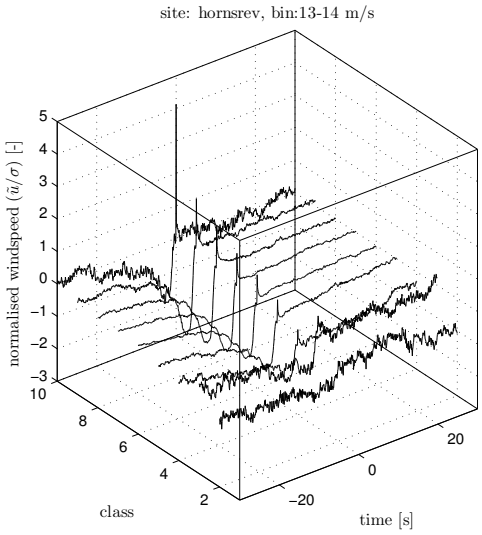
site: hornsrev, bin:13-14 m/s
normalised windspeed $(\tilde{u}/\sigma)$ [-]
class
time [s]

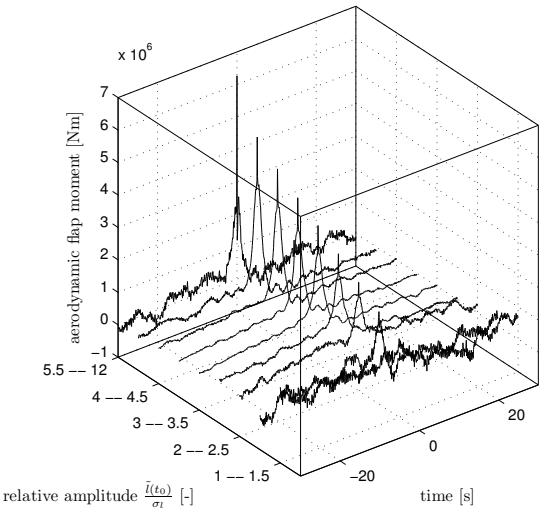
x 10^6
aerodynamic flap moment [Nm]
relative amplitude $\frac{\tilde{l}(t_0)}{\sigma_l}$ [-]
time [s]

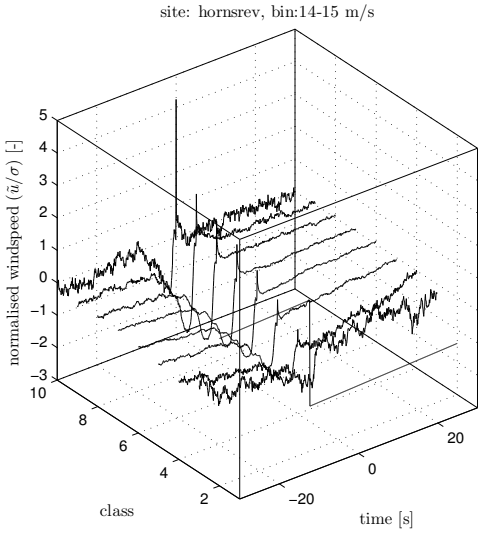
site: hornsrev, bin:14-15 m/s
normalised windspeed $(\tilde{u}/\sigma)$ [-]
class
time [s]

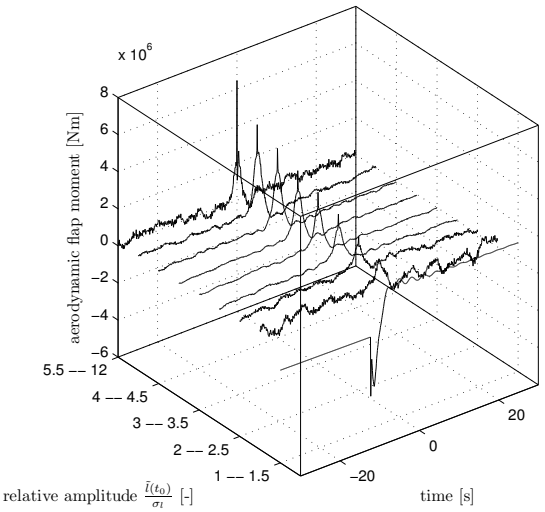
x 10^6
aerodynamic flap moment [Nm]
relative amplitude $\frac{\tilde{l}(t_0)}{\sigma_l}$ [-]
time [s]

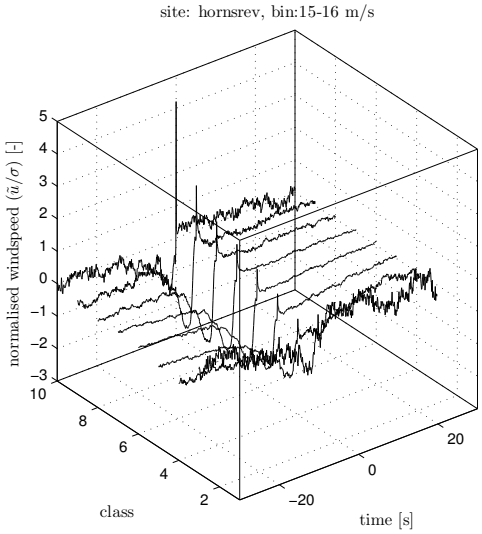
site: hornsrev, bin:15-16 m/s
normalised windspeed $(\tilde{u}/\sigma)$ [-]
class
time [s]

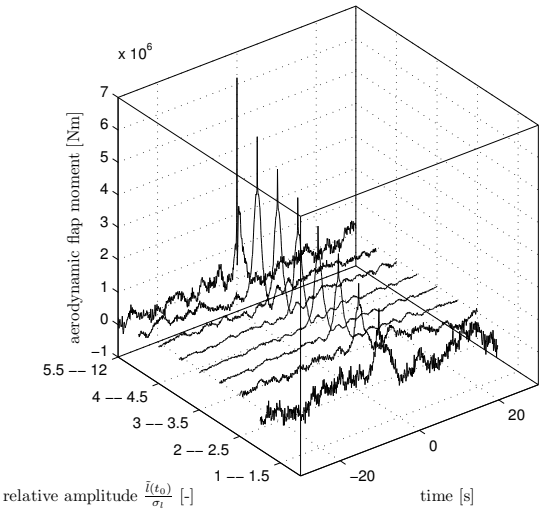
x 10^6
aerodynamic flap moment [Nm]
relative amplitude $\frac{\tilde{l}(t_0)}{\sigma_l}$ [-]
time [s]

K.3 Results for Oak Creek

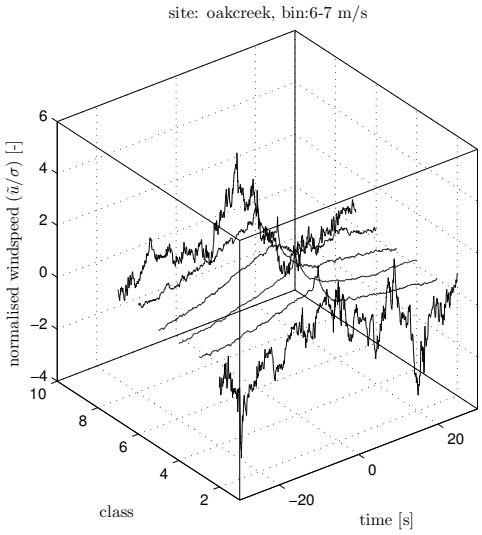
site: oakcreek, bin:6-7 m/s
normalised windspeed $(\tilde{u}/\sigma)$ [-]
class
time [s]

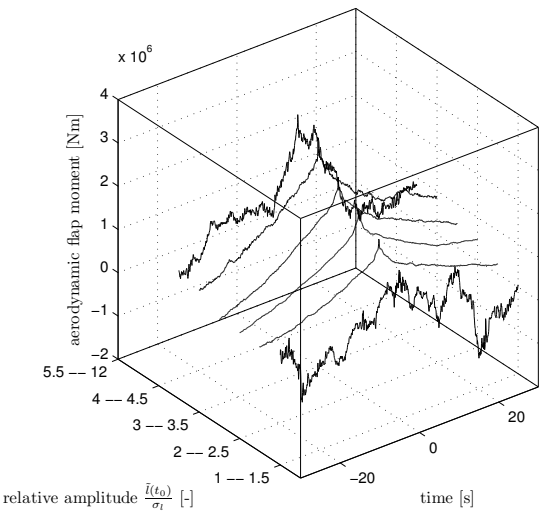
x 10^6
aerodynamic flap moment [Nm]
relative amplitude $\frac{\tilde{l}(t_0)}{\sigma_l}$ [-]
time [s]

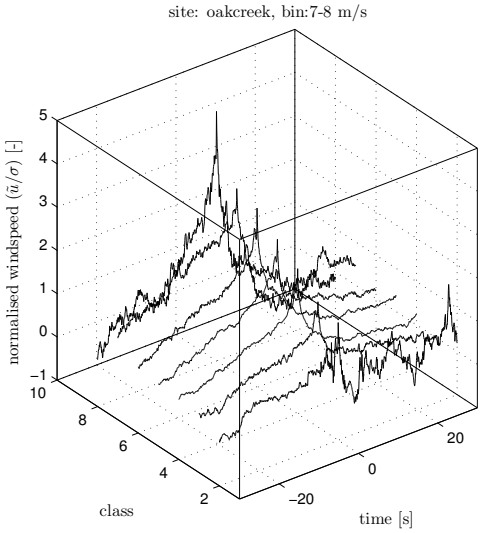
site: oakcreek, bin:7-8 m/s
normalised windspeed $(\tilde{u}/\sigma)$ [-]
class
time [s]

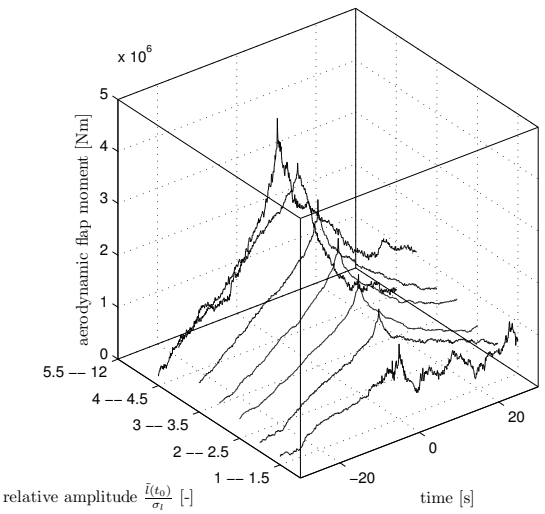
x 10^6
aerodynamic flap moment [Nm]
relative amplitude $\frac{\tilde{l}(t_0)}{\sigma_l}$ [-]
time [s]

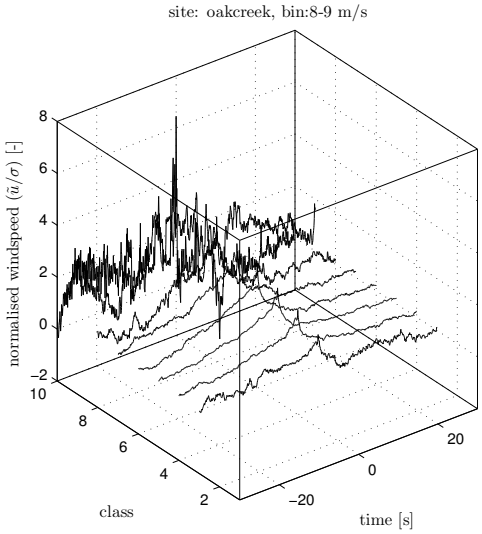
site: oakcreek, bin:8-9 m/s
normalised windspeed $(\tilde{u}/\sigma)$ [-]
class
time [s]

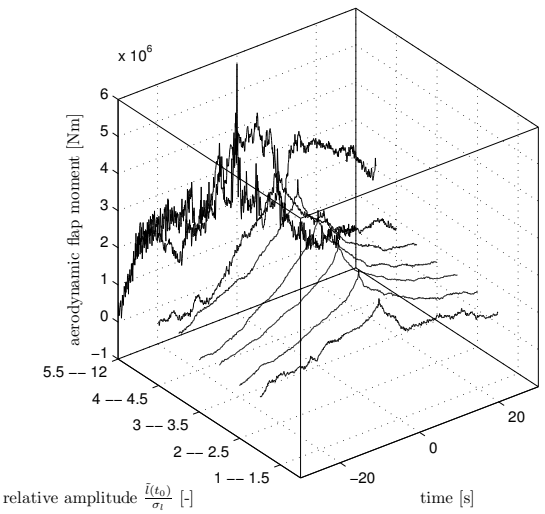
x 10^6
aerodynamic flap moment [Nm]
relative amplitude $\frac{\tilde{l}(t_0)}{\sigma_l}$ [-]
time [s]

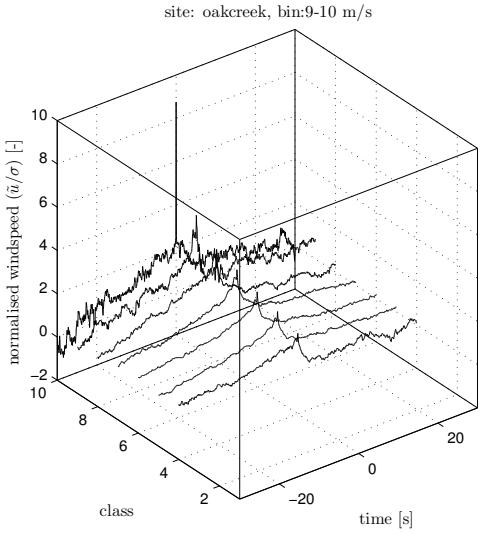
site: oakcreek, bin:9-10 m/s
normalised windspeed $(\tilde{u}/\sigma)$ [-]
class
time [s]

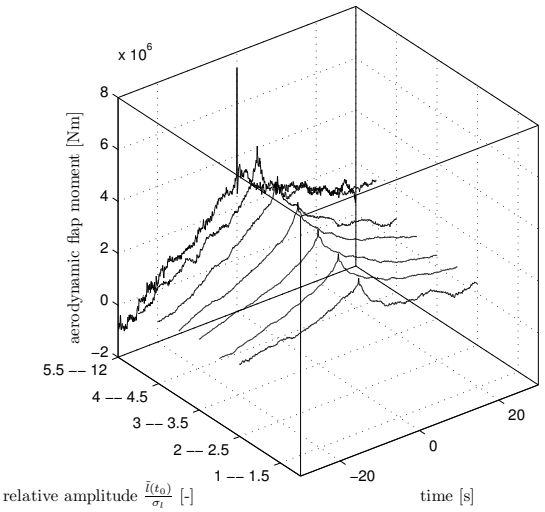
x 10^6
aerodynamic flap moment [Nm]
relative amplitude $\frac{\tilde{l}(t_0)}{\sigma_l}$ [-]
time [s]

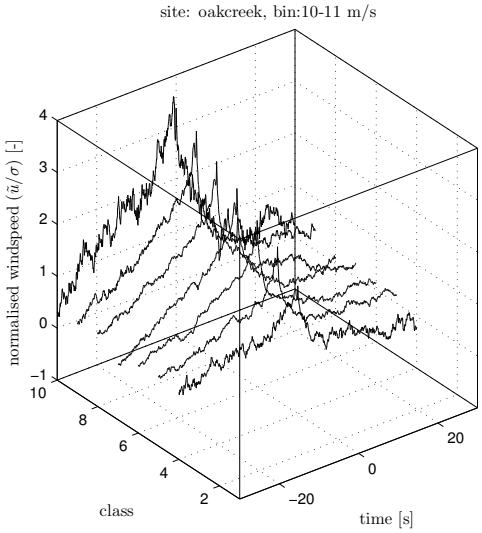
site: oakcreek, bin:10-11 m/s
normalised windspeed $(\tilde{u}/\sigma)$ [-]
class
time [s]

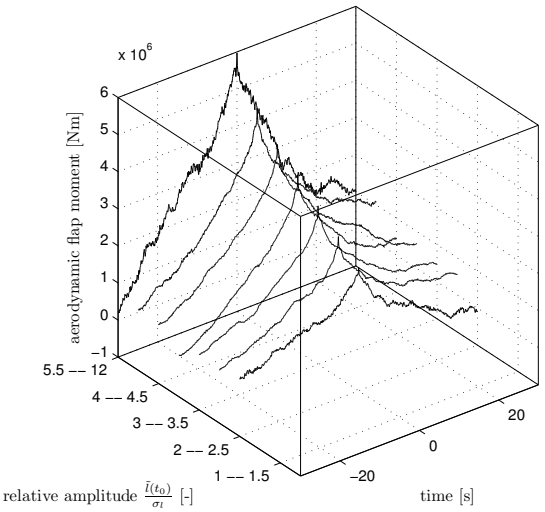
x 10^6
aerodynamic flap moment [Nm]
relative amplitude $\frac{\tilde{l}(t_0)}{\sigma_l}$ [-]
time [s]

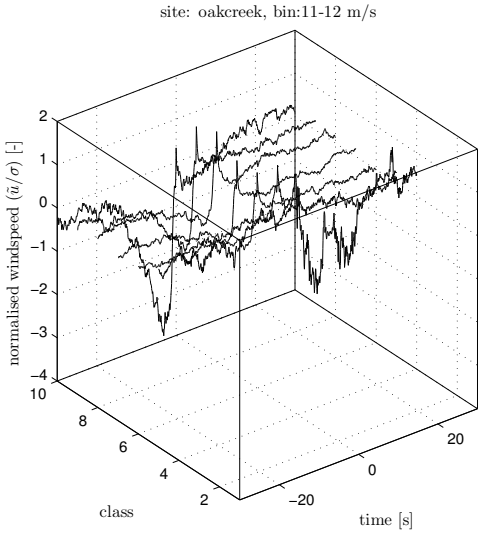
site: oakcreek, bin:11-12 m/s
normalised windspeed $(\tilde{u}/\sigma)$ [-]
class
time [s]

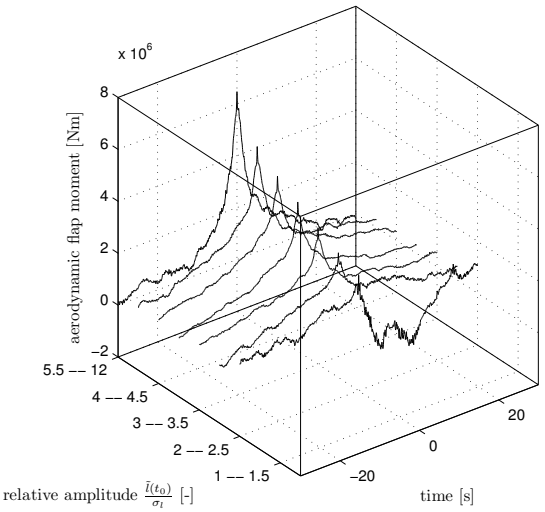
x 10^6
aerodynamic flap moment [Nm]
relative amplitude $\frac{\tilde{l}(t_0)}{\sigma_l}$ [-]
time [s]

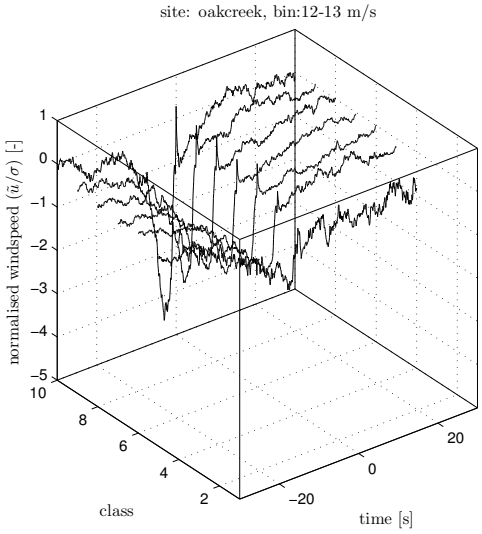
site: oakcreek, bin:12-13 m/s
normalised windspeed $(\tilde{u}/\sigma)$ [-]
class
time [s]

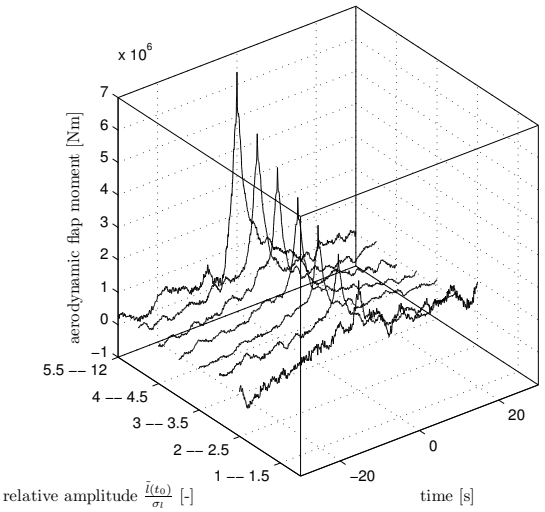
x 10^6
aerodynamic flap moment [Nm]
relative amplitude $\frac{\tilde{l}(t_0)}{\sigma_l}$ [-]
time [s]

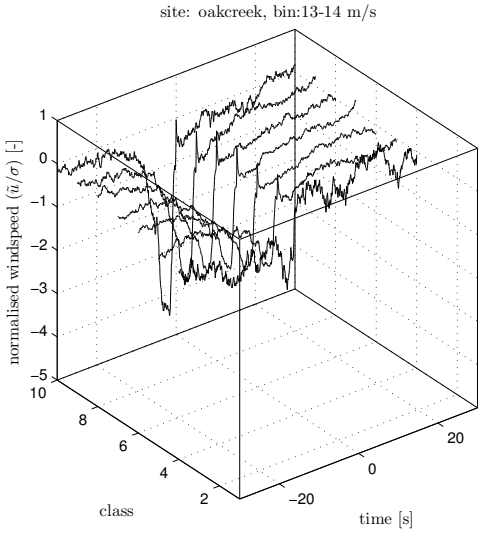
site: oakcreek, bin:13-14 m/s
normalised windspeed $(\tilde{u}/\sigma)$ [-]
class
time [s]

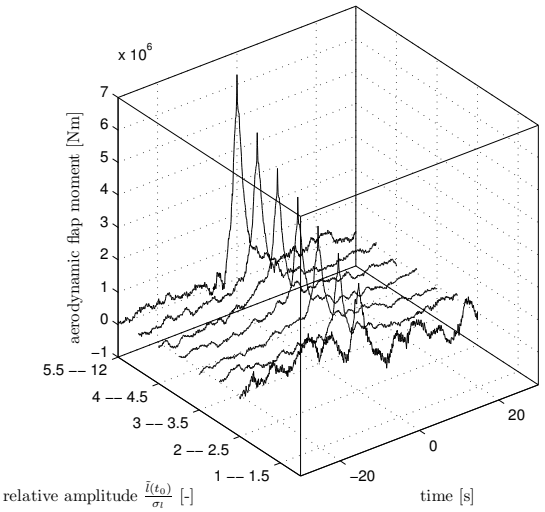
x 10^6
aerodynamic flap moment [Nm]
relative amplitude $\frac{\tilde{l}(t_0)}{\sigma_l}$ [-]
time [s]

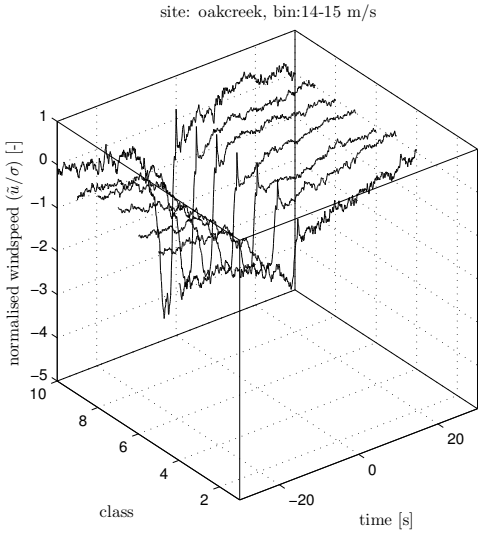
site: oakcreek, bin:14-15 m/s
normalised windspeed $(\tilde{u}/\sigma)$ [-]
class
time [s]

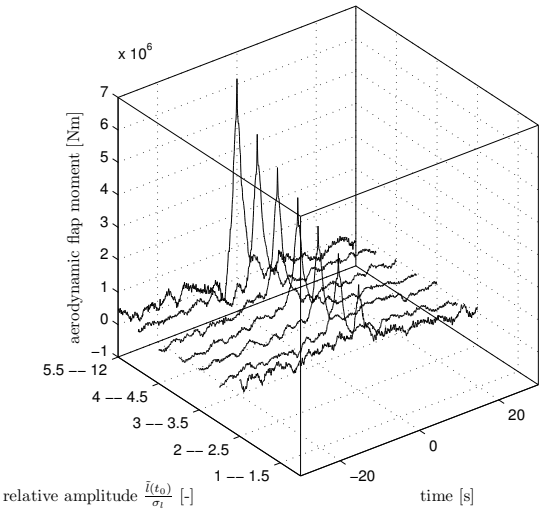
x 10^6
aerodynamic flap moment [Nm]
relative amplitude $\frac{\tilde{l}(t_0)}{\sigma_l}$ [-]
time [s]

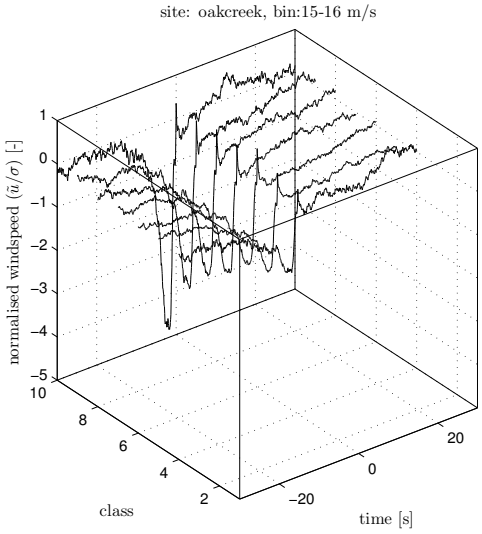
site: oakcreek, bin:15-16 m/s
normalised windspeed $(\tilde{u}/\sigma)$ [-]
class
time [s]

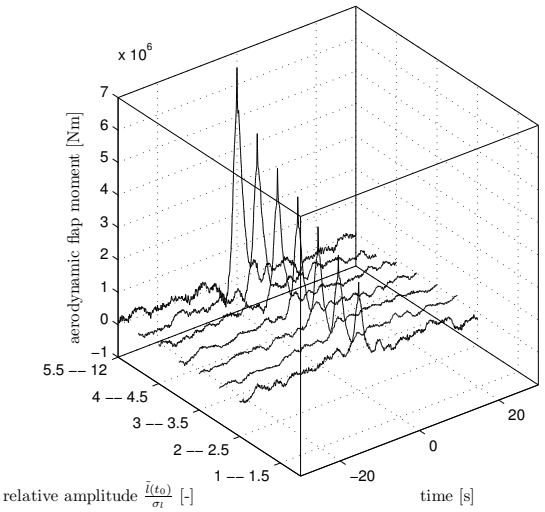
x 10^6
aerodynamic flap moment [Nm]
relative amplitude $\frac{\tilde{l}(t_0)}{\sigma_l}$ [-]
time [s]

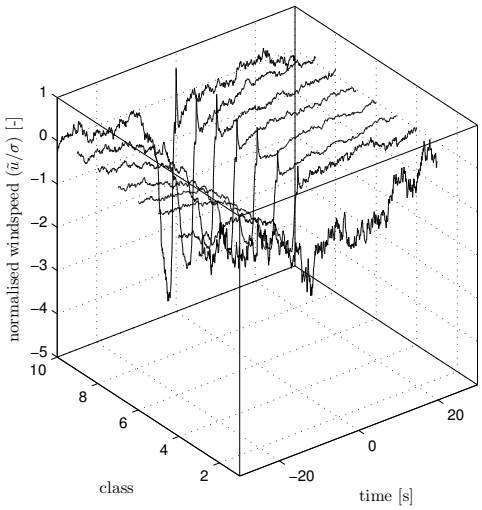
site: oakcreek, bin:16-17 m/s
normalised windspeed $(\tilde{u}/\sigma)$ [-]
class
time [s]

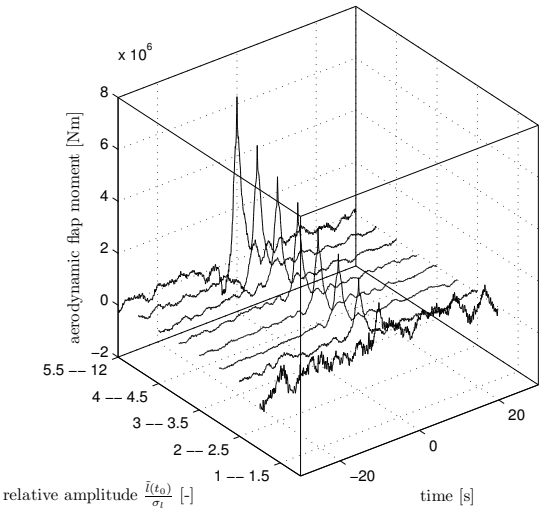
x 10^6
aerodynamic flap moment [Nm]
relative amplitude $\frac{\tilde{l}(t_0)}{\sigma_l}$ [-]
time [s]

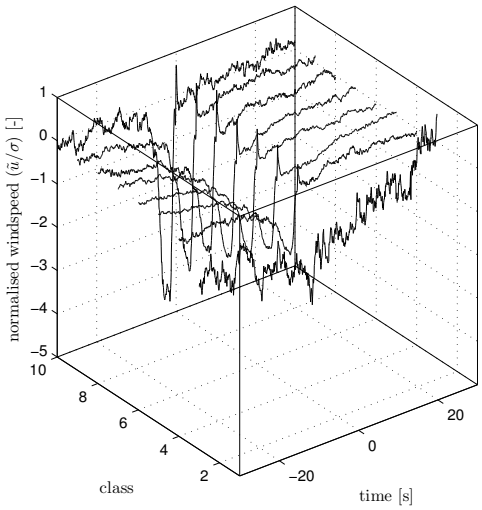
site: oakcreek, bin:17-18 m/s
normalised windspeed $(\tilde{u}/\sigma)$ [-]
class
time [s]

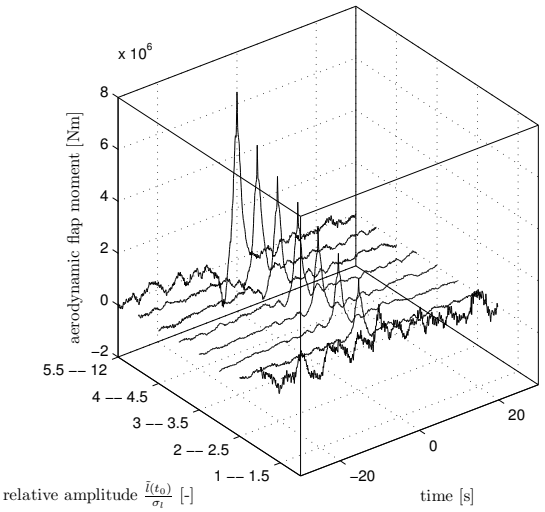
x 10^6
aerodynamic flap moment [Nm]
relative amplitude $\frac{\tilde{l}(t_0)}{\sigma_l}$ [-]
time [s]